MASTER

BNL-NUREG-50773

AN ADVANCED THERMOHYDRAULIC SIMULATION CODE FOR TRANSIENTS IN LMFBRs (SSC-L CODE)

A.K. AGRAWAL, Principal Investigator

Date Published - February 1978

ENGINEERING AND ADVANCED REACTOR SAFETY DIVISION
DEPARTMENT OF NUCLEAR ENERGY, BROOKHAVEN NATIONAL LABORATORY
UPTON, NEW YORK 11973

OFFICIAL FILE COPY

bnl

DISCLAIMER

This report was prepared as an account of work sponsored by an agency of the United States Government. Neither the United States Government nor any agency Thereof, nor any of their employees, makes any warranty, express or implied, or assumes any legal liability or responsibility for the accuracy, completeness, or usefulness of any information, apparatus, product, or process disclosed, or represents that its use would not infringe privately owned rights. Reference herein to any specific commercial product, process, or service by trade name, trademark, manufacturer, or otherwise does not necessarily constitute or imply its endorsement, recommendation, or favoring by the United States Government or any agency thereof. The views and opinions of authors expressed herein do not necessarily state or reflect those of the United States Government or any agency thereof.

DISCLAIMER

Portions of this document may be illegible in electronic image products. Images are produced from the best available original document.

DISCLAIMER

This report was prepared as an account of work sponsored by an agency of the United States Government. Neither the United States Government nor any agency Thereof, nor any of their employees, makes any warranty, express or implied, or assumes any legal liability or responsibility for the accuracy, completeness, or usefulness of any information, apparatus, product, or process disclosed, or represents that its use would not infringe privately owned rights. Reference herein to any specific commercial product, process, or service by trade name, trademark, manufacturer, or otherwise does not necessarily constitute or imply its endorsement, recommendation, or favoring by the United States Government or any agency thereof. The views and opinions of authors expressed herein do not necessarily state or reflect those of the United States Government or any agency thereof.

DISCLAIMER

Portions of this document may be illegible in electronic image products. Images are produced from the best available original document.

AN ADVANCED THERMOHYDRAULIC SIMULATION CODE FOR TRANSIENTS IN LMFBRs (SSC-L CODE)

A.K. AGRAWAL, Principal Investigator

Contributors

E.G. CAZZOLI   T.C. NEPSEE
J.G. GUPPY   E.S. SRINIVASAN
R.J. KENNETT   W.L. WEAVER III
I.K. MADNI   J.W. YANG

ENGINEERING AND ADVANCED REACTOR SAFETY DIVISION
DEPARTMENT OF NUCLEAR ENERGY, BROOKHAVEN NATIONAL LABORATORY
UPTON, NEW YORK 11973

THIS PAGE

WAS INTENTIONALLY

LEFT BLANK

FOREWORD

As a part of the Super System Code (SSC) development project for simulating thermohydraulic transients in LMFBRs, the SSC-L code was developed at Brookhaven. This code is intended to simulate transients in loop-type LMFBR designs. This topical report describes all modeling and coding efforts for the SSC-L code. A users' manual is under preparation and it will be issued as a separate report.

This work, covered under the budget activity No. 60-19-20-01-1, was performed for the Office of the Assistant Director for Advanced Reactor Safety Research, Division of Reactor Safety Research, United States Nuclear Regulatory Commission.

THIS PAGE

WAS INTENTIONALLY

LEFT BLANK

TABLE OF CONTENTS

TABLE OF CONTENTS (Cont)

TABLE OF CONTENTS (Cont)

TABLE OF CONTENTS (Cont)

TABLE OF CONTENTS (Cont)

LIST OF FIGURES

LIST OF FIGURES (Cont)

LIST OF FIGURES (Cont)

LIST OF TABLES

NOMENCLATURE

Symbol	Description	Unit
A	flow or cross sectional area	m^2
C	specific heat capacity	J/kg K
D	diameter	m
D_h	hydraulic diameter	m
D_1	inner diameter of IHX tube	m
D_2	outer diameter of IHX tube	m
e, E	specific enthalpy	J/kg
E_d	droplet entrainment rate	kg/s
f	friction coefficient; fractional power	---
F_K	fraction of flow in k-th channel	---
F_{pk}	fraction of total power in K-th channel	---
F_{rk}	normalized radial power distribution	---
F_{zk}	normalized axial power distribution	---
g	acceleration due to gravity	m/s^2
g_z	acceleration due to gravity in flow direction	m/s^2
G	mass flow rate per unit area	$kg/s\ m^2$
h	normalized pump head (H/H_R)	---
h	heat transfer coefficient	$W/m^2\ K$
h_c	convective heat transfer coefficient	$W/m^2\ K$
h_{cond}	gap conductance	$W/m^2\ K$
h_{rad}	radiation heat transfer coefficient	$W/m^2\ K$
H	height	m

Symbol	Description	Unit
H	specific enthalpy	J/kg
H	pump head	m
I	moment of inertia	kg-m^2
k	thermal conductivity	W/m K
K	loss coefficient	---
L	length of control volume or pipe	m
L	length of liquid slug	m
M	mass	kg
n_t	number of active tubes in IHX	---
Nu	Nusselt number	---
P	pitch	m
P	pressure	N/m^2(Pa)
P	power	W
P_{atm}	atmospheric pressure	N/m^2
Pe	Peclet number	---
P_{ext}	pressure external to the break	N/m^2
P_h	heat perimeter of duct	m
P_{inV}	pressure at reactor vessel inlet	N/m^2
Pr	Prandtl number	---
P_1	inlet pressure to loop	N/m^2
q	surface heat flux	W/m^2
Q	average heat generation per unit volume at steady state	W/m^3
Q	pump volumetric discharge	m^3/s
r	radial coordinate or radius	m

NOMENCLATURE (Cont)

Symbol	Description	Unit
r, R	thermal resistance	m^2 K/W
R	radius of a radial node	m
Re	Reynolds number	---
R_{gas}	gas constant	m^2/s^2 K
t	time	s
T	temperature	K
U	overall heat transfer coefficient	W/m^2 K
V	volume	m^3
v	velocity	m/s
v	specific volume	m^3/kg
$v´$	specific volume for momentum flux	m/kg
V_{GV}	volume of coolant collected in guard vessel	m^3
V_{min}	volume of guard vessel space to lowest elevation of pipes in it	m^3
V_{max}	total capacity of guard vessel space	m^3
W	mass flow rate	kg/s
W_b	break flow rate	kg/s
w_f	thickness of liquid film	m
X	mole fraction of ith component of fission gas mixture	---
x	axial distance	m
x	distance along channel from bubble initiation point	m
Z	vertical coordinate, rod length	m
Z_{GV}	level of coolant in guard vessel, measured from the lowest elevation of pipes in guard vessel	m

NOMENCLATURE (Cont)

Symbol	Description	Unit
Z_R	level of coolant in reservoir	m
Z_L	level of coolant in surge tank	m
Z_{tot}	height of reservoir	m
α	thermal expansion coefficient	m/m K
α	normalized pump spead (Ω/Ω_R)	---
β	normalized pump torque (t_{hyd}/t_R)	---
β_p	fraction of flow bypassing the IHX primary side	---
β	pressure ratio	---
β^*	critical pressure ratio	---
ϵ	pipe roughness	m
ϵ	emissivity	---
η	dynamic viscosity	Ns/m^2
θ	angle made by control volume with horizontal	rad
λ	heat of vaporization	J/kg
ν	normalized pump discharge (Q/Q_R)	---
ρ	density	kg/m^3
σ	Boltzman constant	$W/m^2 \, K^4$
τ	shear stress	N/m^2
τ	torque	N-m
ϕ_{TP}	two-phase friction multiplier	---
Ω	pump rotational speed	Hz

NOMENCLATURE (Cont)

Subscript	Description
BP	bypass flow
BPE	exit of bypass flow
BPM	average value of bypass flow
c	core flow or cladding or contraction
CG	columnar grain growth
ci	inside surface of cladding
co	outside surface of cladding
cw	coolant to wall
e	expansion
EG	equiaxed grain growth
f	fuel
Fi	inside surface of fuel
Fo	outside surface of fuel
g	cover gas in upper plenum
i or in	inlet
i	inner
i	node index
ℓ	liquid sodium
m1,m2,m3	metal in upper outlet plenum
N	sodium
o or out	outlet
o	outer
p	primary; fission gas plenum

NOMENCLATURE (Cont)

Subscript	Description
psh	primary to shell wall
pt	primary to tubewall
PB	primary bypass
R	rated value
ref	reference
res	reservoir
s	secondary
sh	shell
st	secondary to tube wall
t	tube
UN	unrestructured grain growth
w or W	water or wall
1	lower liquid slug and bubble interface
2	upper liquid slug and bubble interface

ACKNOWLEDGEMENT

1. ABSTRACT

Physical models for various processes that are encountered in preaccident and transient simulation of thermohydraulic transients in the entire liquid metal fast breeder reactor (LMFBR) plant are described in this report. A computer code, SSC-L, was written as a part of the Super System Code (SSC) development project for the 'loop'-type designs of LMFBRs. This code has the self-starting capability, i.e., pre-accident or steady-state calculations are performed internally. These results then serve as the starting point for the transient simulation.

A users' manual is being prepared as a separate document.

THIS PAGE

WAS INTENTIONALLY

LEFT BLANK

2. INTRODUCTION

2.1 BACKGROUND

The simulation of a liquid metal cooled fast breeder reactor (LMFBR) plant for a variety of off-normal or accident conditions ('Anticipated,' 'Unlikely,' and 'Extremely Unlikely') is an important part of the overall safety evaluation. Examples of different off-normal or accident conditions include (a) the withdrawal of control rod, (b) pump seizure in one of the loops, (c) after-heat removal in the absence of any forced pumping power, and (d) a major pipe break in the primary heat transport system (PHTS). In all of these events, the plant protection system (PPS) is assumed operative per design. The safety implication here is to assure that in any of these events the plant coolability is not endangered.

In some of the off-normal conditions, a proper design of PPS prevents any loss of fuel pin integrity. In fact, PPS is perhaps designed with this requirement in mind. For some other conditions, such as a massive pipe rupture in the primary heat transport system, one needs to assure that the coolable geometry is maintained. In this case, PPS is expected to initiate reactor scram, and, if possible, the affected loop is isolated. The decay heat will then have to be removed, for both short-term and long-term, in an acceptable manner through the remaining unaffected loops or via alternate emergency heat removal paths. Depending upon the nature and location of pipe rupture and the state of the plant prior to the rupture, coolant flow reversal or coolant stagnation could occur in the reactor core. Even if this condition were to persist for only a few seconds, a significant fraction of the total fuel pins could fail and release fission gases either prior to or subsequent to sodium boiling. Any system analysis code, therefore, must provide a capability to analyze such an accident.

Another important area for the system response evaluation is the plant's capability to dissipate after-heat from an intact system in the absence of any forced pumping power. The natural convection that may be established in the plant needs to be evaluated from the point of view of assuring the long-term cooling capability of the plant. The entire plant, with all of the essential components, needs to be modeled in sufficient detail to predict, in particular, the thermohydraulic behavior of the reactor core.

For some of the problems, the plant simulation may be required only for several tens of seconds. On the other hand, the long-term after-heat dissipation capability may require simulation for up to an hour of transient time. The computational time should, therefore, not be excessive, in order to permit execution of a sufficient number of parametric studies.

Restricted analytical models and associated computer codes such as IANUS,[2.1] DEMO,[2.2] and NATRANS[2.3] have been developed by other organizations to simulate the overall response of a fast reactor plant. The first two codes were specifically designed for the Fast Flux Test Facility (FFTF) and the Clinch River Breeder Reactor Plant (CRBRP). The IANUS code models PHTS, the intermediate heat transport system (IHTS), and the dump heat exchanger. The DEMO code is for CRBRP, with the exception that the dump heat exchanger is replaced by a steam generator and other components of the tertiary water loop.

Another code, called NALAP,[2.4] for the transient simulation of an LMFBR system is also available. This code was obtained by adopting the RELAP 3B[2.5] (BNL version of RELAP 3) by substituting sodium properties in place of those of water. Although this code is capable of providing a rudimentary flow decay for a pipe rupture accident, a number of modeling as well as operating limitations exist.

A number of simplifying assumptions and approximations are made in these codes, which may be acceptable from the design point of view, but are unacceptable for the safety analyses. For example, the modeling of the entire reactor core by a single average channel is highly questionable. The thermohydraulic or neutronic couplings between 'hot,' 'peak,' 'average,' and 'cold' channels must be included to account for the fact that up to 20 to 25 percent of the reactor core could be operating at peak channel conditions. An adequate representation for mixing of coolant coming out of different channels (or assemblies) having different temperatures in the outlet plenum is critical in determining sodium conditions at the vessel outlet. The coolant temperature here influences the natural convection capability in the plant.

There are processes that may be peculiar to the safety analyses. For example, the sodium boiling and the fission gas release are two important phenomena that could be encountered in both of the safety problems discussed earlier. It should, however, be noted that these phenomena may not occur in all of the channels but only in part of the core.

2.2 OBJECTIVES

To provide for a general system code, a work plan was written in fiscal year 1976 to develop Super System Code (SSC). The prime objective of this program is to develop an advanced system transient code for LMFBRs which will be capable of predicting the plant response when subjected to various off-normal and accident conditions. Two major accidents that this code will be designed to simulate are: (1) pipe breaks up to and including a double-ended rupture in the PHTS, and (2) the long-term after-heat removal in the absence of any forced pumping power. In both of these events,

the plant protection system (PPS) will be assumed to be functioning. In addition, the SSC will be able to simulate many of the 'level-2' transients such as withdrawal of a control rod followed by reactor scram through PPS action.

Another key objective of the code is to provide a capability within the code for doing steady-state or preaccident initialization. The initialized conditions will be calculated from the user-specified design parameters and operating conditions. A restart capability will be provided so that a series of transient analyses can be made from a single steady-state computation. A restart option during transient analyses will also be available.

The first in the series of codes in the SSC program is designed to simulate thermohydraulic transients in loop-type LMFBRs. Subsequent versions will include a similar capability for the 'pool'- or 'pot'-type designs of LMFBRs.

2.3 SUMMARY

The SSC Program consists of developing system transient codes for both loop- and pool-type designs of LMFBRs. These series of codes are labeled SSC-L and SSC-P, respectively. The work reported here is on the SSC-L code. The essential components and their arrangements in a loop system, such as the Clinch River Breeder Reactor Plant (CRBRP),[2.6] are schematically shown in Figure 2-1. Under normal operation, liquid sodium flows in both primary and intermediate heat transport systems. The steam generating loop or tertiary loop is also shown in this figure.

A comprehensive description of all of the models that were either developed or adapted to simulate processes of interest is given in Chapter 3. In this chapter, descriptions of models for the steady-state plant characterization, prior to the initiation of transients, are noted before going
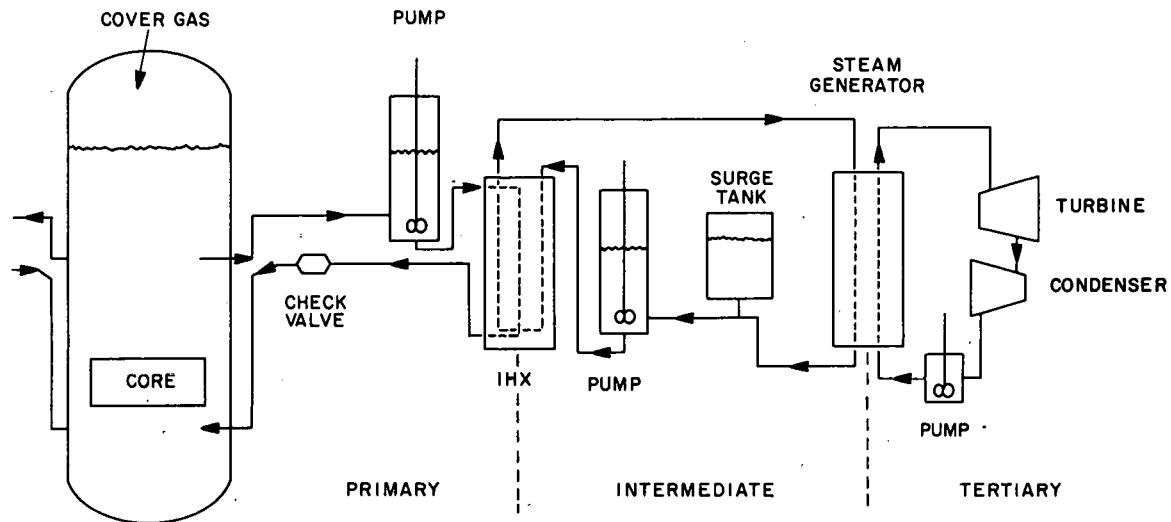
Figure 2-1. Sketch of one set of loops in an LMFBR.

into their transient counterparts.

Numerical methodology, that was developed for the SSC-L code, is discussed in Chapter 4. As a starting point for any transient calculation, a stable and unique steady-state or pretransient solution for the entire plant is obtained. In doing so, the time-independent form for continuity, energy, and momentum conservation equations are reduced to a set of nonlinear algebraic equations. These equations are solved in two steps: first, the global parameters are obtained; then, more detailed characterization is done by using the global conditions, obtained in the first step, as boundary conditions.

The energy and momentum conservation equations which describe water/ steam flow in the tertiary loop are coupled since the consitutive laws depend explicitly on fluid pressure. These equations are represented in the form of a set of algebraic equations for each control volume. These equations are then solved iteratively for the steam generating system.

For sodium loops, the energy and momentum conservation equations are decoupled when the effect of pressure on subcooled liquid sodium properties is neglected. This is a valid assumption. Therefore, the energy equations for both primary and intermediate heat transport systems are solved in conjunction with the detailed solution for the steam generator. The head requirement for sodium pumps is then determined by computing the entire pressure drop in the loop. The actual pressure at any location in either primary or secondary systems is then related directly to the cover gas pressure.

The numerical integration of the transient form of the governing equations is done by the use of a multi-step scheme (MSS) of integration. In this method, different processes are integrated by using different timestep

sizes. This is achieved by dividing the entire system into a number of
subsystems. Each of these subsystems uses a different timestep in time
advancement. In order to keep the logic required for integrating the
different subsystems manageable, a total of five different timestep sizes
are used. These are for (1) hydraulic response of both the primary and
intermediate heat transport systems, (2) thermal response of both the primary
and intermediate heat transport systems, (3) fuel rod heat conduction and
power generation computations, (4) coolant dynamics in the reactor core,
and (5) the computations in the steam generating system.

Individual processes are solved by the numerical algorithm that is most
suitable for the process under consideration. For example, the heat con-
duction equations for a fuel rod are solved by a first-order extrapolated
Crank-Nicolson differencing scheme. The fission heating computations, on
the other hand, are done either under a prompt-jump approximation (for reac-
tivity insertions of up to +50¢) or by a modified Kaganove method which
uses a polynomial method. The overall interfacing of all processes is
achieved by matching boundary conditions at the interface. The overall
timestep is controlled by requiring solutions to be numerically stable as
well as by the user-specified accuracy criteria. A feature that is built
into the code allows the timestep sizes to be automatically reduced or in-
creased.

A large number of options for modeling are built into the code.
These are discussed in detail in Chapter 3. A user can select options
through various flags or switches that are required as a part of the input.

A number of constitutive relations and correlations are required.
These can be input either in a tabular form or in an analytic form. For
the sake of computing efficiency, analytic forms are preferred and, hence,

used in the SSC-L code. Chapter 5 gives a list of all constitutive relations and correlations that are needed by the code. A set of appropriate values for coefficients in these analytic equations is also noted, although no claim for their suitability for any analysis is made (i.e., whether they are best values, conservative values, or desirable values). These coefficients are made available, as default, in the code. They can be overridden through input cards.

The SSC-L code is deliberately structured in a modular fashion. The data transfer between various modules is accomplished by COMMON blocks. The entire code is written in a variably dimensioned format, which allows for most effective usage of computer core space. Standard coding practices were followed so that portability of the code to other institutions can be achieved. Chapter 6 discusses various guidelines that were used in development of the SSC-L code. A naming convention for all global variables, as well as subprograms, was developed and utilized in the code. This considerably simplifies debugging of the code. A simplified flow chart, with brief descriptions of all major subprograms, is also given in Chapter 6.

A word on the units is in order. The SSC-L code is written in a consistent set of SI units.[2.7]

A companion report will give detailed instructions on how to use this code. Included in this report will be a detailed data dictionary, sample input deck, and output of the code.

2.4 APPLICATIONS

The SSC-L code is developed as an advanced thermohydraulic transient code for loop-type designs of LMFBRs. Although the emphasis has been on the safety analysis of transients, this code can be utilized for a variety of other

objectives, including (a) scoping analysis for design of a plant and (b) specification of various components.

REFERENCES

2.1   S.L. Additon, T.B. McCall and C.F. Wolfe, "IANUS - Outline Description," Westinghouse Advanced Reactors Division, Waltz Mill, Pennsylvania, FPC-939.

2.2   "LMFBR Demonstration Plant Simulation Model, DEMO," Westinghouse Advanced Reactors Division, WARD-D-0005 (Rev 3), February 1975.

2.3   D. Brosche, "NATRANS-Ein Rechenmodel zur Berechnung des Dynamischen Verhaltens von Reaktorkuhlkerislaufen bei Storfallen," Laboratorium fur Reaktorregelung and Aulagensicherung Garching, Report MRR-71, April 1971.

2.4   B.A. Martin, A.K. Agrawal, D.C. Albright, L.G. Epel, and G. Maise, "NALAP: An LMFBR System Transient Code," BNL-50457, July 1975.

2.5   "RELAP3B Manual, A Reactor System Transient Code," Brookhaven National Laboratory, RP 1035, December 1974.

2.6   Clinch River Breeder Reactor Project, Preliminary Safety Analysis Report, Vol. 4, Project Management Corporation, 1975.

2.7   "The International System of Units (SI)," C.H. Page and P. Vigoureux Editors, National Bureau of Standards Special Publication 330, 1972 Edition.

3. COMPONENT MODELING

3.1 IN-VESSEL

3.1.1 Description

The in-vessel part of the plant is responsible for the generation of
heat through nuclear fission of both fissile and fertile materials. In
addition, a portion of heat is also produced by decay of the radioactive
nuclides. A schematic of the in-vessel part of a loop-type breeder reactor
plant is shown in Figure 3-1. Although this drawing represents the in-vessel
part of the Clinch River Breeder Reactor Plant (CRBRP),[3.1] it is used
here to illustrate some of the important components that need to be con-
sidered in modeling for the SSC-L code. From the point of view of thermo-
hydraulics modeling, essential in-vessel components include lower and upper
plena, heat generating portion (fuel, blanket, and control assemblies), and
the bypass coolant flow.

Figure 3-2 shows the core midplant details for the CRBRP. Once again,
these details for a plant under simulation may differ from those in the CRBR.
The core internals are represented by fuel, blanket, and control assemblies.
These assemblies are usually made up of closely packed individual rods sep-
arated by a spiral spacer wire. For the purpose of the SSC-L code, these
different types of assemblies are represented as a set of one-dimensional,
parallel, equivalent channels which can be coupled with each other through
(1) hydraulic coupling in lower and upper plena and (2) neutronic coupling.
In all, there can be N5RTYP number of types of rods, each one of which can
have one or more channels such that the total number of channels is N6CHAN
(N6CHAN $\geq$ N5RTYP). A channel represents N6RODS number of rods. The number

COVER GAS

SODIUM LEVEL

CHIMNEY
EXTENSION OF
OUTLET MODULE

SUPPORT COLUMN

CELLULAR FLOW
COLLECTOR

HORIZONTAL BAFFLE

CORE RESTRAINT
FORMER RINGS

FUEL TRANSFER
& STORAGE POSITION

CORE SUPPORT CONE

CORE SUPPORT PLATE

CORE INLET FLOW
MODULE (61)

INLET PLENUM

VESSEL CLOSURE
HEAD

CONTROL ROD
DRIVELINE/SHROUD TUBE

VORTEX SUPPRESSOR
PLATE

IN-VESSEL TRANSFER
MACHINE PLUG

REACTOR VESSEL
THERMAL LINER

REACTOR VESSEL

OUTLET
PLENUM

SODIUM OUTLET
NOZZLE (3)

RADIAL KEY

CONTROL ASSEMBLY

REACTOR CORE

RADIAL BLANKET

CORE BARREL

SODIUM INLET
NOZZLE (3)

Figure 3-1. Reactor schematic.
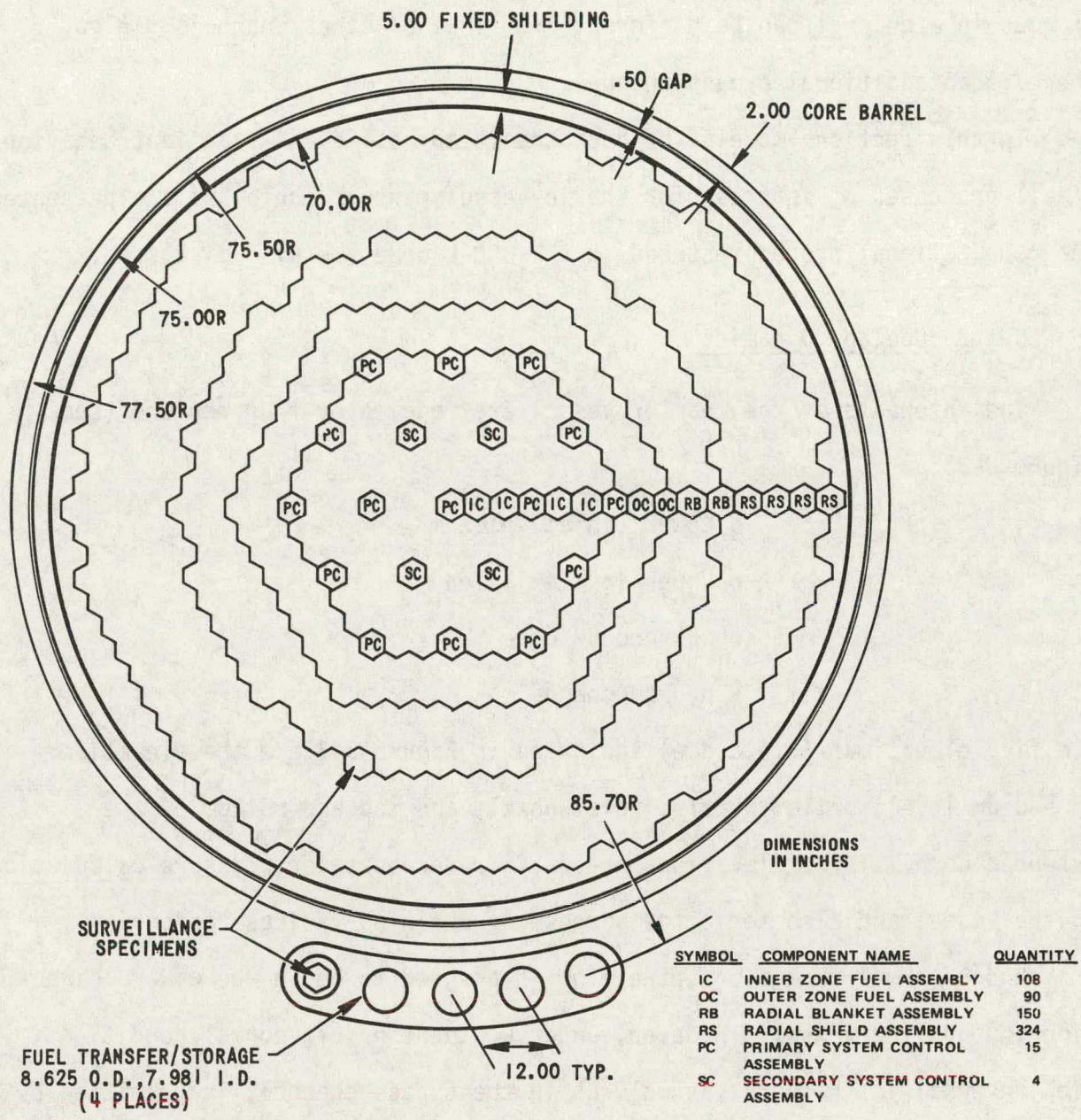
Figure 3-2. CRBRP reactor cross section.

of rods in a channel can be different from that of other channels. Also, there is an additional bypass channel.

In this section, models for both the steady state and transient behavior of all processes of interest for the in-vessel part of the plant are presented. The computational procedures used in the SSC-L code are also discussed.

3.1.2 Coolant Dynamics

The internals of the reactor vessel are modeled by four regions (see Figure 3-3):

- Lower (inlet) plenum
- Upper (outlet) plenum
- "Extended" core
- Bypass channel

The five elevations (a,b,c,d,e) indicated in Figure 3-3 are the elevations of sodium level, outlet nozzle, inlet nozzle, and top and bottom of the extended core. These elevations are basic references for pressure calculation in the vessel and also serve the purpose of defining various regions.

Under normal conditions, the flow is assumed to be in the upward direction through the vessel. However, under accident or off-normal conditions, flow reversal in the core, as well as in the bypass channel, is permitted by the model. The mass flow rate, fluid pressure, and fluid temperature at the inlet and outlet nozzles interconnect the flow dynamics between the vessel and the primary loops.

3.1.2.1 Lower (Inlet) Plenum

At steady-state, the fluid and the metal in the lower plenum are assumed to be in thermal equilibrium. The temperatures are then equal to the fluid
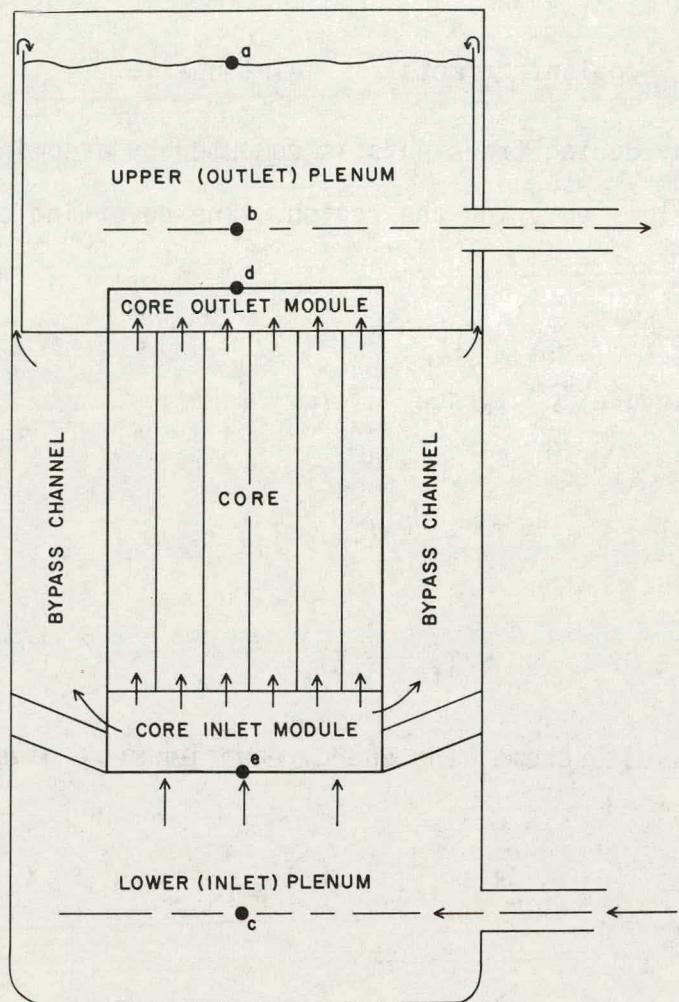
Figure 3-3. Identification of regions in the reactor vessel.

temperature at the inlet nozzle, i.e.,

$$T_{coolant} = T_{metal} = T_{inlet\ nozzle} \quad . \tag{3-1}$$

The coolant enthalpy during transients is computed by assuming complete
mixing of various flows entering the region. The governing energy equations
are

$$\frac{d}{dt} (\rho V E) = \sum_{in} (WE) - \sum_{out} (WE) + UA(T_m - T_f) \quad , \tag{3-2}$$

$$\frac{d}{dt} T_m = \frac{UA}{MC} (T_f - T_m) \quad , \tag{3-3}$$

where

$$T_f = f(E) \quad .$$

Using the semi-implicit scheme, the energy equations are given in the follow-
ing form:

$$a_{11} E^{k+1} + a_{12} T_m^{k+1} = c_1 \quad , \tag{3-4}$$

$$a_{21} E^{k+1} + a_{22} T_m^{k+1} = c_2 \quad , \tag{3-5}$$

where

$$a_{11} = \rho^{k+1} + \frac{\Delta t}{2V} \left(\sum_{out} W^{k+1} \right) + \frac{\Delta t}{2V} \frac{UA}{c_p^k} \quad ,$$

$$a_{12} = - \frac{\Delta t}{2V} UA \quad ,$$

$$a_{21} = - \frac{\Delta t}{2 c_p^k} \left(\frac{UA}{MC} \right) \quad ,$$

$$a_{22} = 1 + \left(\frac{UA}{MC} \right) \frac{\Delta t}{2} \quad ,$$

$$c_1 = (\rho E)^k + \frac{\Delta t}{2V} \left[\sum_{in} (WE)^{k+1} + \sum_{in} (WE)^k - \sum_{out} (WE)^k \right.$$

$$\left. + UA \left(T_m^k - 2T_f^k + \frac{E^k}{C_p^k} \right) \right] ,$$

$$c_2 = T_m^k + \frac{\Delta t}{2} \left(\frac{UA}{MC} \right) \left(2T_f^k - \frac{E^k}{C_p^k} - T_m^k \right) .$$

Equations (3-4) and (3-5) are solved simultaneously for the transient cool-ant enthalpy and metal temperature. The coolant density ρ and heat capacity C_p are obtained from the constitutive relationships for sodium.

3.1.2.2 Upper (Outlet) Plenum

In the upper (outlet) plenum, the coolant from the core exit and the bypass channel mixes with the coolant stored in the region. Along with this mixing process, the heat transfer between sodium and various structural metals and between sodium and the cover gas also takes place. An accurate treatment for this mixing process, coupled with the heat transfer, is re-quired so that the sodium temperature at the outlet nozzle of the reactor vessel may be properly predicted. A detailed three-dimensional (in space) thermohydraulic treatment would be expensive for a system code. Therefore, a simplified treatment was developed.

A schematic of the contents of the outlet plenum is shown in Figure 3-4. The upper plenum contains a large volume of sodium, an annular bypass channel, a small region occupied by the cover gas, and three sections of metal. Fluid leaving the reactor core enters the plenum from the bottom section, while a small percentage of cold bypass flow enters the plenum through the annular space formed by the thin thermal liner and the vessel wall. The vessel out-let flow is represented by an exit nozzle. The support columns, chimney of the
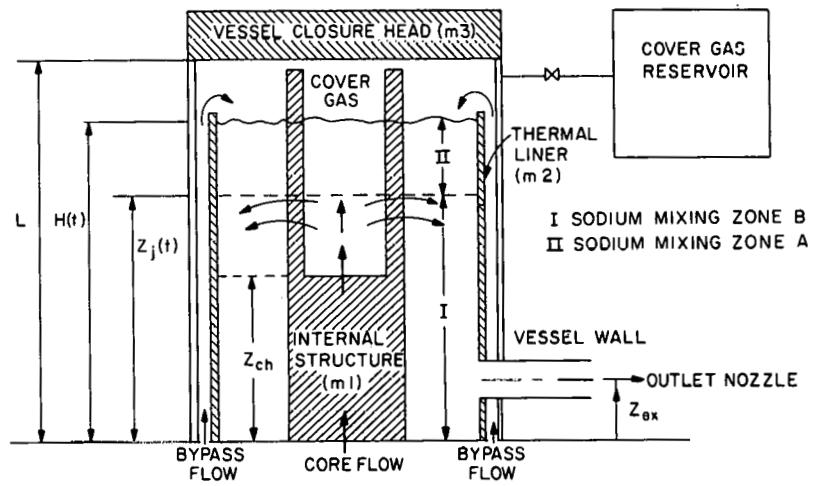
Figure 3-4. A schematic of the outlet plenum of
a reactor vessel.

outlet module, control rod drive mechanism, vertex suppressor plate, control assembly, cellular flow collector, baffle, and all other structures are lumped together and represented by a section of mass (m1) immersed in fluids. The cylindrical thermal liner is indicated as another mass (m2). The vessel closure head and other metals above the cover gas region are considered as mass m3. The cover gas region is connected to a large reservoir which represents all its connections, such as the overflow tank, equalization line header, and gas region of the loop pumps.

The outlet plenum, as described above, is represented by two, one-dimensional (in the direction along the reactor vessel) zones. The maximum penetration of the average core exit flow is used as the criterion for dividing the sodium region with two zones. The upper mixing zone is denoted as zone A and the lower zone as zone B. The basic assumptions are

1) Core flows from different channels into the upper plenum are represented by a single equivalent flow. This flow is associated with the mass-average enthalpy of the different channel flows.

2) The maximum penetration distance, which is related to the initial Froude number, divides the upper plenum into two mixing zones. Full penetration is assumed for flow with positive buoyancy.

3) The mixing process in both zones is described by the lumped-parameter approach, i.e., complete mixing in each zone is assumed.

4) The cover gas obeys perfect gas law, and it is initially in equilibrium with the gas in the reservoir.

At steady state, the core exit flow is at a temperature higher than the mixed-mean sodium temperature of the outlet plenum. In other words, in accordance with our assumption (2) above, the core exit flow is assumed to

penetrate the entire height of the outlet plenum. In this case, we have only one zone, as opposed to up to two zones during transients. The governing energy equations for this complete mixing at steady-state are written for each material as

sodium:

$$W_c(E_c - E_\ell) + W_{BP}(E_{BPE} - E_\ell) + U_g A_{\ell g}(T_g - T_\ell)$$

$$+ U_\ell A_{\ell m1}(T_{m1} - T_\ell) + U_\ell A_{\ell m2}(T_{m2} - T_\ell) = 0 ; \quad (3\text{-}6)$$

cover gas:

$$A_{\ell g}(T_\ell - T_g) + A_{gm1}(T_{m1} - T_g) + A_{gm2}(T_{m2} - T_g) + A_{gm3}(T_{m3} - T_g) = 0; (3\text{-}7)$$

internal structure (m1):

$$U_\ell A_{\ell m1}(T_\ell - T_{m1}) + U_g A_{gm1}(T_g - T_{m1}) = 0 ; \quad (3\text{-}8)$$

thermal liner (m2):

$$U_\ell A_{\ell m2}(T_\ell - T_{m2}) + U_g A_{gm2}(T_g - T_{m2}) + (UA)_{BP}(T_{BPM} - T_{m2}) = 0 ; \quad (3\text{-}9)$$

vessel closure head (m3):

$$T_{m3} - T_{BPE} = 0 ; \quad (3\text{-}10)$$

bypass flow:

$$T_{BPM} = T_{m2} + (T_{BPI} - T_{BPE})\left(\frac{WC}{UA}\right)_{BP} , \quad (3\text{-}11)$$

$$T_{BPE} = T_{m2} + (T_{BPI} - T_{m2})\exp\left(-\left(\frac{UA}{WC}\right)_{BP}\right) . \quad (3\text{-}12)$$

The above seven equations (3-6) through (3-12) are solved simultaneously

to yield a complete solution of coolant mixing in the upper plenum.

During transients, we divide the outlet plenum by up to two zones. As mentioned earlier, this partition is based on the penetration height of the average core exit flow. The governing equations which determine the instantaneous sodium level and various temperatures are expressed for each material as

sodium level:

$$\frac{dH}{dt} = \frac{W_i - W_{ex}}{\bar{\rho}A_{g\ell}} + H\left[(1 - f)\ \alpha(T_B)\ \frac{dT_B}{dt} + f\ \alpha(T_A)\ \frac{dT_A}{dt}\right]; \qquad (3\text{-}13)$$

sodium in the upper mixing zone A:

$$\frac{dE_A}{dt} = \frac{1}{\rho_A\ A_{g\ell}\ Hf}\left\{W_{BP}(E_{BPE} - E_A) + \beta_1 W_C(E_B - E_A) + h\ A_{g\ell}(T_B - T_A)\right.$$
$$\left. + U_g A_{g\ell}(T_g - T_A) + U_\ell f\left[A_{\ell m1}(T_{m1} - T_A) + A_{\ell m2}(T_{m2} - T_A)\right]\right\}; \qquad (3\text{-}14)$$

sodium in the lower mixing zone B:

$$\frac{dE_B}{dt} = \frac{1}{\rho_B\ A_{g\ell}\ H(1-f)}\left\{W_C(E_C - E_B) + \beta_2 W_{BP}(E_A - E_B) + h\ A_{g\ell}(T_A - T_B)\right.$$
$$\left. + U_\ell(1-f)\left[A_{\ell m1}(T_{m1} - T_B) + A_{\ell m2}(T_{m2} - T_B)\right]\right\}; \qquad (3\text{-}15)$$

cover gas:

$$\frac{dT_g}{dt} = \frac{U_g}{(MC)_g}\left[A_{g\ell}(T_A - T_g) + A_{gm1}(T_{m1}\ T_g) + A_{gm2}(T_{m2} - T_g) + A_{gm3}(T_{m3} - T_g)\right];$$
$$(3\text{-}16)$$

metal m1 (internal structure):

$$\frac{dT_{m1}}{dt} = \frac{1}{(MC)_m}\left\{U_\ell\ A_{\ell m1}\left[f\ T_A + (1-f)\ T_B - T_{m1}\right] + U_g\ A_{gm1}(T_g - T_{m1})\right\}; \quad (3\text{-}17)$$

metal m2 (thermal liner):

$$\frac{dT_{m2}}{dt} = \frac{1}{(MC)_{m2}} \left\{ U_\ell \, A_{\ell m2} \left[f(T_A - T_{m2}) + (1-f) \, (T_B - T_{m2}) \right] \right.$$

$$\left. + U_g \, A_{gm2} \, (T_g - T_{m2}) + (UA)_{BP} \, (T_{BPM} - T_{m2}) \right\} ; \qquad (3\text{-}18)$$

metal m3 (vessel closure head):

$$\frac{dT_{m3}}{dt} = \frac{U_g \, A_{gm3}}{(MC)_{m3}} \, (T_g - T_{m3}) \, . \qquad (3\text{-}19)$$

The auxiliary equations required by the above governing equations are

$$T_{BPE} = T_{m2} + (T_{BPI} - T_{m2}) \, \exp \left(- \frac{UA}{WC} \right)_{BP} , \qquad (3\text{-}20)$$

$$T_{BPM} = T_{m2} + (T_{BPI} - T_{BPE}) \left(\frac{WC}{UA} \right)_{BP} , \qquad (3\text{-}21)$$

$$W_i = W_C + W_{BP} , \qquad (3\text{-}22)$$

$$f = 1 - z_j(t)/H(t) , \qquad (3\text{-}23)$$

$$\bar{\rho} = (1-f) \, \rho_B + f \, \rho_A , \qquad (3\text{-}24)$$

and the liquid sodium densities, ρ_A and ρ_B, are obtained from the constitutive relationships for sodium. The contact areas between the cover gas and liquid or metals ($A_{g\ell}$, A_{gm1}, A_{gm2}, A_{gm3}) and between liquid and metals ($A_{\ell m1}$, $A_{\ell m2}$) are obtained by assuming that the cross-sectional areas in a direction perpendicular to the jet are constant during transients.

In the above equations, there are two control indices, β_1 and β_2, which

take values of either 0 or 1 depending upon the relative location of the outlet nozzle and the maximum jet penetration height, z_j. Their values are

$$\beta_1 = 0 \text{ and } \beta_2 = 1 \qquad \text{for } z_j \geq (z_{ex} + \frac{1}{2} D) \quad ,$$

$$\beta_1 = 0 \text{ and } \beta_2 = 0 \qquad \text{for } (z_{ex} - \frac{1}{2} D) < z_j < (z_{ex} + \frac{1}{2} D) \quad ,$$

and

$$\beta_1 = 1 \text{ and } \beta_2 = 0 \qquad \text{for } z_j \leq (z_{ex} - \frac{1}{2} D) \quad \cdot$$

The maximum penetration height is taken from a correlation developed earlier.[3.2] It is given as

$$z_j = (1.0484 \, Fr_0^{0.785}) \, r_0 + z_{ch} \quad , \tag{3-25}$$

where Fr_0 is the local Froude number and is defined as

$$Fr_0 = \left(\frac{W_C}{\pi r_0^2 \rho_C} \right)^2 \left[\frac{\rho_B}{g r_0 (\rho_C - \rho_B)} \right] \quad \cdot \tag{3-26}$$

For the case of full penetration, i.e., for $z_j(t) = H(t)$, f becomes zero. Equations (3-14) and (3-15) are then replaced by the following equations:

$$\frac{dE_B}{dt} = \frac{1}{\rho_B A_{g\ell} H} \left\{ W_C (E_C - E_B) + W_{BP} (E_{BPE} - T_B) + U_g A_{g\ell} (T_g - T_B) \right.$$

$$\left. + U_\ell \left[A_{\ell m1} (T_{m1} - T_B) + A_{\ell m2} (T_{m2} - T_B) \right] \right\} \quad , \tag{3-27}$$

$$E_A = E_B \quad \cdot \tag{3-28}$$

The cover gas mass is determined by assuming that the temperature of the gas in the reservoir remains constant and its pressure equals that of the cover gas in the vessel at any instant. The cover gas mass is then given by

$$M_g(t) = \frac{M_t \, V_g(t) \, T_{res}}{V_{res} \, T_g(t) + V_g(t) \, T_{res}} \quad , \tag{3-29}$$

where

$$V_g(t) = [L - H(t)] A_{g\ell} \cdot$$

These equations, when coupled with the boundary conditions $[W_C(t),$ $W_{BP}(t), E_C(t), T_{BPI}(t)$ and $W_{ex}(t)]$, provide for a complete solution to the problem. The transient differential equations are solved by using the sub-routine DVOGER of IMSL.[3.3] The subroutine integrates a system of first-order ordinary differential equations according to Gear's method. Some of the results that were obtained in a parametric study are given elsewhere.[3.4]

It should be noted that a user can use either a two-zone mixing model, or, through appropriate option flags, a single-zone perfect mixing model.

3.1.2.3 Single-Phase Coolant Dynamics in the Core

The core region is subdivided into N6CHAN parallel channels. These channels represent either fuel, blanket, or control rods. In addition, an additional bypass channel is also included. At steady-state, there are two options that may be used to obtain the fraction of the total flow through these channels. The first option requires that the flow fraction be specified by the user through the parameters F_k and F_{BP}. These are given by the following equations:

$$F_k = \frac{W_k}{W_{total}} , \qquad 1 \leq k \leq N6CHAN , \qquad (3-30)$$

and

$$F_{BP} = \frac{W_{BP}}{W_{total}} \cdot \qquad (3-31)$$

In the second option, these flow fractions are calculated by assuming the same total pressure drop for each channel. Knowing the total pressure

drop and using an iterative procedure, the fraction of the total flow in each channel can be computed from the momentum equations. In either case, it is required that

$$\sum_{k=1}^{\text{N6CHAN}} F_k + F_{BP} = 1 \ . \tag{3-32}$$

Each of the flow channels is divided into a user-controlled number of axial slices. For the case of the single-phase sodium, the flow is assumed to be one-dimensional and incompressible. The axial distributions of coolant enthalpy and pressure in any of the channels are determined, respectively, by the following energy and momentum equations:

$$\frac{dE}{dZ} = \frac{1}{W_k} \frac{P_o F_{pk} F_{zk}(Z)}{L_k} \ , \tag{3-33}$$

$$\frac{dP}{dZ} = - g\rho - \frac{G_k |G_k| f_k}{2\rho \ D_{hk}} - G_k^2 \frac{d}{dZ} \left(\frac{1}{\rho} \right) \ , \tag{3-34}$$

where L_k is the fuel length based on which the normalized axial power distribution is constructed. Details of the power generation (P_o and F_{pk} terms) and the normalization of power distribution, $F_{zk}(Z)$, are discussed in Section 3.1.4. The sodium properties, $\rho(T)$ and $T(E)$, and the correlation for friction coefficient (f) are given in Chapter 5. Rewriting the above equations in finite-difference form, the enthalpy and pressure at any axial slice are computed by

$$E_{j+1} = E_j + \left(\frac{P_o F_{pk} F_{zk,j}}{W_k L_k} \right) \Delta Z_j \ , \tag{3-35}$$

$$P_{j+1} = P_j - \left[g\rho + \frac{f \, G_k |G_k|}{2\rho \, D_{hk}} \right]_j \Delta Z_j - G_k^2 \left[\frac{1}{\rho_{j+1}} - \frac{1}{\rho_j} \right] . \qquad (3\text{-}36)$$

In the case where a core inlet module is attached at the bottom of the active core (see Figure 3-3), the coolant flow is assumed to be isothermal; hence no energy equation is solved for this region. The momentum equation contains three additional loss coefficients as shown in Equation (3-37):

$$P_{j=1} = P_e - \sum_{n=1}^{3} \frac{K_n \, G_k \, G_k}{2\rho} - \left[g\rho + \frac{f_k \, G_k |G_k|}{2\rho \, D_{hk}} \right] \Delta L_k , \qquad (3\text{-}37)$$

where

K_1 = loss coefficient due to area expansion,

K_2 = loss coefficient due to area contraction,

K_3 = loss coefficient of inlet orifice.

The loss coefficients are input values provided by the user. The ΔL_k and D_{hk} are the length and hydraulic diameter of this section. On the top of the core, an additional loss coefficient k_4 is imposed in the core outlet module such that the computed pressure drop in each channel satisfies the overall force balance

$$P_d = P_{last \ slice} - \frac{k_4}{2\rho} G_k |G_k| - \Delta L_4 \, g\rho . \qquad (3\text{-}38)$$

By adjusting the value of k_4 or G_k according to the options discussed before, the calculated P_d can be made to agree with that determined from the upper plenum, since the pressure at d (see Figure 3-3) is given by

$$P_d = P_a + \rho g(Z_a - Z_d) . \qquad (3\text{-}39)$$

This additional loss factor k_4 will be retained in the computation of the

transient state.

The fraction of total coolant flow entering a channel, prior to the initiation of transients, is established by the design of orifice pattern. During transients, this fractional flow in a channel will be altered by the buoyancy effect. A model, therefore, for computation of the flow pattern inside the reactor core is developed in here. This flow redistribution is then used to compute the enthalpy change and the pressure drop in each of the flow channels.

Calculations of flow redistribution in the reactor vessel are based on the following momentum equation for one-dimensional and incompressible flow:

$$\frac{\partial}{\partial t}(W) + \frac{\partial}{\partial z}(W \cdot v) + A \frac{\partial p}{\partial z} + f \cdot \frac{\rho v^2}{2} \frac{A}{D_h} - g\rho \cos(g,W) = 0 . \quad (3\text{-}40)$$

In deriving the above equation, it was assumed that the control volume in the flow circuit satisfies

$$\frac{d \ln A}{dz} = 0 , \quad (3\text{-}41)$$

where W is the coolant flow rate (kg/s), v is the velocity (m/s), p is the pressure (N/m^2), A is the flow area (m^2), D_h is the hydraulic diameter (m), z is the vertical coordinate (m), and ρ is the fluid density (kg/m^3).

The Moody friction coefficient f is expressed in the form

$$f = c_1 (Re)^{-c_2} , \quad (3\text{-}42)$$

where c_1 and c_2 are constants determined by the flow regime.

The differential form of the momentum equation [(Equation 3-40)] can be applied for any of the parallel channels from the elevation e (bottom of the core) to the elevation d (top of the core) in Figure 3-3 by integrating

- 29 -

through different axial regions. We obtain

$$\left(p_e - p_d\right)_j = \left(\frac{L}{A}\right)_j \frac{dW_j}{dt} + \left(\frac{W}{A}\right)_j^2 \left(\frac{1}{\rho_d} - \frac{1}{\rho_e}\right)_j$$

$$+ W_j |W_j|^{c3} I_{f,j} + W_j |W_j| I_{k,j} - g I_{g,j} \quad , \quad (3-43)$$

where j denotes the j-th channel, and

$$\left(\frac{L}{A}\right)_j = \left(\frac{L}{A}\right)_{inlet} + \left(\frac{L}{A}\right)_{core} + \left(\frac{L}{A}\right)_{outlet} \quad , \quad (3-44)$$

$$I_{f,j} = \frac{c_1}{2} \left[\left(\frac{L\mu^{c_2}}{A^{c_5}D^{c_4}\rho}\right)_{inlet} + \frac{1}{A^{c_5}D^{c_4}} \int \frac{\mu^{c_2}}{\rho} dz \bigg|_{core} + \left(\frac{L\mu^{c_2}}{A^{c_5}D^{c_4}\rho}\right)_{outlet} \right], \quad (3-45)$$

$$I_{k,j} = \left[\sum_{i=1}^{4} \left(\frac{K}{2\rho A^2}\right)_i \right]_j \quad , \quad (3-46)$$

$$I_{g,j} = \cos(g, W_j) \left[(L\rho)_{inlet} + \int_{core} \rho dz + (L\rho)_{outlet} \right]_j \quad , \quad (3-47)$$

and

$$c_3 = 1 - c_2 \quad ,$$

$$c_4 = 1 + c_2 \quad ,$$

$$c_5 = 1 + c_3 \quad ,$$

In order to obtain a solution for a finite timestep Δt, the above equation is approximated by using the average values of time-dependent terms. Thus.

$$\left(\overline{p_e - p_d}\right)_j = \left(\frac{L}{A}\right)_j \frac{\Delta W_j}{\Delta t} + \overline{\left(\frac{W}{A}\right)_j^2} \left(\frac{1}{\bar{\rho}_4} - \frac{1}{\bar{\rho}_e}\right)_j$$

$$+ \overline{W_j |W_j| c_3} \cdot \overline{I_{f,j}} + \overline{W_j |W_j|} \cdot \overline{I_{k,j}} - \overline{g I_{g,j}} \quad , (3-48)$$

where $\overline{}$ indicates quantities evaluated at the average values of the density and viscosity as given by

$$\bar{\rho} = \frac{1}{2}\left[\rho(t+\Delta t) + \rho(t)\right], \qquad (3\text{-}49)$$

$$\bar{\mu} = \frac{1}{2}\left[\mu(t+\Delta t) + \mu(t)\right], \qquad (3\text{-}50)$$

Since the density and viscosity of the liquid sodium do not change rapidly with temperature, the values of $\rho(t+\Delta t)$ and $\mu(t+\Delta t)$ can be obtained by linear extrapolation of the coolant temperature from the previous timesteps. The mass flow terms are approximated by using the first-order Taylor series. For a time-dependent function $F(W)$, one has

$$F(W + \Delta W) \cong F(W) + \frac{dF(W)}{dW}\, dW, \qquad (3\text{-}51)$$

and

$$\bar{F} = \frac{1}{2}\left[F(W+\Delta W) + F(W)\right]. \qquad (3\text{-}52)$$

Hence,

$$\overline{W_j|W_j|} = W_j|W_j| + 2|W_j|\Delta W_j, \qquad (3\text{-}53)$$

and

$$\overline{W_j|W_j|^{c_3}} = W_j|W_j|^{c_3} + (c_3 + 1)|W_j|^{c_3}\Delta W_j. \qquad (3\text{-}54)$$

The final form of the integral equation which describes the pressure drop through the jth channel becomes

$$\overline{(P_e - P_d)}_j = \Delta W_j B_j - C_j, \qquad (3\text{-}55)$$

where

$$B_j = \left(\frac{L}{A}\right)_j \frac{1}{\Delta t} + \frac{W_j}{A_j^2}\left(\frac{1}{\bar{\rho}_d} - \frac{1}{\bar{\rho}_e}\right)_j + \frac{c_3 + 1}{2}|W_j|^{c_3}\,\bar{I}_{f,j} + |W_j|\,\bar{I}_{k,j}, \qquad (3\text{-}56)$$

$$C_j = \left(\frac{W_j}{A_j}\right)^2\left(\frac{1}{\bar{\rho}_d} - \frac{1}{\bar{\rho}_e}\right)_j + W_j|W_j|^{c_3}\,\bar{I}_{f,j} + W_j|W_j|\,\bar{I}_{k,j} - g\bar{I}_g. \qquad (3\text{-}57)$$

- 31 -

Similar equations can be obtained for the bypass flow channel.

The flow redistribution in various channels in the vessel is calculated from the pressure-drop equation by using two more assumptions:

1) No radial pressure variation in the lower and upper plena, i.e.,

$$\overline{P_c - P_b} = \Delta W_j B_j - C_j + g\rho_{\ell p}(z_e - z_c) + g\rho_{up}(z_b - z_d)$$

$$\text{for } j = 1,2, \ldots \text{ N6CHAN} \quad , \tag{3-58}$$

$$= \Delta W_{BP} B_{BP} - C_{BP} - g\rho_{BPM}(z_a - z_b) \; .$$

2) At any instant

$$\sum_{j=1}^{\text{N6CHAN}} W_j(t + \Delta t) + W_{BP}(t + \Delta t) = W_{vessel}(t + \Delta t) \quad , \tag{3-59}$$

or

$$\sum_{j=1}^{\text{N6CHAN}} \Delta W_j + \Delta W_{BP} = \Delta W_{vessel} \; , \tag{3-60}$$

where $W_{vessel} = W_{loop\ exit}$, the subscripts BP, ℓp, and up denote bypass flow channel, lower and upper plena, respectively. Equations (3-58) and (3-60) form a set of (N+1) equations with (N+1) unknowns (ΔW_{BP}, ΔW_j, j=1 ... N). These equations can be solved to obtain incremental flow rates. Knowing these flow increments, the new flow rate at t+Δt is given by

$$W(t + \Delta t)_j = W_j(t) + \Delta W_j \; . \tag{3-61}$$

Knowing the transient flow redistribution in core, the enthalpy rise and pressure drop in each channel can be computed by using the one-dimensional,

incompressible flow equations. The energy equation is

$$\frac{\partial(\rho E)}{\partial t} + \frac{\partial(GE)}{\partial z} = S_c q_c + S_s q_s + Q_g \quad , \tag{3-62}$$

where

$$q_c = \frac{T_{CL} - T}{\frac{1}{h} + \frac{\Delta r}{K_{CL}}} \quad , \tag{3-63}$$

$$q_s = \frac{T_s - T}{\frac{1}{h} + R_e} \quad , \tag{3-64}$$

$$Q_g = \text{transient heat generation per unit volume,} \tag{3-65}$$

$$R_e = \text{equivalent thermal resistance in structure,}$$

$$\Delta r = \text{half-thickness of clad.}$$

In finite-difference form, the coolant enthalpy at the (J+1)th node and the (K+1)th timestep is

$$E_{j+1}^{k+1} = \left[E_{j+1}^k (\rho_{j+1}^k - A_2) + E_j^{k+1}(- \rho_j^{k+1} + A_1) \right.$$

$$\left. + E_j^k(\rho_j^k + A_2) + 2\Delta t(S_c q_c + S_s q_s + Q_g) \right] \Big/ (\rho_{j+1}^{k+1} + A_1) \quad , \tag{3-66}$$

where

$$A_1 = \frac{\Delta t}{\Delta z} G^{k+1}, \quad A_2 = \frac{\Delta t}{\Delta z} G^k \quad .$$

The pressure drop is computed from the momentum equation,

$$\frac{\partial P}{\partial z} = - \frac{dG}{dt} - G^2 \frac{\partial}{\partial z}\left(\frac{1}{\rho}\right) - \frac{f}{2} \frac{G|G|}{\rho D_h} + g\rho \cos(g,w), \tag{3-67}$$

or, at the (K+1)th timestep,

$$P_{j+1} = P_j - \frac{\Delta z}{\Delta t}\left[(G^{k+1} - G^k) - (G^{k+1})^2\left(\frac{1}{\rho_{j+1}} - \frac{1}{\rho_j}\right)\right.$$

$$\left. - \frac{\Delta z}{4D_h} G^{k+1} |G^{k+1}| \left[\left(\frac{f}{\rho}\right)_{j+1} + \left(\frac{f}{\rho}\right)_j\right] + \frac{\Delta z}{2}[\rho_{j+1} + \rho_j]g \cos(g,w) \quad , \right.$$

$$\tag{3-68}$$

where

$$\cos(g,w) = -1 \quad \text{for upward flow,}$$

$$= 1 \quad \text{for downward flow.}$$

3.1.2.4 Fission Gas Bubble and Sodium Boiling in the Core

Fission gas release and sodium boiling have been treated by Chawla et al.[3.5] and Cronenberg et al.,[3.6] respectively, and similar models have been employed in accident analysis codes such as SAS2A.[3.7] The model of Chawla et al. for fission gas release is considered to be quite adequate for present use. In a review article on sodium boiling written for SSC-L, Tanaka[3.8] recommends the SAS2A slug-annular flow model for present use, except that, under the conditions of reactor scram, a single-bubble (rather than multi-bubble) treatment is considered to be adequate.

Since the temperature in the reactor core can get quite high under accident conditions, both fission gas release and sodium boiling can occur simultaneously. Therefore, a unified model for a bubble containing both fission gas and sodium vapor is developed. For fission gas release alone, the model reduces to one similar to that of Chawla et al.[3.5] For boiling alone, the model reduces to one similar to that in SAS2A[3.7]; the major difference is that the pressure in the bubble is taken to be uniform in the present work.

The configuration for fission gas release and sodium boiling is illustrated in Figure 3-5. Sodium boiling occurs in the channel forming sodium vapor. Fission gas flows from the gas plenum, through the gap impedance and the rupture, and into the channel. Thus, the bubble may contain sodium vapor and fission gas. Some condensed droplets may also be formed as the vapor is
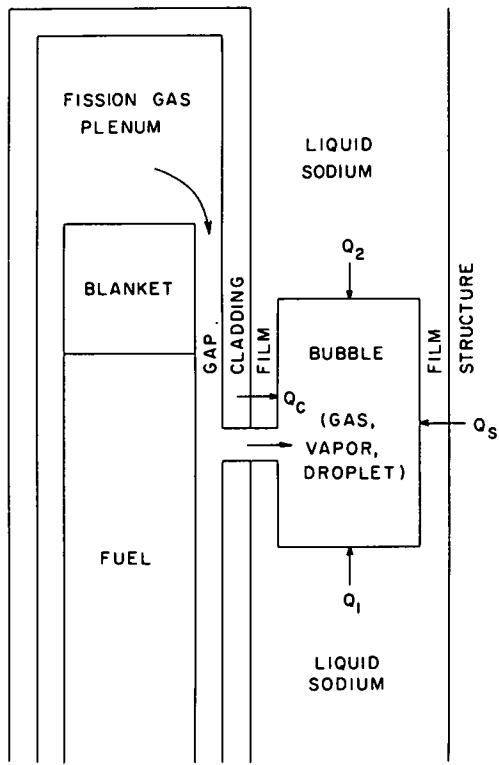
Figure 3-5. A configuration for fission gas release
and sodium boiling model.

mixed with the cooler gas. A primary safety concern is that if the liquid film left on the cladding surface is completely vaporized, the cladding temperature may become so high that melting of the cladding might occur.

The fission gas bubble is considered to be initiated when cladding ruptures. Cladding is assumed to rupture when the gas plenum pressure exceeds the cladding hoop strength. The sodium vapor bubble is considered to be initiated when the temperature of the liquid sodium exceeds the saturation temperature by a specified degree of superheat.

The following assumptions are made:

(1) The bubble fills the entire cross section of the channel except for the liquid films left on the walls of the cladding and structure.

(2) The pressure and temperature are uniform in a bubble.

(3) In a gas bubble, vaporization of the liquid film is initiated when the boiling point corresponding to the bubble is reached.

(4) In a vapor bubble, the vapor remains saturated when gas is introduced.

(5) The saturated vapor undergoes dropwise condensation upon mixing with a cooler gas.

(6) The gas, vapor, and droplet in the bubble are in thermal equilibrium.

(7) The flow of fission gas through the gap impedance is quasi-steady and isothermal.

(8) The liquid film is static and its initial thickness is specified.

Although the bubble is considered to have uniform properties, the liquid film thickness is considered to vary locally. The local vaporization or condensation of the film depends on the local heat transfer from cladding and structure. The motion of each liquid slug (below and above the bubble) is described by the single-mass velocity approximation.[3.9]

The conservation equations for the bubble are

$$\frac{dM_g}{dt} = A_i \, P_p \left[\frac{1 - \beta^2}{2R_g \, T_p \, (F - \ell n\beta)} \right]^{\frac{1}{2}} \qquad \text{for subcritical flow,} \qquad (3\text{-}69a)$$

$$= A_i \, P_p \, \frac{\beta^*}{(R_g \, T_p)^{\frac{1}{2}}} \qquad \text{for critical flow,} \qquad (3\text{-}69b)$$

$$\frac{dM_v}{dt} = \frac{Q}{\lambda} \, , \qquad (3\text{-}70)$$

$$\frac{dM_d}{dt} = \frac{E_g - E_{gp}}{\lambda} \, \frac{dM_g}{dt} + D_e , \qquad (3\text{-}71)$$

$$\frac{d}{dt} (M_g E_g + M_v E_v + M_d E_d) - V_b \frac{dp_b}{dt} = Q + H \, , \qquad (3\text{-}72)$$

where M_g, M_v, and M_d refer to the mass of fission gas, vapor, and droplet, respectively, in the bubble; E_g, E_v, and E_d are the corresponding enthalpies; H is the enthalpy addition rate and D_e is the entrainment rate. All enthalpies are functions of temperature T, and $E_v - E_d = \lambda$ where λ is the heat of vaporization. The V_b and p_b denote volume and pressure of the bubble, respectively, and t denotes time.

In Equations (3-69a) and (3-69b), which describe the quasi-steady iso-thermal flow of fission gas through the gap impedance, A_i denotes the cross-sectional area of the impedance, R_g is the gas plenum, respectively. The pressure ratio β, critical pressure β^*, and resistance factor K are defined by $B = p_b/p_p$, $\beta^{*2} (2K - 2\ell n\beta^* + 1) = 1$, and $K = 2f_i L_i / D_i$, respectively, where f_i, L_i, and D_i are the friction factor, length, and hydraulic diameter, respectively, of the impedance. Subcritical flow occurs when $\beta > \beta^*$ and critical

flow occurs when $\beta \leq \beta^*$.

In Equation (3-70), the mass of vapor at saturation is $M_{vs} = \rho_{vs} V_b$, where the subscript s denotes saturation and ρ_v is vapor density. If the vapor is not saturated, it is taken that the vaporization rate is given by the net rate Q divided by the heat of vaporization.

In Equation (3-71), the droplet condensation rate is related to the heat extraction from a saturated vapor by a cooler fission gas, with E_{gp} denoting plenum gas enthalpy, and it is not considered for an unsaturated vapor. An empirical term, D_e, which is presently unavailable, may be applied to account for droplet entrainment.

In Equation (3-72), the net rate Q and enthalpy addition rate H are given by

$$Q = Q_c + Q_s + Q_1 + Q_2 , \qquad (3-73)$$

$$H = E_{gp} \frac{dM_g}{dt} + E_{\ell i} \frac{dM_{vi}}{dt} - E_{\ell o} \frac{dM_{vo}}{dt} \qquad (3-74)$$

where the subscripts c, s, 1, and 2 appearing in the heat rates refer to cladding, structure, lower liquid slug, and upper liquid slug, respectively (see Figure 3-5). The mass of liquid vaporizing or being entrained into the bubble, M_{vi}, has enthalpy $E_{\ell i}$, and the mass of liquid condensing on the surface, M_{vo}, has enthalpy $E_{\ell o}$.

The heat rates are taken as

$$Q_c = \int_{x_1}^{x_2} \frac{d_c}{R_c} (T_c - T_b) \, dx , \qquad (3-75)$$

$$Q_s = \int_{X_1}^{X_2} \frac{d_s}{R_s} (T_s - T_b) \, dx \quad , \tag{3-76}$$

$$Q_1 = k_{\ell 1} A_\ell \frac{T_{\ell 1} - T_b}{\delta_{\ell 1}} \quad , \tag{3-77}$$

$$Q_2 = k_{\ell 2} A_\ell \frac{T_{\ell 1} - T_b}{\delta_{\ell 2}} \tag{3-78}$$

where d, R, x, k, A, and δ refer to perimeter, resistance, distance from bubble initiation point, conductivity, cross-sectional area, and effective thermal boundary layer thickness between bubble surface and liquid slug, respectively. The subscripts ℓ and b refer to liquid slug and bubble, respectively. The cross-sectional area of the bubble is approximated by the liquid or channel cross-sectional area A_ℓ.

The resistance on the cladding side is given by

$$R_c = \frac{1}{h_c} + \frac{\Delta r_c}{2k_c} + R_{bc} \quad , \tag{3-79}$$

where Δr_c is the cladding thickness (T_c is evaluated at midpoint of cladding), k_c is cladding conductivity, and h_c is an effective convection coefficient. It is taken that $h_c = k_{\ell c}/w_{fc}$, where w_f is the film thickness. The resistance in the bubble, R_b, depends on whether the surface is vaporizing or condensing. If the cladding surface is assumed to have the same temperature as the bubble (zero vapor resistance), then $R_{bc} = 0$. The resistance on the structure side is given by an equation similar to Equation (3-79), except the subscript c is replaced by s. In the simple approximation of Q_1 and Q_2, as presently employed and given by Equations (3-77) and (3-78), the thermal boundary layer thickness is represented by $\delta_\ell = (\alpha_\ell t)^{\frac{1}{2}}$, where α denotes a thermal diffusivity.

The pressures and bubble volume are given by

$$P_p = (M_{gpo} - M_g) R_g T_p / V_p \quad , \tag{3-80}$$

$$P_b = P_g + P_v \quad , \tag{3-81}$$

$$P_g = M_g R_g T_b / V_b \quad , \tag{3-82}$$

$$P_v = (\rho_v / \rho_{vs}) P_{vs} \quad , \tag{3-83}$$

$$V_b = A_\ell (x_2 - x_1) \quad , $$

where M_{gpo} refers to the initial mass of gas in the gas plenum, V_p is plenum volume, and $x_2 - x_1$ is the length of the bubble.

For the liquid slug above the bubble, the governing equations are

$$\frac{dx_2}{dt} = \frac{G_{\ell 2}}{\rho_{\ell b}} \quad , \tag{3-84}$$

$$\frac{dG_{\ell 2}}{dt} = \frac{P_b - P_t - k_{\ell 2}}{L_2} \quad , \tag{3-85}$$

$$\rho_\ell c_\ell \frac{DT_\ell}{Dt} = Q_h + Q_g \quad , \tag{3-86}$$

where $\rho_{\ell b}$ is the liquid density at liquid-bubble interface, the subscript t denotes the top of the liquid slug, and L_2 is the length of the slug. The channel resistance $k_{\ell 2}$ is given by

$$K_{\ell 2} = G_{\ell 2}^2 \left(\frac{1}{\rho_{\ell t}} - \frac{1}{\rho_{\ell b}} \right) + g \int_{L_2} \rho_\ell \, dx + \frac{G_{\ell 2} |G_{\ell 2}|}{2} \int_{L_2} \frac{f}{\rho_\ell D_h} \, dx + \Delta P_{end} \quad , \tag{3-87}$$

where $\rho_{\ell t}$ is the liquid density at the top of the liquid slug, g is the gravitational constant, x is distance along the channel, f denotes friction factor,

D_h is the channel hydraulic diameter, and Δp_{end} accounts for expansion or contraction pressure drop at the end of the channel.

In using Equation (3-84), the effect of mass transfer on the interface velocity has been neglected. Equation (3-86) governs the local liquid temperature and is used in Lagrangian coordinate. The Q_h and Q_g denote convective and direct heating, respectively. The ρ_ℓ is considered to be a function of E_ℓ (or T_ℓ) only.

The governing equations for the liquid slug below the bubble are similar to Equations (3-84) to (3-87), except that subscript 2 is replaced by subscript 1; $p_b - p_t$ in Equation (3-85) is replaced by $p_m - p_b$, where subscript m denotes the bottom of liquid slug; and $(\rho_{\ell t}^{-1} - \rho_{\ell b}^{-1})$ in Equation (3-87) is replaced by $(\rho_{\ell b}^{-1} - \rho_{\ell m}^{-1})$, where $\rho_{\ell m}$ is the liquid density at the bottom of the slug.

For the liquid films on the cladding and structure walls, the local thickness, w_f, is given by

$$\frac{dw_f}{dt} = - \frac{q}{\rho_\ell \lambda} \quad , \tag{3-88}$$

where q denotes the local heat flux.

The Lagrangian calculations for liquid temperatures at fixed axial mesh points are then

$$T_\ell(z, t + \Delta t) = \frac{T_c (z - \Delta z, t)(1 - d \, \overline{h}_1) + d [\varphi + (2\overline{Q}_g/S_c)]}{1 + d \, h_2} \quad , \tag{3-89}$$

where z is the axial distance from inlet of channel, and Δz is the distance traveled by a liquid particle during Δt and is given by

$$\Delta z = \frac{1}{2\overline{\rho}_\ell} \left[G_\ell (t + \Delta t) + G_\ell (t) \right] \Delta t \quad . \tag{3-90}$$

The d, h_1, h_2 and φ are given by

$$d = \frac{S_c \Delta t}{2 \bar{\rho}_\ell \bar{c}_\ell} \quad , \tag{3-91}$$

$$h_1 = \frac{1}{R_c(Z,t)} + \frac{S_s}{R_s(Z,t)} \quad , \tag{3-92}$$

$$h_2(Z) = \frac{1}{R_c(Z,t + \Delta t)} + \frac{S_s}{R_s(Z,t + \Delta t)} \quad , \tag{3-93}$$

$$\varphi = \frac{T_c(Z,t + \Delta t)}{R_c(Z,t + \Delta t)} + \frac{T_c(Z - \Delta Z,t)}{R_c(Z,t)} + S_s \left[\frac{T_s(Z,t + \Delta t)}{R_s(Z,t + \Delta t)} + \frac{T_s(Z - \Delta Z,t)}{R_s(Z,t)} \right] \quad , \tag{3-94}$$

$$S_c = \frac{\text{surface area of cladding}}{\text{volume of coolant}} \quad , $$

$$\tag{3-95}$$

$$S_s = \frac{\text{surface area of structure}}{\text{surface area of cladding}} \quad , $$

$$\bar{\rho}_\ell = \rho \left[T_\ell(Z,t + \Delta t/2) \right] \quad , $$

$$\tag{3-96}$$

$$\bar{c}_\ell = c_\ell \left[T_\ell(Z,t + \Delta t/2) \right] \quad . $$

For the interface:

$$T_{interf}(t + \Delta t) = \frac{T_{interf}(t)(1 - ah_1) + a\phi}{(1 + ah_2)} \quad , \tag{3-97}$$

where

$$a = \frac{S_c}{2} \frac{t}{\rho_\ell c_\ell} \quad , $$

$$h_1 = \frac{1}{R_c(t)} + \frac{S_s}{R_{st}(t)} \quad , \tag{3-98}$$

$$h_2 = \frac{1}{R_c(t + \Delta t)} + \frac{S_s}{R_{st}(t + \Delta t)} \quad , \tag{3-99}$$

$$\phi = \frac{T_c(t + \Delta t)}{R_c(t + \Delta t)} + \frac{T_c(t)}{R_c(t)} + S_s \left[\frac{T_{st}(t + \Delta t)}{R_{st}(t + \Delta t)} + \frac{T_{st}(t)}{R_{st}(t)} \right] \quad , \tag{3-100}$$

$$\bar{\rho}_\ell = \rho \left[T_\ell(t + \frac{\Delta t}{2}) \right] \quad , \tag{3-101}$$

$$\bar{c}_\ell = c \left[T_\ell(t + \frac{\Delta t}{2}) \right] \quad . \tag{3-102}$$

3.1.2.5 Bypass Flow Channel

A bypass channel to represent coolant flow between the barrel and reactor vessel wall is included. The bypass channel is divided into two axial sections as shown in Figure 3-6. The lower section is adjacent to the active core region, and the upper section is separated from the outlet plenum by the thermal liner. The lower section is allowed to have heat generation due to gamma heating.

The momentum and energy equations of the bypass flow are treated in a manner similar to that of the core flow. Two loss coefficients (K_1 and K_2) are incorporated in the momentum equation such that the overall pressure drop through the channel can be balanced. At steady-state, the total pressure drop is given by

$$\Delta P = g \left[(\rho L)_1 + (\rho L)_2 \right] + \frac{W^2}{2} \left[\left(\frac{f L}{\rho D_h A^2} \right)_1 + \left(\frac{f L}{\bar{\rho} D_h A^2} \right)_2 \right]$$
$$+ W^2 \left[\Delta \left(\frac{1}{\rho A^2} \right)_1 + \Delta \left(\frac{1}{\rho A^2} \right)_2 \right] + \frac{W^2}{2} \left[\left(\frac{K}{\rho A^2} \right)_1 + \left(\frac{K}{\rho A^2} \right)_2 \right] \quad . \tag{3-103}$$

HEAT
TRANSFER
FROM
PLENUM

GAMMA
HEATING
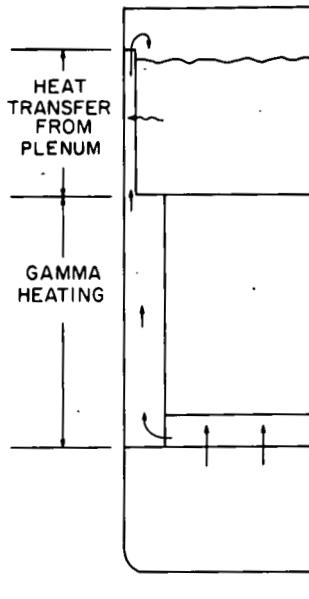
Figure 3-6. Modeling of the bypass flow.

In Equation (3-103), the subscripts 1 and 2 denote the lower and upper section, respectively. The loss coefficient k_1 is an input parameter, and k_2 is the computed value to establish the force balance at steady-state.

During transients the total pressure drop in the bypass channel is determined by the one-dimensional momentum equation:

$$\Delta P = \frac{\Delta W}{\Delta t}\left[\left(\frac{L}{A}\right)_1 + \left(\frac{L}{A}\right)_2\right] + W^2\left[\Delta\left(\frac{1}{\rho A^2}\right)_1 + \Delta\left(\frac{1}{\rho A^2}\right)_2\right]$$

$$+ \frac{W|W|}{2}\left[\left(\frac{fL}{A^2\rho D_h}\right)_1 + \left(\frac{fL}{A^2\rho D_h}\right)_2\right] + g\left[(\rho L)_1 + (\rho L)_2\right] \qquad (3\text{-}104)$$

$$+ \frac{W|W|}{2}\left[\left(\frac{K}{\rho A^2}\right)_1 + \left(\frac{K}{\rho A^2}\right)_2\right] \; .$$

Fluid enthalpy at the exit of the lower sections is computed from the following equation:

$$\frac{\partial}{\partial t}(\rho E) = \frac{P_o \cdot F_{PBP} \cdot P(t)}{AL} - \frac{1}{A}\frac{\partial}{\partial z}(EW) \; , \qquad (3\text{-}105)$$

where A, L, F_{PBP} are the cross-sectional area, height, and fraction of power generation (at steady-state) of the lower section, respectively. In finite difference form, this equation becomes

$$E_{out}^{k+1} = \left[E_{in}^k (1 + A_3 W^k) + E_{out}^k (1 - A_3 W^k)\right.$$

$$\left. - E_{in}^{k+1} (1 - A_3 W^{k+1}) + 2 P_o F_{PBP} P(t) \cdot A_3\right] / (1 + A_3 W^{k+1}),$$

$$(3\text{-}106)$$

where

$$A_3 = \frac{\Delta t}{A L \rho} \quad \text{and} \quad \bar{\rho} = \frac{1}{2} (\rho_{in}^{k} + \rho_{out}^{k}) \ .$$

The computed E_{out}^{k+1} is the inlet enthalpy for computing the enthalpy rise in the upper section of the bypass channel. In the upper section, no internal heat generation is assumed, but heat transfer through the thermal liner is considered as discussed in Section 3.1.2.2. Calculation of enthalpy rise in the upper section is part of the upper plenum mixing model.

3.1.2.6 Computational Procedure

At steady-state, the coolant dynamics and the fuel heat transfer are uncoupled. The coolant temperature and the convective heat transfer coefficient are determined first. These are then used as boundary conditions for the fuel heat transfer calculations. The computational procedure is shown in Figure 3-7.

The coolant temperature and the heat transfer calculations during transients are coupled. In the SSC-L code, these calculations were decoupled either by extrapolating or interpolating boundary conditions. This decoupling was done for the sake of computing efficiency. The actual time-step sizes used by the fuel heat transfer and the coolant dynamics modules are, in general, different as discussed in Chapter 4.

Figure 3-8 shows the procedure of transient coolant computation. There are four major regions in the vessel: lower plenum, core, bypass channel, and upper plenum. Since the core is the most important region of the vessel, its lower and upper boundary conditions are not extrapolated from previous
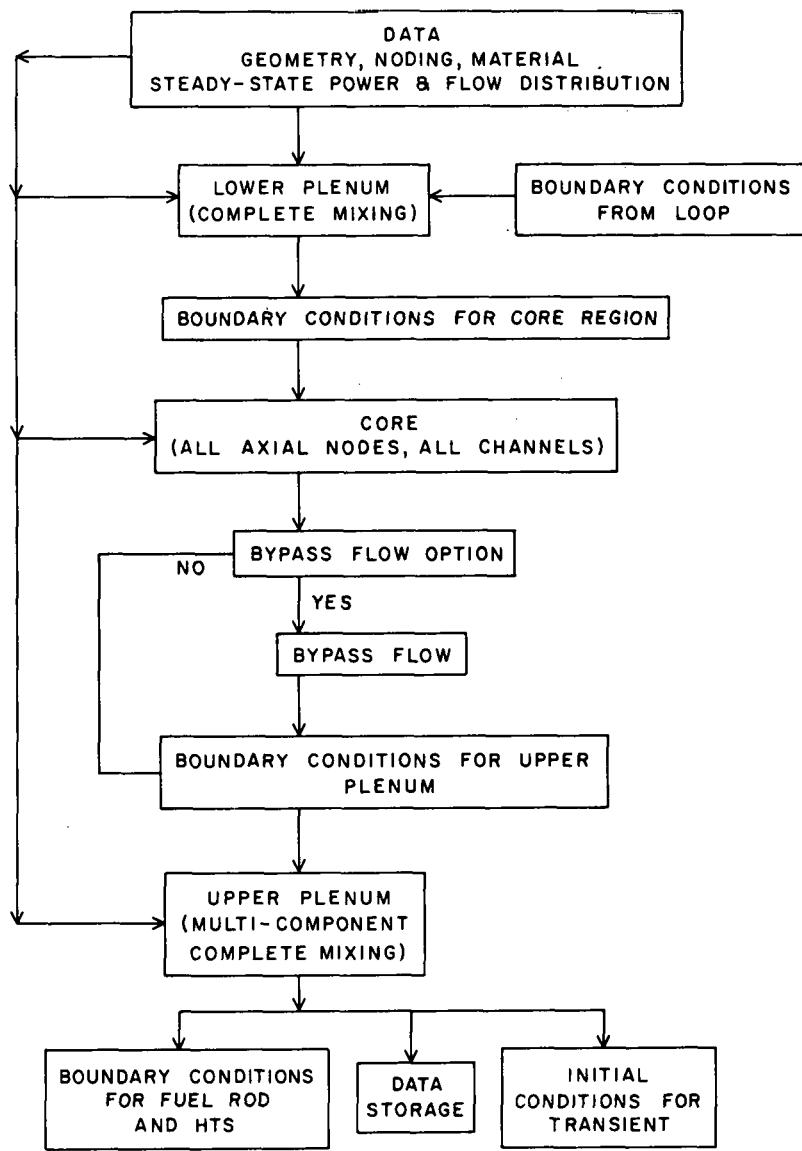
Figure 3-7.   Computational logic for coolant dynamics
at steady state.
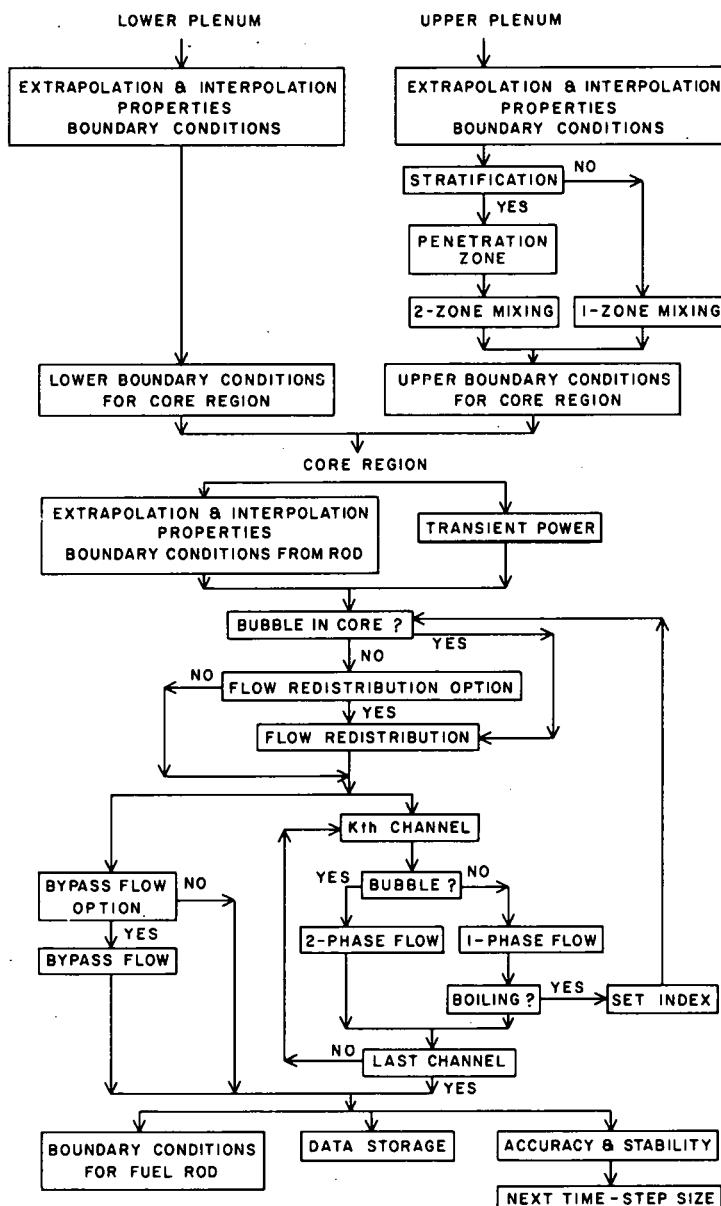
Figure 3-8. Computational logic for the transient
coolant dynamics.

times. The boundary conditions are provided by the lower and upper plena, which are computed in advance, as illustrated in this figure.

3.1.3 Heat Transfer in Fuel Rod and Structure

A general form of fuel rod and its associated coolant and structure are shown in Figure 3-9. The rod is composed of up to five axial regions: lower plenum, lower blanket, active fuel, upper blanket, upper plenum. One or more of these regions may be omitted at the user's request, but the sequence will be maintained. Both fuel and blanket are divided into slices in the axial direction and into concentric rings in the radial direction. The analysis of a blanket is similar to that of a fuel. The geometry, physical properties, and steady-state operating conditions are substituted accordingly.

3.1.3.1 Thermal Expansion, Restructuring and Gap Conductance

The radial nodes are shown in Figure 3-10, in which NF is the number of radial nodes in fuel and is user's input. Only three radial nodes are allowed in the cladding. The radial nodes are determined at the initial reference temperature by either the equal radial increment or the equal area method. The dimensions of the radial nodes are modified by considering thermal expansion at steady-state. Knowing the fuel and cladding size at a reference temperature (usually, the as-fabricated dimensions at room temperature), the inside radius of each radial ring is

$$R_1 = R_{Fi} \quad , \tag{3-107}$$

$$R_2 = R + \frac{1}{2} \Delta R_F \quad , \tag{3-108}$$

$$R_{i+1} = R_i + \Delta R_F \quad \text{for } 2 \le i \le (NF-1), \tag{3-109}$$

and

$$R_{ci+1} = R_{ci} + \frac{1}{2} \Delta R_c \quad , \tag{3-110}$$

$$R_{co} = R_{ci+1} + \Delta R_c \quad , \tag{3-111}$$
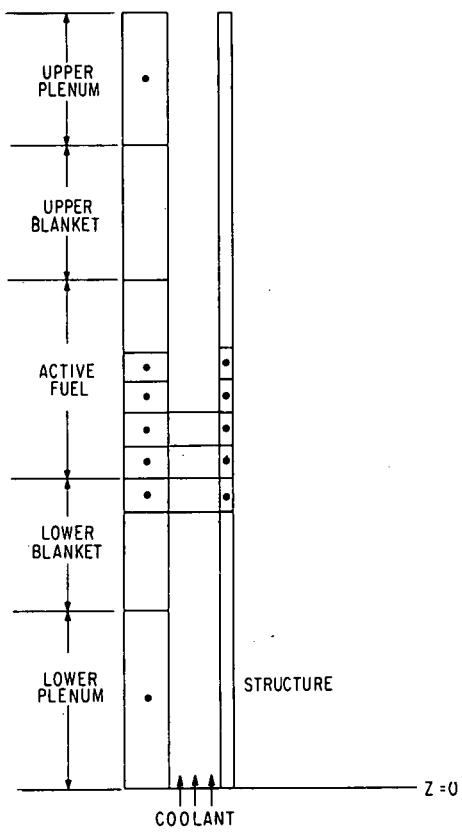
Figure 3-9. Axial noding in a generalized fuel rod.

where, for equal radial increment:

$$\Delta R_F = \frac{R_{Fo} - R_{Fi}}{NF - 1} \quad , \tag{3-112}$$

and

$$\Delta R_c = \frac{R_{co} - R_{ci}}{2} \quad , \tag{3-113}$$

If the nodes are divided on the basis of equal area, then the radial increments are

$$\Delta R_f = \left[\frac{R_{Fo}^2 - R_{Fi}^2}{NF - 1}\right]^{1/2} \tag{3-114}$$

and

$$\Delta R_c = \left[\frac{R_{co}^2 - R_{ci}^2}{2}\right]^{1/2} \quad . \tag{3-115}$$

The inside radius of each radial ring becomes

$$R_1 = R_{Fi} \quad , \tag{3-116}$$

$$R_2 = \left[R_1^2 + \frac{1}{2} \Delta R_F^2\right]^{1/2} \quad , \tag{3-117}$$

$$R_{i+1} = \left[R_i^2 + R_F^2\right]^{1/2} \qquad \text{for } 2 \leq i \leq (NF-1) \quad , \tag{3-118}$$

and

$$R_{ci+1} = \left[R_{ci}^2 + \frac{1}{2} \Delta R_c^2\right]^{1/2} \quad , \tag{3-119}$$

$$R_{co} = \left[R_{ci+1}^2 + \Delta R_c^2\right]^{1/2} \quad . \tag{3-120}$$

Correction due to thermal expansion for any radial node is

$$\Delta R_i = \Delta R_{ref} \left[1 + \alpha\left(T_i - T_{ref}\right)\right] \quad . \tag{3-121}$$

The restructuring of the fuel is calculated for each axial slice for the steady-state condition only. The fuel density is considered to be initially uniform throughout the pellet and is equal to the as-fabricated value. Grain growth is assumed to divide the fuel into three regions. The

characterization of these regions is indicated in Table 3-1. The reference temperatures T_{EG} and T_{CG} are specified by the user. The final radius of the central void is determined by taking the mass balance of fuel in each slice:

$$R_{Fi,s} = \left[R_{EG}^2 + \frac{\rho_2}{\rho_3} \left(R_{UN}^2 - R_{EG}^2 \right) + \frac{\rho_1}{\rho_3} \left(R_{Fi}^2 - R_{UN}^2 \right) \right]^{\frac{1}{2}} , \qquad (3-122)$$

where R_{Fi} is the initial radius of central void of fuel as-fabricated, R_{EG} is the first node in Region II (equiaxed region), and R_{UN} is the first node in Region I (unrestructured region).

The gap between fuel and cladding is calculated explicitly:

$$\Delta R_{gap} = R_{ci,ref} \left[1 + \alpha_c \left(T_{ci} - T_{ref} \right) \right] - R_{Fo,ref} \left[1 + \alpha_F \left(T_{Fo} - T_{ref} \right) \right]. (3-123)$$

It is also required that $\Delta R_{gap} = 0$ if Equation (3-123) indicated that ΔR_{gap} is negative.

The radial gap is used to calculate the gap conductance which is an important parameter for fuel temperature calculation. The gap conductance is computed for two cases: finite gap size and the closed gap. When the gap is closed, a direct input of the contact conductance to the code is required.

For the case of finite gap, heat is transported across the gap by

1) conduction through a mixture of fill gas and fission gases (xenon and krypton),

2) thermal radiation between the outside surface of fuel and the inside surface of cladding,

3) free convection of the gases in the gap.

Heat transfer via free convection in the gap is negligible and hence will not

Table 3-1

Characterization of Fuel Regions in a Fuel Rod

Region	Temperature	Density	Power Generation per unit volume	Thermal Conductivity
I. Unrestructured	$T < T_{EG}$	ρ_1 (as fabricated)	$Q_I = Q_0$	$k = k(\rho_1, T)$
II. Equiaxed Grain Growth	$T_{EG} \leq T < T_{CG}$	ρ_2 $(\rho_2 > \rho_1)$	$Q_{II} = \dfrac{\rho_2}{\rho_1} Q_0$	$k = k(\rho_2, T)$
III. Columnar Grain Growth	$T \geq T_{CG}$	ρ_3 $(\rho_3 > \rho_2)$	$Q_{III} = \dfrac{\rho_3}{\rho_1} Q_0$	$k = k(\rho_3, T)$

be considered in the model.

The heat flux per unit length at the outside surface of fuel is

$$q = 2\pi\, R_{Fo} \left[k_{mix}\, \frac{T_{Fo} - T_{ci}}{\Delta R_{gap}} + \bar{\varepsilon}\sigma\left(T_{Fo}^{\,4} - T_{ci}^{\,4}\right) \right] . \qquad (3\text{-}124)$$

Equation (3-124) can be rewritten as

$$q = 2\pi\, R_{Fo} \left(T_{Fo} - T_{ci}\right)\left(h_{cond} + h_{rad}\right) , \qquad (3\text{-}125)$$

where the gap conductance, h_{cond}, is given by

$$h_{cond} = k_{mix}/\Delta R_{gap}, \qquad (3\text{-}126)$$

and the radiative heat transfer coefficient is written as

$$h_{rad} = \bar{\varepsilon}\,\sigma\, T_{Fo}^{\,3} + \left(T_{Fo}^{\,2}\, T_{ci} + T_{ci}^{\,2}\, T_{Fo} + T_{ci}^{\,3}\right) , \qquad (3\text{-}127)$$

where

$$\bar{\varepsilon} = \left[\frac{1}{\varepsilon_{Fo}} + \frac{R_{Fo}}{R_{ci}}\left(\frac{1}{\varepsilon_{ci}} - 1\right)\right]^{-1} . \qquad (3\text{-}128)$$

The above radiation heat transfer coefficient is defined to eliminate the non-linearity of the equation. It is considered as a temperature-dependent property and is calculated explicitly. There are several correlations to calculate the thermal conductivity of a mixture of monatomic gased. A simple empirical equation was given by Brokaw:[3.10]

$$k_{mix} = 0.5\left[\sum_{i=1}^{N} x_i\, k_i + \frac{1}{\displaystyle\sum_{i=1}^{N} x_i/k_i}\right] . \qquad (3\text{-}129)$$

The mole fractions of the gases, (X_i) are determined from models of fission gas release and are supplied as input by the user.

3.1.3.2 Fuel Rod Radial Temperature Calculation

The radial heat transfer in fuel and blanket at the j-th axial node at steady-state (see Figure 3-10) is given by

node 1:
$$2R_2 k \left(\overline{T}_{1,2}\right) \frac{dT}{dr}\Big|_{R_2} + Q_1 \left(R_1^{\,2} - R_2^{\,2}\right) = 0 \quad ; \qquad (3\text{-}130)$$

node i:
$$-k \left(\overline{T}_{i-1,i}\right) \frac{dT}{dr}\Big|_{R_i} 2R_i + k\left(\overline{T}_{i,i+1}\right) \frac{dT}{dr}\Big|_{R_{i+1}} 2R_{i+1} + Q_i\left(R_{i+1}^{\,2} - R_i^{\,2}\right) = 0$$
$$2 \leq i \leq NF\text{-}1 \quad ; \qquad (3\text{-}131)$$

node NF:
$$-k \left(\overline{T}_{NF-1,NF}\right) \frac{dT}{dr}\Big|_{NF} 2R_{NF} - 2R_{Fo} h_{cond} \left(T_{NF} - T_{ci}\right) - 2R_{Fo}\,\overline{\varepsilon}\,\sigma \left(T_{NF}^{\,4} - T_{ci}^{\,4}\right)$$
$$+ Q_{NF} \left(R_{Fo}^{\,2} - R_{NF}^{\,2}\right) = 0 \quad ; \qquad (3\text{-}132)$$

node ci (cladding inside surface):
$$2R_{Fo} h_{cond} \left(T_{NF} - T_{ci}\right) + 2R_{Fo}\,\varepsilon\,\sigma \left(T_{NF}^{\,4} - T_{ci}^{\,4}\right) + 2R_{ci+1}\,k \left(\overline{T}_{ci,ci+1}\right) \frac{dT}{dr}\Big|_{ci+1}$$
$$+ Q_{ci} \left(R_{ci+1}^{\,2} - R_{ci}^{\,2}\right) = 0 \quad ; \qquad (3\text{-}133)$$

node ci+1 (cladding midplane):
$$-k \left(\overline{T}_{ci,ci+1}\right) \frac{dT}{dr}\Big|_{R_{ci+1}} 2R_{ci+1} + k \left(\overline{T}_{ci+1,ci+2}\right) \frac{dT}{dr}\Big|_{ci+2} 2R_{ci+2}$$
$$+ Q_{ci+1} \left(R_{ci+2}^{\,2} - R_{ci+1}^{\,2}\right) = 0 \quad ; \qquad (3\text{-}134)$$

node ci+2 (cladding outside surface):

$$- 2R_{ci+2}\, k \left(\overline{T}_{ci+1,ci+2}\right) \frac{dT}{dr}\,\Big|_{ci+2} - 2R_{co}\, h_c \left(T_{ci+2} - T_c\right) + Q_{co}\left(R_{co}^{\ 2} - R_{ci+2}^{\ 2}\right) = 0 \ .$$

$$(3\text{-}135)$$

The above equations are expressed in finite difference form which results in a set of simultaneous nonlinear algebraic equations. These equations form a tridiagonal matrix and are solved by using the Gauss eliminations procedure. The final equations are, at a given Z_j,

$$T_i = T_{i+1} + \frac{1}{\beta_{i+1}} \sum_{j=1}^{i} \psi_j \ , \tag{3-136}$$

and

$$T_{ci+3} = T_{coolant} \ , \tag{3-137}$$

where

$$\beta_1 = 0 \ , \tag{3-138}$$

$$\beta_2 = \frac{k \left(\overline{T}_{1,2}\right) R_2}{R_3 + R_2 - 2R_1} \ , \tag{3-139}$$

$$\beta_i = \frac{k \left(\overline{T}_{i-1,i}\right) R_1}{R_{i+1} - R_{i-1}} \qquad \text{for } 3 \le i \le (NF\text{-}1) \tag{3-140}$$

$$\beta_{NF} = \frac{k \left(\overline{T}_{NF-1,NF}\right) R_{NF}}{2R_{Fo} - R_{NF} - R_{NF-1}} \ , \tag{3-141}$$

$$\beta_{ci} = \beta_{cond} + \beta_{rad} \ , \tag{3-142}$$

$$\beta_{ci+1} = \frac{k\,\overline{T}_{ci,ci+1}\,R_{ci+1}}{R_{ci+2} + R_{ci+1} - 2R_{ci}} \ , \tag{3-143}$$

$$\beta_{ci+2} = \frac{k\left(\overline{T}_{ci+1,ci+2}\right) R_{ci+2}}{2R_{co} - R_{ci+2} - R_{ci+1}} \quad , \tag{3-144}$$

$$\beta_{ci+3} = \beta_{conv} \quad , \tag{3-145}$$

$$\beta_{rad} = \frac{R_{Fo}}{2} \, \overline{\varepsilon} \, \sigma \left(T_{NF}^3 + T_{NF}^2 T_{ci} + T_{NF} T_{ci}^2 + T_{ci}^3\right) \quad , \tag{3-146}$$

$$\overline{\varepsilon} = \left[\frac{1}{\varepsilon_F(T_{NF})} + \frac{R_{Fo}}{R_{ci}}\left(\frac{1}{\varepsilon_c(T_{ci})} - 1\right)\right]^{-1} \quad , \tag{3-147}$$

$$\beta_{cond} = \frac{R_{Fo}}{2} \, h_{cond} \quad , \tag{3-148}$$

$$\beta_{conv} = \frac{h_c R_{co}}{2} \quad , \tag{3-149}$$

$$\psi_i = \frac{Q_i\left(R_{i+1}^2 - R_i^2\right)}{4} \qquad \begin{array}{l} \text{for } 1 \le i \le (NF-1) \\ \quad ci \le i \le ci+1 \end{array} \quad , \tag{3-150}$$

$$\psi_{NF} = \frac{Q_{NF}\left(R_{Fo}^2 - R_{NF}^2\right)}{4} \quad , \tag{3-151}$$

$$\psi_{ci+2} = \frac{Q_{ci+2}\left(R_{co}^2 - R_{ci+2}^2\right)}{4} \quad , \tag{3-152}$$

$$Q_i = Q_c F_{z,j} F_{r,i} \qquad \text{for fuel} \quad , \tag{3-153}$$

$$Q_i = Q_c F_{z,j} \qquad \text{for cladding} \quad , \tag{3-154}$$

where Q_f, Q_c are the average heat generation per unit volume for fuel and cladding, respectively.

For transient analysis the time-dependent radial temperature profiles for both fuel and cladding are governed by the heat conduction equation in

the cylindrical geometry:

$$\rho(T)\ c(T)\ \frac{\partial T}{\partial t} = \frac{1}{r}\ \frac{\partial}{\partial r}\ r\ k(T)\ \frac{\partial T}{\partial r} + Q(r)\quad . \tag{3-155}$$

The approximated solution of the above equation is obtained by using the extrapolated Crank-Nicolson differencing scheme for the discretized radial nodes (see Figure 3-10 for the noding arrangement). There are ICO coupled algebraic equations to be solved simultaneously to obtain T_i^{k+1} for all i at each axial node. The final forms of the equations are

$$T_{ICO}^{k+1} = F_{ICO}\quad , \tag{3-156}$$

$$T_{i-1}^{k+1} = F_{i-1} + H_{i-1}\ T_i^{k+1}\qquad \text{for } 2 \le i \le ICO\quad . \tag{3-157}$$

The coefficients are defined as

$$F_1 = d_1/E_1\quad , \tag{3-158}$$

$$F_1 = \frac{d_i + F_{i-1}\ \beta_i}{G_i}\qquad \text{for } 2 \le i \le ICO\ , \tag{3-159}$$

$$H_i = \frac{\beta_{i+1}}{G_i}\qquad \text{for } 1 \le i \le (ICO-1)\ , \tag{3-160}$$

$$G_1 = E_1\quad , \tag{3-161}$$

$$G_i = E_i - \frac{\beta_i^{\ 2}}{G_{i-1}}\qquad \text{for } 2 \le i \le ICO\ , \tag{3-162}$$

$$E_i = \frac{1}{\alpha_i} + \beta_i + \beta_{i+1}\qquad \text{for } 1 \le i \le ICO\ , \tag{3-163}$$

- 58 -

$$\alpha_i = \frac{2\Delta t}{c\,(\overline{T}_i)\,\rho(T_i)\,(R_{i+1}^2 - R_i^2)} \qquad \begin{array}{l} \text{for } 1 \le i \le (NF-1) \\ i = ICI,\ ICI + 1 \end{array} , \qquad (3\text{-}164)$$

$$\alpha_{NF} = \frac{2\Delta t}{c\,(\overline{T}_{NF})\,\rho(\overline{T}_{NF})\,(R_{IGAP}^2 - R_{NF}^2)} , \qquad (3\text{-}165)$$

$$\alpha_{ICO} = \frac{2\Delta t}{c(\overline{T}_{ICO})\,\rho(\overline{T}_{ICO})\,(R_{CO}^2 - R_{ICO}^2)} , \qquad (3\text{-}166)$$

$$\beta_i = 0 , \qquad (3\text{-}167)$$

$$\beta_2 = \frac{k(\overline{T}_{1,2})\,R_2}{R_3 + R_2 - 2R_1} , \qquad (3\text{-}168)$$

$$\beta_i = \frac{k(\overline{T}_{i-1,i})\,R_i}{R_{i+1} - R_{i-1}} \qquad \text{for } 3 \le i \le (NF-1) , \qquad (3\text{-}169)$$

$$\beta_{NF} = \frac{k(\overline{T}_{NF-1,NF})\,R_{NF}}{2R_{Fo} - R_{NF} - R_{NF-1}} , \qquad (3\text{-}170)$$

$$\beta_{ICI} = \beta_{cond} + \beta_{rad} , \qquad (3\text{-}171)$$

$$\beta_{ICI+1} = \frac{k(\overline{T}_{ICI,ICI+1})\,R_{ICI+1}}{R_{ICO} + R_{ICI+1}\ 2R_{ICI}} , \qquad (3\text{-}172)$$

$$\beta_{ICO} = \frac{k(\overline{T}_{ICO-1,ICO})\,R_{ICO}}{2R_{CO} - R_{ICO} - R_{ICO-1}} , \qquad (3\text{-}173)$$

$$\beta_{ICO+1} = \beta_{conv} = \frac{1}{2}\,h_{conv}\,R_{CO} , \qquad (3\text{-}174)$$

$$d_1 = T_1^k \left[\frac{1}{\alpha_1} - \beta_2\right] + T_2^k \left[\beta_2\right] + \psi_1 , \qquad (3\text{-}175)$$

$$d_i = T_{i-1}^k \left[\beta_i\right] + T_i^k \left[\frac{1}{\alpha_i} - \beta_i - \beta_{i-1}\right] + T_{i+1}^k \left[\beta_{i+1}^k\right] + \psi_i$$
$$\text{for } 2 \le i \le (ICO-1) , \qquad (3\text{-}176)$$

$$d_{ICO} = T_{ICO-1}^k \left[\beta_{ICO} \right] + T_{ICO}^k \left[\frac{1}{\alpha_{ICO}} - \beta_{ICO} - \beta_{conv} \right] + \psi_{ICO} \quad , \tag{3-177}$$

$$\psi_i = \frac{Q_i}{2} (R_{i+1} - R_i) \qquad \begin{array}{l} \text{for } 1 \leq i \leq (NF-1) \\ \\ ICI \leq i \leq (ICO-1) \end{array} \tag{3-178}$$

$$\psi_{NF} = \frac{Q_{NF}}{2} (R_{Fo}^2 - R_{NF}^2) \quad , \tag{3-179}$$

$$\psi_{ICO} = \frac{Q_{ICO}}{2} (R_{CO}^2 - R_{ICO}^2) \quad , \tag{3-180}$$

Q_i = transient heat generation per unit volume.

The parameters β_{rad} and β_{cond} are defined by Equations (3-146) to (3-148). All of the thermal properties in the above expressions are determined at the temperature extrapolated to the middle of the (k+1)th time internal, that is

$$\overline{T}_i = T_i^k + \left(\frac{T_i^k - T_i^{k-1}}{2 \Delta t^k} \right) \Delta t^{k+1} \quad . \tag{3-181}$$

The thermal conductivity $k (\overline{T}_{i-1,i})$ is evaluated at

$$T_{i-1,i} = \frac{1}{2} \left[T_{i-1} + \overline{T}_i \right] \quad . \tag{3-182}$$

The wire wrap on the outside surface of cladding is included in the transient analysis. It is assumed that the wire wrap provides an additional mass to the outermost node of cladding. The additional mass increases the heat capacity of that node. An effective mass is given by

$$\rho_{eff} = \rho_{ICO} \left[1 + \frac{r_w^2 \sqrt{1 + \left(\frac{\pi}{p/D} \right)^2}}{R_{ICO}^2 - R_{ICO-1}^2} \right] . \tag{3-183}$$

3.1.3.3 Structure Temperature Calculation

The detailed calculations of radial temperature distribution are not performed for the gas plenum and structures. The structure is divided into the same axial slices as its associated fuel rod. For each slice, the plenum or structure is treated as a lumped mass. The fission heating rate, decay heating rate, and heat convection of coolant flow are used to determine the average temperature of that axial node. The inner surface of plenum and the outside surface of structure are assumed to be adiabatic.

The temperature of the structure (or plenum) at the j-th axial node is given by

$$T_s = T_c + \frac{V_s \, Q_s}{h_c \, A_s} \; .$$

(3-184)

The transient temperature of structure is governed by the single energy balance:

$$\frac{dT_s}{dt} = \frac{h_c A_s}{C_s \rho_s V_s} (T_c - T_s) + \frac{Q_s(t)}{\rho_s C_s} \; .$$

(3-185)

For a given axial node, the structure temperature at (k+1)th timestep is

$$T_s^{k+1} = \frac{T_s^k + B\Delta t + 0.5A \, \Delta t \, T_c^{k+1} + T_c^k - T_s^k}{1 + 0.5A \, \Delta t}$$

(3-186)

where

$$A = \frac{h_c A_s}{C_s \rho_s V_s} \; ,$$

$$B = \frac{Q_s(t)}{\rho_s C_s} \; ,$$
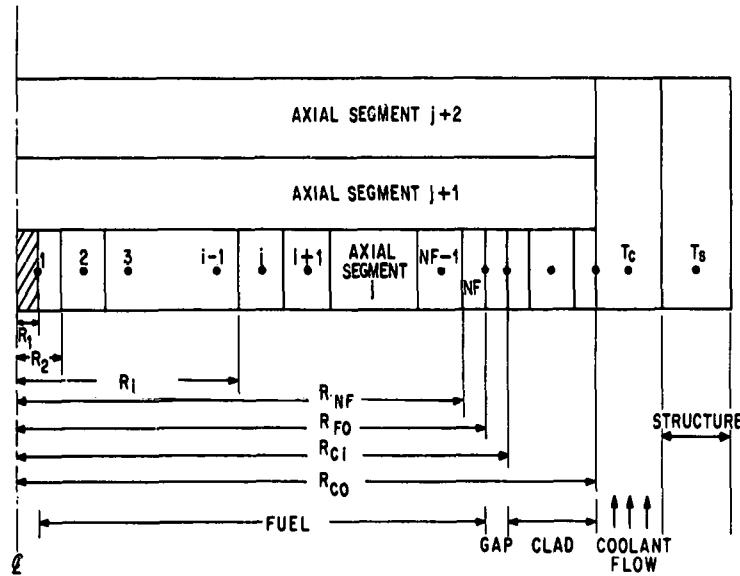
Figure 3-10. Radial noding in the fuel and blanket rods.
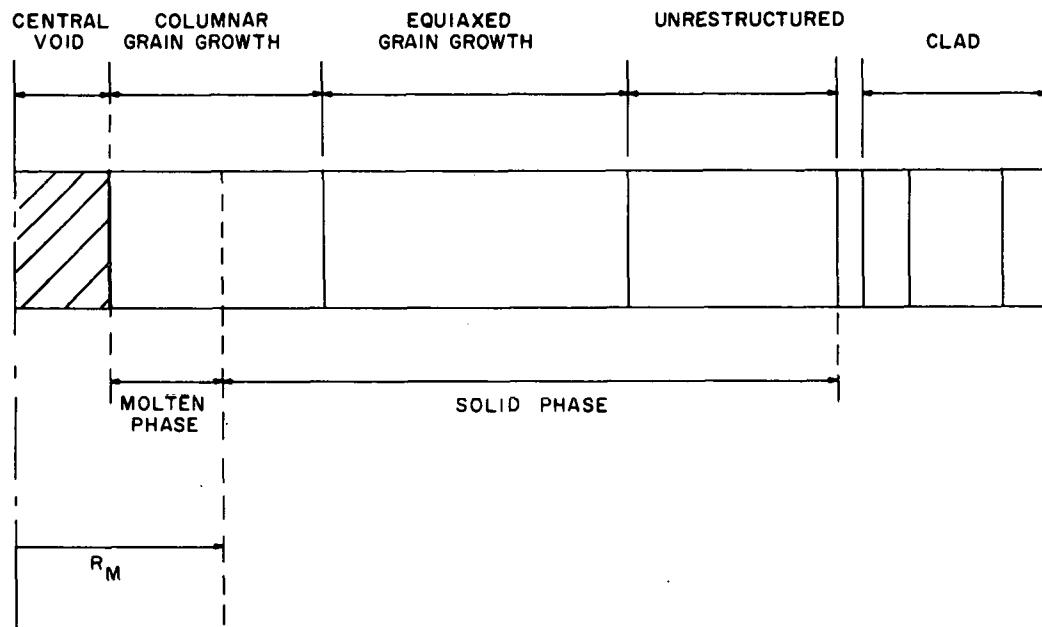
Figure 3-11. A schematic arrangement of radial noding
for a partially molten fuel rod.

and

$$Q_s(t) = \text{transient power generation per unit volume,}$$

$$h_c = \text{convective heat transfer coefficient.}$$

The clad of lower or upper fission gas plenum is treated in a similar manner.

3.1.3.4 Calculation for the Molten Fuel

The computations of transient heat transfer in the core is terminated if

1) clad temperature reaches to its melting temperature, or

2) fraction of fuel melted exceeds a given criterion supplied by user as an input parameter.

The method of computing the fraction of melted fuel is described in this section. According to the steady-state fuel model, there are three possible regions across the radius of fuel: the inner columnar and equiaxed grain-growth regions and the outer unrestructured region. Proper modifications of material properties and volumetric heat generation rate are applied to each of the restructured regions. When the fuel temperature reaches its melting point, which is expected to propagate outward from the center of the rod, a fourth region is identified as the molten fuel region. Figure 3-11 is a schematic representation of an axial segment of the fuel rod.

The basic assumptions used in calculating the fraction of molten fuel are

1) within any radial node, the fraction of molten fuel and the remaining solid fuel are in thermal equilibrium, i.e., both liquidus and solidus phase are at the melting temperature;

2) the melting temperature is specified by user;

3) molten fuel is stationary and is attached to its original axial slice;

4) computation is terminated at $\dfrac{R_m}{R_{Fo}} \geq R_{cr}$, where R_m is the outer radius of the molten region to be calculated, R_{Fo} is the outer radius of the fuel, and R_{cr} is the termination criterion imposed by user $(0 < R_{cr} < 1)$.

The fuel temperature at the i-th radial node is first computed by neglecting any melting during the time increment according to the heat conduction model described in Section 3.1.3.2:

$$T_i^{k+1} = F_i + H_i \, T_{i+1}^{k+1} \quad , \qquad (3\text{-}187)$$

where F_i and H_i are time-dependent coefficients related to the material properties and the heat generation. If the computed T_i^{k+1} is greater then T_{melt}, a pseudo-temperature T_{pse} is defined:

$$T_{pse} = T_i^{k+1} \quad . \qquad (3\text{-}188)$$

The mass of the molten fuel (M_{melt}) and the fractions of mass melted (F_{melt}) are calculated by

$$M_{melt} = \frac{\pi \, (R_{i+1}^2 - R_i^2) \, \Delta Z_j \, \rho_i \, C_i \, (T_{pse} - T_{melt})}{Q_{melt}} \quad , \qquad (3\text{-}189)$$

$$F_{melt} = \frac{C_i \, (T_{pse} - T_{melt})}{Q_{melt}} \quad , \qquad (3\text{-}190)$$

- 64 -

where ρ_i and C_i, respectively, are the density and heat capacity of solidus fuel, and Q_{melt} is the latent heat of fusion. The outer radius of the molten region is then determined by

$$R_m = \left(R_i^2 + \frac{M_{melt}}{\rho_\ell \ \pi \ \Delta Z_j} \right)^{\frac{1}{2}} . \qquad (3-191)$$

For the i-th radial node with mixed solidus and liquidus phase, the material properties are approximated as

$$X_{mix} = (1 - F_{melt}) \ X_{solid} + F_{melt} \ X_{liq} , \qquad (3-192)$$

where X denotes density, heat capacity, thermal expansion coefficient, and thermal conductivity. The volumetric heat generation term in heat conduction equation was determined for solidus fuel and has to be modified:

$$Q = Q_0 \ \frac{\rho_{mix}}{\rho} , \qquad (3-193)$$

where

Q_0 = average volumetric heat generation at steady-state,

ρ = fuel density as fabricated.

The spatial power distribution function and the transient power generation terms are imposed on Equation (3-193).

Finally, if the computed fraction of molten fuel in any radial node is

greater than one, i.e.,

$$C_i (T_{pse} - T_{melt}) > Q_{melt} \quad ,$$

the model will

1) set $F_{melt} = 1$ for this radial node,

2) assume the molten fuel in this radial node is superheated and its temperature is given by

$$T_i^{k+1} = T_{melt} + \frac{C_{i,solid} (T_{pse} - T_{melt}) - Q_{melt}}{C_{i, liquid}} \quad . \tag{3-194}$$

3.1.3.5 Computational Procedure

The fuel heat transfer computation involves three different sections of rod; fuel, blanket, and fission gas plenum. Each section is treated according to the material index specified by the user. At steady-state, the nonlinearity of the heat conduction equations and the option of fuel restructuring require an iterative procedure to obtain the steady-state temperature. The procedure is shown in Figure 3-12. For transients, the temperature-dependent properties are evaluated at extrapolated temperatures and hence no iteration procedure is needed, as shown in Figure 3-13. However, checks of melting of pellet or clad are done during the transient computation. If the computed pellet temperature is above the specified melting temperature, a simple molten fuel model will be used to replace the solid-phase heat transfer model. Melting of clad, as stated previously, is the index of terminating the transient computation. Calculation of hoop stress and comparison with the fission gas pressure are performed for every channel. Release of fission gas is indicated, if the fission gas pressure is higher than the hoop stress. Boundary conditions of gas
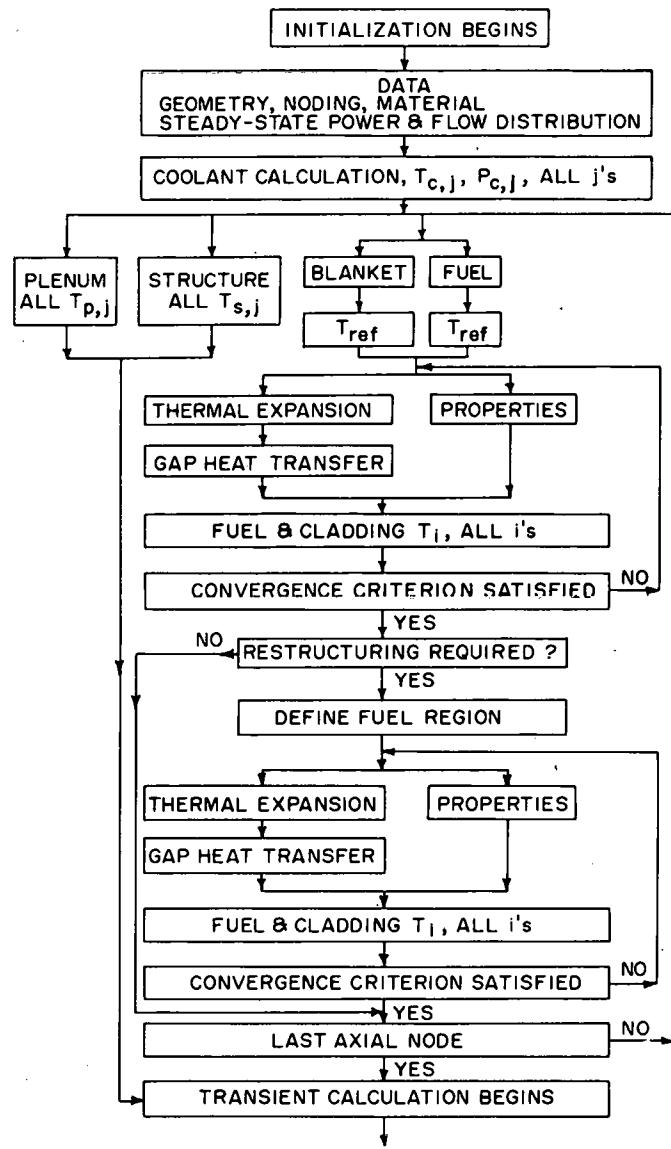
Figure 3-12. Computational logic for the heat transfer
           calculations at steady state.
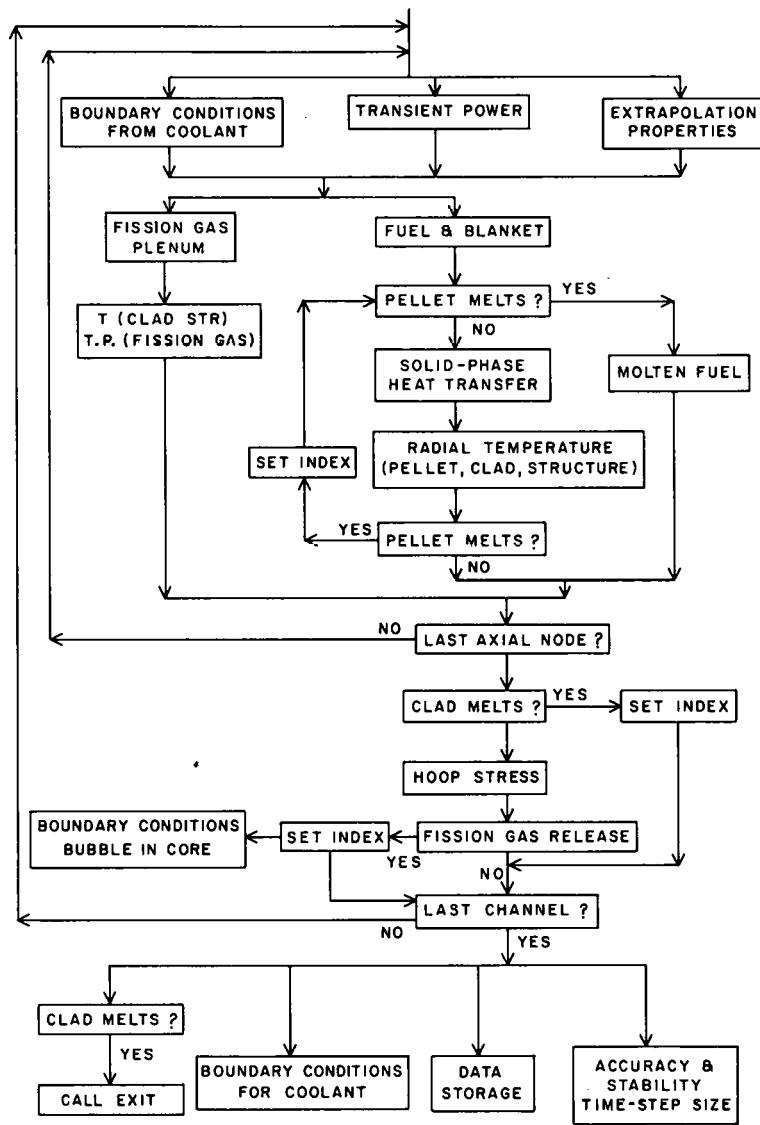
Figure 3-13.   Computational logic for the transient
heat transfer.

bubble formation are transmitted to the coolant model for the initialization of bubble computation. It is assumed that rupture of clad has no effect on clad heat transfer calculations.

3.1.4 Power Generation

The power generated in the reactor core includes both the fission and decay heat contributions. Also, both the time-dependent and spatial-dependent aspects of the power generation are accounted for. In our multi-channel representation of the reactor core, the total reactor power, P5TOT(t), is written as

$$P5TOT(t) = \sum_{K=1}^{N6CHAN} P5FISS\ (K,t) + \sum_{K=1}^{N6CHAN} P5DCY\ (K,t) + P5BYPS\ (t)\ , \qquad (3-195)$$

where

$$P5FISS\ (K,t) = F5PFIS\ (K) \cdot F6TPOW\ (K) \cdot P5TOT\ (0) \cdot n(t)\ , \qquad (3-196)$$

$$P5DCY\ (K,t) = F5PDCY\ (K) \cdot F6TPOW\ (K) \cdot P5TOT\ (0) \cdot d\ (K,t)\ , \qquad (3-197)$$

$$P5BYPS(t) = F6PBYP \cdot P5TOT(0) \cdot \left\{ F5PFIS(N6CHAN+1) \cdot n(t) + \qquad (3-198) \right.$$
$$\left. F5PDCY(N6CHAN+1) \cdot d_B(t) \right\}\ ,$$

subject to the following initial conditions:

$$n\ (t)\ \Big|_{t=0} = 1\ ,$$

$$d\ (K,t)\ \Big|_{t=0} = 1\ ,$$

$$d_B(t)\ \Big|_{t=0} = 1\ .$$

The first two terms on the right hand side of Equation (3-195) represent, respectively, the fission and decay heating contributions. The third term represents gamma heating of coolant in the bypass channel. Equation (3-195) can also be written as

$$P5TOT (t) = P5TOT (0) \cdot \left[\sum_{K=1}^{N6CHAN} F6TPOW (K) \cdot \left\{ F5PFIS (K) \cdot n (t) \right. \right.$$
$$\left. + F5PDCY (K) \cdot d (K,t) \right\} + F6PBYP \cdot \left\{ F5PFIS(N6CHAN+1) \cdot n(t) \right.$$
$$\left. \left. + F5PDCY(N6CHAN+1) \cdot d_B(t) \right\} \right] \cdot \quad (3\text{-}199)$$

Various factors are now defined:

F6TPOW (K) = fraction of total power allocated to the K-th channel,

F5PFIS (K) = fraction of power from fission and gamma heating in the K-th channel,

F5PDCY (K) = fraction of power from decay heating in the K-th channel,

F6PBYP = fraction of power in the bypass channel,

$n(t)$ = normalized time-dependent factor for fission and gamma heating,

$d(K,t)$ = normalized time-dependent factor for decay heating in the K-th channel,

$d_B(t)$ = normalized time-dependent factor for heating of the bypass channel.

Two consistency equations are

$$\sum_{K=1}^{N6CHAN} F6TPOW (K) + F6PBYP = 1 \quad , \qquad (3\text{-}200)$$

and

$$F5PFIS (K) + F5PDCY (K) = 1. \qquad (3\text{-}201)$$

The power generated in a channel is further subdivided into four terms:
(1) portion deposited in the fuel (or blanket or control rod pellets),
F5PWR5 (K); (2) portion deposited in cladding, F5PWR6 (K); (3) portion deposited in coolant, F5PWR1 (K); and (4) portion deposited in structure,
F5PWR7 (K). These numbers are normalized so that

$$F5PWR5 \; (K) + F5PWR6 \; (K) + F5PWR1 \; (K) + F5PWR7 \; (K) = 1.0 \qquad (3-202)$$

for each channel.

3.1.4.1 Spatial Power Normalization

From the power values deposited in the fuel, cladding, coolant, or structure material of any channel, an axial variation along the length of the channel is specified by a profile which must be supplied by the user. These profile data are normalized consistent with the nodal structure (see Figure 3-14). For any channel, five axial regions are available for user specification. These include upper and lower fission gas plena, upper and lower blanket and fuel regions. As shown, for any given region, the associated fuel, cladding, coolant, and structure zones have the same axial mesh. Since the total number of rod axial sections for the K-th channel is N5ASEC(K), the axial distribution profile data supplied by the user are stored in the F5PAX(J,K) array J=1, N5ASEC(K) . The data are taken to apply at the nodal midpoints. These relative axial distribution data are then normalized such that the resulting F5PAX(J,K) array satisfies:

$$\frac{1}{Z_{TOTAL}} \sum_{J=1}^{N5ASEC(K)} F5PAX(J,K) \cdot \Delta Z5_J = 1.0 \quad , \qquad (3-203)$$

UPPER FISSION
GAS PLENUM

UPPER BLANKET

FUEL

GAP

CLADDING

COOLANT

STRUCTURE

FUEL

LOWER BLANKET

LOWER FISSION
GAS PLENUM

₵
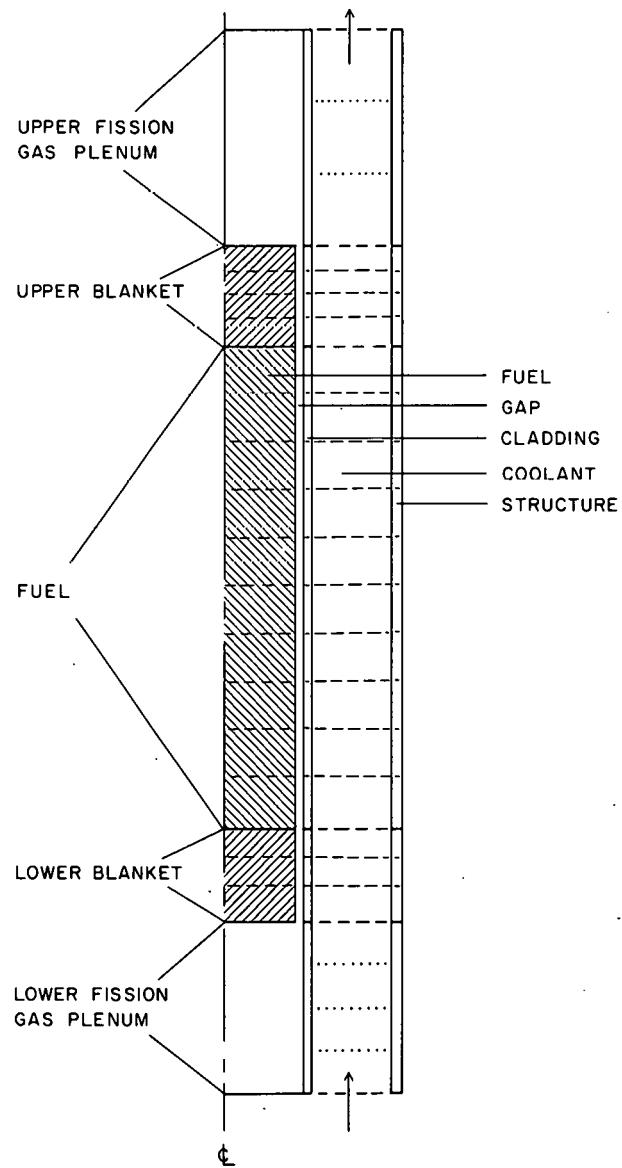
Figure 3-14. Axial noding for power normalization
in fuel and coolant.

where Z_{TOTAL} is the total axial rod length and $\Delta Z5_J$ is the length of the J-th axial rod node. Thus, the user-supplied rod data are normalized on a unit length basis.

The radial power distribution is broken into two sections: (1) the radial distribution on a whole core basis, and (2) the radial variation within a channel. The radial distribution on a whole core basis is incorporated with the fraction of power in the channel, F6TPOW(K), and by specifying the number of rods in this channel, N5RODS(K).

The radial power distribution within a channel, for any given axial section or slice in Figure 3-14, is depicted as follows:

(1) For axial regions containing fuel and/or blanket zones, the user may specify any number of radial nodes. This number is stored in the N5NFR(K) array and is taken to apply to all axial fuel and/or blanket sections in the K-th channel.

(2) For the cladding zone, only three radial nodes are allocated.

(3) The structural zone is allocated one radial node.

(4) The coolant associated with any rod axial section is allocated one radial node.

Any power deposited in the cladding, coolant or structural material is assumed to be distributed uniformly in the radial direction. However, the radial power within the fuel and blanket zones is allowed to vary in the manner specified by the user. The user-input radial power shape is normalized such that the following equation is satisfied:

$$\frac{\displaystyle\sum_{I=1}^{N5NFR(K)} F5PRAD(I,K)\cdot A(I)}{\displaystyle\sum_{I=1}^{N5NFR(K)} A(I)} = 1 \quad , \qquad (3\text{-}204)$$

- 73 -

where F5PRAD(I,K) is the radial power shape in the I-th radial node of the K-th channel, A(I) is the cross-sectional area of the I-th node and N5NFR(K) is the number of radial nodes in the K-th channel.

In summary, the amount of heat generated in the (I,K)th fuel mesh of the K-th channel is given by the following equation:

$$P_{fuel} \; (I,J,K,t) = P5TOT(0) \cdot F6TPOW(K) \cdot \left\{ F5PFIS(K) \cdot n(t) \right.$$

$$\left. + \; F5PDCY(K) \cdot d(K,t) \right\} \cdot F5PWR5(K) \cdot F5PAX(J,K) \cdot F5PRAD(I,K).$$

$$(3-205)$$

Similarily, the power generation in the cladding mesh at the J-th slice of the K-th channel is given by the following equation:

$$P_{clad} \; (J,K,t) = P5TOT(0) \cdot F6TPOW(K) \cdot \left\{ F5PFIS(K) \cdot n(t) \right.$$

$$\left. + \; F5PDCY(K) \cdot d(K,t) \right\} \cdot F5PWR6(K) \cdot F5PAX(J,K) \; ,$$

$$(3-206)$$

since the radial power variation across the cladding is assumed to be constant. The equations for power generation in the coolant or structural materials may be obtained by replacing F5PWR6(K) in Equation (3-206) with F5PWR1(K) or F5PWR7(K), respectively.

3.1.4.2 Fission Heating

The time-dependent portion of the fission power contribution is cal-culated by solving the space-averaged, one-energy group reactor kinetics equations. The one-energy group assumption is reasonable, particularly for a fast reactor. The space-averaged model is quite adequate since the core of an LMFBR responds, due to the relative smallness of the core and the large neutron migration area, more uniformly than a light water reactor core to

changes in reactivity.

The point-kinetics equations written in terms of the prompt neutron generation time (Λ) may be expressed (source term neglected) as

$$\frac{dN}{dt} = \frac{\rho - \beta_T}{\Lambda} N + \sum_i \lambda_i C_i \; , \qquad (3\text{-}207)$$

$$\frac{dC_i}{dt} = \frac{\beta_i N}{\Lambda} - \lambda_i C_i \; , \qquad (3\text{-}208)$$

where

N = neutron density (which is proportional to the power),

ρ = total reactivity ($\Delta k/k$),

β_T = total effective delayed neutron fraction = $\sum_i \beta_i$,

Λ = prompt neutron generation time (s),

λ_i = decay constant of the i-th delayed neutron group (s^{-1}),

C_i = density of the i-th effective delayed neutron precursor,

β_i = fraction of the i-th effective delayed neutron group,

t = time (s),

By rewriting N and C_i in normalized form such that

$$n(t) \equiv \frac{N(t)}{N(o)} \; ; \; c_i(t) \equiv \frac{C_i(t)}{C_i(o)} \; ; \text{ where } C_i(o) = \frac{\beta_i}{\Lambda \lambda_i} N(o),$$

Equations (3-207) and (3-208) become

$$\frac{dn}{dt} = \frac{\rho - \beta_T}{\Lambda} n + \frac{1}{\Lambda} \sum \beta_i c_i \; , \qquad (3\text{-}209)$$

$$\frac{dc_i}{dt} = \lambda_i (n - c_i). \qquad (3\text{-}210)$$

The direct integration of these equations requires very small time-

step sizes due to the small numerical value of the generation time (Λ). To assure numerical stability and accuracy, step sizes of approximately (100 to 1000) · Λ are required. Typically, Λ is about $= 6 \times 10^{-7}$ s, therefore, the step sizes of the order of 0.00006 to 0.0006 s would be required.

The simplest way to circumvent this problem is to utilize the prompt jump approximation (PJA). This approximation makes use of the very fact that Λ is extremely small. By assuming that Λ approaches zero, the product Λ dn/dt in Equation (3-209) also approaches zero. Thus, n may be directly solved for as

$$ n = \frac{1}{\beta_T - \rho} \sum_i \beta_i C_i \; . \tag{3-211} $$

This means that any disturbance in the reactivity (ρ) will be instantaneously reflected in the power (n). Thus, for a step change in ρ, n jumps immediately to some initial level dependent on the size of the reactivity insertion.

The PJA is in excellent agreement (to within < 0.1%) with the exact solution for values of ρ less than +50¢. It should be noted that this approximation gets even closer to the exact solution when the prompt neutron generation is smaller.

The main drawback of using the PJA is the fact that agreement to the exact solution diminishes as ρ approaches β_T. It can be seen from Equation (3-211) that n is discontinuous at $\rho = \beta_T$. To provide for these cases where ρ approaches β_T (or more conservatively, when ρ > 50¢), an option is available in the SSC-L code to solve the equations "exactly." However, it should be stressed that for most cases which the SSC will analyze, the PJA will be adequate. For cases where the plant protection system (PPS) is assumed to

operate, the reactor may be shut down well before reactivity insertions approaching +50¢ are attained.

To provide an "exact" solution to Equations (3-209) and (3-210), without integrating them directly, the method proposed by Kaganove[3.11] was used. Here, Equations (3-210) are solved for c_i in terms of dc_i/dt and substituted into Equation (3-209) such that

$$\frac{dn}{dt} = \frac{\rho n}{\Lambda} - \frac{1}{\Lambda} \sum_i \frac{\beta_i}{\lambda_i} \frac{dc_i}{dt} . \tag{3-212}$$

The assumption is then made that over any integration step (Δt), the normalized power (n) and reactivity (ρ) may be represented by second-order polynomials. Thus,

$$n(t) = n_0 + n_1 t + n_2 t^2 \qquad 0 \le t \le \Delta t , \tag{3-213}$$

$$\rho(t) = \rho_0 + \rho_1 t + \rho_2 t^2 \qquad 0 \le t \le \Delta t , \tag{3-214}$$

where

n_0 = value of n at the end of previous timestep,

ρ_0 = value of ρ at the end of previous timestep,

and n_1, n_2, ρ_1, ρ_2 are constants to be evaluated.

Equation (3-210) is now integrated in a straightforward manner:

$$\int_0^t d\left[c_i(\tau) e^{\lambda_i \tau} \right] = \int_0^t \lambda_i e^{\lambda_i \tau} n(\tau) \, d\tau . \tag{3-215}$$

Then

$$c_i(t) = c_{io} e^{-\lambda_i t} + \lambda_i e^{-\lambda_i t} \int_0^t e^{\lambda_i \tau} n(\tau) \, d\tau , \tag{3-216}$$

where

$$c_{io} = c_i(t)\big|_{t=0} \quad .$$

Making use of Equation (3-213), Equation (3-216) becomes

$$c_i(t) = c_{io} e^{-\lambda_i t} + n_0 (1 - e^{-\lambda_i t}) + \frac{n_1}{\lambda_i} (\lambda_i t - 1 + e^{-\lambda_i t})$$

$$+ \frac{n_2}{\lambda_i^2} \left[\lambda_i^2 t^2 - 2\lambda_i t - 2 (1 - e^{-\lambda_i t}) \right] \quad . \tag{3-217}$$

Likewise, Equation (3-212) becomes

$$n(t) - n(o) = \frac{1}{\Lambda} \int_0^t \rho(\tau) \, n(\tau) \, d\tau - \frac{1}{\Lambda} \sum_i \frac{\beta_i}{\lambda_i} \left[c_i(t) - c_{io} \right] . \tag{3-218}$$

Upon substituting Equations (3-213) and (3-214) into Equation (3-218), one obtains

$$n_1 t + n_2 t^2 = \frac{1}{\Lambda} \left(\rho_0 n_0 t + \rho_0 n_1 \frac{t^2}{2} + \rho_0 n_2 \frac{t^3}{3} + \rho_1 n_0 \frac{t^2}{2} + \rho_1 n_1 \frac{t^3}{3} + \rho_1 n_2 \frac{t^4}{4} \right.$$

$$\left. + \rho_2 n_0 \frac{t^3}{3} + \rho_2 n_1 \frac{t^4}{4} + \rho_2 n_2 \frac{t^5}{5} \right) - \frac{1}{\Lambda} \sum_i \frac{\beta_i}{\lambda_i} \left[c_i(t) - c_{io} \right] . \tag{3-219}$$

The boundary conditions are then imposed that the integral Equation (3-219) be satisfied at the midpoint and end of the step (i.e., at $t=\Delta t/2$ and $t=\Delta t$). Thus, Equation (3-219) yields two equations in the unknowns n_1 and n_2. With the assumption that during any given timestep, the power and reactivity are functions of time only (i.e., decoupled), the solution is now complete. For small timesteps ($\sim.01$ sec or less), this latter assumption is certainly justified.

During a transient, the implementation of the solution in the SSC-L

will proceed as follows (assuming a predictor-corrector type of integrator):

(a) using the predicted value of reactivity at t=Δt and the two previous values, the two constants ρ_1 and ρ_2 in Equation (3-214) are calculated;

(b) using Equation (3-219) solved at Δt/2 and Δt, the constants n_1 and n_2 are calculated;

(c) the predicted power may then be calculated using Equation (3-213);

(d) repeat the above procedure during the correction portion.

3.1.4.3 Reactivity Contributions

The total reactivity at a given time, t, is the sum of an applied reactivity, $\rho_a(t)$ (e.g., control rod movement), plus the sum of the various reactivity feedback contributions, $\rho_i(t)$:

$$\rho(t) = \rho_a(t) + \sum_i \rho_i(t) \ . \tag{3-220}$$

As indicated in Figure 3-15, the total reactivity is then incorporated into the point-kinetics model and used in the evaluation of the normalized time-dependent factor for the fission and gamma heating. It should also be noted that the reactivity effects are inherently spatially-dependent. This is not only due to the fact that the temperatures vary spatially, but even for the same temperatures the magnitude of the effect will depend on the location within the reactor. Since the point-kinetics equations suppress any spatial dependence, an appropriately weighted spatial integration of the evaluated local reactivity feedback effects must be performed.

A survey of several references[3.12-3.16] and existing computer
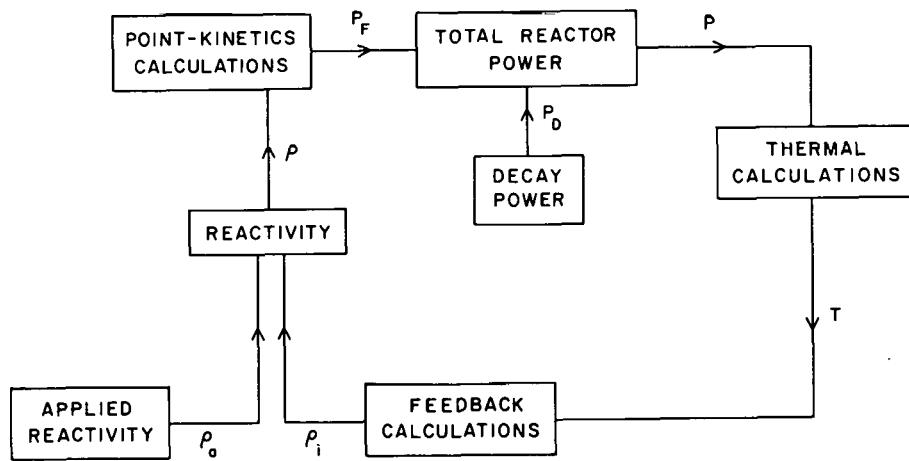
Figure 3-15. Illustration of the reactivity
              feedback loop.

models[3.7,3.17] has identified the following contributions to the feedback effects:

- Doppler
- Sodium density and voiding
- Fuel axial expansion
- Structural expansion
- Bowing
- Fuel slumping

The first three effects will be discussed in more detail in subsequent subsections. Models are presented and equations developed for incorporation of these effects into the present version of SSC. The remainder of this section will briefly discuss the last three effects.

Radial Structural Expansion

As the core heats up there is radial expansion of the fuel assemblies and core support structures which tends to effectively increase the pitch-to-diameter ratio of the fuel lattice, reducing the reactivity. However, this effect has a long time constant relative to the fuel, for example, since it is related to the structural components. From a normal operational viewpoint (e.g., taking the reactor from zero to full power), this effect will be much more important than for those transients that SSC-L will be analyzing.

Bowing

Bowing is caused by differential thermal expansion and is a result of radial temperature gradients. Positive reactivity can be added when fuel

material bows towards the center of the reactor. To reduce this effect, spacers are placed between fuel elements and fuel assemblies. The temperature gradients cause stresses in the contacted material which is designed to be strong enough to prevent appreciable displacements.

Also, as with structural expansion, this effect will have a relatively long time constant since it is the fuel assembly and not the fuel pins themselves that provide the structural strength.[3.12]

Fuel Slumping

In the event of fuel melting, there is the possibility for fuel movement within the cladding material. If the fuel moves (slumps) towards the center of the core, then there will be positive reactivity added to the system. However, the current version of SSC-L does not treat the class of transients that would lead to this condition; hence, fuel slumping is not considered further.

3.1.4.3.1 Doppler Effect

The Doppler effect is the most important and reliable prompt negative reactivity effect in current thermal and fast reactor designs which utilize high fertile (U_{238}) material concentrations. Probably one of the better understood reactivity phenomena, the Doppler effect is due to the increased kinetic motion of the fuel atoms, as measured by an increase in fuel temperature, resulting in the broadening of cross-section resonances and increased resonance absorption.

The Doppler coefficient is defined as the change in multiplication factor, k, associated with an arbitrary change in the absolute fuel tempera-

ture, T. Since in fast reactors this coefficient is found to vary as the inverse of fuel temperature, a temperature independent Doppler parameter, α^{DOP}, can be generally defined as

$$\alpha^{DOP} = T \, dk/dt \; . \tag{3-221}$$

Equation (3-221) may be integrated to yield

$$k^1 - k^2 = \alpha^{DOP} \, \ell n \, T^1/T^2 \quad , \tag{3-222}$$

where T^1 and T^2 represent two different fuel temperatures and k^1 and k^2 are the resulting multiplication factors. Rigorously, reactivity is defined as

$$\rho = \frac{k - 1}{k} \quad ,$$

and changes in reactivity, $\Delta\rho$, as

$$\Delta\rho = \rho^1 - \rho^2 = \frac{k^1 - k^2}{k^1 k^2} \quad .$$

For small reactivity changes (the Doppler effect is of the order of 10^{-4}) and with $k \approx 1$,

$$k^1 - k^2 \approx \rho^1 - \rho^2 \quad ,$$

and the change in reactivity due to the Doppler effect, $\Delta\rho^{DOP}$, can be written as

$$\Delta\rho^{DOP} = \alpha^{DOP} \, \ell n \, \frac{T^1}{T^2} \quad . \tag{3-223}$$

This equation may be applied locally or regionally depending on how the temperatures and Doppler coefficient are defined. Specifically, in discrete

notation, the local Doppler reactivity, ρ_{JK}^{DOP} is

$$\rho_{JK}^{DOP} = \alpha_{JK}^{DOP} \ln \frac{T_{JK}^1}{T_{JK}^2} \quad , \tag{3-224}$$

where K represents the channel, J is the axial position in the channel K, and T_{JK} is the effective local temperature at position JK. This effective fuel temperature can be taken to be the volume-averaged fuel temperature which is defined as

$$T_{JK} = \frac{\sum\limits_{I} V_{IJK} T_{IJK}}{\sum\limits_{I} V_{IJK}} \quad , \tag{3-225}$$

where V_{IJK} is the fuel volume in channel K, axial slice J, and between radial mesh I and I-1, and T_{IJK} is the local fuel temperature at this position.

It should be noted that the Doppler coefficient in Equation (3-224) is shown to be a spatially-dependent variable. Although α_{JK}^{DOP} will be a constant with respect to fuel temperature, there will be spatial variations due to different fuel types (e.g., enrichment, pin size, volume fractions of structural material, coolant, and fuel) and different sodium density. In the present model, α_{JK}^{DOP} will be a spatially-dependent parameter supplied by the user. Thus, the first concern relating to fuel type can be directly addressed.

The sodium density dependence is actually a neutron spectrum dependence--the harder the spectrum, the smaller the Doppler effect (since there are less neutrons in the resonance range). The less sodium present, owing to density decreases or voids, implies a harder spectrum. To treat this effect, an effective isothermal sodium void fraction, X_{JK}^{NA}, is defined

$$X_{JK}^{NA} = \frac{\rho_{JK}^{NA}{}^{ref} - \rho_{JK}^{NA}}{\rho_{JK}^{NA}{}^{ref}} \qquad (3\text{-}226)$$

where ρ_{JK}^{NA} is the local, time-dependent sodium density at position JK, and $\rho_{JK}^{NA}{}^{ref}$ is the local reference sodium density at position JK. Thus, if β_{JK}^{DOP} and γ_{JK}^{DOP} are the Doppler parameters with and without sodium present, respectively, then the net Doppler parameter can be approximated by

$$\alpha_{JK}^{DOP} = \beta_{JK}^{DOP\,\prime}\left(1 - X_{JK}^{NA}\right) + \gamma_{JK}^{DOP} X_{JK}^{NA} \quad . \qquad (3\text{-}227)$$

To get an overall Doppler reactivity, ρ^{DOP}, for use in the point-kinetics equation, a summation of Equation (3-224) must be performed. Thus,

$$\rho^{DOP} = \sum_{J,K} \rho_{JK}^{DOP} = \sum_{J,K} \alpha_{JK}^{DOP} \, \ell n \, \frac{T_{JK}}{T_{JK}} \quad . \qquad (3\text{-}228)$$

The values of the Doppler coefficients, α_{JK}^{DOP}, for each JK-th region must be supplied by the user in units of reactivity ($\Delta k/k$) for that mesh.

3.1.4.3.2 Sodium Density and Void Effects

Heating of the sodium coolant decreases the coolant density and can ultimately lead to vaporization (voiding). These density decreases affect the reactivity of the reactor through two competing effects: increased leakage, which adds negative reactivity and is important away from the center of the core; and spectral hardening due to a decrease in the macroscopic sodium scattering cross-section which adds positive reactivity. The net effect depends primarily upon the location in the reactor.

In modeling this effect, both sodium density changes and voiding can

be treated in a similar fashion. Basically, what is required along with the spatial sodium density distribution is a table of spatially-dependent sodium reactivity worths. The sodium density will be determined internally by SSC-L from knowledge of the sodium temperature distribution. However, the reactivity worths are user supplied.

There are several ways to present this reactivity effect depending on the form in which the reactivity worth data are known. For application in SSC-L, Equation (3-229), which can treat either sodium density or voiding reactivity effects, is used:

$$\rho^{NA} = \sum_{JK} \beta_{JK} M_{JK} \quad , \qquad (3\text{-}229)$$

where ρ^{NA} is the overall sodium density and voiding reactivity for use in the point-kinetics equations, β_{JK} is the sodium reactivity worth in axial slice J, channel K, in units of reactivity per unit mass of sodium effectively voided, and M_{JK} is the effective mass of sodium voided in segment JK, and is defined in the following equation:

$$M_{JK} = \left(\rho_{JK2}^{NA} - \rho_{JK1}^{NA} \right) V_{JK}^{NA} \qquad (3\text{-}230)$$

In this equation, ρ_{JK}^{NA} is the local average, time-dependent sodium density and V_{JK}^{NA} is the local coolant volume in segment JK.

3.1.4.3.3 Fuel Axial Expansion Effect

Axial expansion of the fuel pellets tends to increase the active core height while decreasing the fuel density, resulting in a net decrease in

reactivity. An upper limit to the magnitude of this effect is obtained if it is assumed that the fuel pellets are free to move within the cladding. However, the actual mechanisms for expansion are difficult to model, especially for ceramic fuel. Fuel pellet cracking or friction between the pellet surface and inner clad wall will reduce the expansion significantly. On the other hand, if the fuel pellets are not stacked in perfect contact within the clad, then there may be negative fuel expansion if the fuel pellets settle.

Physics calculations for CRBRP[3.1] indicate a maximum overall reactivity of -0.12¢ per mil of fuel axial expansion. The range of this effect is quoted to be 0.0¢/mil to -0.12¢/mil owing to the uncertainties previously discussed. In fact, neglecting this feedback effect would tend to yield higher positive reactivity values during a positive temperature transient. This would result in a high estimate of the reactor power level and a conservative (i.e., more severe) prediction of the thermal-hydraulic performance.

Nevertheless, for inclusion in SSC-L, the reactivity due to fuel axial expansion, ρ^{AX}, is based on a model which parallels the treatment of sodium density reactivity effects:

$$\rho^{AX} = \sum_{JK} C_{JK} N_{JK}^* , \qquad (3-231)$$

where C_{JK} is the fuel reactivity worth in axial slice J, channel K, in units of reactivity per unit mass of fuel effectively voided from segment JK and N_{JK}^* is the effective mass of fuel voided in segment JK.

The user will supply values for the C_{JK} constants. An expression for the internal evaluation of N_{JK}^* is now derived based on the logic that as the fuel temperature increases, the fuel expands axially according to the

following equation:

$$Z_{JK}^2 = \left[1 + \alpha(T_{JK}^2 - T_{JK}^1)\right] Z_{JK}^1 \quad , \tag{3-232}$$

where α is the linear fuel expansion coefficient in units of cm/cm-K̄ and T_{JK} is the fuel volume average temperature as evaluated by Equation (3-225). To conserve mass, an axial increase in the fuel length (FL) implies a decrease in the fuel density, ρ_{JK}^{FL}, (ignoring other dimensional changes); thus

$$\rho_{JK}^{FL_1} Z_{JK}^1 = \rho_{JK}^{FL_2} Z_{JK}^2 \quad , \tag{3-233}$$

or

$$\rho_{JK}^{FL_1} - \rho_{JK}^{FL_2} = \rho_{JK}^{FL_1} \left[\frac{\alpha\,(T_{JK}^2 - T_{JK}^1)}{1 + \alpha(T_{JK}^2 - T_{JK}^1)} \right] . \tag{3-234}$$

The difference in density time the original fuel volume (before expansion), $V_{JK}^{FL_1}$, will give the amount of fuel voided from location JK, N_{JK}:

$$N_{JK} = \rho_{JK}^{FL_1} \; X_{JK}^{FL} \; V_{JK}^{FL_1} \quad , \tag{3-235}$$

where X_{JK}^{FL} is the fuel void fraction at location JK and follows from Equation (3-234) to be

$$X_{JK}^{FL} = \frac{\alpha\,(T_{JK}^2 - T_{JK}^1)}{1 + \alpha(T_{JK}^2 - T_{JK}^1)} \quad , \tag{3-236}$$

The effective amount of fuel voided from location JK, N_{JK}^*, and the resulting net reactivity effect associated with fuel axial expansion are

given by the following equations:

$$N^*_{JK} = \varepsilon \, N_{JK} \quad , \tag{3-237}$$

$$\rho^{AX} = \varepsilon \sum C_{JK} \, N_{JK} \quad , \tag{3-238}$$

where ε is a user-supplied constant that accounts for the fact that the present model does not account for the uncertainties associated with the mode of fuel expansion and does not explicitly evaluate the increase in reactivity because the fuel that was calculated to be voided from location JK [Equation (3-235)] actually causes a net increase in axial fuel height, reducing leakage. An estimate on the size of these effects is given in Reference 3.14. A recommended upper limit for ε is thus given to be 0.3.

3.1.4.4 Decay Heating

The time-dependent portion of the decay heat contribution is handled in one of two ways:

(1) tabular look-up of user supplied data, or

(2) solution of user-supplied empirical relationships.

The decay heat calculations are handled in one subroutine (PDCY5T). If the tabular look-up option is used, then paired points of time v/s decay heat fraction must be supplied on input. If the user wishes to supply empirical correlations, they must be inserted into PDCY5T at the appropriate place.

Both the relative magnitude and the time-dependent shape of the decay heating are allowed to be channel-dependent, as discussed earlier. A user will have to provide F5PDCY(K) as well as d(K,t). An additional time-

dependent function $d_B(t)$ for gamma heating of coolant in the bypass channel must also be provided. Both $d(K,t)$ and $d_B(t)$ are normalized so that at steady-state their values are 1.0.

3.2 HEAT TRANSPORT SYSTEM

3.2.1 System Description

The heat transport system provides the vital function of removing reactor generated heat and transporting it to the steam generator while maintaining an adequate flow rate for controlling reactor temperatures within safe limits under all plant operating conditions.

In this section of the report, a detailed analysis to predict the thermal and hydraulic response of the heat transport system under both pre-accident and transient conditions will be presented.

Figure 3-16 shows an example configuration of the heat transport system for a loop-type LMFBR plant. Only one circuit has been shown. It consists of the primary loop carrying radioactive liquid sodium and the intermediate loop carrying nonradioactive liquid sodium. The number of parallel heat transport circuits usually depends on total flow rate, allowable pressure drops, degree of plant reliability, size of available components, and allowable coolant velocities.[3.18] The Clinch River Breeder Reactor Plant (CRBRP) has three heat transport circuits operating in parallel.[3.1]

Each primary loop contains a variable speed, centrifugal, liquid metal pump, a check valve, an intermediate heat exchanger (shell side), and the associated piping interconnecting these components. The pump circulates coolant through the reactor where it picks up the heat generated in the core and exits at a higher temperature. The coolant transfers this heat during its passage through the shell side of the intermediate heat exchanger and returns to the reactor to complete the cycle. All primary loops share a common heat source at the reactor core and a common flow path through the reactor vessel, but otherwise each circuit operates independently.
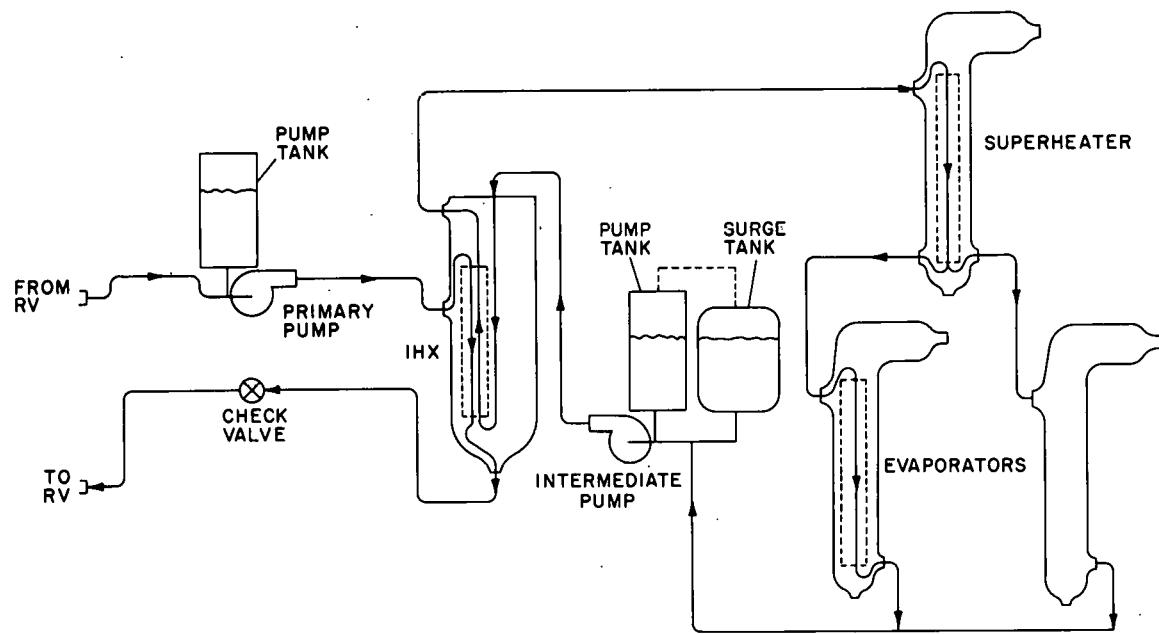
Figure 3-16.   Example configuration of the heat
transport system.

The primary and intermediate loops are thermally linked at the Intermediate Heat Exchanger (IHX). Here, the intermediate coolant, as it rises in the heat transfer tubes, picks up the heat from the primary coolant. It then passes to the shell side of the steam generator, where it gives up this heat to produce steam in the tubes, and returns to the IHX to complete the cycle. The coolant is circulated by a variable speed centrifugal pump. An expansion (surge) tank is also provided in the intermediate loop to accommodate coolant volume changes due to thermal expansion. In the case of the primary heat transport loops, the reactor vessel also serves the purpose of the surge tank.

In the example configuration of Figure 3-16, which corresponds to the CRBRP design, heated intermediate sodium leaving the IHX flows through hot leg piping and enters the steam generation system superheater module. At the superheater exit, the piping consists of two parallel runs, each extending to an evaporator inlet. Cooled sodium from the evaporators flows through two parallel runs, joined at a tee, and continues as a single run to the pump situated in the cold leg and then back to the IHX. The expansion tank is located just upstream of the pump.

Transfer of reactor power by the heat transport system is achieved by varying system flow rates, which in turn are controlled by changing pump speeds. The piping runs are insulated on the outside to minimize heat loss.

3.2.2 Analysis

For modeling purposes, the primary loop is understood to extend from the reactor vessel outlet to its inlet. The intermediate loop is assumed to

start at the IHX secondary outlet and includes the shell side of the steam generator. The heat transport system calculations thus interface with the reactor calculations at the vessel inlet and outlet, and with the tertiary loop calculations at the steam generator.

The analysis is aimed at allowing considerable flexibility in the arrangement of components in the loop for future PLBRs. In the CRBRP arrangement illustrated in Figure 3-16, the primary pump is placed in the hot leg. However, it could be located in the cold leg at the user's option, as also the check valve could be anywhere in the loop. or be absent altogether. The figure also shows one superheater and two evaporators in the intermediate loop, with the intermediate pump in the cold leg and the expansion (surge) tank just upstream of it. The model could accommodate variations in this arrangement such as none or more than one superheater, and one or more evaporators at the user's option. Also, the pump and surge tank could be located away from each other.

3.2.2.1 General Assumptions

The following basic assumptions are inherent in the analysis:

(1) one-dimensional (space) flow, i.e., uniform velocity and temperature profiles normal to the flow direction;

(2) single-phase liquid coolant, i.e., temperatures in the loop are always below coolant saturation temperature;

(3) incompressible liquid, i.e., coolant properties are not pressure dependent;

(4) single mass flow rate model, i.e., the effect of time rate of change of density on mass flow rate distribution in space is neglected,

so that at any instant of time, the mass flow rate would be uniform everywhere in a circuit, except at a free surface, or at a break where there is flow loss, or at a junction where flows meet, or at a branch where flows separate;

(5) axial heat conduction in walls is neglected.

3.2.2.2 Model Features

Aside from its flexibility, the model has several other features. Some of these are

(1) temperature-dependent material properties, expressed as curve-fitted polynomial functions of temperature,

(2) gravity effects included in detail,

(3) flow-dependent friction factor encompassing the full range of flow conditions from turbulent to laminar,

(4) loss-coefficients included for area changes,etc.,

(5) heat transfer with pipe walls considered.

3.2.2.3 Steady-State Simulation

Figure 3-17 shows a skeleton flow chart for the overall solution approach to the heat transport system. Certain boundary conditions and input data are necessary to start the calculations. These are the system geometry, i.e., pipe lengths, diameters, angles at nodes, loss coefficients, heat transfer tube dimensions, etc., and certain reference parameters, such as the loop flow rates W_p and W_s, the coolant temperature at reactor outlet $T_{1,1}$ the pressure at inlet to the primary loop P_1, the reactor pressure drop ΔP_{RV}, cover gas pressure in the pump tank P_{gas}, etc. Of these,
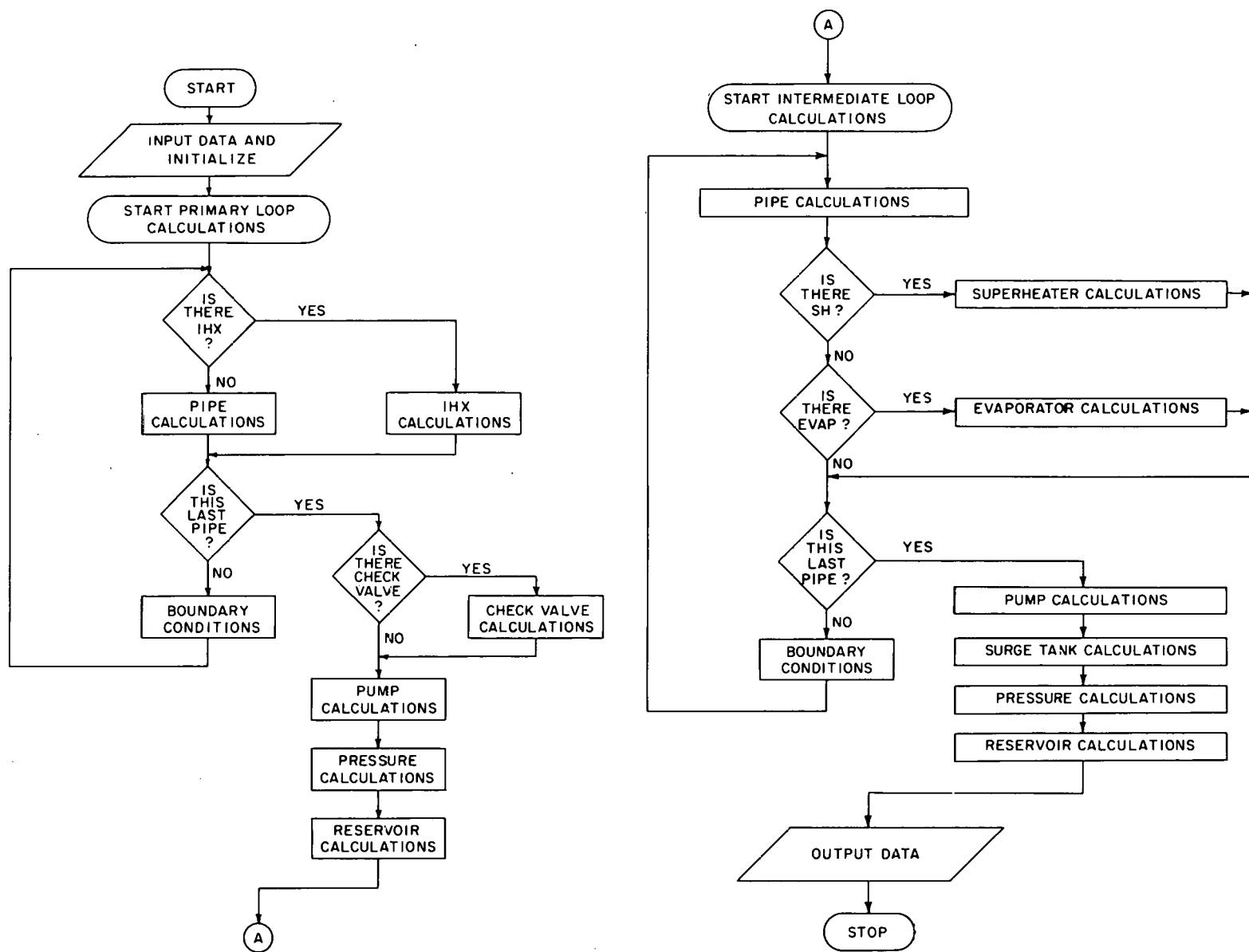
Figure 3-17. Flow diagram for steady state solution
of heat transport system.

W_p, W_s, $T_{1,1}$ are determined from overall plant thermal balance, and P_1 and ΔP_{RV} are obtained from the in-vessel simulation.

With this information, along with the constitutive relations, the calculation begins at the entrance of the primary loop and marches in the direction of coolant flow. The conservation equations for flow in piping are solved first, unless an IHX is encountered (see Figure 3-17) in which case the energy and momentum equations at the IHX are solved. Following each component or pipe run, the boundary conditions are set for the next component or pipe run. This process continues until the outlet of the loop has been reached and temperatures and pressure drops in all piping runs and the IHX have been computed. At this point, the check valve pressure drop, pump pressure rise and operating speed, and height of coolant in the pump tank are all determined. The intermediate loop calculations now begin at the IHX secondary outlet, and a similar process continues until the steady-state thermal-hydraulic conditions in both loops are completely specified.

3.2.2.4 Transient Solution Approach

The simulation approach is strongly influenced by the nature of the flowing medium within the range of conditions of interest to the model. Thus, for liquid sodium loops, the time-dependent energy and momentum equations can be decoupled since the effect of pressure on subcooled liquid sodium properties is considered negligible. However, whereas the momentum equations are only loosely dependent on temperature through the sodium properties, the converse is not true, since convective terms in the energy equations are directly flow dependent. So, if hydraulic equations are solved first with coolant properties evaluated at temperatures

corresponding to the earlier time (one time step behind), the energy equations can then be readily solved, using the flow rates calculated from hydraulics at advanced time. More details on hydraulic and thermal simulation procedures will be presented in subsections 3.2.10 and 3.2.11.

The next few subsections will be devoted to description of the model equations for the individual components of the heat transport system.

3.2.3 Coolant Flow in Piping

By far the longest time the coolant spends in its passage through the heat transport circuit is in the piping runs interconnecting the different components. Hence, a thermal-hydraulic model for coolant flow in piping should form an important part of the overall system simulation model.

3.2.3.1 Heat Transfer

A detailed model with discrete parameter representation has been formulated for the heat transfer process in the piping. This is preferable to a simple transport delay model as used in other codes[3.19, 3.20] for two reasons. Firstly, the temperature signal is not only delayed in its passage from inlet to outlet of a pipe run, but also altered. Secondly, a detailed temperature distribution will aid in a more accurate determination of the gravitational heads, hence, the natural circulation capability of the heat transport system under loss of forced flow conditions.

Figure 3-18 shows the model configuration. In the axial direction the number of nodes in a pipe section is user specified, the number being influenced by the pipe length and the coolant velocity at full flow. In the radial direction, there are two nodes - coolant and pipe wall. Perfect
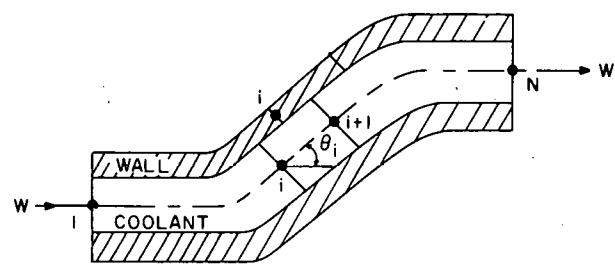
Figure 3-18. Nodal diagram for flow in piping.

insulation (i.e., negligible heat losses) is assumed on the wall outer surface. As shown in the figure, the coolant and wall nodes form a staggered arrangement.

Governing Equations

The governing equations are obtained by the nodal heat balance method, where energy balance is applied over the control volume formed between two adjacent fluid nodes to give the coolant equation, and the wall equation is related to the coolant equation through the heat flux term. These equations can be written for i=1, N-1, as follows:

Coolant:
$$\rho_{ii+1} A \Delta x \frac{de_{i+1}}{dt} = W(e_i - e_{i+1}) - U_{cw} A_{cw} \left[T_{ii+1} - T_{w_i} \right], \qquad (3\text{-}239)$$

where e_{i+1} is the coolant enthalpy at node i+1, T_{ii+1} is the average coolant temperature in the control volume between nodes i and i+1, expressed as

$$T_{ii+1} = \frac{T_i + T_{i+1}}{2}, \qquad (3\text{-}240)$$

ρ_{ii+1} is the coolant density corresponding to T_{ii+1}, W is the flow rate in the pipe, A is the cross-sectional area for flow given by $\frac{\pi D_i^2}{4}$, U_{cw} is the overall heat transfer coefficient between coolant and wall, evaluated at the midpoint between coolant nodes i and i+1, and A_{cw} is the area for heat transfer between coolant and wall, given by

$$A_{cw} = \pi D_i \Delta x. \qquad (3\text{-}241)$$

Inherent in Equation (3-239) is the assumption that

$$\frac{de_i}{dt} \approx \frac{de_{i+1}}{dt} \approx \frac{de_{i\,i+1}}{dt} \ . \tag{3-242}$$

Wall:

$$M_w \ C_{w_i} \ \frac{dT_{w_i}}{dt} = U_{cw} \ A_{cw} \left[T_{i\,i+1} - T_{w_i} \right], \tag{3-243}$$

where M_w = mass of wall for length Δx.

Finite Difference Forms

A fully implicit single-layer time integration scheme is applied to Equation (3-239) and the wall heat flux is allowed to be determined explicitly. With this, Equation (3-239) becomes

$$\rho_{i\,i+1}^{k} \ A\Delta x \ \frac{\left(e_{i+1}^{k+1} - e_{i+1}^{k} \right)}{h} = W^{k+1} \left(e_{i}^{k+1} - e_{i+1}^{k+1} \right)$$

$$- U_{cw}^{k} \ A_{cw} \left(T_{i\,i+1}^{k} - T_{w_i}^{k} \right), \tag{3-244}$$

and Equation (3-243) becomes

$$M_w \ C_{w_i}^{k} \ \frac{\left(T_{w_i}^{k+1} - T_{w_i}^{k} \right)}{h} = U_{cw}^{k} \ A_{cw} \left(T_{i\,i+1}^{k} - T_{w_i}^{k} \right), \tag{3-245}$$

where the index k represents previous time, $(k+1)$ represents the current (advanced) time, and h is the size of the timestep.

The flow rate W^{k+1} in Equation (3-244) is known since hydraulic calculations precede thermal calculations. Equations (3-244) and (3-245) are now

uncoupled and unknowns e_{i+1}^{k+1} and $T_{w_i}^{k+1}$ can be determined algebraically in a marching fashion going from i=1 to N-1.

It is worth noting that Equations (3-244) and (3-245) are for forward flow only. However, the code has the formulation in terms of general node counters so that the equations and the marching direction in each pipe section are automatically adjusted depending on the flow direction, be it forward or reverse.

Overall Heat Transfer Coefficients

In Equations (3-239) and (3-243), U_{cw} represents the overall heat transfer coefficient between coolant and pipe wall, and it is defined, based on the resistance concept (see Figure 3-19), as

$$\frac{1}{U_{cw}} = \frac{1}{h_{film}} + r_{wall} \cdot \tag{3-246}$$

The film heat transfer coefficient is given in terms of Nusselt number Nu_c as

$$h_{film} = \frac{Nu_c k_c}{D_i} , \tag{3-247}$$

where Nu_c is obtained from established correlations (see Chapter 5).

The wall resistance term is obtained by considering half the wall thickness (since that is where T_{w_i} is defined), and is expressed as

$$r_{wall} = \frac{D_i}{2} \frac{\ln\left(\frac{D_i + D_o}{2D_i}\right)}{k_w} , \tag{3-248}$$

- 102 -
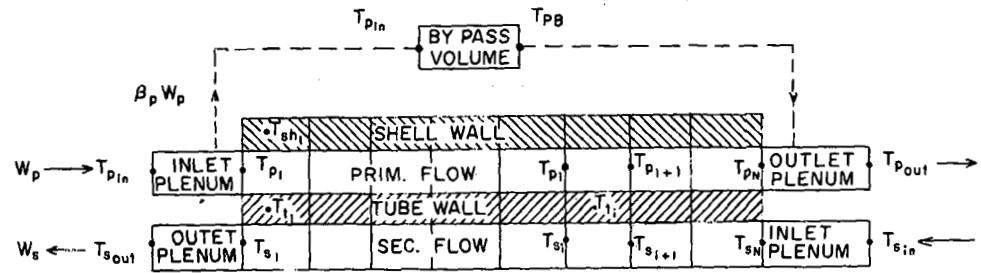
Figure 3-19. Nodal diagram for thermal balance.

where D_i, D_o are the pipe inner and outer diameters, respectively.

Since U_{cw} is dependent on material (k_c, k_w) and flow (Nu_c) properties, which are functions of temperature, it is evaluated at each nodal section of the pipe.

3.2.3.2 Pressure Losses

The hydraulic model essentially calculates the pressure losses in the pipe section as

$$(\Delta P_{f,g})_{pipe} = \text{acceleration loss} + \text{frictional loss}$$
$$+ \text{gravity loss} + \text{other losses}.$$

$$= \frac{W^2}{A^2}\left(\frac{1}{\rho_N} - \frac{1}{\rho_1}\right) + \frac{1}{2}\frac{W|W|}{DA^2}\int_0^L \frac{f}{\rho}\,dx + g\int_0^L \rho\sin\theta\,dx + K\frac{W|W|}{\overline{\rho}A^2},$$

$$(3\text{-}249)$$

where f is a flow-dependent friction factor (see Chapter 5 for details). K is a user-specified loss coefficient to account for losses due to bends, fittings, etc. Since $\frac{f}{\rho}$ is a continuous function, $\int_0^L \frac{f}{\rho}\,dx$ is evaluated using Simpon's rule. However, $\rho\sin\theta$, unlike $\frac{f}{\rho}$, is a discontinuous function, dependent on the pipe geometry; hence $\int_0^L \rho\sin\theta\,dx$ is evaluated rather as the summation $\Delta x\sum_{i=1}^{N-1}\rho_i\sin\theta_i$, where $\rho_i = \rho(T_i)$.

The importance of these pressure loss evaluations will be seen later under transient hydraulic simulation.

3.2.3.3 Steady-State Model

The energy equations are considerably simplified because of the

absence of time derivatives. In fact, with the assumption of perfect
insulation, the wall equation, i.e., Equation (3-243), disappears, and the
coolant equation simply gives

$$T_i = T_1 \qquad \text{for } i = 1,N \ . \qquad\qquad (3\text{-}250)$$

This equation also implies constant fluid properties over the pipe run.

The formulation for pressure losses in the piping is the same as for
transient, except that the acceleration term drops out, and f, ρ are constant,
simplifying the evaluation of frictional loss term. Since under steady-
state, momentum balance yields

$$\text{pressure drop} = \text{pressure losses}, \qquad\qquad (3\text{-}251)$$

there being no flow acceleration, the terms loss and drop can be used
interchangeably. Generally, the term "drop" has been used in the steady-
state analysis.

3.2.4 Intermediate Heat Exchanger

3.2.4.1 Description and Summary

The IHX in an LMFBR serves to physically separate the radioactive primary
coolant from the nonradioactive intermediate coolant while at the same time
thermally connecting the two circuits in order to transfer the reactor-
generated heat to the steam generator. Its location in each circuit of
current loop-type reactor system designs was illustrated by the example
configuration of Figure 3-16.

The IHX incorporates a liquid metal-to-liquid metal cylindrical shell-and-tube heat exchanger where primary coolant flows in the baffled shell and gives up its heat to secondary coolant flowing at a higher pressure in the tubes. The higher pressure in the secondary side is to assure no radioactive coolant entering into the secondary circuit in the event of a leak in any of the heat transfer tubes. Secondary fluid in the tubes is a natural choice because it is more economical to put the higher pressure fluid in the tubes,[3.18] besides the fact that primary coolant in the shell allows more design freedom.[3.21] All current designs use essentially counterflow arrangement. However, the model to be described is equally valid for parallel flow as well.

The thermal response, in terms of temperature distribution in the IHX and heat transfer from primary to secondary coolant within the heat exchanger, is predicted by the thermal model, which involves dividing the heat transfer region into a user-specified number of sections, and then applying energy balance over each section. The analysis includes mixing in plena, heat transfer with wall, fouling,and primary bypass flow. Fouling resistance is included as a user-specified parameter to allow the code to analyze the preaccident conditions of the plant at any stage of its operating life. The hydraulic response is obtained in terms of pressure drop characteristics on both primary and secondary sides of the IHX. The model includes variable friction factor in the heat transfer section, gravity heads, and losses due to contractions, expansions, etc. A loss coefficient has been introduced into the hydraulic model in order to absorb uncertainties in the evaluation of various losses within the heat exchange unit.

3.2.4.2 Energy Equations

If a detailed model is needed to describe the heat transfer process in the piping, there is even greater justification for a detailed model here, apart from the need to evaluate accurately the heat removal capability of the heat exchange unit at all times.

Figure 3-19 is a model diagram for the thermal model (under counterflow arrangement). All the heat transfer tubes have been shown as one representative tube. As in the piping, the coolant equations are derived using the nodal heat balance method.

Essential Features

Some features of the model are enumerated:

(1) user-specified number of equidistant axial nodes;

(2) variable material properties and heat transfer coefficients (functions of temperature, flow, etc.) which are evaluated locally;

(3) presence of bypass flow stream on primary side accounted for;

(4) ideal mixing plena at the inlet and outlet of each coolant stream;

(5) four radial nodes (secondary coolant, tube metal, primary coolant, shell wall);

(6) axial heat flow due to conduction in the metal wall is assumed negligible;

(7) fully developed convective heat transfer is assumed, i.e., entrance effects are neglected.

The tube and shell wall nodes (see Figure 3-19) lie in the midplane

between the fluid nodes, giving rise to a staggered nodal arrangement. Representative time-dependent equations are noted below.

Plenum primary inlet:

$$\rho V_{in} \frac{d}{dt} (e_{p_1}) = W_p' (e_{p_{in}} - e_{p_1}) , \qquad (3\text{-}252)$$

where

$$e_{p_{in}} = e(T_{p_{in}}) \text{ and } e_{p_1} = e(T_{p_1}) , \qquad (3\text{-}253)$$

V_{in} is the stagnant volume in the primary inlet plenum, and ρ is the average coolant density in the plenum. Further, from mass conservation, we have

$$W_p' = (1 - \beta_p) W_p , \qquad (3\text{-}254)$$

where β_p is the fraction of flow bypassing the active heat transfer region.

Plenum primary outlet:

$$\rho V_{out} \frac{d}{dt} (e_{p_{out}}) = W_p' e_{p_N} + \beta_p W_p e_{PB} - W_p e_{p_{out}} . \qquad (3\text{-}255)$$

Plenum primary bypass:

$$\rho V_{PB} \frac{d}{dt} (e_{PB}) = \beta_p W_p (e_{p_{in}} - e_{PB}) . \qquad (3\text{-}256)$$

Similar equations can be written for the inlet, outlet plena and downcomer

in the secondary side.

Active Heat-Transfer Region

Primary coolant:

$$\rho V_p \frac{d}{dt} (e_{p_{i+1}}) = W_p' (e_{p_i} - e_{p_{i+1}}) - U_{pt} A_{pt} (T_{p_{i\,i+1}} - T_{t_i})$$

$$- U_{psh} A_{psh} (T_{p_{i\,i+1}} - T_{sh_i}) . \qquad (3\text{-}257)$$

Secondary coolant:

$$\rho V_s \frac{d}{dt} (e_{s_i}) = W_s (e_{s_{i+1}} - e_{s_i}) + U_{st} A_{st} (T_{t_i} - T_{s_{i\,i+1}}) . \qquad (3\text{-}258)$$

Tube wall:

$$M_t C_{t_i} \frac{d}{dt} (T_{t_i}) = U_{pt} A_{pt} (T_{p_{i\,i+1}} - T_{t_i}) - U_{st} A_{st} (T_{t_i} - T_{s_{i\,i+1}}). \qquad (3\text{-}259)$$

Shell wall:

$$M_{sh} C_{sh_i} \frac{d}{dt} (T_{sh_i}) = U_{psh} A_{psh} (T_{p_{i\,i+1}} - T_{sh_i}) . \qquad (3\text{-}260)$$

In the above equations V_p, V_s are the control volumes between i and i+1 on primary and secondary sides, respectively. U_{pt}, U_{st}, U_{psh} denote the overall heat transfer coefficients and A_{pt}, A_{psh}, and A_{st} are the areas per length Δx for heat transfer between primary coolant and tube wall, primary coolant and shell wall, and secondary coolant and tube wall, respectively defined as

$$A_{pt} = \pi D_2 n_t \Delta x , \qquad (3\text{-}261)$$

$$A_{st} = \pi D_1 n_t \Delta x , \qquad (3\text{-}262)$$

$$A_{psh} = \frac{A_{sh}}{L} \Delta x \, , \qquad\qquad (3\text{-}263)$$

where n_t = number of active heat transfer tubes, A_{sh} is the shell heat transfer area, and L is the length of the active heat transfer region.

Equations (3-257) to (3-260), along with the plena equations, are integrated by a fully implicit single-layer scheme. The heat flux terms in Equations (3-257) and (3-258) are allowed to be determined explicitly, which uncouples them. These equations are then solved in a marching fashion without resorting to matrix inversion. At the same time since the heat fluxes in Equations (3-259) and (3-260) are evaluated implicitly, no stability limitations are imposed on the integration step size. The timestep control is achieved by regulating the relative change of the integrated variables from the standpoint of accuracy. This is required particularly since the heat flux terms, being allowed to lag in the coolant equations, could swamp the solution if unlimited step sizes were attempted.

The above equations, in the form shown, are valid for counterflow arrangement, positive flow only. However, they have been coded with general node counters to allow for reverse flow in either coolant stream, as also a choice of parallel or counterflow arrangement.

All functional relationships between enthalpy and temperature and vice versa were obtained from property relations (see Chapter 5).

Overall Heat Transfer Coefficients

In Equations (3-257) to (3-260), U_{pt}, U_{st}, and U_{psh} represent the over-all heat transfer coefficients from primary fluid to tube wall, from secondary fluid to tube wall, and from primary fluid to shell wall, respectively, and

are defined, based on the resistance concept, by:

$$\frac{1}{U_{pt}} = \frac{1}{h_{film,p}} + r_{wall,p} + \frac{1}{h_{foul,p}} \; , \tag{3-264}$$

$$\frac{1}{U_{st}} = \frac{1}{h_{film,s}} + r_{wall,s} + \frac{1}{h_{foul,s}} \; , \tag{3-265}$$

$$\frac{1}{U_{psh}} = \frac{1}{h_{film,p}} \; , \tag{3-266}$$

where the film heat transfer coefficients are calculated in terms of Nu by

$$h_{film,p} = \frac{Nu_{pt} \; k_p}{D_{h,p}} \; , \tag{3-267}$$

$$h_{film,s} = \frac{Nu_{st} \; k_s}{D_1} \; . \tag{3-268}$$

The Nusselt numbers, Nu_{pt} and Nu_{st}, are obtained from established correlations (see Chapter 5).

The wall resistance terms are obtained by dividing the tube wall thickness equally between primary and secondary sides, since T_t is defined at the midpoint of wall thickness.

$$r_{wall,p} = r_2 \frac{\ell n\left(\dfrac{2r_2}{r_1 + r_2}\right)}{k_t} \; , \tag{3-269}$$

and

$$r_{wall,s} = r_1 \frac{\ell n\left(\dfrac{r_1 + r_2}{2r_1}\right)}{k_t} \; . \tag{3-270}$$

Fouling is a time-dependent phenomenon, and the fouling resistances $\frac{1}{h_{foul,p}}$ and $\frac{1}{h_{foul,s}}$ are included as a user input quantity in order to lend capability to the model to better analyze the response of the heat exchange unit at any stage of its operating life.

The overall heat transfer coefficients, U_{pt} and U_{st}, are dependent on material (k_p, k_t, k_s) and flow (Nu_{pt}, Nu_{st}) properties, which are functions of temperature and, therefore, are evaluated at each nodal section along with the temperatures. Referring to Figure 3-19, for each i, k_t would be evaluated at i on the tube wall node whereas all other variables (k_p, k_s, Nu_{pt}, Nu_{st}) would be evaluated at the midpoint between the fluid nodes i and (i+1). The Nusselt numbers are obtained from established correlations.

There are three options available to the user in which either

(1) he supplies both A_p and $D_{h,p}$, or

(2) A_p is user input and $D_{h,p}$ is calculated from

$$D_{h,p} = \frac{4A_p}{n_t \pi D_2} \text{ , or}$$
(3-271)

(3) both A_p and $D_{h,p}$ are calculated by the code as follows:

$$A_p = n_t \frac{\pi D_2^2}{4} \left[\frac{2\sqrt{3}}{\pi} \left(\frac{P}{D_2} \right)^2 - 1 \right] ,$$
(3-272)

and $D_{h,p}$ is given by Equation (3-271). The Reynolds number for the primary side is defined as

$$Re = \frac{W_p D_{h,p}}{A_p \mu} ,$$
(3-273)

where A_p is the flow area on the shell-side. On the tube side, the Reynolds number is given by

$$Re = \frac{W_s D_1}{A_s \mu} \; ,$$

(3-274)

where A_s, the flow area through the tubes, is given as

$$A_s = n_t \frac{\pi D_1^2}{4} \; .$$

(3-275)

3.2.4.3 Pressure Losses

Figure 3-20 illustrates an example hydraulic profile of the IHX. The primary coolant rises in the inlet region, turns around, flows down around the tubes, and exits at the bottom through the outlet nozzle. The secondary (intermediate) coolant flows down the central downcomer into the bottom header (inlet plenum region) where it turns upward and distributes itself into the heat transfer tubes. The pressure losses on both primary and secondary sides of the IHX can be expressed as follows:

$$(\Delta P_{f,g})_{IHX} = \text{acceleration loss} + \text{frictional loss} + \text{gravity loss} + \text{inlet loss} + \text{exit loss} + \text{other losses}.$$

For the primary side this equation gives

$$(\Delta P_{f,g})_{IHX,p} = \frac{W_p'^2}{A_p^2} \left(\frac{1}{\rho_N} - \frac{1}{\rho_1} \right) + \frac{1}{2} \frac{W_p' |W_p'|}{D_{h,p} A_p^2} \int_0^1 \frac{f}{\rho} \, dx + \Delta P_g$$

$$+ K_{p_{in}} \frac{W_p |W_p|}{(\rho A^2)_{in}} + K_{p_{out}} \frac{W_p |W_p|}{(\rho A^2)_{out}} + K_p \frac{W_p |W_p|}{\overline{\rho A}_p^2} \; ,$$

(3-276)
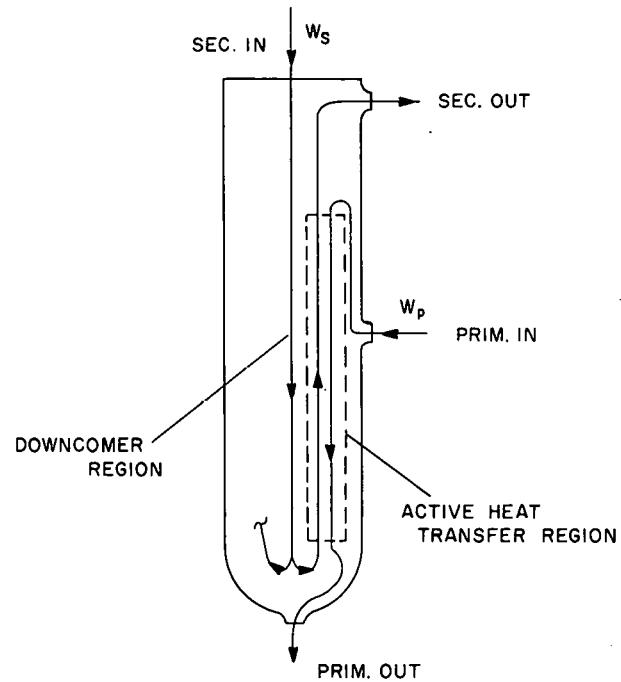
Figure 3-20. Hydraulic profile of IHX.

where

$$\Delta P_g = g(\rho \sin\theta \, \Delta x)_{inlet \ plenum} + g \int_0^L \rho \sin\theta \, dx + g(\rho \sin\theta \, \Delta x)_{outlet \ plenum},$$

(3-277)

$$W_p' = (1 - \beta_p) \, W_p,$$

(3-278)

and

$$\bar{\rho} = \frac{\rho_{in} + \rho_{out}}{2}.$$

(3-279)

K_{in} (K_{out}) is user specified and can represent expansion loss (contraction loss) from inlet pipe to the inlet plenum and nozzle losses, or it can also include inlet plenum losses due to turning, flow distribution, etc. A_{in} represents the area of primary piping at the IHX inlet. K_p is an uncertainty absorber that is either calculated during steady state if $\Delta P_{IHX,p}$ is known from flow testing (or other means), or is input by the user if $\Delta P_{IHX,p}$ is not known. Once determined or known, the value of K_p remains constant for transients. This is a useful parameter especially because of the difficult task of determining accurately all the losses in the complex internal geometry of the heat exchange unit.

Similarly, for the secondary side,

$$(\Delta P_{f,g})_{IHX,s} = \frac{W_s^2}{A_s^2} \left(\frac{1}{\rho_1} - \frac{1}{\rho_N} \right) + \frac{1}{2} \frac{W_s |W_s|}{D_1 A_s^2} \int_0^L \frac{f}{\rho} \, dx + \Delta P_g$$

$$+ K_{s_{in}} \frac{W_s |W_s|}{(\rho A^2)_{in}} + K_{s_{out}} \frac{W_s |W_s|}{(\rho A^2)_{out}} + \Delta P_{c,e} + K_s \frac{W_s |W_s|}{\bar{\rho} A_s^2},$$

(3-280)

where

$$\Delta P_g = g(\rho \sin\theta \, \Delta x)_{downcomer} + g(\rho \sin\theta \, \Delta x)_{inlet\ plen}$$

$$+ g \int_0^L \rho \sin\theta \, dx + g(\rho \sin\theta \, \Delta x)_{outlet\ plen} \, , \qquad (3\text{-}281)$$

and

$$\Delta P_{c,e} = K_c \frac{W_s |W_s|}{(\rho A^2)_{tube\ in}} + K_e \frac{W_s |W_s|}{(\rho A^2)_{tube\ out}} \, . \qquad (3\text{-}282)$$

K_s in Equation (3-280) is the uncertainty absorber for the secondary side. The friction factor f is a function of Reynolds number Re and the relative roughness of the channel $\frac{\varepsilon}{D_h}$. The same approach has allowed formulation of hydraulics in the shell (sodium) side of the superheater and evaporator as well.

3.2.4.4 Steady State Model

Energy Equations

To start the calculations, the boundary temperatures at one end of the IHX, in this case $T_{p_{in}}$ and $T_{s_{out}}$, are assumed to be known ($T_{p_{in}}$ is known from pipe calculations and $T_{s_{out}}$ is selected by the overall plant thermal balance). Applying thermal balance at the primary inlet plenum (see Figure 3-17) gives

$$W_p e_{p_{in}} - \left(\beta_p W_p e_{p_{in}} + W_p' e_{p_1} \right) = 0 \, . \qquad (3\text{-}283)$$

On simplification, this yields

$$T_{p_1} = T_{p_{in}} \, . \qquad (3\text{-}284)$$

Similarly, at the secondary outlet plenum,

$$T_s = T_{s_{out}}. \tag{3-285}$$

Thus, the boundary temperatures at one end of the active heat transfer section are known. Now, energy balance at each nodal section (see Figure 3-21) gives, for i=1, N-1:

primary fluid:

$$(1 - \beta_p) \; W_p \left[e_{p_i} - e_{p_{i+1}} \right] - U_{pt} \; A_{pt} \left[\frac{T_{p_i} + T_{p_{i+1}}}{2} - T_{t_i} \right] = 0; \tag{3-286}$$

tube wall:

$$U_{pt} \; A_{pt} \left[\frac{T_{p_i} + T_{p_{i+1}}}{2} - T_{t_i} \right] - U_{st} \; A_{st} \left[T_{t_i} - \frac{T_{s_i} + T_{s_{i+1}}}{2} \right] = 0; \tag{3-287}$$

secondary fluid:

$$(-L_{fd}) \; W_s \left[e_{s_{i+1}} - e_{s_i} \right] + U_{st} \; A_{st} \left[T_{t_i} - \frac{T_{s_i} + T_{s_{i+1}}}{2} \right] = 0, \tag{3-288}$$

where

$$L_{fd} = 1 \text{ for parallel flow,}$$
$$= -1 \text{ for counter flow,}$$

and

$$e_p = e(T_p),$$
$$e_s = e(T_s).$$

Equations (3-286) to (3-288), together with the functional relationships

- 117 -
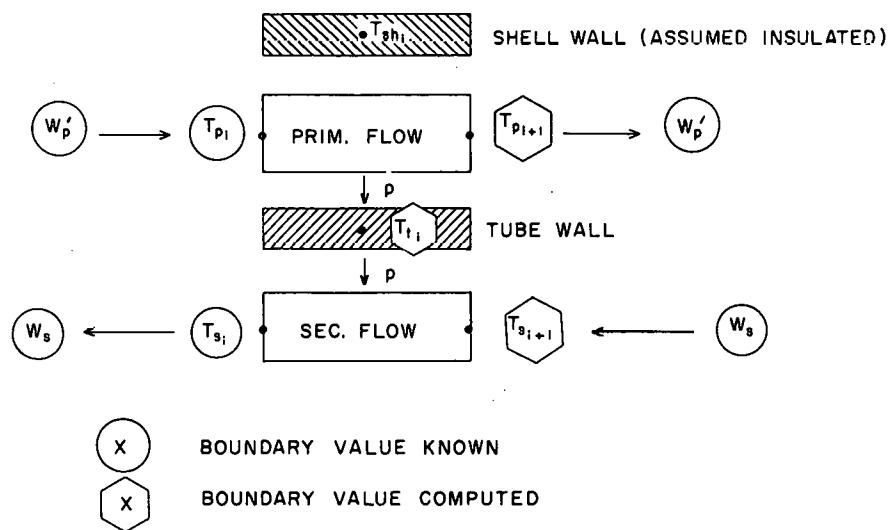
Figure 3-21. Steady state boundary conditions for an IHX nodal section.

of the enthalpies to temperatures, form a system of coupled, independent, nonlinear algebraic equations that are solved iteratively for each i to determine $T_{p_{i+1}}$, $T_{s_{i+1}}$, and T_{t_i}. For bypass mixing volume, referring back to Figure 3-19, we have

$$e_{PB} = e_{p_1} ,$$

or

$$T_{PB} = T_{p_1} , \tag{3-289}$$

and, at the primary outlet plenum:

$$e_{p_{out}} = (1 - \beta_p) e_{p_N} + \beta_p e_{PB} . \tag{3-290}$$

This yields

$$T_{p_{out}} = T\left(e_{p_{out}}\right) \tag{3-291}$$

At the secondary outlet plenum:

$$e_{s_{in}} = e_{s_N} ,$$

or

$$T_{s_{in}} = T_{s_N} . \tag{3-292}$$

With all temperatures thus obtained, an overall energy balance yields the heat transferred in the IHX as:

$$P_{loss,p} = W_p \left[e_{p_{in}} - e_{p_{out}} \right] , \tag{3-293}$$

and

$$P_{gain,s} = W_s \left[e_{s_{out}} - e_{s_{in}} \right] \qquad (3\text{-}294)$$

Equations (3-293) and (3-294) should yield results that match as closely as possible. Also, the heat transferred at the IHX should equal the reactor heat plus heat addition at the pump, to within specified limits. If not, the secondary outlet temperature has to be reselected and the computations repeated until convergence is obtained.

Pressure Drop

The formulation for hydraulics in the IHX is the same for steady state as in transient, except that "pressure drop" (ΔP_{IHX}) is used instead of "pressure loss" i.e., $(\Delta P_{f,g})_{IHX}$.

3.2.5 Centrifugal Pump

Liquid metal pumps for LMFBRs are vertically mounted, free-surface, centrifugal pumps driven by a variable speed motor. The impeller is attached to the bottom of a long shaft while the drive motor and its bearings are located at the upper end. The shaft is surrounded by a tank which extends upward from the pump casing to the motor mounting. In order to protect the bearings of the motor, the level of sodium in this tank is maintained well below the bearings, and an inert gas such as argon is used in the region above the liquid level.[3.22]

The sodium tank thus essentially sees only the inlet pressure to the pump at its lower end, and the cover gas pressure acting on the sodium free surface at its upper end. Hence, for modeling purposes, the pump is most

conveniently divided so that a free-surface pump tank is located just upstream of the pump impeller (see Figure 3-22). The impeller is modeled in terms of homologous head and torque relations which describe pump characteristics, and angular momentum balance to determine impeller speed during transient. The behavior of the free surface in the pump tank is described by a mass balance at the tank. The pump equations are solved together with the hydraulic equations in the loop, as part of hydraulic simulation, to account for the interaction between the impeller and the flow resistance in the circuit.

3.2.5.1 Impeller Dynamics

Homologous characteristics: Any given turbomachine, flowing full, has definite relationships between head and discharge, torque and discharge, horsepower and discharge, etc. for any given speed. These are the pump characteristics relating the different parameters. However, there are very few complete sets of data available. Also, we need characteristics for all ranges of flow and speed conditions. Here, homologous theory[3.23] can be used to advantage in two ways. Firstly, it permits the results of model tests with units of the same specific speed to be used. Secondly, by using dimensionless, homologous relationships, one can use one set of relationships to represent a whole series of different pumps having nearly the same specific speed.

In a severe accident such as a double-ended pipe break in the cold leg of a primary heat transport loop, the pump can go through several regimes of operation. These are illustrated in Figure 3-23. If the pump parameters are nondimensionalized through division by the appropriate

COVER GAS

PUMP TANK

COOLANT

H_{tot}

H_1

PUMP

$P_{in}, T_{in}, \rho_{in}$
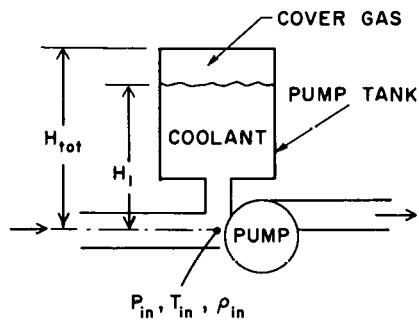
Figure 3-22. Schematic diagram for the pump model.

$\nu = Q/Q_R$
$a = \Omega/\Omega_R$

Ω Q

NORMAL PUMP
$(+\nu, +a)$

ENERGY DISSIP.
$(-\nu, +a)$

NORMAL TURBINE
$(-\nu, -a)$

REVERSE PUMP
$(+\nu, -a)$
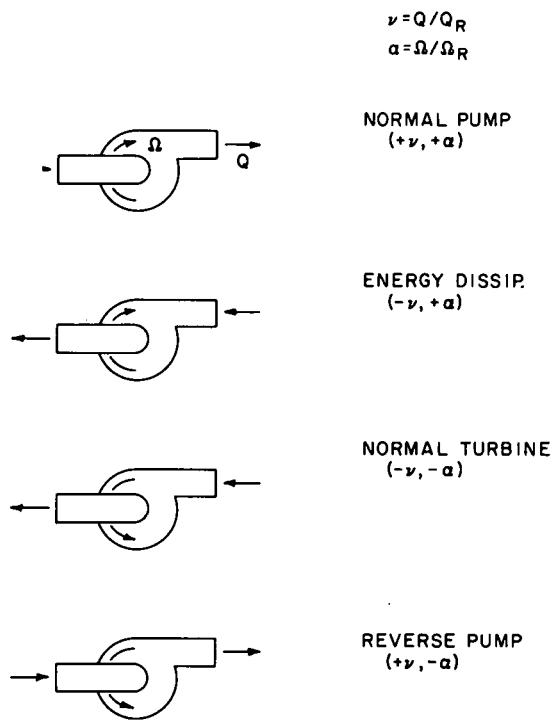
Figure 3-23. Pump configurations under different regimes of operation.

rated values as follows:

$$h = H/H_R, \quad \nu = W/W_R, \quad \alpha = \Omega/\Omega_R, \quad \beta = T_{hyd}/T_R, \qquad (3\text{-}295)$$

then these variables can be related by homologous curves, which are dimensionless extensions of the four-quadrant pump characteristics. Homologous curves for head discharge can be drawn by plotting

$$\frac{h}{\alpha^2} \quad \text{vs.} \quad \frac{\nu}{\alpha} \quad \text{in the range} \quad 0 \le \left|\frac{\nu}{\alpha}\right| \le 1 \; ,$$

$$\frac{h}{\nu^2} \quad \text{vs.} \quad \frac{\alpha}{\nu} \quad \text{in the range} \quad 0 \le \left|\frac{\alpha}{\nu}\right| < 1 \; ;$$

and, for torque-discharge, by plotting

$$\frac{\beta}{\alpha^2} \quad \text{vs.} \quad \frac{\nu}{\alpha} \quad \text{in the range} \quad 0 \le \left|\frac{\nu}{\alpha}\right| \le 1 \; ,$$

$$\frac{\beta}{\nu^2} \quad \text{vs.} \quad \frac{\alpha}{\nu} \quad \text{in the range} \quad 0 \le \left|\frac{\alpha}{\nu}\right| < 1 \; .$$

Figures 3-24 and 3-25 show these curves encompassing all four quadrants and all regions of pump operation. The curves can be read either in tabular form, as is done in the RELAP3B code,[3.24] or in the form of curve-fitted polynomials. In this analysis, the latter approach has been used. The polynomial relations are of the following form (up to 5th order):

$$\frac{\beta}{\alpha^2} \text{ or } \frac{h}{\alpha^2} = a_1 + a_2 \frac{\nu}{\alpha} + a_3 \left(\frac{\nu}{\alpha}\right)^2 + a_4 \left(\frac{\nu}{\alpha}\right)^3 + \ldots \qquad (3\text{-}296)$$

$$\text{in the range } 0 \le \left|\frac{\nu}{\alpha}\right| \le 1 \; ,$$
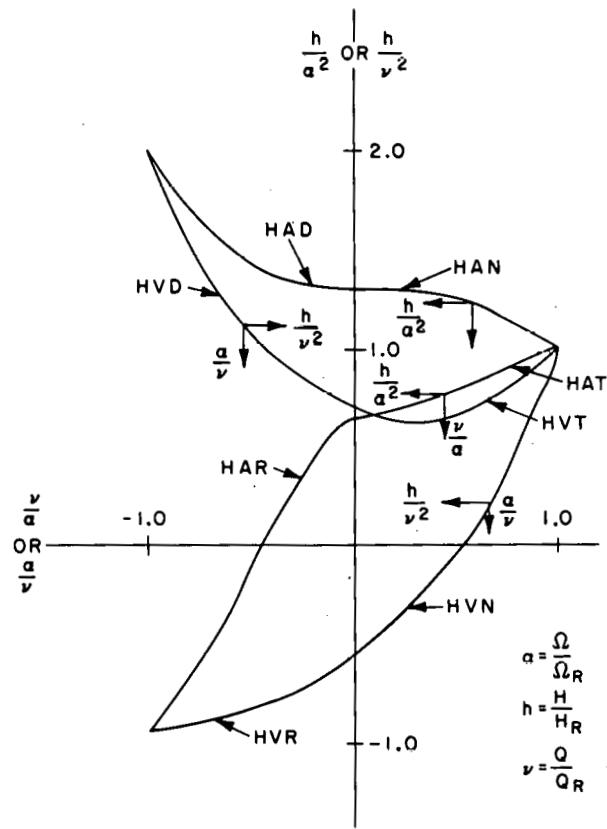
Figure 3-24. Complete homologous head curves.

- 124 -
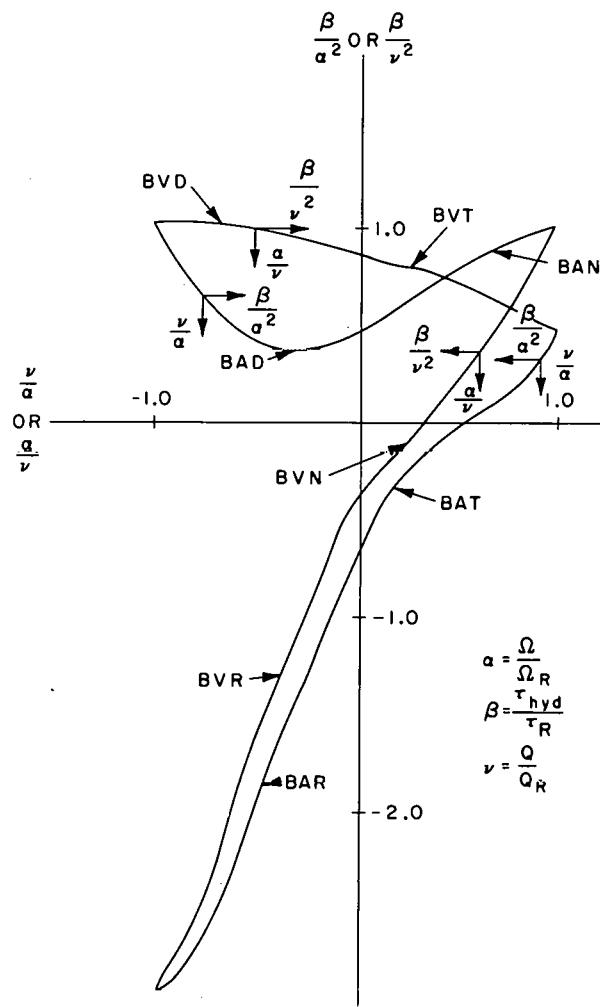
Figure 3-25. Complete homologous torque curves.

$$\frac{\beta}{\nu^2} \text{ or } \frac{h}{\nu^2} = a_1 + a_2 \frac{\alpha}{\nu} + a_3 \left(\frac{\alpha}{\nu}\right)^2 + a_4 \left(\frac{\alpha}{\nu}\right)^3 + \ldots \qquad (3\text{-}297)$$

$$\text{in the range } 0 \leq \left|\frac{\alpha}{\nu}\right| \leq 1 \text{ , }$$

where a_1, $a_2 \ldots a_6$ are user-specified constants for each polynomial. There are seven polynomials for head discharge and seven for torque discharge. This is a very convenient representation and avoids tabular look-ups during computation. The code has built in coefficients for a pump with specific speed 1800 (gpm units). This is in the range of specific speeds for LMFBR pumps. They have been obtained by curve-fitting the data points in[3.23] for all regions except reverse pump, where the values are not available. The reverse pump region corresponds to positive flow and negative impeller rotational speed (see Figure 3-23) and can occur during the later stages (t > 60 s) of the transient following pipe break, without pony motor. Values for this regime were generated from the Karman Knapp Circle diagram[3.25] and then curve-fitted.

Once the characteristics are available in this fashion, the head H and torque T_{hyd} can be determined, knowing rated values, operating speed, and flow rate at any time during transient. The head then yields the pressure rise across the pump as

$$(\text{PRISE})_{pump} = \rho_{in} \, gH \text{ , } \qquad (3\text{-}298)$$

where ρ_{in} is the density of coolant at pump inlet.
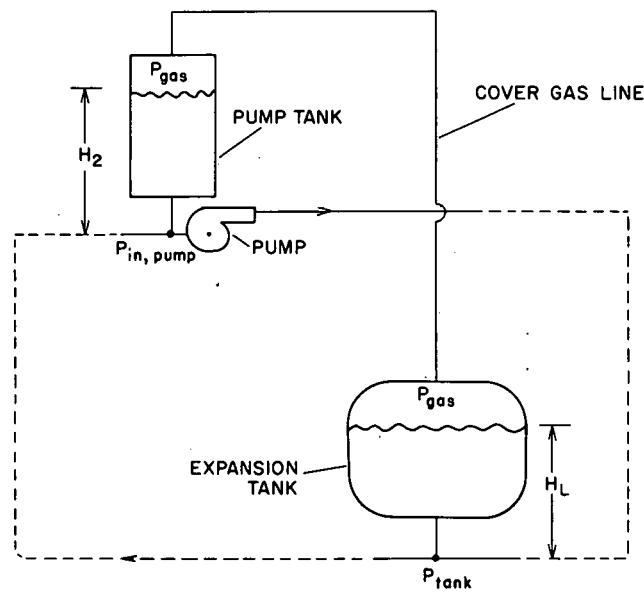
Figure 3-26. Schematic arrangement of surge and pump tanks.

Angular Momentum Balance

The hydraulic torque is used to determine the operating speed of the impeller. At any time during the transient, the rotational speed of the pump is obtained by integrating

$$I \frac{d\Omega}{dt} = \tau_m - \tau_{hyd} - \tau_{fr} \, , \qquad (3\text{-}299)$$

where I is the moment of inertia of shaft, impeller and rotating elements inside the motor, τ_m is the applied motor torque (= 0 during coastdown), τ_{hyd} is the hydraulic load torque due to fluid at the impeller, τ_{fr} is frictional torque, and Ω is the angular speed of the pump (rad/s).

3.2.5.2 Pump Tank (Reservoir)

Mass conservation at the pump tank (reservoir) yields the equation describing the level of coolant free surface below the cover gas as

$$A_{res} \frac{d}{dt} (\rho Z_R) = W_{in} - W_{out} \, , \qquad (3\text{-}300)$$

where A_{res} is the cross-sectional area of the pump tank, W_{in} is the mass flow rate into the pump, W_{out} is the mass flow rate out of the pump, Z_R is the height of coolant in the pump tank, and ρ is the density of coolant in the pump tank.

Assuming negligible gas flow to and from the cover gas volume in the reservoir and applying ideal gas law, the pressure of cover gas is determined from

$$P_{gas} = \frac{m_{gas} \, R_{gas} \, T_{gas}}{A_{res} \, (Z_{tot} - Z_R)} \, , \qquad (3\text{-}301)$$

- 128 -

where Z_{tot} is the total height of the pump tank. The temperature of cover gas is assumed to be the same as that of the coolant below it.

The inlet pressure to the pump impeller is governed by the behavior of coolant and cover gas in the pump tank, as follows:

$$P_{in} = P_{gas} + \rho g Z_R + K_{res} (W_{in} - W_{out}) \mid (W_{in} - W_{out}) \mid , \qquad (3\text{-}302)$$

where K_{res} is a user-specified loss coefficient for the tank orifice. Knowing P_{in}, $(PRISE)_{pump}$ from Equations (3-302) and (3-298), respectively, the pressure at pump discharge is simply obtained as the sum

$$P_{out} = P_{in} + (PRISE)_{pump} . \qquad (3\text{-}303)$$

3.2.5.3 Steady-State Model

The aim of the steady-state pump model is two-fold:

(1) to determine the pump operating conditions from its characteristics, and

(2) to determine the level of sodium in the pump tank.

Impeller

In the current approach, it was felt more logical to determine pump operating speed during steady state by matching pump head with load (total hydraulic resistance) in the circuit. Thus, for the primary loop, the required pressure rise across the pump is obtained from

$$(PRISE)_{pump} = \sum_{j} \Delta P_j + \Delta P_{CV} + \Delta P_{RV} , \qquad (3\text{-}304)$$

- 129 -

where ΔP_j's are the pressure drops in the piping runs and the IHX. ΔP_{CV} and ΔP_{RV} are, respectively, the pressure drops in the check valve and the reactor vessel.

Similarly, for the intermediate loop

$$(PRISE)_{pump} = \sum_j \Delta P_j + \Delta P_{IHX,s} + \Delta P_{SH} + \Delta P_{EV} , \qquad (3\text{-}305)$$

where ΔP_{SH}, ΔP_{EV} are the shell side pressure drops in the superheater and evaporator, respectively.

Pump head is related to $(PRISE)_{pump}$ by

$$H = (PRISE)_{pump} \ (\rho_{in} g). \qquad (3\text{-}306)$$

Knowing the head and flow rate, the pump operating speed can be obtained from the homologous head curve. Equation (3-296) can be re-arranged to give

$$a_1 \alpha^5 + a_2 \nu \alpha^4 + (a_3 \nu^2 - h)\alpha^3 + a_4 \nu^3 \alpha^2 + a_5 \nu^4 \alpha + a_6 \nu^5 = 0. \qquad (3\text{-}307)$$

This is a fifth degree polynomial equation in α, and is solved by a Newton's iteration method specially adapted for polynomials.[3.26] Pump steady-state operating speed can now be obtained from Equation (3-295), since both α and Ω_R are known.

Pump Tank

The cover gas pressure in the tank at steady state is assumed known.

For the primary loop, the gas pressure is generally equal to the gas pressure in the reactor vessel. In the case of the secondary loop, the gas pressure is generally equal to that in the surge tank. Thus, static pressure balance yields the height of coolant in the pump tank:

$$Z_R = (P_{in} - P_{gas}) / (\rho_{in} g),\tag{3-308}$$

where P_{in}, ρ_{in} are, respectively, the pressure and coolant density at pump inlet.

3.2.5.4 Pony Motor Option

While the arrangement of the primary and intermediate loops is intended to be such that natural circulation will provide sufficient heat transport for safe decay heat removal in the event of loss of all pumping power, the pumps may be equipped with pony motors (as is the case with CRBRP) supplied with normal and emergency power to provide forced circulation decay heat removal. Therefore, an option for pony motor has been included in the pump model. The pony motor is assumed to come into play when the main motor coasts down to a user-specified fraction of its rated speed. Once the pony motor takes over, the angular momentum balance equation i.e., Equation (3-299), is bypassed since pump speed remains constant. All other calculations remain the same.

3.2.6 Check Valve

A check valve in the heat transport system serves two purposes:

(1) to prevent thermal shock and flow reversal in a non-operating loop, and

- 131 -

(2) to allow operation of the plant while one loop is out of commission. The valve generally closes on reverse flow. The most commonly used type utilizes a pivoted disk which closes against a seat if flow is reversed.

The modeling approach for the check valve is similar to that employed in the RELAP3B code.[3.24] The flow-dependent pressure losses are assumed to be represented by

$$\Delta P_{CV} = c_i \frac{W|W|}{\rho_{CV}} , \qquad (3\text{-}309)$$

where ρ_{CV} is the coolant density at the check valve location. The model allows for three regions of operation for the valves, hence, three pressure loss coefficients are required:

(1) c_1 for positive flow with valve open,

(2) c_2 for negative flow with valve open,

(3) c_3 for negative flow with valve in closed position,

where c_1, c_2, c_3 are user-specified constants, in addition to P_{CV}, the back pressure required to close the valve. The code, however, has default values for these built in.

For positive flow, the valve remains open at all times. On reverse flow, the valve remains open as long as ΔP_{CV} with $c_i = c_2$ is less than P_{CV}. So far, both valves behave identically, but from the closed position, type 1 valve opens when ΔP_{CV} with $c_i = c_2$ is less than P_{CV}, whereas type 2 valve opens when ΔP_{CV} with $c_i = c_3$ is less than P_{CV}. At the user's option, the valve can also remain open in the failed position on reverse flow.

3.2.7 Surge Tank

The expansion (surge) tank in each intermediate loop serves to accommodate the coolant volume change due to thermal expansion over the operating range. Figure 3-26 shows a schematic diagram of the expansion tank and pump tank. Much like the reactor vessel upper plenum in the primary system, the surge tank adds another free surface in the intermediate loop. During steady-state operation, the pressure in the loop at the location of the surge tank is evaluated, assuming that the level in the tank is known by

$$P_{tank} = P_{gas} + \rho g Z_L \, . \qquad (3\text{-}310)$$

Here, ρ is the density of coolant at the tank location, and P_{gas} is the pressure of cover gas in the surge tank.

Equation (3-310) gives the starting point for evaluating all other pressures in the intermediate loop, once pressure drops in the different piping runs and components have been computed.

During transient, the equations are very similar to those for the pump tank and will not be repeated here.

3.2.8 Pipe-Break Model

During a pipe-break accident in an LMFBR, the coolant flow in the system is coupled to the break discharge rate. Since a coolant pipe is usually surrounded by an outer pipe, the discharge fluid, depending on the gap size between pipes, may expand freely or be space limited. In the current models,[3.20, 3.27] only two limiting types of breaks are

considered. One is the small leak for which a discharge coefficient of 0.611 is used. Another is the guillotine break with large separation distance so that the flow interaction between the two sides of the break can be neglected. The medium size breaks are treated as either small leaks or guillotine breaks. Furthermore, the effect of the sleeve or guard pipe flow confinement is not considered.

The existing models result in a conservative prediction for the discharge rate. However, this may not necessarily result in a conservative impact on the reactor core since the most conservative discharge rate results in an optimistic reactor scram time. This effect may be illustrated in Figure 3-27, which is a sketch of the flow rate and power versus time. For a predicted fast coolant loss, one predicts an early scram operation which is initiated by a sensing device; while in reality, with a slower coolant loss, the scram may be initiated at a later time, or it may not occur at all. Thus, it is important to employ a realistic rather than a conservative model to determine the discharge rate.

The model to be described[3.28] covers the entire range of break/pipe area ratios (from small leaks to guillotine breaks with large separation distance) as well as gap/pipe area ratios (from free-jet flow to confined flow).

The flow in the break region is considered to be quasi-steady and incompressible, and gravity effects are neglected. When the break area is small compared to the space between the coolant and outer pipes, the discharge fluid is assumed to behave as a free jet. When the break area is large such that the discharge fluid is limited by the gap space, confined flow theory accounting for dissipation pressure losses is employed.
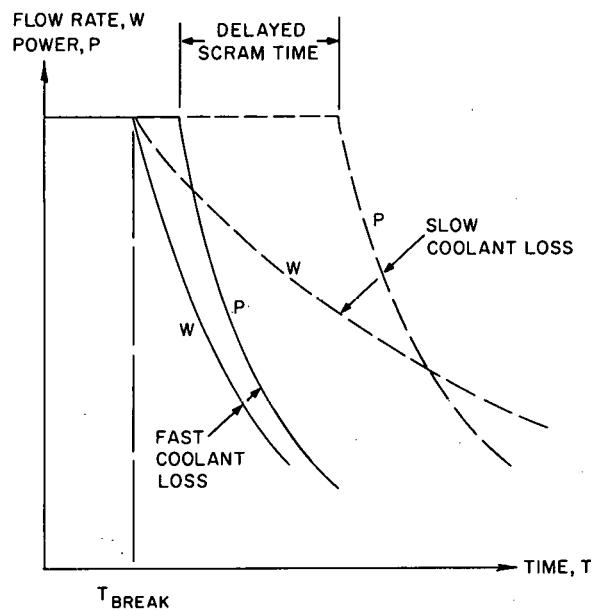
Figure 3-27. Effect of flow rate on scram time.

3.2.8.1 Free-Jet Discharge

Consider the case of small break/gap area ratio in Figure 3-28(a).
The jet then expands freely (i.e., with a free stream surface), and the
following conservation equations apply:

$$(v_1 - v_2)A_p = v_j (A_3 + A_4), \tag{3-311}$$

$$(p_1 - p_2)A_p = \rho(v_2^2 - v_1^2) A_p + \rho v_j^2 (A_4 - A_3), \tag{3-312}$$

$$P_\alpha + \frac{1}{2}\rho v^2 = p_j + \frac{1}{2}\rho v_j^2, \quad \alpha = 1,2, \tag{3-313}$$

where A, p, ρ, and v denote area, pressure, density, and velocity, res-
pectively. Here, A_p denotes the inside cross-sectional area of the pipe.

The pressure-velocity relations for upstream and downstream pipe
flows are given in the form

$$F_\alpha (P_\alpha, v_\alpha) = 0, \quad \alpha = 1,2. \tag{3-314}$$

In addition, if the discharge coefficient based on two-dimensional free
streamline analysis[3.29] without wall impingement effect is employed, one
deduces

$$\frac{2}{\pi}\left[(1 + r_1^2)\tanh^{-1} r_1 - (1 + r_2^2)\tanh^{-1} r_2 - \frac{1}{2}(r_1^2 - r_2^2)\tanh^{-1} \frac{1}{2}(r_1 + r_2)\right]$$

$$+ (r_1 - r_2)\left[1 - (r_1 + r_2)^2/4\right]^{\frac{1}{2}} = A_b/A_p , \tag{3-315}$$

PIPE BREAK MODEL

(a) FREE-JET EXPANSION

(b) CONFINED FLOW
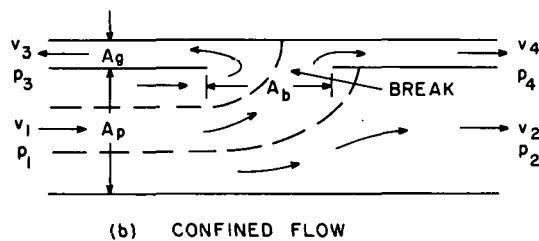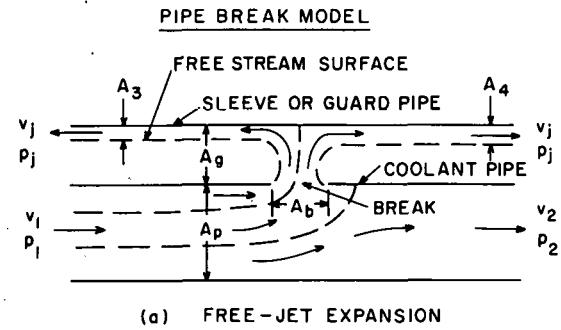
Figure 3-28. Illustration of pipe break flowfields.

where $r_1 = v_1/v_j$ and $r_2 = v_2/v_j$.

For given geometry and p_j, Equations (3-311) to (3-315) may be solved for p_1, p_2, v_1, v_2, v_j, A_3, and A_4. If coolant is discharged from both sides of pipe, v_2 is negative. The contraction (discharge) coefficient may be defined as $C_c = (A_3 + A_4)/A_b$. The discharge rate is then given by $Q = C_c A_b v_j$.

Equations (3-311) to (3-314) are applicable for jet discharge between two pipes as well as between two plane walls. Equation (3-315) is based on two-dimensional (planar) flow considerations. However, two-dimensional results have been known to be very good approximations for circular geometry,[3.29, 3.30] and it is expected that Equation (3-315) is a valid first approximation for various break configurations. It should be emphasized, however, that the impingement effect of the outer wall on the discharge coefficient has not been considered.

It may be noted that, using Equations (3-311) and (3-313), one may replace Equation (3-312) by

$$(v_1 + v_2)(A_3 + A_4) = 2v_j(A_4 - A_3) . \qquad (3-316)$$

3.2.8.2 Confined Flow

When the break/gap area ratio is large, the discharge rate is limited by the gap space [Figure 3-28(b)]. Confined flow is accompanied by significant dissipation losses in pressure. The governing equations are

$$(v_1 - v_2)A_p = (v_3 + v_4)A_g ; \qquad (3-317)$$

$$p_1 + \frac{1}{2}\rho v_1^2 = p_\beta + \frac{1}{2}\rho v_\beta^2 + \zeta_{1\beta}\frac{1}{2}\rho v_1^2, \quad \beta = 2,3,4 ; \tag{3-318}$$

$$F_\alpha(p_\alpha, v_\alpha) = 0, \quad \alpha = 1,2,3,4 ; \tag{3-319}$$

where $\zeta_{1\beta}$ denotes the loss coefficient from stream 1 to stream β, and Equation (3-319) represents a pipe flow relation for each stream. For given geometry, Equations (3-317) to (3-319) may be solved for p_α and v_α, where $\alpha = 1,2,3$, and 4.

The loss coefficients need to be determined by experiment. Meanwhile, however, a momentum principle employed by Taliev and described by Ginsberg[3.31] for converging and diverging pipe flows may be generalized to the present configuration to obtain the idealized formulas for the loss coefficients.

Consider the control volume for each separate stream as shown in Figure 3-29. The effective average pressure at a separating stream surface is assumed to be of the form $\bar{p} = p_1 + k\frac{1}{2}\rho v_1^2$, where k is a correction coefficient. For example, consider stream 1-2 shown at the bottom of Figure 3-29. A momentum balance for the control volume yields

$$p_1 A_{12} + (p_1 + k_b\frac{1}{2}\rho v_1^2)(A_2 - A_{12}) + \rho v_1^2 A_{12} = p_2 A_2 + \rho v_2^2 A_2 . \tag{3-320}$$

Simplified by the continuity relation of $v_1 A_{12} = v_2 A_2$, Equation (3-320) becomes

$$p_1 - p_2 = \rho v_2(v_2 - v_1)(1 + \frac{1}{2}k_b v_1/v_2) ; \tag{3-321}$$

similarly, for streams 1-3 and 1-4, one obtains

$$p_1 - p_3 = \rho v_3(v_3 + v_1)\cdot(1 - \frac{1}{2}k_a v_1/v_3) , \tag{3-322}$$
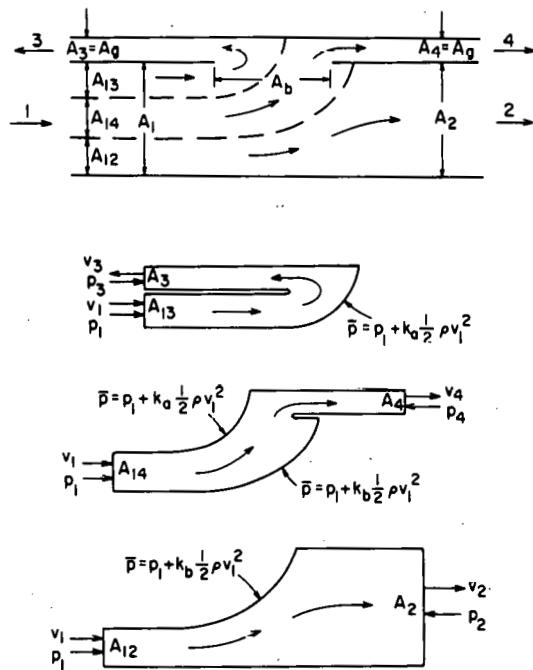
Figure 3-29. Control volumes for confined flow.

$$p_1 - p_4 = \rho v_4 (v_4 - v_1) + \frac{1}{2} \rho v_1 \left[(k_b - k_a) v_3 + k_b v_4 - k_a v_1 \right].$$

(3-323)

Comparison of Equations (3-321) to (3-323) with Equation (3-318) yields

$$\zeta_{12} = \left(1 - \frac{v_2}{v_1} \right)^2 + k_b \left(\frac{v_2}{v_1} - 1 \right),$$

(3-324)

$$\zeta_{13} = \left(1 + \frac{v_3}{v_1} \right)^2 - k_a \left(\frac{v_3}{v_1} + 1 \right),$$

(3-325)

$$\zeta_{14} = \left(1 - \frac{v_4}{v_1} \right)^2 + \left[(k_b - k_a) \frac{v_3}{v_1} + k_b \frac{v_4}{v_1} - k_a \right].$$

(3-326)

The correction factors k_a and k_b remain to be determined from experiments. Presently, however, the idealized values of $k_a = 0$ and $k_b = 0$ are assumed.

If the fluid is discharged from both sides of the pipe (v_2 is negative), then there exists only one separating stream surface, and the analysis is modified accordingly. Consider stream 2 to mix with part of stream 1 to exit at stream 4. Then, following the momentum principle, Equations (3-321) to (3-323) are replaced by

$$p_1 - p_2 = k_d \frac{1}{2} \rho v_1^2,$$

(3-327)

$$p_1 - p_3 = \rho v_3 (v_3 + v_1) (1 - \frac{1}{2} k_c v_1 / v_3),$$

(3-328)

$$p_1 - p_4 = \rho \left[v_4 (v_4 - v_1)_1 - v_2 (v_3 + v_4) \right]$$
$$+ \frac{1}{2} \rho v_1 \left[K_d v_1 \frac{v_3 + v_4}{v_1 - v_2} - k_c (v_3 + v_1) \right],$$

(3-329)

and Equations (3-324) to (3-326) are replaced by

$$\zeta_{12} = \left(1 - \frac{v_2}{v_1}\right)^2 + k_d , \tag{3-330}$$

$$\zeta_{13} = \left(1 + \frac{v_3}{v_1}\right)^2 - k_c \left(\frac{v_3}{v_1} + 1\right) , \tag{3-331}$$

$$\zeta_{14} = \left(1 - \frac{v_4}{v_1}\right)^2 - \frac{2v_2(v_3 + v_4)}{v_1^2} + k_d \frac{v_3 + v_4}{v_1 - v_2} - k_c \frac{v_3 + v_1}{v_1} . \tag{3-332}$$

Again, k_c and k_d are correction factors which are to be determined experimentally. These are presently given the idealized value of zero.

The equations for confined flow are applicable for both circular pipes and plane walls. However, for the unsymmetrical case such as a circular break on the inner pipe, it is implied in the analysis that the discharge fluid spreads out circumferentially to fill the cross-sectional gap area between the inner and outer pipes.

3.2.9 Guard Vessel

As a safety feature to minimize the effects of a pipe-break accident, guard vessels are provided around the reactor vessel, IHX, primary pump and all piping which is below the elevation of the tops of the guard vessels while their volume is such that reactor vessel coolant level does not fall below the outlet nozzle, so that the core is always submerged in coolant. If a break occurs such that coolant spills into the guard vessel eventually the vessel will fill up to the break height. Any level rise above that will create back pressure against further leakage.

An example configuration of a guard vessel for a break in the reactor vessel inlet region is shown in Figure 3-30. At any time t during the
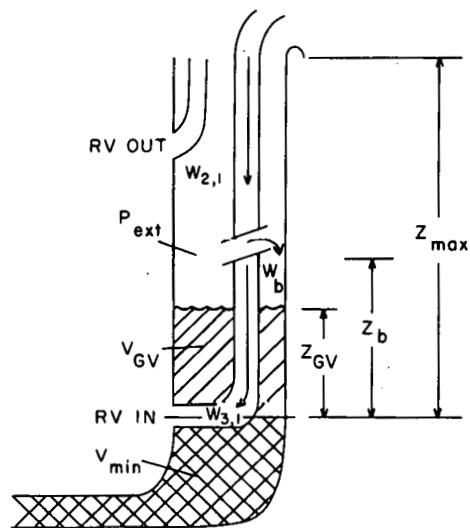
Figure 3-30. Guard vessel configuration for break
in the inlet region of the reactor vessel.

transient following a pipe break within a guard vessel, the volume of
sodium collected in the guard vessel can be determined by

$$V_{GV} = \int_{o}^{t} \frac{W_b}{\rho} \, dt \, , \tag{3-333}$$

where W_b, the break flow rate (for the case illustrated), is

$$W_b = W_{2,1} - W_{3,1} \, , \tag{3-334}$$

and ρ is the coolant density at break.

To determine the height of sodium in the guard vessel (Z_{GV}), a
detailed knowledge of configuration and dimensions of the annular and
bottom space between the component and its guard vessel is required. However,
a simpler and more general approach is to have a functional relationship between
Z_{GV} and V_{GV} in the form of a polynomial equation as follows:

$$Z_{GV} = c_1 + c_2 (V_{GV} - V_{min}) + c_3 (V_{GV} - V_{min})^2 \qquad \text{if } V_{GV} > V_{min} \, ,$$

and $\tag{3-335}$

$$Z_{GV} = 0 \qquad \qquad \text{if } V_{GV} \leq V_{min} \, ,$$

where c_1, c_2, c_3 are user-input coefficients depending on the geometry
of the guard vessel space. V_{min} is the volume required to fill up to the
lowest elevation of piping in the guard vessel. This is also a user-input
quantity and will be different for different guard vessels. V_{GV} is limited
by V_{max}, the maximum capacity of the guard vessel. It seems reasonable

to assume V_{max} to be the same for all guard vessels based on the volume contained in the upper plenum between the operating level and the minimum safe level. Z_{GV} is limited by Z_{max}, the height of the guard vessel. This can be different for different guard vessels.

With Z_{GV} known from Equation (3-335), the pressure external to the break can be determined by

$$P_{ext} = P_{atm} \qquad \text{if } Z_{GV} \leq Z_b \; ;$$

$$= P_{atm} + \rho g \, (Z_{GV} - Z_b) \quad \text{if } Z_{GV} > Z_b \; . \qquad (3\text{-}336)$$

3.2.10 Transient Hydraulic Simulation

The equations describing the behavior of pumps, free surface levels, pressure losses in different components, and flow rates in the loops, together constitute the hydraulic model for the heat transport system. Since the primary and intermediate systems are only thermally coupled, their hydraulic equations do not have to be solved together, even though it is advantageous to solve them at the same time.

In this section, the hydraulic model will be presented for the primary system. Similar analysis is performed for the intermediate loop also. Figure 3-31 is an example configuration for two loop simulation with a break near the reactor vessel in one of the loops and all intact loops being lumped together as the other loop. Note that the code has the more general formulation.

The model equations are described on the following page:
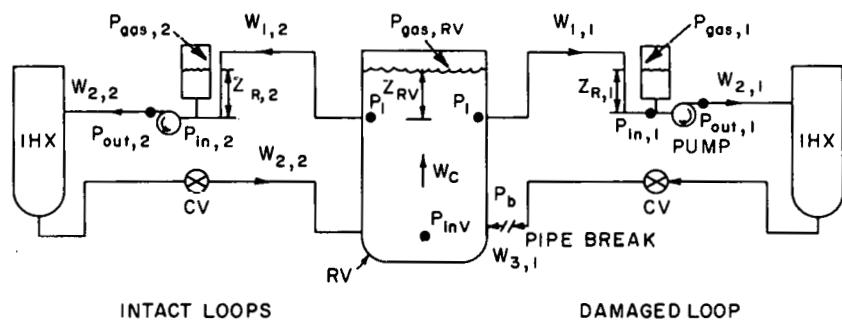
Figure 3-31.   Hydraulic profile of PHTS for test case.

Momentum: The uniform mass flow rate model implies that at any instant in time, flow rates are constant throughout the loops except at a free surface, or junction where several flows meet, or a break where there is flow loss. With this as background, the flow rates have been indicated in Figure 3-31. Volume-averaged momentum equations can be written relating rate of change of mass flow rate in a constant mass flow rate section to the terminal pressures and losses in that section.   These are

$$\frac{dW_{1,1}}{dt} \sum_{1,1} \frac{L}{A} = P_1 - P_{in,1} - \sum_{1,2} \Delta P_{f,g} \, , \tag{3-337}$$

$$\frac{dW_{2,1}}{dt} \sum_{2,1} \frac{L}{A} = P_{out,1} - P_{in,b} - \sum_{2,1} \Delta P_{f,g} \, , \tag{3-338}$$

$$\frac{dW_{3,1}}{dt} \sum_{3,1} \frac{L}{A} = P_{out,b} - P_{inV} - \sum_{3,1} \Delta P_{f,g} \, , \tag{3-339}$$

$$\frac{dW_{1,2}}{dt} \sum_{1,2} \frac{L}{A} = P_1 - P_{in,2} - \sum_{1,2} \Delta P_{f,g} \, , \tag{3-340}$$

$$\frac{dW_{2,2}}{dt} \sum_{2,2} \frac{L}{A} = P_{out,2} - P_{inV} - \sum_{2,2} \Delta P_{f,g} \, . \tag{3-341}$$

Here, $P_{in,b}$ and $P_{out,b}$ represent the pressure just upstream and downstream of the break, respectively.

Pump: The pressure in the loop at pump exit is obtained from Equation (3-303) in the pump model description.

Reservoir: The inlet pressure to the pump is obtained from Equation (3-302).   Level changes are described by Equation (3-300).

Reactor Vessel: The primary loop has interfaces with RV at inlet to loop and inlet to RV.   The level of sodium in the upper plenum is determined by

$$A_{RV} \frac{d}{dt} (\rho Z_{RV}) = W_c - W_{1,1} - n\, W_{1,2} \,, \qquad (3\text{-}342)$$

where

$$W_c = W_{3,1} + n\, W_{2,2} \,. \qquad (3\text{-}343)$$

P_1, the pressure at the inlet to the loop, is given by

$$P_1 = P_{gas,RV} + \rho g Z_{RV} \,. \qquad (3\text{-}344)$$

Equations (3-342) and (3-344), as well as the equation for $P_{gas,RV}$, are described in more detail under the "In-Vessel" section.

An equation to determine the vessel inlet pressure, which utilizes information from the primary loop hydraulic equations, as well as from vessel coolant dynamics, has been included as part of primary loop hydraulic model. The equation is obtained as follows (again, a two loop simulation is used for illustrative purposes):

Mass conservation at vessel inlet yields

$$W_c = n\, W_{2,2} + W_{3,1} \,, \qquad (3\text{-}345)$$

or, differentiating both sides,

$$\frac{dW_c}{dt} = n\, \frac{dW_{2,2}}{dt} + \frac{dW_{3,1}}{dt} \,. \qquad (3\text{-}346)$$

From loop hydraulics

$$\frac{dW_{2,2}}{dt} = \frac{P_{out,2} - P_{inV} - \sum_{2,2} \Delta P_{f,g}}{\sum_{2,2} \frac{L}{A}} \,, \qquad (3\text{-}347)$$

and, assuming break after pump:

$$\frac{dW_{3,1}}{dt} = \frac{P_{out,b} - P_{inV} - \sum_{3,1} \Delta P_{f,g}}{\sum_{3,1} \frac{L}{A}} \,. \qquad (3\text{-}348)$$

The core flow can be expressed as

$$W_c = \sum_j W_j \ , \quad j = 1, \ (N6CHAN + 1) \ , \tag{3-349}$$

where (N6CHAN + 1) represents the number of channels simulated in core, including bypass. Differentiating both sides of Equation (3-349) and substituting along with Equations (3-347) and (3-348) in Equation (3-346), one obtains

$$\sum_j \frac{dW_j}{dt} = n \frac{\left[P_{out,2} - P_{inV} - \sum_{2,2} \Delta P_{f,g} \right]}{\sum_{2,2} \frac{L}{A}} + \frac{\left[P_{out,b} - P_{inV} - \sum_{3,1} \Delta P_{f,g} \right]}{\sum_{3,1} \frac{L}{A}} \ . \tag{3-350}$$

Also, applying momentum balance across the core yields

$$\sum_j \frac{dW_j}{dt} = \sum_j \left[\frac{P_{inV} - P_1 - \left(\sum \Delta P_{f,g} \right)_j}{\left(\sum \frac{L}{A} \right)_j} \right] \ . \tag{3-351}$$

Substituting into Equation (3-350) and simplifying yields the vessel inlet pressure as

$$P_{inV} = (A + B + C) \Bigg/ \left\{ \sum_j \left[\frac{1}{\left(\sum \frac{L}{A} \right)_j} \right] + \frac{n}{\sum_{2,2} \frac{L}{A}} + \frac{1}{\sum_{3,1} \frac{L}{A}} \right\} \ , \tag{3-352}$$

where

$$A = \sum \left[\frac{P_1 + \left(\sum \Delta P_{f,g} \right)_j}{\left(\sum \frac{L}{A} \right)_j} \right] \ , \tag{3-353}$$

$$B = n \left[\frac{P_{out,2} - \sum_{2,2} \Delta P_{f,g}}{\sum_{2,2} \frac{L}{A}} \right] \ , \tag{3-354}$$

$$C = \left[\frac{P_{out,b} - \sum_{3,1} \Delta P_{f,g}}{\sum_{3,1} \frac{L}{A}} \right] . \qquad (3-355)$$

Equations (3-337) to (3-344), together with equations for pump, break, guard vessel, vessel inlet pressure, etc., form a system of ordinary differential equations and associated algebraic equations to be solved together to yield the flow rates, pressures, and free-surface levels in the system. These equations are solved using a predictor-corrector algorithm of the Adams type.

The solution procedure is shown in Figures 3-32 and 3-33 by means of simple flow charts. Only the main calculations involved during each timestep are indicated. During each step, several detailed subroutines, which are not shown here, are called.

3.2.11 Transient Thermal Simulation

On the primary side, the loop thermal calculations interface directly with the reactor vessel at loop inlet and outlet. On the intermediate side, the coupling is through heat fluxes at the steam generator.

As mentioned earlier, since the wall equations are decoupled from the coolant equations in each module, the solution can march in the direction of flow. Figures 3-34 and 3-35 show flow charts for the simulation procedure. To keep the illustration simple, the overall logic shown is for forward flow only; however, the code has the more general logic to handle reverse flow as well.

ENTER FLOWIT

STOP

NO

ARE ALL Z_R'S >0?

YES

DEFNIT

DEFINE W IN PIPES AND PUMP FOR EACH PRIMARY LOOP (K = 1, NILOOP)

PDFGIT

COMPUTE PRESSURE LOSSES IN ALL PRIMARY COMPONENTS

RESIT

COMPUTE P_{gas}, P_{in} & e_{in} TO PUMP, AND $\frac{d}{dt}(\rho Z_R)$ FOR ALL PRIMARY PUMP TANKS

PUMPIT

CALCULATE Q, H, τ_{hyd}, τ_{fr}, $(e\,RISE)_{pump}$, $(P\,RISE)_{pump}$, P_{out}, T_{out} OF PUMP, AND $\frac{d\Omega}{dt}$, FOR ALL PRIMARY PUMPS

PLOSIT

COMPUTE $\Sigma \Delta P_{f,g}$'s FOR ALL UNIFORM W SECTIONS IN EACH PRIMARY LOOP

K = 1

$P_{ext} = P_{atm}$

IS THERE A BREAK IN LOOP?

NO

YES

IS BREAK WITHIN GUARD VESSEL?

NO

YES

GVSLIT

CALCULATE Z_{gv}, P_{ext}, AND $\frac{d}{dt}(V_{gv})$

IS K = NILOOP?

NO

K = K + 1

YES

VESLIT (CALLS BREKIT)

OBTAIN P_l, etc. FROM R.V. COMPUTE P_{in} V_{in} IF THERE IS BREAK, COMPUTE $P_{in,b}$ & $P_{out,b}$

PRESIT

EVALUATE P_{in}, P_{out} FOR ALL UNIFORM W SECTIONS IN PRIMARY LOOPS

FUNCIT

CALCULATE ALL $\frac{dW}{dt}$'s

RETURN TO TRANSIENT HYDRAULIC DRIVER

Figure 3-32. Flow diagram for transient hydraulic simulation (primary system).

ENTER FLOW 2T

ARE ALL Z_R's >0? — NO → STOP

YES

DEFINE W FOR ALL INTERMEDIATE PIPES & PUMPS

COMPUTE PRESSURE LOSSES IN ALL INTERMEDIATE SYSTEM COMPONENTS

COMPUTE P_{gas}, P_{tank}, $\frac{d}{dt}(\rho Z_L)$ FOR ALL SURGE TANKS

COMPUTE $\frac{d}{dt}(\rho Z_R)$ P_{gas}, P_{in} & e_{in} TO PUMP FOR ALL PUMP TANKS

CALCULATE Q, H, T_{hyd}, T_{fr}, (e RISE)$_{pump}$, (P RISE)$_{pump}$, P_{out}, T_{out} OF PUMP, AND $\frac{d\Omega}{dt}$, FOR ALL INTERMEDIATE PUMPS.

COMPUTE $\sum \Delta P_{f,g}$'s FOR ALL UNIFORM W SECTIONS IN EACH INTERMEDIATE LOOP

IF THERE ARE BREAKS IN INTERMEDIATE SYSTEM, COMPUTE $P_{in,b}$, $P_{out,b}$ FOR EACH

EVALUATE P_{in}, P_{out} FOR ALL UNIFORM W SECTIONS IN INTERMEDIATE SYSTEM

CALCULATE ALL $\frac{dW}{dt}$'s

RETURN TO TRANSIENT HYDRAULIC DRIVER

Figure 3-33. Flow diagram for transient hydraulic simulation (intermediate system).

- 152 -
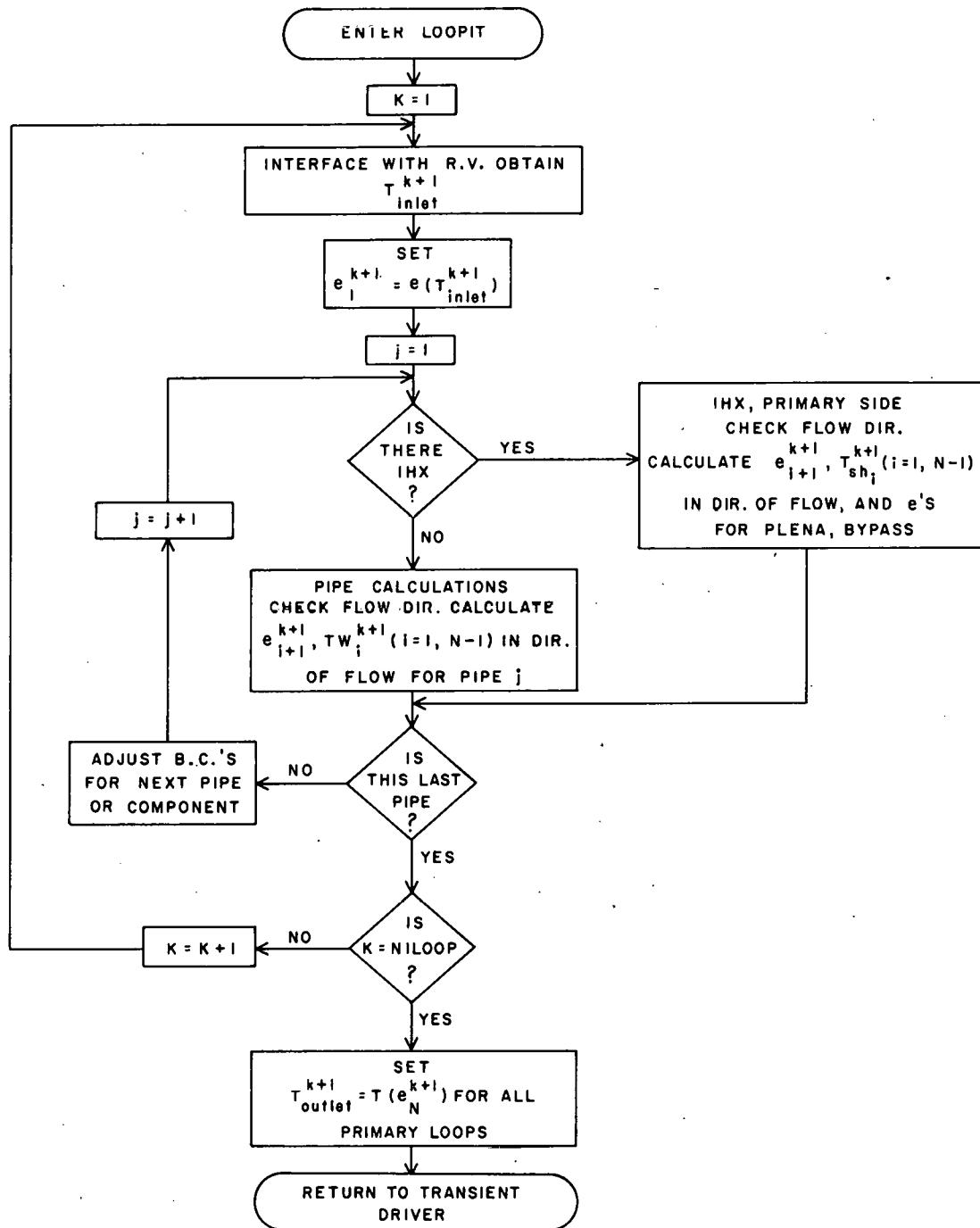
Figure 3-34. Flow diagram for transient thermal
simulation (primary system).

Left column:

ENTER LOOP 2T

K = 1

IS THERE SH ?

YES → $j_{START} = L2SH + 1$

SET B.C.'s FROM SH. $e_1^{K+1} = e_{out,SH}^{K+1}$

NO → $j_{START} = L2EV + 1$

SET B.C.'s FROM EV $e_1^{K+1} = e_{out,EV}^{K+1}$

$j = j_{START}$

IS THERE SH ?

NO → $j = j + 1$

YES

IS THIS PIPE AFTER EV ?

NO

YES

SET B.C.'s FROM EV $e_1^{K+1} = e_{out,EV}$

PIPE CALCULATIONS CHECK FLOW DIR. CALCULATE e_{i+1}^{K+1}, $T_{W_i}^{K+1}$ (i = 1, N−1) IN DIR. OF FLOW FOR PIPE j

ADJUST B.C's FOR NEXT PIPE OR COMPONENT

IS THIS LAST PIPE ?

NO → $j = j + 1$

YES → A

Right column:

A

IHX, SECONDARY SIDE CHECK FLOW DIR, AND FLOW CONFIG. CALCULATE e_{i+1}^{K+1}, $T_{t_i}^{K+1}$ (i = 1, N−1) IN DIRECTION OF FLOW. ALSO e's FOR PLENA, DOWNCOMER

$j_{START} = 1$

IS THERE SH ?

NO → $j_{END} = L2EV$

YES → $j_{END} = L2SH$

SET B.C.'s FROM IHX $e_1^{K+1} = e_{out,HX}^{K+1}$

$j = j_{START}$

PIPE CALCULATIONS

ADJUST B.C.'s FOR NEXT PIPE OR COMPONENT

IS THIS LAST PIPE

NO → $j = j + 1$

YES

SET B.C.'s FOR SH $e_{in,SH}^{K+1} = e_N^{K+1}$

IS K = NILOOP ?

NO → K = K + 1

YES

RETURN TO TRANSIENT DRIVER

Figure 3-35. Flow diagram for transient thermal simulation (intermediate system).

3.3 STEAM GENERATING SYSTEM

3.3.1 Introduction

The steam generator module of the SSC-L code is intended to be a general purpose simulation model for forced-recirculation or once-through sodium heated steam generating systems. The function of the steam generating system is to remove the reactor-generated heat from the intermediate heat transport system. The energy removed from the intermediate heat transport system is used to generate superheated steam which is fed to a steam turbine. The turbine converts the thermal energy contained in the superheated steam to mechanical energy which is in turn converted to electrical energy by a generator. The low pressure, saturated steam from the turbine exhaust is condensed to water in a condenser and the condensate returned to the steam generator through a series of feedwater heaters. As an example, a schematic diagram of the steam generating system for the CRBRP is shown in Figure 3-36. It consists of two forced-recirculation evaporators, a steam drum with internal separators, a recirculation pump, a superheater, a steam header, a steam turbine, a condenser, feedwater heaters, and all interconnecting pipings. Any other plant could very well use this recirculating type or once-through type steam generating system.

The complexity of the model is determined by the user who constructs the simulation model by interconnecting individual models of four types of components. These four components are a pipe, a heat exchanger, a pump, and an accumulator. These components are represented in the simulation model by a user-specified number of control volumes in pipes and heat exchangers and single-control volumes for pumps and accumulators. The steam turbine, condenser, and feedwater heating equipment are modeled, in the first order of approximation, in terms of user-supplied performance characteristics, such as the
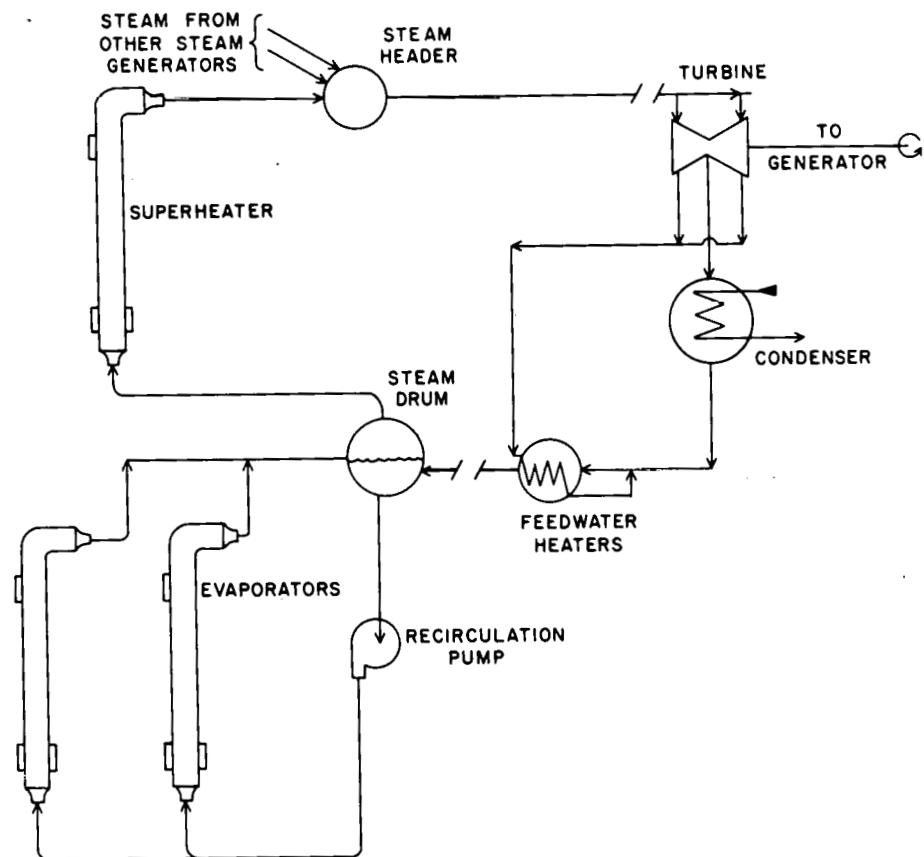
Figure 3-36. Schematic diagram of a steam
generating system.

turbine inlet pressure as a function of time and the feedwater enthalpy as a function of feedwater flow rate.

Once the geometry of the steam generating system has been defined by the user, it is divided into two groups of components for calculational purposes. These two groups are flow segments and accumulators. A flow segment is a linear series of components and contains only pipes, pumps, and heat exchangers. The division of a steam generating system into flow segments and accumulators can be illustrated using the CRBRP steam generating system. This system is divided into three flow segments and two accumulators. The steam drum and steam header are modeled as accumulators. The first flow segment represents the recirculation loop, beginning at the steam drum, proceeding to the recirculation pump, from the recirculating pump to the evaporator, then from the evaporator back to the steam drum. The second flow segment also begins at the steam drum, proceeds to the superheater and then to the steam header. The third and last flow segment consists of the piping from the steam header to the turbine inlet.

3.3.2 Model for Flow Segments

The type of flow model used to describe the flow segments in the simulation model is dictated by the type of transients to be analyzed by the model. The transients to be analyzed by the initial version of the SSC-L code are initiated by faults in the reactor core, the primary heat transport system, or the intermediate heat transport system. Their effect on the steam generating system is to change the amount of heat transported to the steam generators. This results in changes in the surface heat fluxes in the heat exchangers. Flow transients initiated by changes in the surface heat fluxes are classified as intermediate speed transients for which the momentum integral flow model is appropriate.[3.9]

- 157 -

3.3.2.1 Conservation Equations

The basic one-dimensional conservation equations for a constant area duct are[3.32]

mass:

$$\frac{\partial \rho}{\partial t} + \frac{1}{A} \frac{\partial W}{\partial z} = 0 \quad ; \qquad (3\text{-}356)$$

energy:

$$\frac{\partial}{\partial t}(\rho E - P) + \frac{1}{A} \frac{\partial}{\partial z}(WE) = \frac{P_h}{A} q \quad ; \qquad (3\text{-}357)$$

momentum:

$$\frac{1}{A} \frac{\partial W}{\partial t} + \frac{1}{A^2} \frac{\partial}{\partial z} \frac{W^2}{\rho} = -\frac{\partial P}{\partial z} - \frac{f|W|W}{2\rho A^2 D_h} - \rho g \quad . \qquad (3\text{-}358)$$

The sonic effects associated with the fluid compressibility can be eliminated by assuming that the fluid density is a function of enthalpy only,

$$\rho = \rho(E, P_r) \quad , \qquad (3\text{-}359)$$

where P_r is a suitably chosen spatially constant reference pressure.[3.9] It will be shown later that this reference pressure must be constant in order to remove the sonic effects associated with the fluid compressibility.

In order to integrate these equations to determine the time-dependent behavior of the enthalpy and flow, their spatial derivatives must be approximated. A nodal approximation, rather than a finite difference approximation, was chosen in order to stabilize and increase the accuracy of the calculations. This was done because when discontinuities in the material properties and their derivatives are encountered (i.e., the density derivatives are discontinuous across the two saturation lines, the largest discontinuity being

at the liquid saturation line)[3.33, 3.34] the conventional finite differ-
ence approximation would require placing a movable node at this discon-
tinuity.[3.35] There are other methods of reducing the effects of discon-
tinuities in the derivatives of the fluid properties,[3.36] but they can
be seen to be variants of the nodal approximation of spatial derivatives.

3.3.2.2 Nodal Form of Conservation Equations

3.3.2.2.1 Thermal Equations

The nodal form of the one-dimensional conservation equations for mass
and energy are formed by integrating the partial differential form of these
equations over a control volume extending from Z_{i-1} to Z_i:

mass:

$$A \int_{Z_{i-1}}^{Z_i} \frac{\partial \rho}{\partial t} \, dz + A \int_{Z_{i-1}}^{Z_i} \frac{1}{A} \frac{\partial W}{\partial z} \, dz = 0 \quad ; \qquad (3\text{-}360)$$

energy:

$$A_i \int_{Z_{i-1}}^{Z_i} \frac{\partial}{\partial t} (\rho E - P_r) \, dz + A_i \int_{Z_{i-1}}^{Z_i} \frac{1}{A} \frac{\partial}{\partial z} (WE) \, dz = A_i \int_{Z_{i-1}}^{Z_i} \frac{P_h}{A} q \, dz. \qquad (3\text{-}361)$$

Defining the volume averages as

$$m_i = \frac{1}{Z_i - Z_{i-1}} \int_{Z_{i-1}}^{Z_i} \rho \, dz \quad , \qquad (3\text{-}362)$$

$$e_i = \frac{1}{Z_i - Z_{i-1}} \int_{Z_{i-1}}^{Z_i} \rho E \, dz \quad , \qquad (3\text{-}363)$$

$$\langle q \rangle_i = \frac{1}{Z_i - Z_{i-1}} \int_{Z_{i-1}}^{Z_i} q \ dz \quad , \tag{3-364}$$

the nodal form of the conservation equations becomes:

mass:

$$(\Delta Z_i) \frac{\partial m_i}{\partial t} + \frac{1}{A_i} (W_i - W_{i-1}) = 0 \quad ; \tag{3-365}$$

energy:

$$(\Delta Z_i) \frac{\partial e_i}{\partial t} - (\Delta Z_i) \frac{\partial P_r}{\partial t} + \frac{1}{A_i} (W_i E_i - W_{i-1} E_{i-1}) = \left(\frac{P_h}{A}\right)_i (\Delta Z_i) \langle q \rangle_i \quad . \tag{3-366}$$

Remembering that the fluid density is a function of enthalpy only, and assuming that enthalpy varies linearly with position in the control volume, the volume averages may be written as

$$m_i = \frac{1}{E_i - E_{i-1}} \int_{E_{i-1}}^{E_i} \rho(E, P_r) \ dE = m_i(E_{i-1}, E_i, P_r) \tag{3-367}$$

and

$$e_i = \frac{1}{E_i - E_{i-1}} \int_{E_{i-1}}^{E_i} \rho(E, P_r) E \ dE = e_i(E_{i-1}, E_i, P_r) \quad . \tag{3-368}$$

Here, the volume averages were defined in terms of the enthalpy at the ends of the control volume.[3.33] The derivations of m_i and e_i in terms of E_i and E_{i-1} are given in Appendix A. Using these definitions of the volume averages, the mass and energy equations become

mass:

$$\left(\frac{\partial m_i}{\partial E_{i-1}}\right) \frac{dE_{i-1}}{dt} + \left(\frac{\partial m_i}{\partial E_i}\right) \frac{dE_i}{dt} + \left(\frac{\partial m_i}{\partial P_r}\right) \frac{dP_r}{dt} + \frac{1}{A_i} \left(\frac{W_i - W_{i-1}}{\Delta Z_i}\right) = 0 \quad ; \tag{3-369}$$

energy:

$$\left(\frac{\partial e_i}{\partial E_{i-1}}\right) \frac{dE_{i-1}}{dt} + \left(\frac{\partial e_i}{\partial E_i}\right) \frac{dE_i}{dt} + \left(\frac{\partial e_i}{\partial P_r}\right) \frac{dP_r}{dt} - \frac{dP_r}{dt} + \frac{1}{A_i} \left(\frac{W_i E_i - W_{i-1} E_{i-1}}{\Delta Z_i}\right) = \left(\frac{P_h}{A}\right)_i \langle q \rangle_i \tag{3-370}$$

This particular form of the conservation equations has been found to an unrealistic (false) numerical diffusion. To reduce this diffusion, the assumption is made that the time rate of change of enthalpy at the upstream end of the control volume is equal to the time rate of change of enthalpy at the downstream end of the control volume, i.e.,

$$\frac{dE_{i-1}}{dt} = \frac{dE_i}{dt}$$

(3-371)

Using this assumption, the mass and energy equations become,

mass:

$$\left(\frac{\partial m_i}{\partial E_{i-1}} + \frac{\partial m_i}{\partial E_i}\right)\frac{dE_i}{dt} + \frac{\partial m_i}{\partial P_r}\frac{dP_r}{dt} + \frac{1}{A_i}\frac{(W_i - W_{i-1})}{\Delta Z_i} = 0 \quad ;$$

(3-372)

energy:

$$\left(\frac{\partial e_i}{\partial E_{i-1}} + \frac{\partial e_i}{\partial E_i}\right)\frac{dE_i}{dt} + \left(\frac{\partial e_i}{\partial P_r} - 1\right)\frac{dP_r}{dt} + \frac{1}{A_i}\left(\frac{W_i E_i - W_{i-1} E_{i-1}}{\Delta Z_i}\right) = \left(\frac{P_h}{A_i}\right)\langle q \rangle_i \quad .$$

(3-373)

which is equivalent to donor cell differencing. It should be noted that this approximation was also used in Section 3.2.2. These equations are applied to each control volume in the pipes, heat exchangers, and pumps in each flow segment.

3.3.2.2.2 Hydraulic Equations

Because the pressure is assumed to be constant with respect to position in the flow segment, the momentum equation must be integrated over all control volumes in the flow segment. This integration yields

$$I\frac{d}{dt}\langle W \rangle = (\Delta P - F) \quad ,$$

(3-374)

where the average flow rate $\langle W \rangle$ is given by

$$\langle W \rangle = \frac{\int_{Z_I}^{Z_0} \frac{W}{A} \, dz}{I} \quad , \tag{3-375}$$

and the inertance of the flow segment is given by

$$I = \int_{Z_I}^{Z_0} \frac{dz}{A} \quad . \tag{3-376}$$

The total pressure force, ΔP, acting on the flow loop is the difference between the sum of the imposed pressure drop and the pump pressure rise given by

$$\Delta P = P_I - P_0 + \Delta P_p \quad , \tag{3-377}$$

and the total flow resistance, F, given by

$$F = \int_{Z_I}^{Z_0} \frac{1}{A^2} \frac{\partial}{\partial z} \left(\frac{W^2}{\rho}\right) dz + \int_{Z_I}^{Z_0} \frac{f|W|W}{2\rho A^2 D_h} \, dz + \int_{Z_I}^{Z_0} \rho g \, dz + \sum_j \left(\frac{K|W|W}{2\rho A^2}\right)_j \cdot \tag{3-378}$$

Note that the last term in the above equataion has been added to represent pressure losses due to changes in flow area, fittings, valves, etc. The total resistance, F, may be written as the sum of the flow resistance of the individual control volumes,

$$F = \sum_{i=1}^{N} \frac{1}{A_i^2} \left(\frac{W_i^2}{\rho_i} - \frac{W_{i-1}^2}{\rho_{i-1}}\right) + \sum_{i=1}^{N} \int_{Z_{i-1}}^{Z_i} \frac{f|W|W}{2\rho A^2 D_h} \, dz + \sum_{i=1}^{N} \int_{Z_{i-1}}^{Z_i} \rho g \cdot dz$$

$$+ \sum_j \left(\frac{K|W|W}{2\rho A^2}\right)_j \quad . \tag{3-379}$$

- 162 -

Assuming that the flow rate in any control volume varies linearly with position in the control volume, the average flow rate in the flow segment may be written as

$$\langle W \rangle = \frac{1}{I} \sum_{i=1}^{N} \frac{\Delta Z_i}{2A_i} (W_i + W_{i-1}) \quad . \tag{3-380}$$

The integrated momentum equation gives only one equation relating the (N+1) flow rates in a flow segment containing N control volumes so that N additional equations are needed. One way in which these N additional equations, which define the flow rate distribution, may be found is by eliminating the enthalpy derivative from the mass equation [Equation (3-356)] by use of the energy equation [Equation (3-357)]. The mass and energy equations written in terms of pressure and enthalpy are, respectively,

mass:

$$\left(\frac{\partial \rho}{\partial E}\right) \frac{dE}{dt} + \left(\frac{\partial \rho}{\partial P_r}\right) \frac{dP_r}{dt} + \frac{1}{A} \frac{\partial W}{\partial z} = 0 \quad , \tag{3-381}$$

energy:

$$\rho \frac{dE}{dt} - \frac{dP_r}{dt} + \frac{W}{A} \frac{\partial E}{\partial z} = \frac{P_h}{A} q \quad . \tag{3-382}$$

Eliminating the time derivative of the enthalpy, we obtain

$$\frac{1}{A} \frac{\partial W}{\partial z} = -\frac{1}{\rho} \left(\frac{\partial \rho}{\partial E}\right) \left[\frac{P_h}{A} q + \frac{dP_r}{dt} - \frac{W}{A} \frac{\partial E}{\partial z}\right] - \frac{\partial \rho}{\partial P_r} \frac{dP_r}{dt} \quad . \tag{3-383}$$

Collecting the pressure terms, we find

$$\frac{1}{A} \frac{\partial W}{\partial z} = -\frac{1}{\rho} \frac{\partial \rho}{\partial E} \left[\frac{P_h}{A} q - \frac{W}{A} \frac{\partial E}{\partial z}\right] - \frac{1}{a_r^2} \frac{dP_r}{dt} \quad , \tag{3-384}$$

where

$$a_r^2 = \left[\frac{1}{\rho} \left(\frac{\partial \rho}{\partial E}\right) + \left(\frac{\partial \rho}{\partial P_r}\right)\right]^{-1} \quad . \tag{3-385}$$

- 163 -

We can see from Equation (3-384) that the sonic effects are included. They are removed when the reference pressure is constant in time. This relation can now be integrated over the N control volumes to yield N equations relating the flow rates at the ends of the control volumes to the reference pressure and the enthalpies at the ends of the control volumes.

3.3.2.3 Pump Model

The hydraulic model of the pump is very simple. The pump pressure rise is given by

$$\Delta P_p = \rho g \, H_p \quad , \tag{3-386}$$

where H_p is the pump head. The pump head is determined from the pump characteristics as a function of pump speed and pump flow rate. For this simple model, quadratic characteristics are assumed, so that the pump head is given by

$$H_p = H_r \left[(1 - \alpha) \, \omega_{rel}^2 - \alpha \, W_{rel}^2 \right] \quad . \tag{3-387}$$

The relative pump speed, ω_{rel}, and the relative pump flow rate, W_{rel}, are their instantaneous values divided by pump speed and flow rate at rated conditions, respectively. The relative pump speed is constant during operation until it is turned off, after which it decays according to

$$\omega_{rel} = \frac{1}{1 + t/\tau_p} \tag{3-388}$$

where t is the time since the pump was turned off and τ_p is a user input decay constant. The instantaneous pump flow rate is the flow at the inlet of the pump determined from the overall hydraulic model. Mass storage in the pump

as well as the enthalpy rise in the pump are neglected.

3.3.3 Model for Accumulators

3.3.3.1 Conservation Equations

The conservation equations for the accumulators are

mass:

$$\frac{\partial \rho}{\partial t} + \frac{1}{A} \frac{\partial W}{\partial z} = 0 \quad ; \qquad (3\text{-}389)$$

energy:

$$\frac{\partial}{\partial t} (\rho E - P) + \frac{1}{A} \frac{\partial}{\partial z} (WE) = 0 \quad \cdot \qquad (3\text{-}390)$$

The fluid in the accumulators is assumed to be stagnant. Therefore, the momentum equation for the accumulators is satisfied identically.

3.3.3.2 Nodal Form of Conservation Equations

The nodal form of the conservation equations are found by integrating the partial differential equations over the volume of the accumulator. Thus,

mass:

$$\int_V \frac{\partial \rho}{\partial t} \, dv + \int_V \frac{1}{A} \frac{\partial W}{\partial z} \, dv = 0 \quad ; \qquad (3\text{-}391)$$

energy:

$$\int_V \frac{\partial}{\partial t} (\rho E - P) \, dv + \int_V \frac{1}{A} \frac{\partial (WE)}{\partial z} \, dv = 0 \quad \cdot \qquad (3\text{-}392)$$

Defining the volume averages as before, we obtain

$$V \frac{d\rho}{dt} = \sum_{j=1}^{J} W_j \quad , \qquad (3\text{-}393)$$

and

$$V \frac{d}{dt} (\rho E) - V \frac{dP}{dt} = \sum_{j=1}^{J} W_j E_j \quad , \qquad (3\text{-}394)$$

- 165 -

where V is the volume of the accumulator and the summations are over all flows into or out of the accumulator. Note that each accumulator is represented by a single control volume. Using the equation or state to eliminate the time derivatives of the density, we obtain

$$\frac{\partial \rho}{\partial E} \cdot \frac{dE}{dt} + \frac{\partial \rho}{\partial P} \cdot \frac{dP}{dt} = \frac{1}{V} \sum_{j=1}^{J} W_j \qquad (3\text{-}395)$$

and

$$\left(\rho + E \cdot \frac{\partial \rho}{\partial E} \right) \frac{dE}{dt} + \left(E \cdot \frac{\partial \rho}{\partial P} - 1 \right) \frac{dP}{dt} = \frac{1}{V} \sum_{j=1}^{J} W_j E_j \cdot \qquad (3\text{-}396)$$

3.3.4 Transient Integration Scheme

The choice of the integration scheme for the simulation was dictated by two considerations. First and foremost, the integration scheme must be capable of taking large timesteps so that the amount of time spent in computing the state of the steam generating system is as small as possible. The second reason is related to the first by the desire to use a reference pressure for each flow segment, which is calculated by the code and which varies during the transient, rather than require the user to specify the reference pressure. The reference pressure for each flow segment was chosen to be the average of the pressures at the inlet and outlet ends of the flow segment. This reference pressure could have been chosen to be constant in time at its value before the transient begins, but has been allowed to vary in time during the transient to better model the effects of the absolute pressure level on each flow segment. However, because the time varying reference pressure reintroduces the sonic effects removed by the assumption of a reference pressure in the derivation of the equations, an implicit integration technique must be used to allow longer timesteps to be taken.

- 166 -

3.3.4.1 Implicit Form of Flow Segment Equations

3.3.4.1.1 Thermal Model

The reduction of the conservation equations for mass and energy from ordinary differential equations to algebraic equations is accomplished by integrating the conservation equations [Equation (3-372) and (3-373)] over a time interval Δt^{k+1} (where $\Delta t^{k+1} = t^{k+1} - t^k$).

mass:

$$\int_{t^k}^{t^{k+1}} \left(\frac{\partial m_i}{\partial E_{i-1}} + \frac{\partial m_i}{\partial E_i}\right) \frac{dE_i}{dt} \cdot dt + \int_{t^k}^{t^{k+1}} \left(\frac{\partial m_i}{\partial P_r}\right) \frac{dP_r}{dt} \cdot dt$$

$$+ \frac{1}{A_i} \int_{t^k}^{t^{k+1}} \frac{(W_i - W_{i-1})}{\Delta Z_i} \, dt = 0 \quad ; \qquad (3\text{-}397)$$

energy:

$$\int_{t^k}^{t^{k+1}} \left(\frac{\partial e_i}{\partial E_{i-1}} + \frac{\partial e_i}{\partial E_i}\right) \frac{dE_i}{dt} \cdot dt + \int_{t^k}^{t^{k+1}} \left(\frac{\partial e_i}{\partial P_r} - 1\right) \frac{dP_r}{dt} \cdot dt$$

$$+ \frac{1}{A_i} \int_{t^k}^{t^{k+1}} \frac{W_i E_i - W_{i-1} E_{i-1}}{\Delta Z_i} \, dt = \int_{t^k}^{t^{k+1}} \left(\frac{P_h}{A}\right) \langle q \rangle_i \, dt \quad . \qquad (3\text{-}398)$$

Assuming that the coefficients of the time derivative terms and the heat flux are constant during the timestep, we obtain

mass:

$$\left(\frac{\partial m_i}{\partial E_{i-1}} + \frac{\partial m_i}{\partial E_i}\right)^k \Delta E_i^{k+1} + \left(\frac{\partial m_i}{\partial P_r}\right)^k \Delta P_r^{k+1}$$

$$\frac{\Delta t^{k+1}}{\Delta Z_i A_i} \left[\Theta W_i^{k+1} + (1-\Theta)W_i^k - \Theta W_{i-1}^{k+1} - (1-\Theta)W_{i-1}^k\right] = 0 \quad ; \qquad (3\text{-}399)$$

energy:

$$\left(\frac{\partial e_i}{\partial E_{i-1}} + \frac{\partial e_i}{\partial E_i}\right)^k \Delta E_i^{k+1} + \left(\frac{\partial e_i}{\partial P_r} - 1\right)^k \Delta P_r^{k+1} + \frac{\Delta t^{k+1}}{\Delta Z_i A_i} \left[\Theta W_i^{k+1}\right.$$

$$\left. + (1-\Theta)W_i^k E_i^k - \Theta W_{i-1}^{k+1} E_{i-1}^{k+1} - (1-\Theta)W_{i-1}^k E_{i-1}^k\right] = \Delta t^{k+1} \left(\frac{P_h}{A}\right)_i \langle q \rangle_i^k \quad .$$

$$(3\text{-}400)$$

where

$$\Delta E_i^{k+1} = E_i^{k+1} - E_i^k \quad \text{and} \quad \Delta P_r^{k+1} = P_r^{k+1} - P_r^k$$

The time integrals of the flow terms are approximated by the theta difference method. Accordingly, we write

$$\int_{t^k}^{t^{k+1}} g(t) \, dt = \Delta t^{k+1} \left[\Theta \, g(t^{k+1}) + (1-\Theta) \, g(t^k) \right] \tag{3-401}$$

where $g(t)$ is an arbitrary function of time, and the value of Θ ($0 \leq \Theta \leq 1$) controls the degree of implicitness. For example, $\Theta = 0$ gives a fully explicit method, and $\Theta = 1$ implies fully implicit.

The nonlinear flow term in the energy equation is linearized by the use of a first-order Taylor expansion. Thus,

$$W_\ell^{k+1} E_\ell^{k+1} = W_\ell^k E_\ell^k + W_\ell^k \Delta E_\ell^{k+1} + E_\ell^k \Delta W_\ell^{k+1} \quad . \tag{3-402}$$

This equation is now rewritten as:

$$W_\ell^{k+1} E_\ell^{k+1} = W_\ell^k \Delta E_\ell^{k+1} + E_\ell^k W_\ell^{k+1} \tag{3-403}$$

Expanding the flow terms in the energy equation in terms of the relation given by Equation (3-403), we obtain

$$\left(\frac{\partial e_i}{\partial E_{i-1}} + \frac{\partial e_i}{\partial E_i} \right)^k \Delta E_i^{k+1} + \left(\frac{\partial e_i}{\partial P_r} - 1 \right)^k \Delta P_r^{k+1} + \frac{\Delta t^{k+1}}{A_i \Delta Z_i} \left[\Theta (W_i^k \Delta E_i^{k+1} + E_i^k W_i^{k+1}) \right.$$

$$\left. + (1-\Theta) W_i^k E_i^k - \Theta (W_{i-1}^k \Delta E_{i-1}^{k+1} + E_{i-1}^k W_{i-1}^{k+1}) - (1-\Theta) W_{i-1}^k E_{i-1}^k \right]$$

$$= \Delta t^{k+1} \left(\frac{P_h}{A} \right)_i \langle q \rangle_i^k \quad . \tag{3-404}$$

Solving Equations (3-399) and (3-404) simultaneously for ΔE_i^{k+1} and W_i^{k+1} in terms of ΔE_{i-1}^{k+1}, W_{i-1}^{k+1}, and ΔP_r^{k+1} gives

$$\Delta E_i^{k+1} = c_1 \, \Delta E_{i-1}^{k+1} + c_2 \, \Delta P_r^{k+1} + c_3 \, W_{i-1}^{k+1} + c_4 \quad , \qquad (3\text{-}405)$$

$$W_i^{k+1} = c_5 \, W_{i-1}^{k+1} + c_6 \, \Delta E_{i-1}^{k+1} + c_7 \, \Delta P_r^{k+1} + c_8 \quad , \qquad (3\text{-}406)$$

where

$$c_1 = \frac{1}{c_0} \cdot \Delta t^{k+1} \frac{\Theta W_{i-1}^k}{V_i} \quad , \qquad (3\text{-}407)$$

$$c_2 = \frac{1}{c_0} \cdot \left\{ E_i^k \left(\frac{\partial m_i}{\partial P_r} \right)^k - \left(\frac{\partial e_i}{\partial P_r} \right)^k + 1 \right\} \quad , \qquad (3\text{-}408)$$

$$c_3 = \frac{1}{c_0} \cdot \frac{\Delta t^{k+1} \Theta}{V_i} \left(E_{i-1}^k - E_i^k \right) \quad , \qquad (3\text{-}409)$$

$$c_4 = \frac{1}{c_0} \cdot \Delta t^{k+1} \left[\left(\frac{P_h}{A} \right)_i \langle q \rangle_i + \frac{(1-\Theta) W_{i-1}^k}{V_i} \left(E_{i-1}^k - E_i^k \right) \right] , \qquad (3\text{-}410)$$

$$c_5 = 1 - \frac{c_3 V_i}{\Theta \Delta t^{k+1}} \left(\frac{\partial m_i}{\partial E_{i-1}} + \frac{\partial m_i}{\partial E_i} \right)^k \quad , \qquad (3\text{-}411)$$

$$c_6 = \frac{-V_i}{\Theta \Delta t^{k+1}} c_1 \left(\frac{\partial m_i}{\partial E_i} + \frac{\partial m_i}{\partial E_{i-1}} \right)^k \quad , \qquad (3\text{-}412)$$

$$c_7 = \frac{-V_i}{\Theta \Delta t^{k+1}} \left\{ \left(\frac{\partial m_i}{\partial P_r} \right)^k + c_2 \left(\frac{\partial m_i}{\partial E_{i-1}} + \frac{\partial m_i}{\partial E_i} \right)^k \right\} \quad , \qquad (3\text{-}413)$$

$$c_8 = \frac{-V_i}{\Theta \Delta t^{k+1}} \left\{ (1-\Theta) (W_i^k - W_{i-1}^k) + c_4 \left(\frac{\partial m_i}{\partial E_{i-1}} + \frac{\partial m_i}{\partial E_i} \right)^k \right\} \quad , \qquad (3\text{-}414)$$

$$c_0 = \left(\frac{\partial e_i}{\partial E_{i-1}} + \frac{\partial e_i}{\partial E_i} \right)^k - E_i^k \left(\frac{\partial m_i}{\partial E_{i-1}} + \frac{\partial m_i}{\partial E_i} \right)^k + \frac{\Delta t^{k+1} \Theta W_i^k}{V_i} \quad , \qquad (3\text{-}415)$$

and

$$V_i = \Delta Z_i A_i \quad \cdot \qquad (3\text{-}416)$$

Equations (3-405) and (3-406) relate the conditions at the downstream end (i) of a control volume with those at the upstream end (i-1) of the control volume. Defining the conditions at the downstream end (i) of the control volume in terms of the condition at the inlet end (I) of the flow segment,

$$\Delta E_i^{k+1} = C_i^1 \Delta E_I^{k+1} + C_i^2 \Delta P_r^{k+1} + C_i^3 W_I^{k+1} + C_i^4 \quad , \tag{3-417}$$

$$W_i^{k+1} = C_i^5 W_I^{k+1} + C_i^6 \Delta E_I^{k+1} + C_i^7 \Delta P_r^{k+1} + C_i^8 \quad , \tag{3-418}$$

and substituting these definitions into Equations (3-405) and (3-406), the following recursion relations are obtained:

$$C_i^1 = c_1 C_{i-1}^1 + c_3 C_{i-1}^6 \quad , \tag{3-419}$$

$$C_i^2 = c_1 C_{i-1}^2 + c_3 C_{i-1}^7 + c_2 \quad , \tag{3-420}$$

$$C_i^3 = c_1 C_{i-1}^3 + c_3 C_{i-1}^5 \quad , \tag{3-421}$$

$$C_i^4 = c_1 C_{i-1}^4 + c_3 C_{i-1}^8 + c_4 \quad , \tag{3-422}$$

$$C_i^5 = c_5 C_{i-1}^5 + c_6 C_{i-1}^3 \quad , \tag{3-423}$$

$$C_i^6 = c_5 C_{i-1}^6 + c_6 C_{i-1}^1 \quad , \tag{3-424}$$

$$C_i^7 = c_5 C_{i-1}^7 + c_6 C_{i-1}^2 + c_7 \quad , \tag{3-425}$$

$$C_i^8 = c_5 C_{i-1}^8 + c_6 C_{i-1}^4 + c_8 \quad , \tag{3-426}$$

where $C_0^1 = 1$, $C_0^2 = C_0^3 = C_0^4 = 0$ and $C_0^5 = 1$, and $C_0^6 = C_0^7 = C_0^8 = 0$.

3.3.4.1.2 Hydraulic Model

The momentum equation for the flow segment is given by

$$I \frac{d}{dt} \langle W \rangle = (\Delta P - F) \quad , \tag{3-427}$$

where

$$\Delta P = P_I - P_o + \Delta P_p \tag{3-428}$$

and

$$F = \sum_{i=1}^{N} \frac{1}{A_i^2} \left(\frac{W_i^2}{\rho_i'} - \frac{W_{i-1}^2}{\rho_{i-1}'} \right) + \sum_{i=1}^{N} \frac{\overline{f} |W_i + W_{i-1}| \cdot (W_i + W_{i-1}) \, \Delta Z_i}{8 A_i^2 \, m_i \, D_{hi}}$$

$$+ \sum_{i=1}^{N} m_i \, (g \cdot \Delta Z_i) + \sum_{j} \left(\frac{K |W| W}{2 \rho A^2} \right)_j \quad . \tag{3-429}$$

Expanding the time derivative as a backward difference and linearizing the square terms in the flow resistance and pump pressure rise, we obtain

$$I \frac{\langle W \rangle^{k+1} - \langle W \rangle^k}{\Delta t^{k+1}} = \Delta P^{k+1} - F^{k+1} \quad , \tag{3-430}$$

where

$$\Delta P^{k+1} = P_I^{k+1} - P_o^{k+1} + \Delta P_p^{k+1} \quad , \tag{3-431}$$

and

$$F^{k+1} = \sum_{i=1}^{N} \frac{1}{A_i^2} \left(\frac{W_i^k W_i^{k+1}}{\rho'_i^k} - \frac{W_{i-1}^k W_{i-1}^{k+1}}{\rho'_{i-1}^k} \right) + \sum_{i=1}^{N} \frac{\overline{f}_i |W_i^k + W_{i-1}^k| \cdot (W_i^{k+1} + W_{i-1}^{k+1}) \, \Delta Z_i}{8 m_i^k \, A_i^2 \, D_{hi}}$$

$$+ \sum_{i=1}^{N} m_i^{k+1} \, (g \cdot \Delta Z_i) + \sum_{j} \left(\frac{K |W^k| W^{k+1}}{2 \rho^k A^2} \right)_j \quad . \tag{3-432}$$

The flow resistance F^{k+1} and pump pressure rise ΔP_p^{k+1} are expanded in terms of the conditions at the inlet of the flow segment which gives,

$$\Delta P_p^{k+1} - F^{k+1} = SW_I^{k+1} + T \Delta E_I^{k+1} + U \Delta P_r^{k+1} + V \quad , \tag{3-433}$$

where the definitions of the coefficients S, T, U, and V are given in Appendix B. Next, the average flow rate is determined in terms of the flow rate at the inlet of the flow segment;

$$\langle W \rangle^{k+1} = \frac{1}{I} \left[\langle C^5 \rangle W_I^{k+1} + \langle C^6 \rangle \Delta E_I^{k+1} + \langle C^7 \rangle \Delta P_r^{k+1} + \langle C^8 \rangle \right] \qquad (3\text{-}434)$$

where

$$\langle C^5 \rangle = \sum_{i=1}^{N} \frac{\Delta Z_i}{2A_i} (C_i^5 + C_{i-1}^5) \quad , \qquad (3\text{-}435)$$

$$\langle C^6 \rangle = \sum_{i=1}^{N} \frac{\Delta Z_i}{2A_i} (C_i^6 + C_{i-1}^6) \quad , \qquad (3\text{-}436)$$

$$\langle C^7 \rangle = \sum_{i=1}^{N} \frac{\Delta Z_i}{2A_i} (C_i^7 + C_{i-1}^7) \quad , \qquad (3\text{-}437)$$

$$\langle C^8 \rangle = \sum_{i=1}^{N} \frac{\Delta Z_i}{2A_i} (C_i^8 + C_{i-1}^8) \quad , \qquad (3\text{-}438)$$

Substituting Equation (3-433) and Equation (3-434) into the momentum equation for the flow segment, Equation (3-430), yields,

$$\langle C^5 \rangle W_I^{k+1} + \langle C^6 \rangle \Delta E_I^{k+1} + \langle C^7 \rangle \Delta P_r^{k+1} + \langle C^8 \rangle =$$

$$I \langle W \rangle^k + \Delta t^{k+1} \left[P_I^k + \Delta P_I^{k+1} - P_o^k - \Delta P_o^{k+1} - \right.$$

$$\left. SW_I^{k+1} - T \Delta E_I^{k+1} - U \Delta P_r^{k+1} - V \right] \cdot \qquad (3\text{-}439)$$

The change in the reference pressure is defined in terms of the changes in the pressures at the inlet and outlet ends of the flow segment,

$$\Delta P_r = \frac{1}{2} (\Delta P_I^{k+1} + \Delta P_o^{k+1}) \quad , \qquad (3\text{-}440)$$

so that the flow rate at the inlet of the flow segment can be written as

$$W_I^{k+1} = M_1 \, \Delta P_I^{k+1} + M_2 \, \Delta P_O^{k+1} + M_3 \, \Delta E_I^{k+1} + M_4 \tag{3-441}$$

where

$$M_1 = \frac{-\frac{1}{2}\left[\langle C^7 \rangle - \Delta t^{k+1} \cdot (2-U)\right]}{\langle C^5 \rangle + \Delta t^{k+1} \, S} \tag{3-442}$$

$$M_2 = \frac{-\frac{1}{2}\left[\langle C^7 \rangle + \Delta t^{k+1} \, (2+U)\right]}{\langle C^5 \rangle + \Delta t^{k+1} \, S} \tag{3-443}$$

$$M_3 = \frac{-\left[\langle C^6 \rangle + \Delta t^{k+1} \, T\right]}{\langle C^5 \rangle + \Delta t^{k+1} \, S} \tag{3-444}$$

$$M_4 = \frac{-\left[\langle C^8 \rangle - I \langle W \rangle^k - \Delta t^{k+1} \cdot (P_I^k - P_O^k - V)\right]}{\langle C^5 \rangle + \Delta t^{k+1} \, S} \tag{3-445}$$

Substituting Equation (3-441) into the flow distribution equation, Equation (3-418), gives,

$$W_i^{k+1} = (C_i^5 M_1 + \tfrac{1}{2} C_i^7) \, \Delta P_I^{k+1} + (C_i^5 M_2 + \tfrac{1}{2} C_i^7) \, \Delta P_O^{k+1}$$
$$+ (M_3 + C_i^6) \, \Delta E_I^{k+1} + (M_4 + C_i^8) \quad , \tag{3-446}$$

for the flow rate at any point in the flow segment. The enthalpy can also be expressed in this form by,

$$E_i^{k+1} = (C_i^3 M_1 + \tfrac{1}{2} C_i^2) \, \Delta P_I^{k+1} + (C_i^3 M_2 + \tfrac{1}{2} C_i^2) \, \Delta P_O^{k+1}$$
$$+ (C_i^3 M_3 + C_i^1) \, \Delta E_I^{k+1} + (C_i^3 M_4 + C_i^4). \tag{3-447}$$

These two equations can be written in a more compact form as

$$\underline{X}_i^{k+1} = \underline{C}_i^k + \underline{\underline{D}}_i^k \underline{Y}_i^{k+1} + \underline{\underline{E}}_i^k \underline{Y}_o^{k+1} \quad , \qquad (3\text{-}448)$$

where

$$\underline{X}_i = \begin{bmatrix} E \\ W \end{bmatrix}_i \quad ,$$

$$\underline{Y}_i = \begin{bmatrix} \Delta E \\ \Delta P \end{bmatrix}_I \quad ,$$

$$\underline{Y}_o = \begin{bmatrix} \Delta E \\ \Delta P \end{bmatrix}_O \quad , \qquad (3\text{-}449)$$

and the coefficient matrices $\underline{C}$, $\underline{\underline{D}}$, and $\underline{\underline{E}}$ are evaluated using the state of the flow segment at time k.

3.3.4.2 Implicit Form of Accumulator Equations

Expanding the conservation equations for the accumulators using backward time differences, we obtain

$$\left(\frac{\partial \rho}{\partial E}\right)^k \frac{\Delta E^{k+1}}{\Delta t} + \left(\frac{\partial \rho}{\partial P}\right)^k \frac{\Delta P^{k+1}}{\Delta t} = \frac{1}{V} \sum_{j=1}^{N} W_j^{k+1} \quad , \qquad (3\text{-}450)$$

$$\left(\rho + E \frac{\partial \rho}{\partial E}\right)^k \frac{\Delta E^{k+1}}{\Delta t} + \left(E \frac{\partial \rho}{\partial P} - 1\right) \frac{\Delta P^{k+1}}{\Delta t} = \frac{1}{V} \sum_{j=1}^{J} W_j^{k+1} E_j^{k+1} \quad . \qquad (3\text{-}451)$$

The sums on the right hand sides of these equations are the flows and flow enthalpies at the interface between the accumulator and all flow segments attached to it. Flow out of a flow segment (into an accumulator) is considered a positive flow.

These equations may also be written in a more compact form as

$$\underline{\underline{A}}_i \, \underline{Z}_i = \underline{B}_i \quad , \tag{3-452}$$

where

$$\underline{Z}_i = \begin{bmatrix} \Delta E \\ \Delta P \end{bmatrix}_i \quad .$$

and the coefficient matrix $\underline{\underline{A}}_i$ is evaluated using the state of the accumulator at time k.

3.3.4.3 Solution Procedure for Steam/Water Conditions

The state of the steam generating system at the advanced time (t^{k+1}) can be determined by solving the conservation equations for the flow segments and accumulators simultaneously. The set of equations can be reduced considerably by observing that the unknown boundary conditions for the flow segments are just the conditions in the accumulators at the inlet and outlet of the flow segment. Likewise, the flows and flow enthalpies which appear on the right-hand side of the accumulator equations are just the flows and enthalpies at the ends of the flow segments attached to each accumulator.

The set of equations are reduced by writing the flow and flow enthalpies at the inlet and outlet ends of each flow segment as a function of the conditions in the accumulators:

$$W_j^{k+1} = \sum_{m=1}^{M} \underline{F}_{mj} \, \underline{Z}_m + G_j$$

and

$$W_j^{k+1} \, E_j^{k+1} = \sum_{m=1}^{M} \underline{R}_{mj} \, \underline{Z}_m + S_j \quad , \tag{3-453}$$

where the steam generating system contains M accumulators.

These relations are then used to express the right-hand-side vector $\underline{B}$ in the accumulator equations [Equation (3-452)] in terms of the state of the accumulators only. The set of equations for all the accumulators can now be solved. In the derivation of the flows and flow enthalpies in the flow segments in terms of the accumulator conditions, cross terms (order Δ^2) which appear in the flow enthalpy term have been neglected so that the flow and flow enthalpies can be expressed as linear combinations of the unknown states of the accumulators. Once the state of the accumulators at the advanced time has been determined, the state of the flow segments can be determined by back substitution of the accumulator states into the conservation equations for the flow segments [Equation (3-448)].

3.3.4.4 Evaluation of Surface Heat Fluxes

In the integration of the energy equation in the flow segments, the surface heat fluxes, where they are different from zero (i.e., in the heat exchangers), were assumed to be constant. Before the next timestep can be taken, they must be updated for the conditions existing in the flow segment at the end of the timestep.

The multi-tube heat exchanger is modeled by a single representative heat transfer tube, and the arrangement of the control volumes in this representative tube is shown in Figure 3-37.

The heat fluxes on the two surfaces of the tube are given by

$$\langle q \rangle_{ws}^{k+1} = h_{ws}^{k+1} \left(T_w^{k+1} - \overline{T}_{ws}^{k+1} \right) \tag{3-454}$$

and

$$\langle q \rangle_{WS}^{k+1} = h_N^{k+1} \left(\overline{T}_N^{k+1} - T_W^{k+1} \right) \ . \tag{3-455}$$

where the average temperatures in the two fluids (sodium on the outside of the tube and water inside the tube) are computed from

$$\overline{T}_{WS}^{k+1} = T \left(\overline{E}_{WS}^{k+1}, \ P_r^{k+1} \right) \tag{3-456}$$

and

$$\overline{T}_N^{k+1} = T \left(\overline{E}_N^{k+1} \right) \ , \tag{3-457}$$

and the average fluid enthalpy in the control volume is given by

$$\overline{E}_{WS}^{k+1} = e_{WS}^{k+1} / m_{WS}^{k+1} \ , \tag{3-458}$$

$$\overline{E}_N^{k+1} = e_N^{k+1} / m_N^{k+1} \ . \tag{3-459}$$

The heat transfer coefficients h_{WS}^{k+1} and h_N^{k+1} are also computed using the average conditions in the control volume. The enthalpies in the sodium at the advanced time are found from the energy equation for the control volumes representing the sodium side of the heat exchanger. The energy equation for the control volumes representing the sodium side of the heat exchanger is identical in form to the energy equation for the control volumes on the water side of the heat exchanger [Equation (3-373)] except that the properties of sodium are assumed to be independent of pressure. The sodium flow rate and the sodium enthalpy at the inlet of the heat exchanger are provided as boundary conditions by other modules in the SSC-L code and are known functions of time.
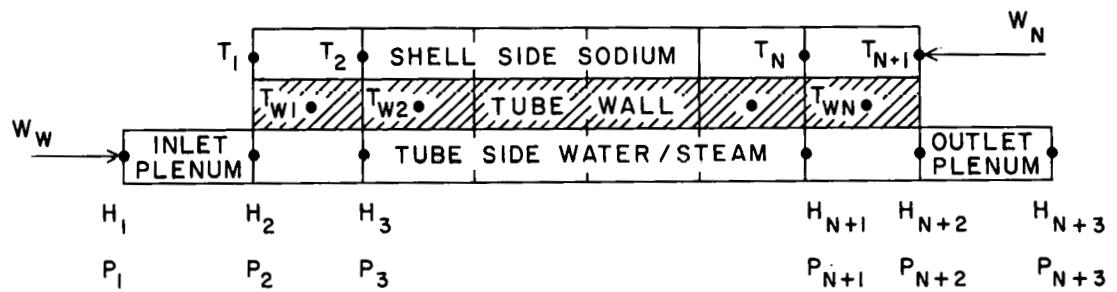
Figure 3-37. Nodal diagram for steam generator
thermal balance.

In order to evaluate the heat fluxes, the tube wall temperature at the advanced time must also be known. The tube wall temperature is found from the energy equation for the control volume representing the tube wall,

$$(\rho C_p) \frac{dT_w}{dt} = \frac{4(D_N \langle q \rangle_N - D_{ws} \langle q \rangle_{ws})}{\Delta Z(D_N^2 - D_{ws}^2)} \quad . \tag{3-460}$$

Expanding the time derivative of the tube wall temperature as a backward difference, we find

$$(\rho C_p)^k \frac{T_w^{k+1} - T_w^k}{\Delta t^{k+1}} = \frac{4}{\Delta Z(D_N^2 - D_{ws}^2)} \left[D_N h_N^{k+1} (\overline{T}_N^{k+1} - T_w^{k+1}) - D_{ws} h_{ws}^{k+1} (T_w^{k+1} - \overline{T}_{ws}^{k+1}) \right], \tag{3-461}$$

where the heat fluxes have been expanded in terms of the respective heat transfer coefficients. This equation can now be solved iteratively for the tube wall temperature at the advanced time,

$$T_w^{k+1} = T_w^k + \frac{D_N h_N^{k+1} \overline{T}_N^{k+1} + D_{ws} h_{ws}^{k+1} \overline{T}_{ws}^{k+1}}{\left(\dfrac{(\rho C_p)^k \Delta Z(D_N^2 - D_{ws}^2)}{4\Delta t^{k+1}} \right) + D_N h_N^{k+1} D_{ws} h_{ws}^{k+1}} \quad , \tag{3-462}$$

where the heat transfer coefficients h_{ws}^{k+1} and h_N^{k+1} are functions of the tube wall temperature T_w^{k+1}.

The modes of heat transfer on the water side and the correlation used to calculate the heat transfer coefficient for that mode are

1) forced convection to subcooled water (Dittus-Boelter),[3.37]

2) subcooled or saturated nucleate boiling (Thom),[3.38]

3) saturated film boiling (Bishop),[3.39] and

4) forced convection to superheated steam (Heineman).[3.40]

Only forced convection to liquid sodium (Graber-Reiger)[3.41] is allowed on the sodium side of the heat exchanger. The location of the departure from nucleate boiling is determined, using the Atomics International correlation.[3.42] The heat flux on the water side in the control volume containing the departure from nucleate boiling is computed as the area-weighted average of the heat fluxes for the pre-DNB and post-DNB portions of the control volume.

Once the tube wall temperature at a particular axial location in the heat exchanger has been determined, the surface heat fluxes at that axial location can be found using Equations (3-454) and (3-455).

3.3.4.5 Overall Solution Procedure

A simplified flow chart of the overall solution procedure is shown in Figure 3-38. The flow rates and enthalpies for all control volumes containing water and/or steam are advanced in time, using the procedure described in Section 3.3.4.3. Then the enthalpy in all the control volumes representing the sodium side of the heat exchanger is advanced in time. Next, the tube wall temperatures at the advanced time are computed, using the enthalpies and flows in the two fluids (water and sodium) computed in the first two steps. Finally, the surface heat fluxes are computed from the enthalpies, flows, and tube wall temperatures at the advanced time. This completes the sequence of computations for a single integration step.

In order to use this procedure, one additional variable must be chosen, the integration timestep. In the initial version of the steam generation module, the timestep will be chosen so that the maximum change in any flow rate or enthalpy during a timestep is equal to a user specified value. Because the magnitude of the changes in flow rate and enthalpy cannot be known
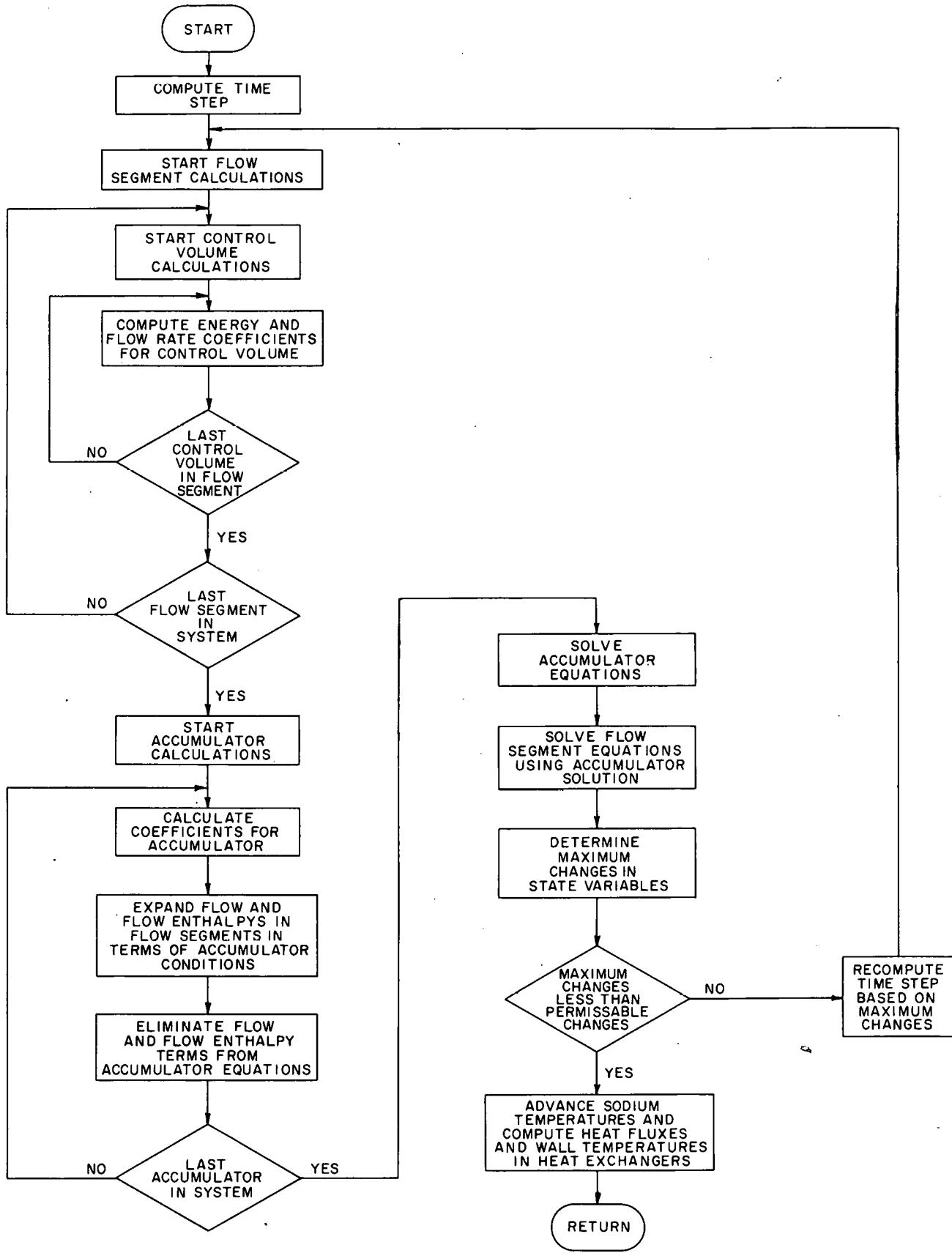
Figure 3-38. Flow chart for transient solution of steam generator.

until after the integration has been performed, the timestep will be esti-
mated based upon the past performance of the system, using a first-order
extrapolation formula. Using this procedure, the timestep will be continu-
ously adjusted so that the maximum permissible timestep which corresponds
to the user-input maximum change in the flows or enthalpies during the time-
step will always be taken.

3.3.5 Steady-State Computations

The transient integration procedure requires as its initial conditions
the values of flow rate and enthalpy for all nodes in the steam/water side,
temperatures of the tube wall nodes, and enthalpies for all nodes on the
sodium side of the heat exchangers at steady-state conditions. Rather than
performing the transient integration procedure until a steady-state is
achieved, the steady-state is determined by setting all the time derivatives
in the conservation equations identically to zero. This yields a large set
of nonlinear algebraic equations for the steady-state values of flow and
enthalpy in the flow segments, pressure, and enthalpy in the accumulators;
the temperatures in the tube wall, and the enthalpies in the sodium nodes in
the heat exchangers. This large set of equations is partitioned into the
flow segment equations and the accumulator equations. A simplified flow chart
for the steady-state computation is shown in Figure 3-39.

3.3.5.1 Accumulator Conditions

The user is required to input the pressure and liquid level (or enthalpy)
in each accumulator. These conditions are used to establish the inlet condi-
tions for the flow segments connected to the accumulators and uncouple the
thermal and hydraulic calculations in the flow segments.
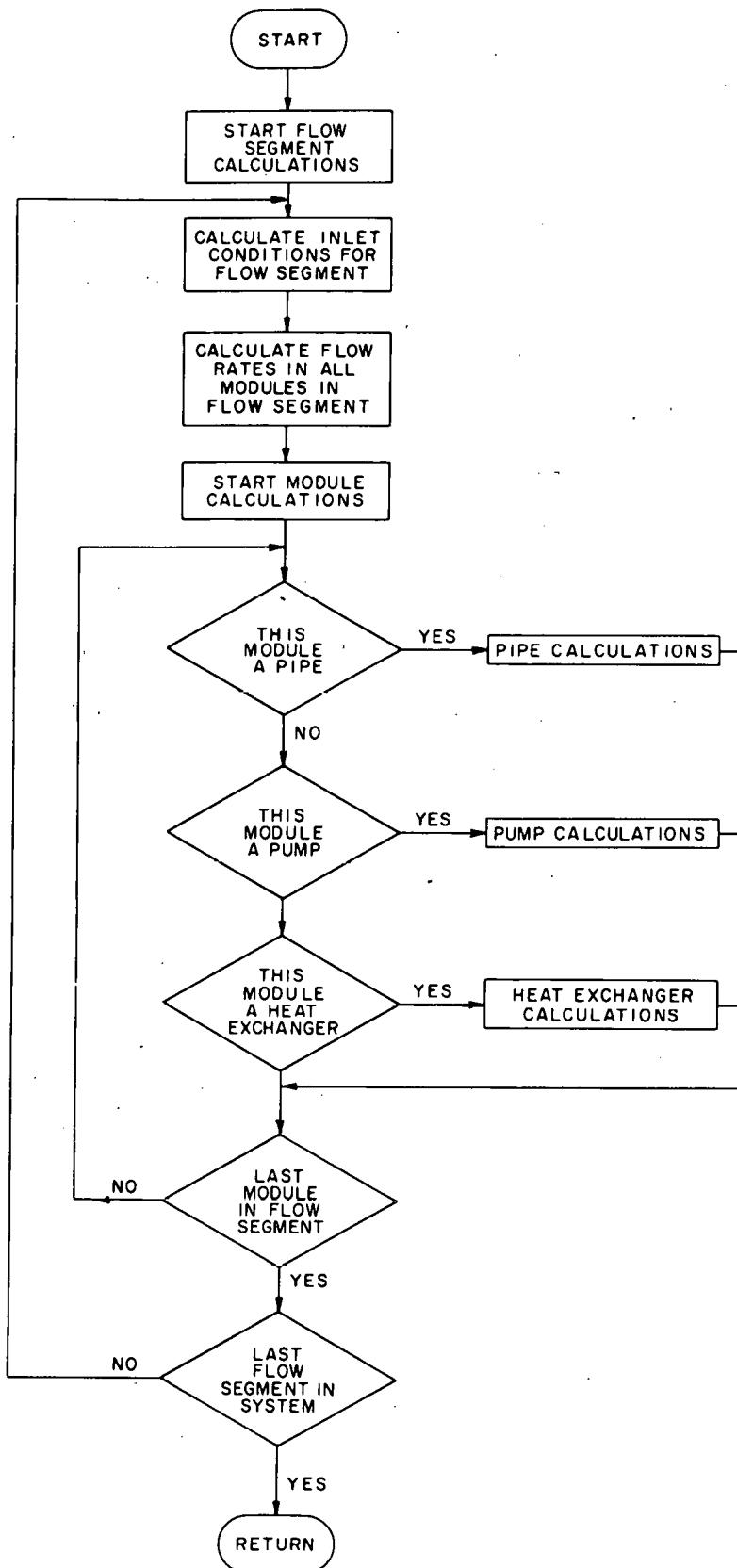
Figure 3-39. Flow chart for steady state solution
of steam generator.

3.3.5.2 Flow Segment Inlet Conditions

The conditions in the accumulators are used to determine the inlet conditions (pressure and enthalpy) for the flow segments attached to them. The pressure at the inlet of any flow segment is the pressure (user specified) in the accumulator to which it is attached. The determination of the average specific enthalpy in an accumulator and the calculation of the enthalpy of the flow into the flow segment attached to that accumulator depend upon the liquid level in the accumulator, whether there is a fill junction adding feedwater to the accumulator, and the height (relative to the liquid level) of the connection between the accumulator and the flow segment. If the liquid level is either zero (no liquid) or one (all liquid), the average specific enthalpy of the fluid in the accumulator and the enthalpy of the fluid into the next downstream flow segment are equal to the enthalpy of the flow into the accumulator from the preceding flow segment. If the liquid level in the accumulator is greater than zero but less than one, the average specific enthalpy in the accumulator corresponds to the saturated enthalpy at a quality equal to the liquid level.

The enthalpy of the flow into the next flow segment depends upon the height (relative to the liquid level) of the connection of the loop to the volume. If the connection is above the liquid level, the enthalpy of the fluid entering the next flow segment is the enthalpy of saturated steam determined from the pressure in the accumulator. If the connection between the next downstream flow segment is below the liquid level, the enthalpy of the fluid entering the next flow segment is the enthalpy of saturated water evaluated at the accumulator pressure. However, if a fill junction is adding subcooled liquid to the accumulator, the user may specify that the enthalpy of

the flow into the next downstream flow segment is the mixed enthalpy of the saturated liquid in the accumulator and the subcooled feedwater. The mixing fractions are determined from the fill junction flow rate and the flow rate in the flow segment under consideration.

Once the enthalpy of the flow into a flow segment is determined, the flow rate in that flow segment may be found. If the flow segment contains a pump, the pump reference flow rate is used as the flow rate in the flow segment. If no pump is present in the flow segment, the flow rate is determined from the flow rate in the previous flow segment of the phase entering the flow segment under consideration.

Once the inlet pressure, flow, and enthalpy have been established, the conditions in each component in the flow segment are calculated beginning with the first or most upstream component and proceeding in the direction of flow.

3.3.5.3 Water/Steam Computations in Pipes

The flow model for a pipe utilizes the volume-averaged momentum equation to determine the pressure change in the direction of flow along a length of pipe. Pressure changes due to wall and interphase friction and changes in elevation and flow acceleration due to flashing are included.

The pipe is divided into a user specified number of control volumes, and the pressure change in each control volume is determined beginning at the upstream end of the pipe and marching downstream until the last control volume is reached. An additional pressure change is located at the downstream end of the pipe and is calculated using a user specified loss coefficient. This loss coefficient can be used to represent the pressure changes in valves,

flanges, area changes, etc. The pipe must be a straight length of pipe, but may be oriented at any angle to the vertical. The user may also specify the pressure at the end of the pipe. If the pressure is specified at the end of a pipe, the loss coefficient is adjusted to produce that pressure. Flow in all pipes is adiabatic so that the enthalpy at the outlet of the pipe (E_o) is identical to the enthalpy at the inlet of the pipe (E_I).

The pressure at the outlet of any control volume (P_o) is the pressure at the inlet of the control volume (P_I) minus the pressure drop in the control volume (ΔP). The designations of inlet and outlet are based on the local water flow direction. The pressure drop in the control volume is determined from

$$\Delta P = \frac{W^2}{A^2} \left(\frac{1}{\rho_o} - \frac{1}{\rho_I} \right) + \frac{\overline{f} \, \Delta Z \, W^2 \, \phi_{TP}}{2m \, A^2 \, D_h} + mg \cdot \Delta Z \ . \tag{3-463}$$

The two-phase friction multiplier (ϕ_{TP}) is given by the homogeneous flow model. The friction factor is a function of the Reynolds number which is determined from the average fluid properties in the segment, and the pipe surface roughness to diameter ratio. The pressure change at the end of a pipe is given by

$$\Delta P = \frac{KW^2}{2A^2 \, \rho_o} \ , \tag{3-464}$$

where K is the loss coefficient.

3.3.5.4 Computations in the Heat Exchangers

The heat transfer in the evaporator/superheater model is calculated using a single-tube representation of the multi-tube heat exchanger. Pressure losses in the inlet and outlet plena on the steam/water side are

calculated from user-supplied loss coefficients (or loss coefficients are calculated using user-supplied pressure losses). The active length of the heat transfer tube is divided into a user-supplied number of control volumes. The volume-averaged energy equations are utilized to determine the water/steam enthalpy, sodium temperature, and tube wall temperature, as shown in Figure 3-40. The volume-averaged momentum equation is used to determine the steam/water pressure at the downstream end of each control volume, beginning with the most upstream control volume (upstream relative to the steam/water flow) and proceeding in the direction of steam/water flow until the end of the heat transfer tube is reached.

The enthalpy change in each of the fluids (steam/water and sodium) is calculated using an average surface heat flux for each control volume. The average surface heat fluxes are calculated based on the average thermodynamic state of the respective fluid, the thermal resistance of the tube wall, and the thermal resistance of the surface fouling on the steam/water side as well as on the sodium side. The enthalpy rise in a control volume of the steam/water side is given by

$$E_O = E_I + f_q \frac{(\pi D_{WS} \, \Delta Z) \, \langle q \rangle_{WS}}{W_{WS}} \, , \qquad (3\text{-}465)$$

where the average surface heat flux is given by [Equation (3-442)]

$$\langle q \rangle_{WS} = h_{WS} \, (T_W - \overline{T}_{WS}) \, . \qquad (3\text{-}466)$$

The corresponding equation for the sodium side is

$$C_p T_I = C_p T_O + f_q \frac{(\pi D_N \, \Delta Z) \, \langle q \rangle_N}{W_N} \, , \qquad (3\text{-}467)$$

where the average surface heat flux on the sodium side is given by
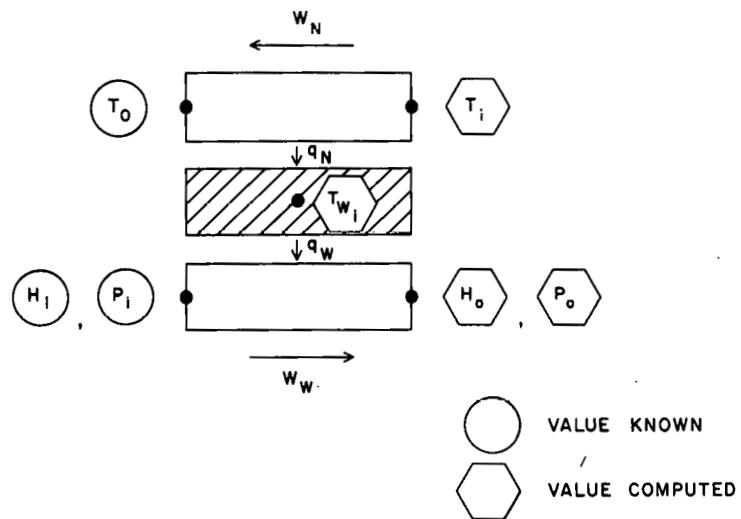
Figure 3-40. Steady-state boundary condition for
steam generator nodal section.

$$\langle q \rangle_N = h_N (\overline{T}_N - T_w) \quad . \tag{3-468}$$

The overall heat transfer coefficients h_{ws} and h_N are given by

$$\frac{1}{h_{ws}} = \frac{1}{h_{film,ws}} + R_{w,ws} + \frac{1}{h_{foul,ws}} \tag{3-469}$$

$$\frac{1}{h_N} = \frac{1}{h_{film,N}} + R_{w,N} + \frac{1}{h_{foul,N}} \quad , \tag{3-470}$$

where the film heat transfer coefficients are given by standard correlations and the fouling heat transfer coefficients are user-input quantities. The tube wall resistances are given by

$$R_{w,ws} = \frac{D_{ws}}{2k_w} \ln \frac{D_w}{D_{ws}} \tag{3-471}$$

$$R_{w,N} = \frac{D_N}{2k_w} \ln \frac{D_N}{D_w} \quad , \tag{3-472}$$

where

$$D_w = \frac{1}{2} (D_N + D_{ws}) \quad . \tag{3-473}$$

The tube wall temperature is given by

$$D_N \langle q \rangle_N = D_{ws} \langle q \rangle_{ws} \quad , \tag{3-474}$$

which can be rearranged to give

$$T_w = \frac{D_{ws} h_{ws} \overline{T}_{ws} + D_N h_N \overline{T}_N}{D_{ws} h_{ws} + D_N h_N} \quad . \tag{3-475}$$

Because the CRBRP evaporators and superheaters are counterflow heat exchangers, the steam/water inlet and the sodium outlet are located at the same end of an axial segment. A cocurrent heat exchanger may be simulated by considering the sodium flow rate to be in the negative direction. The

three energy equations [Equations (3-465), (3-467) and (3-475)] must be solved simultaneously with the momentum equation to determine the steam/water outlet enthalpy, the sodium inlet temperature, the tube wall temperature, and the steam/water outlet pressure for a given control volume.

On the sodium side, the mode of heat transfer is forced-convection heat transfer, while on the steam/water side, three modes are considered for heat transfer to subcooled and saturated water, and a single mode is included for heat transfer to superheater steam. The forced convection, nucleate boiling and film boiling modes are included for heat transfer to subcooled or saturated water, and forced convection is considered for heat transfer to superheated steam. The heat transfer correlations that represent these regions are included in Chapter 5.

Because the departure from nucleate boiling (DNB) is accompanied by a large drop in the surface heat flux, the control volume in which the departure from nucleate boiling occurs is treated differently. When DNB is detected to have occurred in a control volume (the DNB is detected by comparing the outlet quality of a control volume to the quality at DNB computed from a correlation), the control volume is divided into two portions. The length of each portion is adjusted so that the DNB point lies on the boundary between the two pieces of the control volume. Only film boiling heat transfer is allowed in the downstream portion of the divided control volume and all other control volumes downstream of the DNB location, while either forced convection or nucleate boiling are allowed for control volumes upstream of the DNB location.

The calculations use the actual (user input) length of the heat exchanger tube unless the user specifies the heat exchanger steam/water outlet enthalpy,

the heat exchanger steam/water outlet quality, or the heat exchanger sodium inlet temperature. When any one of these are specified, an area correction factor, f_q, is calculated. This area correction factor modifies the length of the heat transfer tube in such a way as to produce the specified outlet (or inlet) conditions for the heat exchanger.

3.3.5.5 Pump Computations

The model adopted for the recirculation pump is extremely simple. The outlet pressure (P_O) from the pump is determined from the inlet pressure of the pump (P_I) and the pressure rise in the pump (ΔP_p). The pressure rise in the pump is given by

$$P_O - P_I = \Delta P_p = H_p \, \rho_I g \, . \tag{3-476}$$

The pump head is determined from the pump characteristics as functions of pump speed and flow rate through the pump. For the simplified model, quadratic characteristics are assumed, and the pump head is given by

$$H_p = H_{ref} \left[(1 + \alpha) \, \omega_{rel}^2 - \alpha W_{rel}^2 \right] , \tag{3-477}$$

where

E_{ref} = pump head at rated speed and flow rate,

ω_{ref} = pump speed relative to rated pump speed, and

W_{rel} = pump flow rate relative to rated flow rate.

The pump is assumed to operate at rated speed unless the user specifies the pump outlet pressure. If the pump outlet pressure is specified, the pump

speed is adjusted to produce the specified outlet pressure. The flow in the pump is assumed to be adiabatic so that the enthalpy of the flow out of the pump is equal to the enthalpy of the flow into the pump.

3.3.5.6 Sodium-Side Hydraulics in Heat Exchangers

The momentum equations are very similar to that for the shell side of the IHX except that bypass flow is not considered. The mass flow entering the superheater will be

$$W = W_s/n_s \, , \qquad (3\text{-}478)$$

where n_s = number of superheaters per loop. Each superheater will have n_e outlets where n_e is the number of evaporators per superheater, and the mass flow entering the evaporator will be

$$W = W_s/(n_s n_e) \qquad (3\text{-}479)$$

unless there are no superheaters, in which case

$$W = W_s/n_e \, . \qquad (3\text{-}480)$$

The momentum equation can be written for the superheater as

$$\Delta P_{SH} = \frac{W^2}{A_{SH}^2} \left(\frac{1}{\rho_N} - \frac{1}{\rho_1} \right) + \frac{1}{2} \frac{W|W|}{D_h A_{SH}^2} \int_0^L \frac{f}{\rho} \, dx + \Delta P_g$$

$$+ K_{in} \frac{W|W|}{(\rho A^2)_{in}} + K_o \frac{\frac{W|W|}{n_e^2}}{(\rho A^2)_{out}} + K_{SH} \frac{W|W|}{(\rho A_{SH})^2} \qquad (3\text{-}481)$$

where W in this equation is given by Equation (3-478), and for the evaporator as:

$$\Delta P_{EV} = \frac{W^2}{A_{EV}^2} \left(\frac{1}{\rho_N} - \frac{1}{\rho_1} \right) + \frac{1}{2} \frac{W|W|}{D_h A_{EV}^2} \int_0^L \frac{f}{\rho} \, dx + P_g$$

$$+ K_{in} \frac{W|W|}{(\rho A^2)_{in}} + K_o \frac{W|W|}{(\rho A^2)_{out}} + K_{EV} \frac{W|W|}{\rho A_{EV}^2} \,, \tag{3-482}$$

where W in this equation is given by Equation (3-479). K_{SH} and K_{EV} in Equations (3-481) and (3-482) are the uncertainty absorbers similar to K_p, as defined for the IHX.

APPENDIX A

Derivation of Volume-Averaged Enthalpy and Density

The volume-averaged density m and volume-averaged enthalpy e can be found by assuming that the density of subcooled liquid varies linearly with enthalpy and that the specific volume of saturated and superheated fluid varies linearly with enthalpy. Using these approximations, the volume-averaged density becomes

$$m_i = \frac{1}{E_i - E_{i-1}} \int_{E_{i-1}}^{E_i} \rho(E, P_r) dE \; , \qquad (A-1)$$

$$m_i = (\rho_i + \rho_{i-1})/2 \qquad \text{for } E_{i-1} < E_i < E_f; \quad (A-2)$$

$$m_i = \frac{1}{2} \beta(\rho_{i-1} + \rho_f) + (1-\beta) \frac{\ell n(v_i/v_f)}{(v_i - v_f)} \qquad \text{for } E_{i-1} < E_f < E_i; \quad (A-3)$$

$$m_i = \frac{\ell n(v_i/v_{i-1})}{v_i - v_{i-1}} \qquad \text{for } E_f < E_{i-1} < E_i; \quad (A-4)$$

where

$$\beta_i = \frac{E_f - E_{i-1}}{E_i - E_{i-1}} \qquad (A-5)$$

and E_f is the liquid saturation enthalpy at the reference pressure P_r.

The volume-averaged enthalpy is given by

$$e_i = \frac{1}{6} \left[(2E_i + E_{i-1}) \rho_i + (2E_{i-1} + E_i) \rho_{i-1} \right] \qquad \text{for } E_{i-1} < E_i < E_f, \quad (A-6)$$

$$e_i = \frac{\beta}{6} \left[(2E_f + E_{i-1}) \rho_f + (2E_{i-1} + E_f) \rho_{i-1} \right]$$
$$+ (1-\beta) \left[\frac{E_i - E_f}{v_i - v_f} + \frac{(E_f v_i - E_i v_f) \ell n(v_i/v_f)}{(v_i - v_f)^2} \right] \qquad \text{for } E_{i-1} < E_f < E_i, \quad (A-7)$$

$$e_i = \frac{E_i - E_{i-1}}{v_i - v_{i-1}} + \frac{(E_{i-1} v_i - E_i v_{i-1})}{(v_i - v_{i-1})^2} \ln(v_i/v_{i-1}) \quad \text{for } E_f < E_{i-1} < E_i. \quad \text{(A-8)}$$

The partial derivatives of m_i and e_i may be written in a simple form as

$$\frac{\partial m_i}{\partial E_{i-1}} = \frac{\partial}{\partial E_{i-1}} \left(\frac{1}{E_i - E_{i-1}} \int_{E_{i-1}}^{E_i} \rho\,dE \right) = \frac{m_i - \rho_{i-1}}{E_i - E_{i-1}}, \quad \text{(A-9)}$$

$$\frac{\partial m_i}{\partial E_i} = \frac{\rho_i - m_i}{E_i - E_{i-1}}, \quad \text{(A-10)}$$

$$\frac{\partial e_i}{\partial E_{i-1}} = \frac{e_i - \rho_{i-1} E_{i-1}}{E_i - E_{i-1}}, \quad \text{(A-11)}$$

$$\frac{\partial e_i}{\partial E_i} = \frac{\rho_i E_i - e_i}{E_i - E_{i-1}}. \quad \text{(A-12)}$$

APPENDIX B

Expansion of Flow Resistance and Pump Pressure Rise

The flow resistance term in the momentum equation may be found by direct substitution of the formula for the flow rate at any point in the flow segment in terms of the flow rate at the inlet of the flow segment into the individual terms in the flow resistance.

The total flow resistance is given as the sum of the flow resistances in the individual control volumes. The flow resistance in an individual control volume is given by

$$F_i = \frac{1}{A_i} \left(\frac{W_i^k \, W_i^{k+1}}{\rho_i^k} - \frac{W_{i-1}^k \, W_{i-1}^{k+1}}{\rho_{i-1}^k} \right) + \frac{\bar{f} \, (W_i^k + W_{i-1}^k)(W_i^{k+1} + W_{i-1}^{k+1}) \, \Delta Z_i}{8 A_i^2 \, m_i^k \, D_h}$$

$$+ \, m_i^{k+1} \, (g \cdot \Delta Z_i) + \frac{K_i \, (W_i^k) \, W_i^{k+1}}{2\rho_i \, A_i^2} \quad . \tag{B-1}$$

Expanding the flow rates at the advanced times as

$$W_i^{k+1} = C_i^5 \, W_I^{k+1} + C_i^6 \, \Delta E_I^{k+1} + C_i^7 \, \Delta P_r^{k+1} + C^8 \tag{B-2}$$

and

$$W_{i-1}^{k+1} = C_{i-1}^5 \, W_I^{k+1} + C_{i-1}^6 \, \Delta E_I^{k+1} + C_{i-1}^7 \, \Delta P_r^{k+1} + C_{i-1}^8 \tag{B-3}$$

and collecting terms, the flow resistance for control volume i can be written as

$$F_i^{k+1} = s_i \, W_I^{k+1} + t_i \, \Delta E_I^{k+1} + u_i \, \Delta P_r^{k+1} + v_i \tag{B-4}$$

where

$$s_i = \frac{1}{A_i^2} \left(\frac{W_i^k \, C_i^5}{\rho_i^{'k}} - \frac{W_{i-1}^k \, C_{i-1}^5}{\rho_{i-1}^{'k}} \right) + \frac{\bar{f} \, (W_i^k + W_{i-1}^k) \, \Delta Z_i \, (C_i^5 + C_{i-1}^5)}{8 A_i^2 \, m_i \, D_{hi}}$$

$$+ \, (g \cdot \Delta Z_i) \, C_i^3 \left(\frac{\partial m_i}{\partial E_i} + \frac{\partial m_i}{\partial E_{i-1}} \right) + \frac{K_i \, W_i^k \, C_i^5}{2\rho_i^k \, A_i^2} \quad . \tag{B-5}$$

- 196 -

$$t_i = \frac{1}{A_i^2}\left(\frac{W_i^k\, C_i^6}{\rho_i'^k} - \frac{W_{i-1}^k\, C_{i-1}^6}{\rho_{i-1}'^k}\right) + \frac{\overline{f}\,(W_i^k + W_{i-1}^k)\,\Delta Z_i\,(C_i^6 + C_{i-1}^6)}{8A_i^2\, m_i\, D_{hi}}$$

$$+ (g \cdot \Delta Z_i)\, C_i^1\left(\frac{\partial m_i}{\partial E_i} + \frac{\partial m_i}{\partial E_{i-1}}\right) + \frac{K_i\, W_i^k\, C_i^6}{2\rho_i^k\, A_i^2} \quad ; \qquad (B\text{-}6)$$

$$u_i = \frac{1}{A_i^2}\left(\frac{W_i^k\, C_i^7}{\rho_i'^k} - \frac{W_{i-1}^k\, C_{i-1}^7}{\rho_{i-1}'^k}\right) + \frac{\overline{f}\,(W_i^k + W_{i-1}^k)\,\Delta Z_i\,(C_i^7 + C_{i-1}^7)}{8A_i^2\, m_i\, D_{hi}}$$

$$+ (g \cdot \Delta Z_i)\left[C_i^2\left(\frac{\partial m_i}{\partial E_{i-1}} + \frac{\partial m_i}{\partial E_i}\right) + \frac{\partial m_i}{\partial P_r}\right] + \frac{K_i\, W_i^k\, C_i^7}{2\rho_i^k\, A_i^2} \quad ; \qquad (B\text{-}7)$$

$$v_i = \frac{1}{A_i^2}\left(\frac{W_i^k\, C_i^8}{\rho_i'^k} - \frac{W_{i-1}^k\, C_{i-1}^8}{\rho_{i-1}'^k}\right) + \frac{\overline{f}\,(W_i^k + W_{i-1}^k)\,\Delta Z_i\,(C_i^8 + C_{i-1}^8)}{8A_i^2\, m_i\, D_{hi}}$$

$$+ (g \cdot \Delta Z_i)\left[m_i^k + C_i^4\left(\frac{\partial m_i}{\partial E_{i-1}} + \frac{\partial m_i}{\partial E_i}\right)\right] + \frac{K_i\, W_i^k\, C_i^8}{2\rho_i^k\, A_i^2} \cdot \quad (B\text{-}8)$$

The total flow resistance is the sum of the individual flow resistances,

$$F^{k+1} = SW_I^{k+1} + T\,\Delta E_I^{k+1} + U\,\Delta P_r^{k+1}\, V \quad , \qquad (B\text{-}9)$$

where

$$S = \sum_{i=1}^{N} s_i \quad ,$$

$$T = \sum_{i=1}^{N} t_i \quad ,$$

$$U = \sum_{i=1}^{N} u_i \quad ,$$

$$V = \sum_{i=1}^{N} v_i \quad \cdot \qquad (B\text{-}10)$$

The pump pressure rise, ΔP_p^{k+1}, is evaluated at the advanced time in terms of the pump head at the advanced time.

$$\Delta P_p^{k+1} = \rho^k \, g \, H_p^{k+1} \quad , \tag{B-11}$$

where the pump head at the advanced time is given by

$$H_p^{k+1} = H_{ref} \left[(1+\alpha) \, (\omega^{k+1})^2 - \alpha \, \frac{W_p^k \, W_p^{k+1}}{W_{ref}^2} \right] \cdot \tag{B-12}$$

The flow rate term in the pump head equation has been linearized. Using the expansion of flow rate in terms of the flow rate at the inlet of the flow segment and collecting terms, the pump pressure rise can be expressed as

$$\Delta P_p = s_p \, W_I^{k+1} + t_p \, \Delta E_I^{k+1} + u_p \, \Delta P_r^{k+1} + v_p \quad , \tag{B-13}$$

where

$$s_p = - \rho^k \, g \, \alpha \, H_r \, \frac{W_p^k \, C_p^5}{W_{ref}^2} \quad ,$$

$$t_p = - \rho^k \, g \, \alpha \, H_r \, \frac{W_p^k \, C_p^6}{W_{ref}^2} \quad ,$$

$$u_p = - \rho^k \, g \, \alpha \, H_r \, \frac{W_p^k \, C_p^7}{W_{ref}^2} \quad ,$$

$$v_p = + \rho^k \, g \, H_r \left[(1+\alpha) \, (\omega^{k+1})^2 - \alpha \, \frac{W_p^k \, C_p^8}{W_{ref}^2} \right] \cdot \tag{B-14}$$

REFERENCES

3.1 Clinch River Breeder Reactor Plant, _Preliminary Safety Analysis Report_, Project Management Corporation.

3.2 J.W. Yang, "Penetration of Core Flow in Upper Plenum of an LMFBR," _Trans. Am. Nucl. Soc._ _23_, 414, 1976.

3.3 _Reference Manual_, _IMSL Library 3_, Edition 6, International Mathematical and Statistical Libraries, Incorporated, Houston, Texas, July 1977.

3.4 J.W. Yang and A.K. Agrawal, "An Analytical Model for Transient Fluid Mixing in Upper Outlet Plenum of an LMFBR," in _Proc. Int. Conf. Fast Reactor Safety and Related Phys._, Chicago, Illinois, October 5-8, 1976, p. 1448, CONF-761001.

3.5 T.C. Chawla et al., "The Recovery of Coolant Flow Following Rapid Release of Fission Gas from a Postulated Multiple Pin Failure in a Liquid Metal Fast Breeder Reactor Subassembly," _Nucl. Sci. Eng._ _58_, 21, 1975.

3.6 A.W. Cronenberg et al., "A Single-Bubble Model for Sodium Expulsion from a Heated Channel," _Nucl. Eng. Design 16_, 285, 1971.

3.7 F.E. Dunn et al., "The SAS2A LMFBR Accident Analysis Computer Code," ANL-8138, 1974.

3.8 N. Tanaka, "Sodium Boiling Model," in _SSC - An Advanced Thermohydraulic Code for LMFBRs, Quarterly Progress Report (July 1 - September 30, 1976)_, Brookhaven National Laboratory, BNL-NUREG-50607, December 1976.

3.9 J.E. Meyer, "Hydrodynamic Models for the Treatment of Reactor Thermal Transients," _Nucl. Sci. Eng. 10_, 269, 1961.

3.10 R.S. Brokaw, "Estimating Thermal Conductivities for Non-Polar Mixtures: Simple Empirical Method," _Ind. Eng. Chem._ _47_, 2398, 1955.

3.11 J.J. Kaganove, "Numerical Solution of the One-Group, Space-Independent Reactor Kinetics Equations for Neutron Density Given the Excess Reactivity," Argonne National Laboratory, ANL-6132, February 1960.

3.12 H. Hummel and D. Okrent, _Reactivity Coefficients in Large Fast Power Reactors_, American Nuclear Society, 1970.

3.13 J. Graham, _Fast Reactor Safety_, Academic Press, Inc., New York, 1971.

3.14 J. Yevick, _Fast Reactor Technology and Plant Design_, M.I.T. Press, Cambridge, Mass., 1966.

3.15 R.G. Palmer and A. Platt, _Fast Reactors_, Temple Press Ltd., 1961.

REFERENCES (Cont)

3.16 The Technology of Nuclear Reactor Safety, Vol. I, T. J. Thompson and
      J.G. Beckerly, Editors, M.I.T. Press, Cambridge, Mass., 1964.

3.17 F.E. Dunn et al., "The SAS2A LMFBR Accident Analysis Computer Code,"
      ANL/RAS 75-17, April 1975.

3.18 W.L. Chase, "Heat-Transport Systems," in Fast Reactor Technology:
      Plant Design, Ch. 4, edited by J.G. Yevick, The M.I.T. Press, Cambridge,
      Mass., 1966.

3.19 S.L. Additon, T.B. McCall, and C.F. Wolfe, "IANUS - Outline Description,"
      Westinghouse Advanced Reactors Division, Waltz Mill, Pennsylvania,
      FPC-939.

3.20 "LMFBR Demonstration Plant Simulation Model, Demo," Westinghouse
      Advanced Reactors Division, WARD-D-0005 (Rev 3), February 1975.

3.21 W.H. McAdams, Heat Transmission, 2nd Edition, McGraw-Hill, New York,
      1942.

3.22 N.J. Palladino, "Mechanical Design of Components for Reactor Systems,"
      in The Technology of Nuclear Reactor Safety, Vol 2, Ch. 14, edited
      by T.J. Thompson and J.G. Beckerley, The M.I.T. Press, Cambridge,
      Mass., 1973.

3.23 V.L. Streeter and E.B. Wylie, Hydraulic Transients, McGraw-Hill, New
      York, 1967.

3.24 "RELAP 3B Manual, A Reactor System Transient Code," Brookhaven National
      Laboratory, RP 1035, December 1974.

3.25 B. Donsky, "Complete Pump Characteristics and the Effects of Specific
      Speeds on Hydraulic Transients," Trans. ASME, J. Basic Eng., pp. 685-
      696, December 1967

3.26 E. Isaacson and H.B. Keller, Analysis of Numerical Methods, John Wiley
      & Sons, Inc., New York, 1966.

3.27 B.A. Martin, A.K. Agrawal, D.C. Albright, L.A. Epel, and G. Maise,
      "NALAP: An LMFBR System Transient Code," BNL-50457, July 1975.

3.28 V. Quan and A.K. Agrawal, "A Pipe-Break Model for LMFBR Safety Analysis,"
      BNL-NUREG-50688, 1977.

3.29 J.S. McNown and E.Y. Hsu, "Application of Conformal Mapping to Divided
      Flow," Proc. Midwest Conf. Fluid Dynamics, pp. 143-155, 1951.

3.30 H. Rouse and A.H. Abul-Fetouh, "Characteristics of Irrotational Flow
      Through Axially Symmetric Orifices," J. Appl. Mech. 17, pp. 421-426,
      1950

3.31 I.P. Ginzburg, <u>Applied Fluid Dynamics</u>, Chap. VI, NTIS N63-21073, 1963.

3.32 J.E. Meyer, "Conservation Laws in One-Dimensional Hydrodynamics," <u>Bettis Technical Reviews</u>, WAPD - BT - 20, pp. 61-72, September 1960.

3.33 J.E. Meyer and E.A. Reinhard, "Numerical Techniques for Boiling Flow Stability Analysis," <u>J. Heat Transfer</u>, ASME Series C, <u>87</u>, 311, 1965.

3.34 G. Birkhoff, T.F. Kines, and L.L. Lynn, "CHIC Numerical Studies for Reactor Thermal Transients," <u>Bettis Technical Reviews</u>, WAPD - BT - 27, pp. 73-83.

3.35 W.G. Mather, W.W. Zuzak, B.H. McDonald, and W.J. Hancoz, "On Finite Difference Solutions to the Transient Flow-Boiling Equations," presentation at Committee on the Safety of Nuclear Installations Specialists Meeting on Transient Two-Phase Flow, Toronto, August 1976.

3.36 G.D. Trimble and J.W. Turner, "NAIID - A Computer Program for Calculations of the Steady State and Transient Behavior (including LOCA) of Compressible Two-Phase Coolant in Networks," AAEC/E-378, 1976.

3.37 F.W. Dittus and L.M.K. Boelter, <u>Univ. Calif. Eng.</u>, <u>2</u>, 433, 1930.

3.38 J.R.S. Thom, J.A. Clark, E.R. Lady, and H. Merte, "Boiling Heat Transfer at Low Heat Fluxes," <u>Trans. ASME</u>, <u>J. Heat Transfer</u>, <u>89</u>, 235, 1969.

3.39 A.A. Bishop, R.O. Sandberg, and L.S. Tang, "Forced Convection Heat Transfer at High Pressure after Critical Heat Flux," ASME Paper 65-HT-31, 1965.

3.40 J.B. Heineman, "An Experimental Investigation of Heat Transfer to Superheated Steam in Round and Rectangular Channels," ANL-6213, 1960.

3.41 H. Graber and M. Rieger, "Experimental Study of Heat Transfer to Liquid Metals Flowing In-Line thru Tube Bundles," <u>Progress in Heat and Mass Transfer</u>, Vol. 7, pp. 151-166, O.E. Dwyer, ed. Pergamon Press, Inc. Elmsford, New York, 1973.

3.42 R.B. Harty, "Modular Steam Generator Final Project Report," TR - 097 - 330 - 010, September 1974.

4. NUMERICAL TECHNIQUE

The thermohydraulic transient simulation of an entire LMFBR system is, by its very nature, complex. Physically, the entire plant consists of many subsystems which are coupled by various processes and/or components. Mathematically, each subsystem constitutes a set of differential equations with appropriate boundary conditions. The connections between different subsystems are made through interface conditions. The numerical method employed in the SSC-L code is discussed in this chapter.

4.1 STEADY-STATE SOLUTION

4.1.1 Description

The essential components and their arrangement in a loop-type LMFBR are schematically shown in Figure 4-1. Although only one set of loops is explicitly shown in this figure, any plant can, and does, have two or more sets of loops. In the SSC-L code, the number of such sets of loops is an input parameter. In actual running of the code, one can simulate most transients by one or two sets of loops.

As shown in Figure 4-1, the primary heat transport system (PHTS) consists of reactor vessel and its internals, pump, primary side of the intermediate heat exchanger (IHX), check valve, and piping connecting these major components. The centrifugal pump is a variable speed pump. It provides pumping head for offsetting the pressure losses due to friction, change in elevation, and other considerations. The absolute pressure in this closed loop is determined when the cover gas pressure is specified. Typically, the cover gas pressure is very close to the atmospheric pressure.

The intermediate heat transport system (IHTS) consists of the secondary

- 203 -
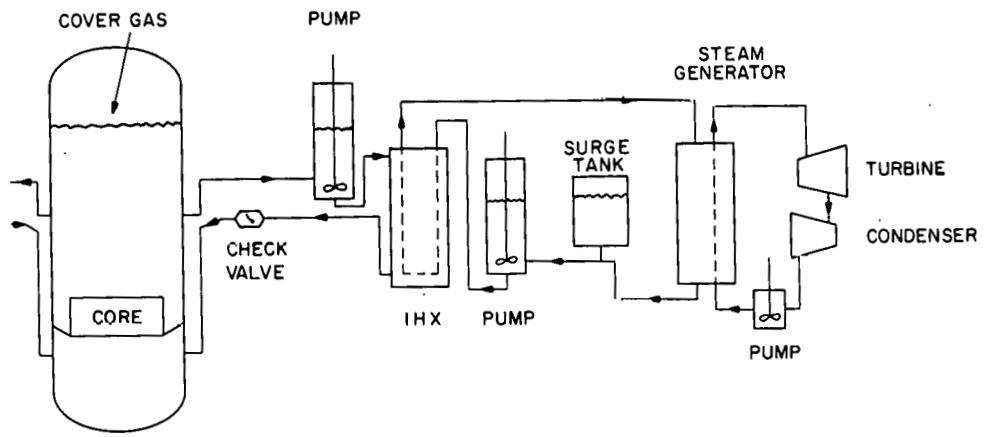
Figure 4-1. Sketch of the heat transport system.

sodium side of IHX, sodium side in the steam generator, surge tank to accommo-
date change in sodium volume, pump, and piping connecting these components. The
hydraulic characterization of this closed loop is very similar to that of the
PHTS.

The steam generator, which constitutes the essential part of the tertiary
heat transport system, can be either a recirculating type similar to the design
used in the CRBRP or a once-through type. In either case, the prime emphasis,
as far as modeling of the water/steam loop is concerned, is on adequate
representation of the steam generator. Details pertaining to the turbine and
condenser are not included.

4.1.2 Numerical Method

The main objective of the SSC preaccident calculations is to provide a
unique and stable plant-wide solution for the initialization of the transient
analysis. The preaccident calculations for the entire plant including all of
the essential components in the primary, secondary, and intermediate heat trans-
port system (HTS) can be time consuming if the overall conservation equations
are solved simultaneously. One way to reduce demand on computing time is to
take advantage of special features of the plant.

For example, the energy and momentum equations for liquid sodium can be
decoupled since thermal properties are independent of pressure. Thus, the
energy conservation equations for the primary and intermediate sodium loops can
be solved first. The required pumping head is obtained by solving the momentum
conservation equation. The energy and momentum equations for the water loop,
however, cannot be decoupled since the pressure-dependent nature of the two-
phase water properties must be considered.

The resulting system of equations to be solved is a typical set of "m"

nonlinear coupled algebraic equations with "n" unknowns (n>m). Certain groups of these equations representing the IHX and steam generator (on a component basis) must be solved iteratively. As the number of unknowns is greater than the number of independent equations, some plant variables must be known (i.e., specified) "a priori." Since uncertainties may exist as to which operating conditions are known or unknown, the user is allowed some flexibility in the selection of plant variables which are input and those which are to be calculated.

The overall logic for the plant thermal and hydraulic steady-state balance is as follows:

1. Determine the exact initialization scheme for the plant thermal balance from the input option the user has specified.

2. Iterate with the detailed steam generator and IHX thermal balances and the core gross thermal balance to achieve an overall plant thermal balance.

   (a) The steam generator water-side hydraulic balance must be determined in conjunction with the thermal balance due to the pressure-dependent nature of water-side properties and correlations.

   (b) The detailed thermal balance in the core is not required during the iterative phase of the overall thermal balance.

3. Determine the detailed in-core thermal and hydraulic balance.

4. Initialize:

   (a) primary loop hydraulics;

   (b) secondary loop hydraulics.

5. Initialize:

   (a) primary pump speed;

   (b) secondary pump speed.

Since the calculation of the plant hydraulic balance (see steps 4 and 5 above) can be done on a per loop basis and requires no iteration or special techniques, it is not discussed further here. The detailed in-vessel balance is described in Section 3.1. However, the gross plant thermal balance warrants some discussion.

A plant schematic of an equivalent single-loop system is presented in Figure 4-2. The steam generator model is for illustrative purposes of the gross energy balance only. This treatment given here would apply to a forced recirculation or once-through steam generator design.

For the purpose of illustration only, a simplified example is used in the following discussions. The gross energy balance equations may be given by the following set of five independent equations:

$$P = W_p \left[e(T_{Ro}) - e(T_{Ri}) \right], \tag{4-1}$$

$$P = U_I A_I \Delta T_I^{LM}, \tag{4-2}$$

$$P = W_I \left[e(T_{Io}) - e(T_{Ii}) \right], \tag{4-3}$$

$$P = U_{SG} A_{SG} \Delta T_{SG}^{LM}, \tag{4-4}$$

$$P = W_S \left[e_{So} - e_{FW} \right], \tag{4-5}$$

where ΔT^{LM} denotes the log-mean temperature difference and it is defined by the following expression:

$$\Delta T^{LM} = \frac{(\Delta T)_{outlet} - (\Delta T)_{inlet}}{\ln \left[\frac{(\Delta T)_{outlet}}{(\Delta T)_{inlet}} \right]}. \tag{4-6}$$

Equations (4-2) and (4-4) were obtained by assuming that U_I and U_{SG}, the overall heat transfer coefficients of the IHX and steam generator, respectively, are
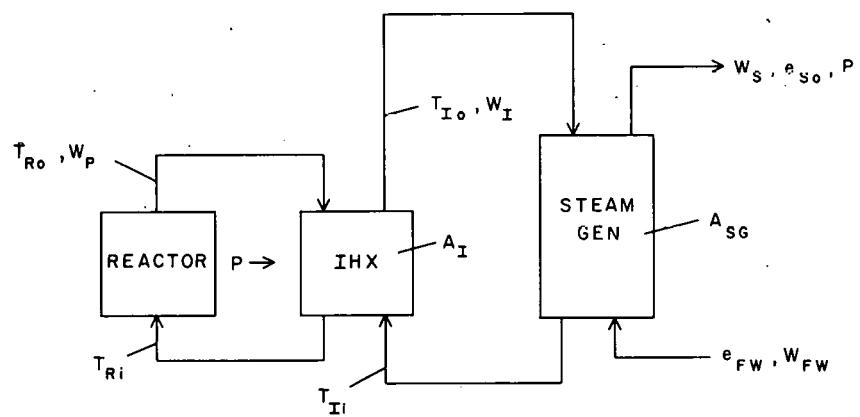
Figure 4-2. Plant schematic.

constant throughout the heat transfer portions in the IHX and steam generator. They are assumed to be known from empirical relationships. The sodium enthalpies are assumed to be functions of temperature only, while the water-side enthalpies are functions of temperature and pressure.

In actual computations for the steady-state in SSC-L, Equations (4-2) and (4-4) are replaced by a series of nodal heat balances. The overall effective heat transfer coefficients for each of these nodes are computed as a function of flow conditions, temperature, and fouling. More details of the procedure can be found in Chapter 3. Approximate forms of the heat transfer as given by Equations (4-2) and (4-4) were used to illustrate the method only.

In solving equations (4-1) through (4-5), it is assumed that A_I and A_{SG} are known from the design (although a steam generator area option is available, see Section 3.3). Also, the current version of the steam generator computational module assumes that

$$e_{FW} = f_1(W_{FW}) , \qquad (4-7)$$

thus,

$$W_S = P/(e_{So} - e_{FW}) . \qquad (4-8)$$

Relationship (4-7) is user-supplied input.

Thus, in Equations (4-1) through (4-5), nine variables remain to be determined (i.e., P, W_p, T_{Ro}, T_{Ri}, W_I, T_{Io}, T_{Ii}, e_{So} and P_{SG}). Of these nine, five can be determined by using Equations (4-1) through (4-5). The remaining four must be specified as input.

To allow some latitude in user flexibility, but to keep the total number of initialization options within reason, several constraints are placed upon which parameters may or may not be specified as input. As the reactor side and steam

generator side contain the more important parameters from the stand point of plant design and operation, it was decided to leave the entire intermediate loop as unspecified (i.e., to be determined by Equations (4-1) to (4-5)). Thus, T_{Io}, T_{Ii} and W_I may not be specified as input. Furthermore, since the total power (or power per loop P) is the prime variable, it is assumed to be always specified.

On the steam generator side, it is also assumed that the pressures (P_{SG}) at the module (e.g., evaporator, superheater) endpoints are specified. This assumption results from the particular method used to solve the steam generator initialization (see Section 3.3). It provides an efficient computational algorithm and is not felt to be overly restrictive from a user's standpoint.

Thus, in addition to five equations (Equations (4-1) through (4-5)), two other parameters (P and P_{SG}) have been assumed to be specified as input. Two additional variables, and only two, from the remaining four quantities (i.e., W_p, T_{Ro}, T_{Ri} and e_{So}) are required to specify the system completely. Various combinations of four items taken two at a time, without regard for ordering, yield six possible pairs of input specifications. These are:

Option	Parameters Specified
1	W_p, e_{So}
2	T_{Ri}, e_{So}
3	T_{Ro}, e_{So}
4	T_{Ro}, W_p
5	T_{Ri}, T_{Ro}
6	T_{Ri}, W_p

Depending on the option the user desires, the iteration logic scheme for solving the gross plant balance Equations $\left[(4\text{-}1) \text{ to } (4\text{-}5)\right]$ is selected. The iterative schemes for the various options are shown in Figure 4-3. Once the overall plant
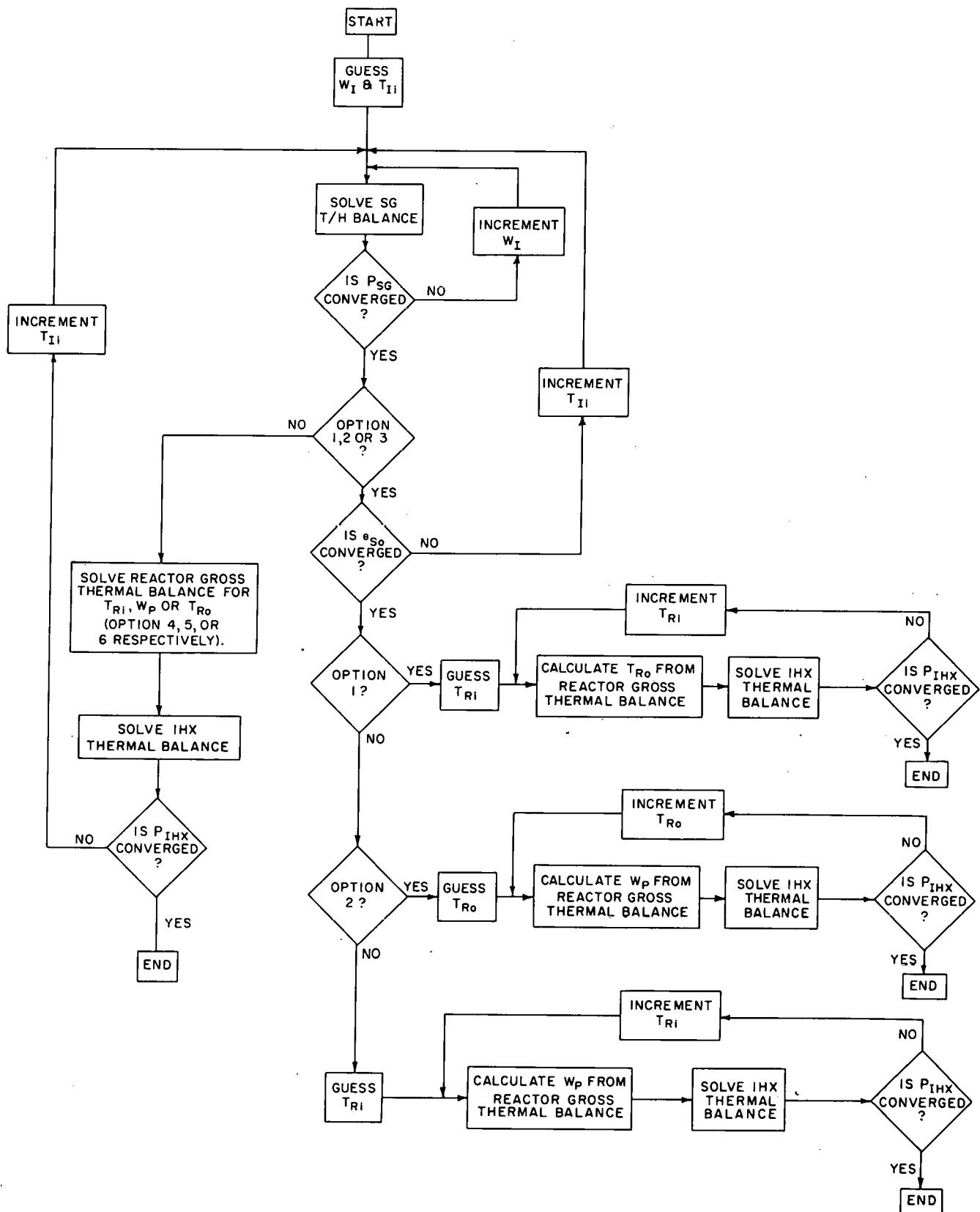
Figure 4-3. Iterative logic for plant thermal
balance at steady-state.

balance is obtained, the steady-state solution proceeds to step 3 mentioned earlier.

The above results are consistent with the fact that for a single-phase fluid in a closed loop only three state variables (temperature or enthalpy, flow rate, and pressure), either at any point in the system or at a combination of different locations, are required to specify the system completely. It should be noted that the third state variable, i.e., pressure, for the sodium loop is obtained by solving the momentum conservation equation.

4.2 INTEGRATION METHOD

The numerical integration in time of the entire system may be carried out in various ways. Two such integration strategies, geared to digital computer applications, are discussed further in this section: (1) integration of all variables at a common timestep (i.e., a single step scheme, SSS), or (2) integration of various processes/components at different timesteps (i.e., a multi-step scheme, MSS).

4.2.1 Single-Step Scheme(SSS)

The integration of the entire set of governing differential equations can be readily handled by advancing all time-dependent variables at a common timestep. This single-step scheme (SSS) is the simplest method from the standpoint of the computational logic involved.

In order to satisfy both stability and accuracy requirements, the timestep size (h) has to be the smallest of all h's for different processes. Depending upon the integration method used, the smallest h may or may not be a variable one, i.e., h(t) may or may not be allowed. Nevertheless, the entire system is solved using a common, single value for h at any instant.

For the various processes/components modeled in the SSC-L simulation, estimates for characteristic integration timesteps are shown schematically in Figure 4-4. As seen in Figure 4-4, the allowable h may be quite small. Thus, although the logic is reduced, a penalty in terms of computation time spent in various parts of the system where variations are occurring less rapidly or where, by the nature of the particular process, a larger timestep could be allowed, must be paid. Indeed, even for test cases run at BNL where highly simplified models were studied (eleven differential equations representing two components), factors of 3 in computational running times were seen between identical cases analyzed using the SSS versus the MSS.

The ratio of SSS to MSS computational time required can only increase as more detailed system models (i.e., more variables and components) are analyzed since the logic involved remains the same, while the number of equations being integrated is increased. For this reason, the MSS method is used to handle the integration in time of the SSC-L code.

4.2.2 Multi-Step Scheme(MSS)

A computationally more efficient integration strategy, which takes advantage of the fact that different components/processes may have widely varying timestep size requirements, is being used in the SSC-L code.[4.1] In this method, various portions of the overall system are advanced at different timesteps, all being controlled, however, by a master clock. This method is labeled the multi-step scheme (MSS). It should be noted that the MSS is closely related to the method of fractional steps of Yanenko.[4.2] In this section, the division of the overall system into subsystems and the resulting timestep hierarchy and computational logic are discussed. Later sections address the individual subsystem integration method and timestep
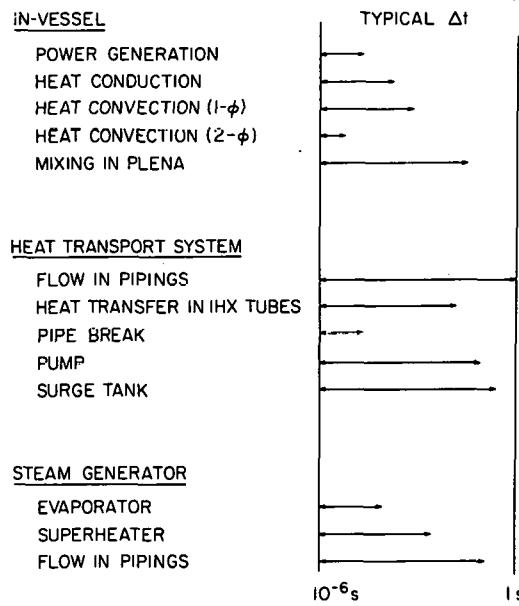
Figure 4-4. An estimate of timestep sizes by processes.

control, as well as the overall interfacing between subsystems.

The application of the MSS to the SSC code is based on physical considerations. For example, some of the subsystems or processes are known to respond rapidly while others change slowly. In general, hydraulic response is more rapid than energy/temperature response.

An important assumption used in the SSC-L code which has bearing here needs to be reiterated. In all regions of the system containing single-phase sodium coolant (i.e., primary loops, intermediate loops, and reactor plena), the appropriate sodium properties are assumed to be functions of temperature only (i.e., not of pressure). Once this assumption is made and the sodium properties investigated, they are found to be slowly varying functions of temperature.

The convective energy equations are coupled to their respective sodium flow rates, and the flow rates are coupled to the plant temperatures. However, while the coupling of the convective energy equations to the sodium flow rates is very strong, the coupling of the flow rates to the temperatures is weak and enters only through the temperature-dependent nature of the sodium properties. Since the properties vary slowly, the possibility exists to solve for the sodium flow rates at a different timestep than the energy equations.

4.2.2.1 Division of Overall System into Subsystems

In the SSC-L code, the momentum equations governing the flow rates for all the sodium loops are handled separately. These are advanced in time first. The sodium properties required are evaluated using the plant temperatures at the end of the previously completed timestep. For the purpose of the hydraulic equations only, these temperatures (and, consequently, the

- 215 -

sodium properties used in the momentum equations) are assumed to remain constant during the hydraulic timestep. Subsequently, once all the energy equations have been advanced to the hydraulic time, the updated values of temperature are then used to calculate the sodium properties for the next hydraulic timestep.

Because of the existence of two phases on the tertiary side of the stream generators, the required water properties are highly pressure and temperature dependent. Thus, the thermal and hydraulic equations on the water side cannot be treated separately, but must be advanced in time simultaneously. Also included within this set of equations are the energy equations on the sodium side of the steam generators.

The remainder of the system energy equations are segmented into three groups. The first group encompasses all the energy equations in the primary and intermediate loops, inclusive of the IHX, but exclusive of those on the steam generator sodium-side.

The in-vessel equations are distinguished by those dealing with heat conduction and power generation in the rods and those associated with the sodium coolant convection and coolant dynamics. This separation is made since, when interchannel flow redistribution is computed or when sodium boiling and/or fission gas release occur, the timestep required for the sodium convection and coolant dynamics can be drastically shorter than that for heat conduction in the rods.

Thus, the various required computations can be grouped into five separate categories. Specifically, (1) loop hydraulic calculations; (2) in-vessel sodium coolant energy and coolant dynamic calculations; (3) in-vessel rod heat conduction and power generation calculations; (4) steam generator thermal and water-side hydraulic calculations; (5) loop energy calculations.

With the preceding discussion in mind, Figure 4-5 should be referred to. Shown here is a schematic of the plant indicating the major components. Also shown are the names of those subroutines which are the main driver modules controlling the advancement in time of various blocks of the SSC-L transient segment.

The various driver modules are:

FLOW1T \
FLOW2T / Drivers (called by the same DRIV1T module) for the primary and intermediate loop sodium coolant hydraulics, respectively.

COOL6T   Driver for the in-vessel sodium coolant energy and coolant dynamics calculations

FUEL5T   Driver for the in-vessel rod heat conduction and power generation calculations

STGN3T   Driver for the steam generator energy and water-side hydraulic calculations

LOOP1T \
LOOP2T / Drivers for the primary and intermediate loop energy calculations, respectively.

A further breakdown of all subroutines which are associated with each driver is provided in Chapter 6.

Also shown in Figure 4-5, listed under each subroutine name, is the respective variable name of the simulation time of that associated section of the code. For example, S5FUEL is the current time (in s) at which the rod heat conduction and power generation calculations are being computed (driven by FUEL5T). Note that since the primary and intermediate loop hydraulics are advanced at a common timestep, their respective simulation times are identical (i.e., S1FLOW = S2FLOW). The same is true for the primary and intermediate loop energy calculations (i.e., S1LOOP = S2LOOP).
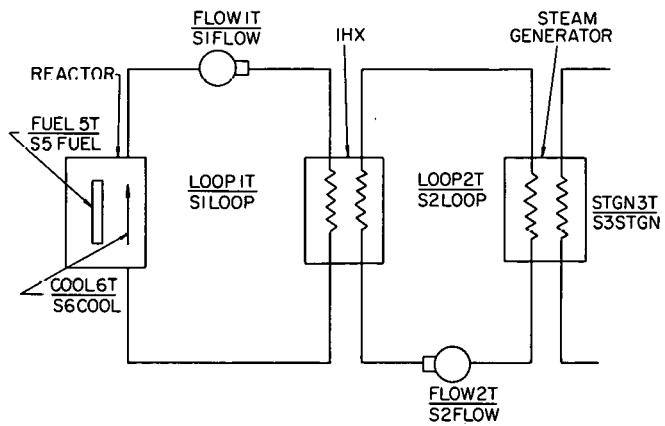
Figure 4-5. A schematic of transient computational modules and respective times.

4.2.2.2 Timestep Hierarchy

In conjunction with the partitioning of the SSC-L transient segment
as discussed above, a timestop hierarchy for the advancement in time of the
entire system must be established. The variable name for the master clock,
to which all sections must be advanced, is designated S9MSTR. The corres-
ponding master timestep is designated S9DELT. Table 4-1 indicates the various
transient code sections, their corresponding simulation time variable names,
and respective timestep names.

As in the partitioning of the SSC-L transient segment, knowledge of
the system was used in the selection of the specific hierarchy of the
various timesteps. Since the loop temperatures are assumed to respond more
slowly, in general, than any other temperatures in the system, the respective
timesteps at which those variables are advanced are set equal to the master
clock timestep (i.e., S9DELT ≡ S1DELT = S2DELT).

Although the loop hydraulics are driven separately, the plant sodium
temperatures are very tightly coupled to them. Thus, the hydraulic timestep
must exert some influence on the master timestep, since S9DELT controls how
rapidly the loop energy equations may advance. As discussed in the preceding
section, the loop hydraulics may be advanced for one timestep using the values
of the sodium temperatures at the end of the previous timestep. Since the sodium
temperatures depend strongly on the loop flow rates, the hydraulic calculations
must be executed first during any given master timestep. Once the hydraulics
are advanced one timestep (i.e., S1DELW = S2DELW), a check is immediately made.
If the hydraulic timestep had to be reduced (as dictated by the hydraulic
integration package's accuracy and/or stability requirements), the master
timestep is also immediately reduced. If the hydraulic timestep may be in-
creased, this is not allowed until the succeeding timestep, so the master timestep

Table 4-1

Code Sections with Corresponding
Simulation Times and Timestep Names

Section	Simulation Time (s)	Timestep (s)
Master Clock	S9MSTR	S9DELT
FLOW1T	S1FLOW	S1DELW
FLOW2T	S2FLOW	S2DELW
FUEL5T	S5FUEL	S5DELT
COOL6T	S6COOL	S6DELT
STGN3T	S3STGN	S3DELT
LOOP1T	S1LOOP	S1DELT
LOOP2T	S2LOOP	S2DELT

is not altered yet. The hydraulic timestep is by far the more restrictive of
the two (i.e., S1DELW is more restrictive than S1DELT), because of the
sensitive nature of the hydraulic equations. Thus, in general, once the
hydraulic timestep is allowed to increase, the loop energy timestep immediately
follows. Summarizing for the hydraulic timestep limits then, S1DELW, which
is the same as S2DELW, will never be less than, will most always equal, but
occasionally may be greater than (for one time increment) the master timestep
(S9DELT ≡ S1DELT = S2DELT). It should also be noted again, that the hydraulic
equations must be advanced first (i.e., before any other part of the system).

As discussed previously, the in-vessel calculations are handled in
two sections: (1) sodium coolant convection and coolant dynamics calculations,
and (2) rod heat conduction and power generation calculations. In general,
the required timestep for the coolant calculations is less than that for rod
calculations. This is particularly true when the flow redistribution cal-
culations are being conducted, or when sodium boiling or fission gas release
occurs. Thus, the calculations controlled by COOL6T (see Figure 4-5) are
nested within those controlled by FUEL5T and so, consequently, are their
respective timesteps. This yields a timestep hierarchy for these calculations
as follows:

$$\text{S6DELT} \leq \text{S5DELT} \leq \text{S9DELT} \quad . \qquad (4\text{-}9)$$

The remaining section of code to be assigned encompasses the steam
generator calculations, driven by STGN3T. In the steam generator, both the
thermal and water-side hydraulic calculations are advanced at a common timestep
(S3DELT). Since the only interface with the steam generator is through the
intermediate loop, the STGN3T calculations and its corresponding timestep

are nested within the loop energy calculations. Thus, S3DELT ≤ S9DELT.

The various criteria used for the timestep control of these five code sections, as well as the logic and computational algorithm involved, are discussed in detail in succeeding sections of this chapter.

4.2.3 Individual Component/Process Solver

As presented in Section 4.2.2, the time integration of the entire SSC-L transient is divided into five sections.

(1) Primary and intermediate loop hydraulic calculations.

(2) In-vessel sodium coolant convection and coolant dynamics calculations.

(3) In-vessel rod heat conduction and power generation calculations.

(4) Steam generator energy (including the steam generator, sodium, and tube wall) and water-side hydraulic calculations.

(5) Primary and intermediate loop energy (exclusive of the steam generator sodium side) calculations.

The following discussion will proceed in the order just mentioned. Only the integration method used in the various components/processes will be mentioned here. For a description of the models and/or equations which represent any particular system, refer to the appropriate section in Chapter 3. The timestep control is discussed in Section 4.3.

The momentum equations describing the hydraulic response of the primary and intermediate loops are integrated explicitly. The integration scheme is a fifth-order predictor-corrector method[4.3] of the Adams type. Algorithms are provided within the package for automatically changing the step size (by factors of 2.0) according to the accuracy requested by the user. Checks are included to test for the stability of the numerical method and to test for accuracy requests which cannot be met because of round-off error.

The majority of the differential equations in the vessel are handled

by a first-order (i.e., single layer) semi-implicit integration scheme. By semi-implicit is meant a theta-differencing method where $\theta = \frac{1}{2}$.

The energy equations in the lower plenum are handled by this first-order semi-implicit scheme. The differential equations in the upper mixing plenum encompass various energy and level calculations. These equations are currently solved by a package which integrates a system of first-order ordinary differential equations according to Gear's method.[4.4]

In the core region, the coolant dynamic equations (flow redistribution) are advanced first by the first-order semi-implicit scheme, once certain required spatial integrations are done by a finite differencing method in each axial channel (including the bypass channel). The coolant energy equations are decoupled from the fuel heat conduction equations at the cladding wall. Extrapolations of the heat flux are computed on the basis of current and previous information. Once this decoupling is done, the time integration of the energy equations can be handled by a simple marching technique, up or down each channel depending on the direction of flow. The first-order semi-implicit scheme is applied to these equations.

The transient heat conduction equations in the rod are handled by applying a first-order extrapolated Crank-Nicolson differencing scheme[4.5] to the discretized radial nodes. The solution proceeds inward from the cladding/coolant interface for each axial slice in each channel.

The method used in advancing the transient neutron fission power depends on whether the prompt jump approximation (PJA) or an "exact" solution to the point reactor kinetics equations is desired. If the PJA option is selected, the kinetics equations are handled by a fifth-order predictor-corrector package similar to that used for the flow hydraulics integration. If the "exact" solution is desired, a modified version of the method proposed by Kaganove[4.6]

- 223 -

is used to integrate the kinetics equations.

The steam generator thermal and water-side hydraulics equations are advanced using a first-order, fully-implicit integration scheme. The solution procedure involves marching first through the steam generator segments and secondly through the accumulators. The steam generator water-side flow conditions and the heat fluxes are lagged one timestep. This effectively decouples the various steam generator flow segments and heat exchangers and allows a simple marching procedure to be used. The accumulator conditions are advanced first. These conditions are then back-substituted so that the advanced steam generator water-side enthalpies and sodium temperatures in all control volumes and the advanced flow rates can be solved for. Finally, the advanced conditions for the heat fluxes and tube wall temperatures are computed.

As with the steam generator, the loop energy equations are integrated by a first-order fully-implicit scheme. The wall heat fluxes are lagged one timestep. This decouples the energy equations and allows them to be solved in a simple marching fashion (in the direction of flow) without resorting to matrix inversions.

4.2.4 Overall Interfacing

The advancement in time of the entire SSC-L transient segment has been divided into five sections, as discussed earlier in Section 4.2.2. Each section has its own individual timestep and uses various methods to handle the integration (see Section 4.2.3). Discussed here are the overall interface conditions required between these five sections and how they are computed. The impact of these interface conditions on the overall timestep control is addressed in Section 4.3.

The interface conditions are presented in the order in which they are

required by the SSC-L code. Specifically:

(1) Primary and intermediate loop hydraulics interface conditions.

(2) In-vessel sodium coolant energy and coolant dynamics interface conditions.

(3) In-vessel rod heat conduction and power generation interface conditions.

(4) Steam generator interface conditions.

(5) Primary and intermediate loop energy interface conditions.

The primary and secondary loop hydraulics calculations interface with other SSC-L sections through various system temperatures and pressure-related conditions. As discussed in Section 4.2.2, the coupling of the hydraulic response to temperature variations is weak (through sodium properties), and, consequently, temperature conditions updated at the end of the previous timestep are used during the succeeding hydraulic timestep. However, two pressure-related values are important interface conditions for the primary loop hydraulics; (1) the pressure at the vessel outlet nozzle, and (2) the overall vessel inlet nozzle to outlet nozzle pressure drop.

The pressure at the outlet nozzle is computed as the reactor cover gas pressure plus the sodium head to the outlet nozzle level. The overall nozzle-to-nozzle pressure loss is required in the complicated vessel inlet pressure calculation (see Section 3.2.10) and is evaluated using the detailed core pressure drop distributions described in Section 3.1.2. Currently, values of both the vessel outlet nozzle pressure and nozzle-to-nozzle pressure drop from the end of the preceding coolant dynamics timestep are used during the succeeding loop hydraulics timestep.

The in-vessel coolant dynamics calculations require updated interface information for the vessel inlet flow rate(s) from the primary loop(s), plus the pressure at the vessel inlet nozzle. Since the loop hydraulics

equations are integrated first, this information is available for any advanced in-vessel coolant time (i.e., S6COOL, which is advanced by increments of S6DELT as dictated by the COOL6T driver module, see Section 4.2.2). These values are linearly interpolated from previously stored values provided by the loop hydraulics calculations.

The in-vessel coolant energy equations require interface conditions of temperature at the vessel inlet nozzle(s), plus the heat fluxes at the rod cladding coolant boundaries. Since advanced values of neither the vessel inlet temperature(s) nor the heat fluxes have been calculated when the coolant energy equations are updated, extrapolations are required. Currently, linear extrapolations based on values of inlet temperature(s) and heat fluxes at the two most recently completed timesteps are provided.

The rod heat conduction calculations interface with the in-vessel coolant energy calculations at the cladding-coolant boundaries. As discussed in Section 4.2.2.2, the coolant energy calculations are nested within the rod calculations and are executed (i.e., advanced in time) first. Thus, updated coolant temperatures (and required heat transfer coefficients) at the advanced fuel time (S5FUEL, see Section 4.2.2.2) are already available.

The required interface conditions at the steam generator boundaries are the intermediate loop sodium flow rate(s) and the intermediate loop temperature(s) at the steam generator heat exchanger sodium-side inlet(s). The intermediate loop flow rate(s) at the advanced steam generator time is already available, since the sodium loop hydraulics equations have been integrated previously. A cubic spline interpolation method is used to compute the required sodium flow rate(s). A cubic spline extrapolation method (utilizing information from previously completed sodium loop energy calculations) is used to provide the necessary sodium temperature(s) at the sodium-side inlet(s) of the steam

generator heat exchanger(s).

The interface conditions required for the primary and intermediate loop energy calculations are (1) the vessel outlet temperature, (2) the sodium-side temperature(s) at the steam generator heat exchanger outlet(s),and (3) the sodium flow rate in each primary and intermediate loop. Since the loop energy equations are integrated last, all these required interface conditions from the other SSC-L transient sections are available at the advanced loop energy time (S1LOOP = S2LOOP = S9MSTR, see Section 4.2.2).

4.3 TIMESTEP CONTROL

To provide for the automatic control of the five separate timesteps utilized in the SSC-L transient segment, certain accuracy, numerical stability, and interface condition criteria must be established. The accuracy and numerical stability criteria apply to the specific integration method(s) (see Section 4.2.3) used in each of the five transient sections. The inter-face criteria apply to the boundary conditions (see Section 4.2.4) connecting the five sections to each other. In this section, the various criteria used to determine the timestep control are first discussed, then the specific algorithm used for the actual control of all timesteps in the SSC-L transient segment is described.

4.3.1 Numerical Stability and Accuracy Criteria

As discussed in Section 4.2.3, all the integration methods used in SSC-L, with the exception of the primary and intermediate loop sodium hydraulics and reactor fission power generation (when using the prompt jump approximation) integration schemes are either of a fully-implicit or semi-implicit type. Any scheme using an implicit technique is, by its very nature, inherently

- 227 -

stable in a numerical sense.

The integration schemes used to advance the primary and intermediate loop hydraulics and the fission power generation equations for the prompt jump approximation (PJA) option are identical (i.e., the same method, but different subroutines). This integration scheme uses a fifth-order predictor-corrector method of the Adams type. An algorithm is provided within the integration package to test for the stability of the numerical method. Thus, automatic control of the timesteps (i.e., S1DELW and S2DELW for the loop hydraulics and S5DELT for the PJA, see Section 4.2.2.2) for numerical stability criteria is handled within the integration scheme itself. The user is allowed no control over these numerical stability criteria.

The accuracy criteria provided within the SSC-L code enable the user to select the degree of accuracy one desires for the various system variables being integrated. All accuracy criteria require a relative accuracy limit, which is supplied by the user. A value of the relative accuracy limit desired for each of the five transient sections must be input.

These relative accuracy limits are used such that any variable being integrated in any of the five transient sections is not allowed to change, in a relative sense, by more than the specified limit during any timestep. Thus, for any variable (θ_{ij}) being integrated, the following holds:

$$\varepsilon_{ij} \equiv \left| \frac{\theta_{ij}^{k+1} - \theta_{ij}^{k}}{\theta_{ij}^{k}} \right| \leq \varepsilon_i \ , \tag{4-10}$$

where:

ε_{ij} = absolute relative deviation of variable θ_{ij} from timestep k to k+1,

θ_{ij}^{k+1} = value of θ_{ij} at timestep k+1,

θ_{ij}^k = value of θ_{ij} timestep k, and

ϵ_i = relative accuracy limit specified for transient section i.

Table 4-2 lists the five SSC-L transient sections and the names of their corresponding ϵ_i.

Within each transient section, after a timestep advancement has been completed, Equation (4-10) is applied to all variables just integrated. The maximum absolute relative change (ϵ_{ij}-max) is selected and compared to the relative accuracy limit for that transient section. If the limit has been exceeded, the timestep for that section, which will be used during the next integration step, is decreased by a factor of 2.0. Conversely, if ϵ_{ij}-max is less than a certain value (set equal to $\epsilon_i/2.0$), the timestep for that section is allowed to increase by a (factor of 2.0) during the next integration step.

This evaluation after each and every timestep of the various ϵ_{ij}-max values from each transient section forms the basis for the overall SSC-L automatic timestep control from an accuracy standpoint. For all sections integrated by fully-implicit or semi-implicit methods, the calculations of the specific ϵ_{ij}-max values are handled in separate subroutines developed expressly for this purpose (see Chapter 6). The ϵ_{ij} values for those variables integrated explicitly are calculated internally within the predictor-corrector package.

4.3.2 Interface Condition Criteria

As discussed in Section 4.2.4, the five SSC-L transient sections are coupled together through various interface conditions at component/process boundaries. Some interface conditions involve variables which have already been computed (i.e., already advanced/updated in time) at the point in the

- 229 -

Table 4-2

SSC-L Transient Sections and
Corresponding Names for Accuracy Criterion Limits

Section	Relative Accuracy Criterion Limit (ϵ_i)
FLOW1T } FLOW2T }	F1WMXA
COOL6T	F6MAXA
FUEL5T	F5MAXA
STGN3T	F3MAXA
LOOP1T } LOOP2T }	F1EMXA

execution logic when they are required. The remaining interface conditions involve variables whose advanced/updated values have not yet been computed at the point they are needed. Only these latter ("unknown") interface conditions need to be considered in establishing the interface condition criteria.

Listed in order of their requirement by the five SSC-L transient sections, these "unknown" interface conditions are (see Section 4.2.4 for a further discussion of how they are computed):

(1) For the primary and intermediate loop hydraulics calculations:

    a) reactor vessel outlet pressure,

    b) overall vessel inlet nozzle to outlet nozzle pressure drop.

(2) In-vessel sodium coolant dynamics and coolant energy calculations:

    a) sodium coolant temperature at vessel inlet nozzle(s),

    b) rod cladding-coolant heat fluxes.

(3) Rod heat conduction and power generation calculations: None.

(4) Steam generator energy and water-side hydraulics calculations: Intermediate loop temperature(s) at the steam generator heat exchanger sodium-side inlet(s).

(5) Primary and intermediate loop energy calculations: None.

At the end of each master clock step, all previously "unknown" interface conditions will have been computed. Thus, the values of the "unknown" interface conditions that were predicted during the just completed master clock timestep can be compared with the computed values for consistency. The following consistency check is made for each "unknown" interface conditions (Y_{ij}):

$$\Delta_{ij} \equiv \left| \frac{{}^{p}Y_{ij}^{k+1} - {}^{c}Y_{ij}^{k+1}}{{}^{c}Y_{ij}^{k+1}} \right| \leq \Delta_i , \qquad (4\text{-}11)$$

where

Δ_{ij} = relative absolute deviation of interface condition Y_{ij} at end of timestep k+1.

$^P Y_{ij}^{k+1}$ = predicted value of Y_{ij} at end of timestep k+1 as used in transient section i.

$^c Y_{ij}^{k+1}$ = value of Y_{ij} as computed at end of timestep k+1

Δ_i = relative absolute acceptance limit for interface conditions required by transient section i.

The values of Δ_i are specified by the user for all transient sections where

appropriate.

Equation (4-11) is applied to all Y_{ij} at the end of each master timestep,

with the exception of the rod cladding-coolant heat flux interface conditions.

As discussed in Section 4.2.2.2, the timestep for the in-vessel sodium coolant

dynamics and coolant energy calculations is nested within the timestep for the

rod heat conduction and power generation calculations, which, in turn, is nested

within the master clock timestep (i.e., S6DELT $\leq$ S5DELT $\leq$ S9DELT). Of the

five transient sections of the SSC-L code, these sections are the only ones

where a double nesting occurs. This simply means that Equation (4-11) must

be applied to the cladding-coolant heat flux interface conditions whenever

S6COOL = S5FUEL instead of delaying until S6COOL = S5FUEL = S9MSTR. The

specific logic involved in implementing all these criteria is discussed in

Section 4.2.4.

The purpose of the consistency checks performed using Equation (4-11)

is to provide a means for establishing acceptance limit criteria for the

"unknown" interface conditions. Whenever any Δ_{ij} fails to pass the consistency

test (i.e., $\Delta_{ij} > \Delta_i$), the entire system time advancement is interrupted.

The solution automatically reverts back to the end of the previously completed

master clock integration step. The timestep in the transient section whose

interface condition just failed the consistency test is decreased substantially. The solution of the overall system is then allowed to proceed once again.

4.3.3 Modifications at Print and Subset Intervals

The discussion of the overall timestep control for the SSC-L code is now complete with the exception of modifications made at print and subset intervals. For print interval control, the user supplies the input data quantity S9PINT. This is the time interval (in seconds) at which the user desires various plant variables to be printed/stored. To ensure that the master clock time (S9MSTR, see Section 4.2.2.2) falls exactly on the print interval, modification to the master clock timestep (S9DELT) is occasionally necessary.

Additionally, whenever a subset interval time is reached, modification to the individual timestep for that transient section is required occasionally. As discussed in Section 4.2.2.2, the following subsets of timesteps are established within SSC-L:

(1) S6DELT $\leq$ S5DELT $\leq$ S9DELT ,

(2) S3DELT $\leq$ S9DELT.

As seen in Table 4-1, timestep S6DELT corresponds to time S6COOL, S5DELT to S5FUEL, and S3DELT to S3STGN. Thus, to ensure that S6COOL falls exactly on S5FUEL, modification to S6DELT is sometimes required. In a like manner, modifications to S5DELT and S3DELT are occasionally necessary to ensure that S5FUEL and S3STGN fall exactly on S9MSTR, respectively. The timestep control techniques used in SSC-L to handle modifications at both print intervals and subset intervals are identical.

A test is made before any transient section time is advanced to check if a print/subset interval would be exceeded using the current value of timestep. If a print/subset interval would be exceeded, the following is done:

- 233 -

(1) The present allowed value of the affected timestep is stored.

(2) The affected timestep is set equal to the print/subset interval time minus the current time for the affected transient section.

(3) A control flag is set indicating that a modification (reduction) to the affected timestep has been made for reasons other than accuracy or stability.

(4) For the next integration step taken past the print/subset interval, the affected timestep is set equal to the presently allowed value for that timestep as dictated by accuracy, stability, and interface criteria.

4.3.4 Algorithm

The algorithm used in the SSC-L code to effect the overall automatic timestep control is shown in the logic diagram Figure 4-6. The various calculative drivers, transient section times, and timesteps are described in Section 4.2.2 and Table 4-1. Variables not identified in Table 4-1 include

- S9PRNT - Time at which certain plant variables are to be printed/ stored (seconds).

- S9PINT - Print interval increment (seconds).

- S9LAST - Problem termination time (seconds).

In Figure 4-6, the numbers in parentheses indicate the locations in the logic flow where the calculations for the five major sections of the SSC-L transient segment are executed. The remaining logic described in Figure 4-6 indicates how the criteria and modifications to the various SSC-L timesteps, discussed in Sections 4.3.1 to 4.3.3, are implemented.
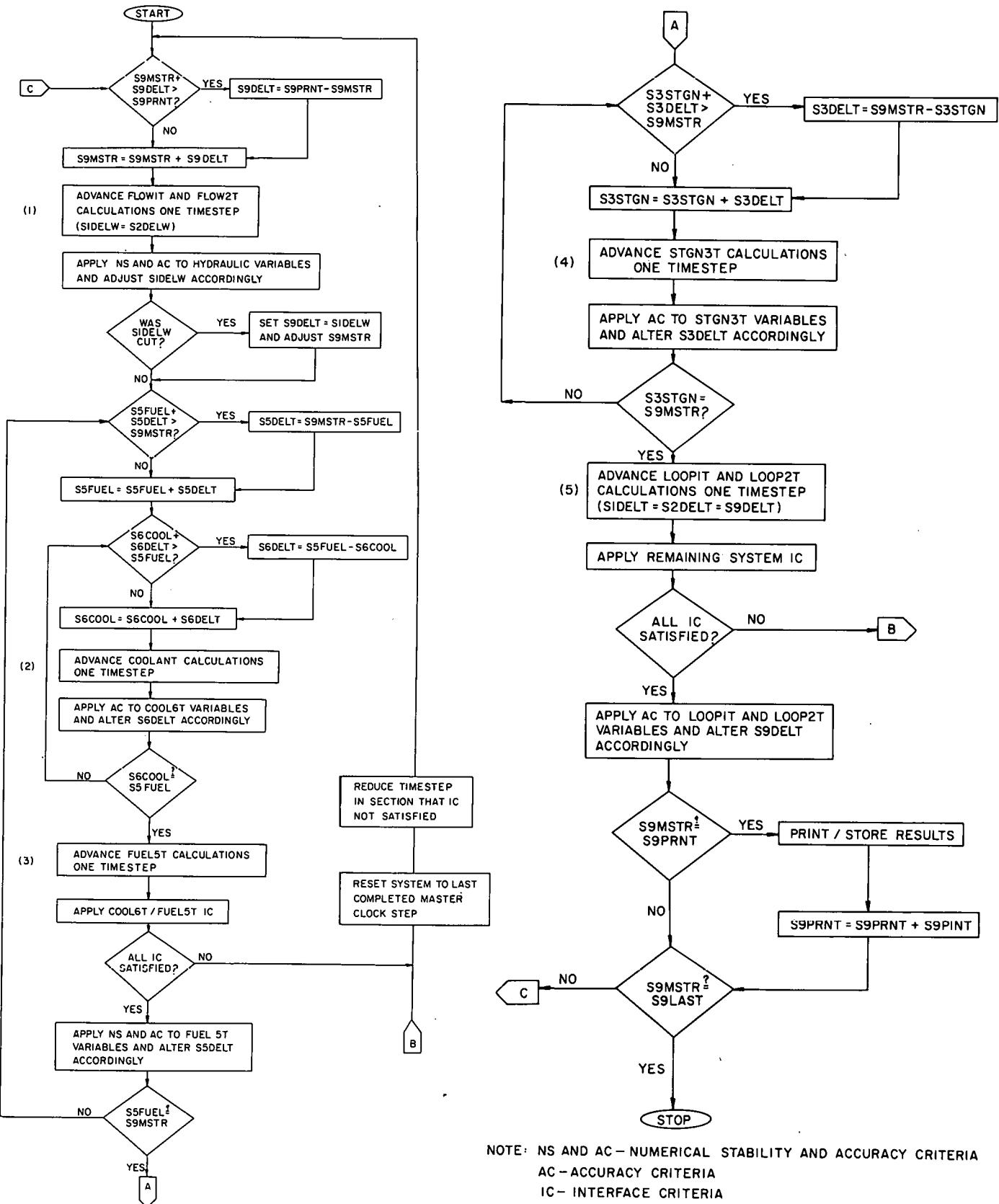
Figure 4-6. Logic diagram for overall SSC-L
timestep control.

REFERENCES

4.1 A. K. Agrawal, J. G. Guppy, I. K. Madni, V. Quan, W. L. Weaver III, and
     J. W. Yang, "Simulation of Transients in Liquid Metal Fast Breeder
     Reactor Systems," Nucl. Sci. Eng. 64, 480, 1977.

4.2 N. N. Yanenko, The Method of Fractional Steps, Springer-Verlag,
     New York, 1971.

4.3 F. T. Krogh, "Variable Order Integrators for the Numerical Solution
     of Ordinary Differential Equations," Jet Propulsion Laboratory
     Report, May 1, 1969.

4.4 M. Lees, "An Extrapolated Crank-Nicholson Difference Scheme for
     Quasi-linear Parabolic Equations," Proceedings of the Symposium on
     Non-linear Partial Differential Equations, Academic Press, 1966.

4.5 A. C. Hindmarsh, "Linear Multistep Methods for Ordinary Differential
     Equations: Method Formulations, Stability, and the Methods of
     Nordsieck and Gear," UCRL-51186 Rev. 1, March 20, 1972.

4.6 J. J. Kaganove, "Numerical Solution of the One-Group, Space-Independent
     Reactor Kinetics Equations for Neutron Density Given the Excess
     Reactivity," ANL-6132, 1960.

5. CONSTITUTIVE LAWS AND CORRELATIONS

A number of constitutive laws and correlations will be required in order to execute the SSC code. Our approach is based on providing the best available data into the code. The entire collection or part of these data may be overwritten by the user. This section provides for a collection of data that have been incorporated so far. All of the correlations and numerical values used in them are noted in the SI units.

5.1 CONSTITUTIVE LAWS

The required thermophysical and transport properties for all of the materials of interest are provided for in the form of correlations. Reasonable values for the coefficients in these correlations are provided in the SI units. These values may be changed by the user through input cards. Various constitutive laws are grouped according to materials.

5.1.1 Core and Blanket Fuel

Thermal-conductivity (W/m K)

The thermal conductivity of mixed oxide[5.1] core (UO_2-20 w/o PuO_2) and blanket (oxide) materials is given by the following relation:

$$K(T,P) = \frac{K_0 (1-P)}{1 + (1 + 10P) P} \left[\frac{1}{k_1 + k_2 T} + k_3 T^3 \right] , \qquad (5-1)$$

where typical values for k_0, k_1, k_2, and k_3 are noted in Table 5-1, and P is the fractional porosity (= 1 - fractional density).

Specific heat capacity (J/kg K)

The specific heat capacity of mixed-oxide[5.2] core and blanket materials is given by the following relations:

Table 5-1

Parameters in Fuel Thermal Conductivity
and Specific Heat Correlations

Parameter	Core material	Blanket material
k_0	113.3	113.3
k_1	0.78	0.78
k_2	0.02935	0.02935
k_3	6.60×10^{-13}	6.60×10^{-13}
P	input	input
c_0	194.319	194.319
c_1	1.3557×10^{-3}	1.3557×10^{-3}
c_2	-9.3301×10^{-7}	-9.3301×10^{-7}
c_3	2.4482×10^{-10}	2.4482×10^{-10}
c_4	502.951	502.951
c_5	0	0
T_1	3020.0	3020.0
T_2	3060.0	3060.0

$$C_p(T) = c_0 \left[1 + c_1T + c_2T^2 + c_3T^3\right] \qquad \text{for } T \leq T_1 \ , \qquad (5\text{-}2)$$

$$C_p(T) = c_p(T_1) + \frac{C_p(T_2) - C_p(T_1)}{T_2 - T_1} (T - T_1) \quad \text{for } T_1 \leq T \leq T_2 , \quad (5\text{-}3)$$

$$C_p(T) = c_4 + c_5T \qquad \text{for } T \geq T_2 \ , \qquad (5\text{-}4)$$

where values of various parameters are noted in Table 5-1, and

$$C_p(T_1) = c_0 \left[1 + c_1T_1 + c_2T_1{}^2 + c_3T_1{}^3\right] \ , \qquad (5\text{-}5)$$

and

$$C_p(T_2) = c_4 + c_5T_2 \ . \qquad (5\text{-}6)$$

Coefficient of thermal expansion (m/m K)

The average linear coefficient of thermal expansion from T_0 to T for core and blanket materials is represented by the following equation[5.3, 5.4]:

$$\overline{\alpha}(T) = \alpha_0 + \alpha_1 T \qquad \text{for } T \leq T_3 \ . \qquad (5\text{-}7)$$

For higher temperatures, the average linear coefficient of thermal expansion is given by the following relation:

$$\overline{\alpha}(T) = \alpha_2 \qquad \text{for } T \geq T_4 \ . \qquad (5\text{-}8)$$

For intermediate temperatures,

$$\overline{\alpha}(T) = \overline{\alpha}(T_3) + \frac{\overline{\alpha}(T_4) - \overline{\alpha}(T_3)}{T_4 - T_3} \qquad \text{for } T_3 \leq T \leq T_4 \ , \qquad (5\text{-}9)$$

where

$$\overline{\alpha}(T_3) = \alpha_0 + \alpha_1 T_3 \ , \qquad (5\text{-}10)$$

$$\overline{\alpha}(T_4) = \alpha_2 \ , \qquad (5\text{-}11)$$

and other parameters are noted in Table 5-2.

Table 5-2

Parameters in Fuel Coefficient of Thermal
Expansion, Density and Emissivity Correlations

Parameter	Core material	Blanket material
α_0	5.7506×10^{-6}	5.7506×10^{-6}
α_1	2.997×10^{-9}	2.997×10^{-9}
α_2	3.1×10^{-5}	3.1×10^{-5}
T_0	295.4	295.4
T_3	3020.0	3020.0
T_4	3060.0	3060.0
ρ_0	11.04×10^3	10.0×10^3
ρ_1	8.733×10^3	8.744×10^3
P	input	input
ε_0	0.75	0.75
ε_1	5×10^{-5}	5×10^{-5}
T_5	400.0	400.0

Density (kg/m^3)

The core and blanket fuel materials density is given by the following set of correlations:

$$\rho(T,P) = \frac{\rho_0(1 - P)}{\left[1 + \overline{\alpha}(T) \ (T - T_0)\right]^3} \qquad \text{for } T_0 \leq T \leq T_3 \ , \quad (5\text{-}12)$$

$$\rho(T,P) = \rho(T_3, P) + \frac{\rho(T_4, P) - \rho(T_3, P)}{T_4 - T_3}(T - T_3) \qquad \text{for } T_3 \leq T \leq T_4 \ , \quad (5\text{-}13)$$

$$\rho(T,P) = \frac{\rho_1}{\left[1 + \overline{\alpha}(T) \ (T - T_4)\right]^3} \qquad \text{for } T \geq T_4 \ , \quad (5\text{-}14)$$

where P is the fractional porosity. The above correlations imply that (a) the core fuel density for different restructured regions have the same temperature dependence below fuel solidus temperature (T_3), and (b) the molten fuel density, i.e., density beyond its liquidus temperature (T_4), does not depend upon its pre-molten fractional density. The following two equations are noted for the sake of clarity:

$$\rho(T_3,P) = \frac{\rho_0(1 - P)}{\left[1 + \overline{\alpha}(T_3)(T_3 - T_0)\right]^3} \qquad (5\text{-}15)$$

and

$$\rho(T_4,P) = \rho_1 \ . \qquad (5\text{-}16)$$

The average linear coefficient of thermal expansion is already noted above; other parameters are noted in Table 5-2.

Emissivity (-)

The core and blanket material emissivity[5.5] is given by the following correlations:

$$\epsilon = \epsilon_0 \qquad \text{for } T \leq T_5 \qquad (5\text{-}17)$$

and

$$\varepsilon = \varepsilon_0 + \varepsilon_1(T - T_5) \qquad\qquad \text{for } T \geq T_5 , \qquad\qquad (5\text{-}18)$$

where ε_0, ε_1 and T_5 are given in Table 5-2.

5.1.2 Cladding and Structural Materials

The thermal conductivity (W/mK),[5.6] specific heat (J/kgK),[5.6] and the average linear coefficient of thermal expansion (m/mK),[5.7] are represented by a polynomial fit of data. These equations for temperatures up to melting point are given by the following:

$$k(T) = k_0 + k_1 T + k_2 T^2 + k_3 T^3 , \qquad\qquad (5\text{-}19)$$

$$C(T) = c_0 + c_1 T + c_2 T^2 + c_3 T^3 , \qquad\qquad (5\text{-}20)$$

$$\overline{\alpha}(T) = \alpha_0 + \alpha_1 T + \alpha_2 T^2 , \qquad\qquad (5\text{-}21)$$

where values for various parameters for both cladding and structural materials are noted in Table 5-3. The structural or cladding material density is related to the average thermal coefficient of linear expansion as follows:

$$\frac{\rho(T)}{\rho_0} = \frac{1}{\left[1 + \overline{\alpha}(T)(T - T_0)\right]^3} , \qquad\qquad (5\text{-}22)$$

where ρ_0 is the density at temperature T_0.

The cladding and structural emissivity[5.8] are given by the following relations:

$$\varepsilon = \varepsilon_0 \qquad\qquad \text{for } T \leq T_1 \qquad\qquad (5\text{-}23)$$

and

$$\varepsilon = \varepsilon_0 + \varepsilon_1(T - T_1) \qquad\qquad \text{for } T \geq T_1 , \qquad\qquad (5\text{-}24)$$

where values for ε_0, ε_1 and T_1 are also noted in Table 5-3.

Table 5-3

Parameters for Cladding and
Structural Material Properties

Parameter	Cladding material	Structural material
k_0	9.01748	9.01748
k_1	1.62997×10^{-2}	1.62997×10^{-2}
k_2	-4.80329×10^{-6}	-4.80329×10^{-6}
k_3	2.18422×10^{-9}	2.18422×10^{-9}
c_0	380.962	380.962
c_1	0.535104	0.535104
c_2	-6.10413×10^{-4}	-6.10413×10^{-4}
c_3	3.02469×10^{-7}	3.02469×10^{-7}
α_0	1.7887×10^{-5}	1.7887×10^{-5}
α_1	2.3977×10^{-9}	2.3977×10^{-9}
α_2	3.2692×10^{-13}	3.2692×10^{-13}
T_0	298.15	298.15
ε_0	0.55	0.55
ε_1	2.5×10^{-4}	2.5×10^{-4}
T_1	400	400

5.1.3 Control Rod Material

The thermal conductivity (W/m K), the specific heat (J/kg K), the average linear thermal coefficient of expansion (m/m K), and the density (kg/m³) are represented by a polynomial fit.[5.9] These equations are:

$$k(T) = \frac{1}{k_0 + k_1 T} \left(\frac{1 - P}{1 + k_2 P}\right)(\theta - k_3) \quad , \qquad (5\text{-}25)$$

$$C_p(t) = c_0(1 + c_1 T + c_2/T^2) \quad , \qquad (5\text{-}26)$$

$$\overline{\alpha}(T) = \frac{\alpha_0 + \alpha_1 T}{T - T_0} \quad , \qquad (5\text{-}27)$$

and

$$\rho(T) = \frac{\rho_0(1 - P)}{[1 + \overline{\alpha}(T)(T - T_0)]^3} \quad , \qquad (5\text{-}28)$$

where values for the various parameters are noted in Table 5-4, and P is the porosity. These correlations are valid in the temperature range from 500 K to 1250 K.

5.1.4 Sodium

All of the required thermophysical properties for liquid sodium and sodium vapor are taken from Golden and Tokar.[5.10] These are noted in the following.

Thermal conductivity (W/m K)

The thermal conductivity of liquid sodium is given by the following equation:

$$k(T) = k_0 + k_1 T + k_2 T^2 \quad , \qquad (5\text{-}29)$$

Table 5-4

Parameters for Control Rod Material Properties

Parameter	Value
k_0	21.6178
k_1	0.05381
k_2	2.2
k_3	334.13
c_0	1741.79
c_1	2.34856×10^{-4}
c_2	$-46{,}634.7$
α_0	-1.4886×10^{-3}
α_1	4.124×10^{-6}
ρ_0	2381.0
T_0	295.4

where

$$k_0 = 109.7 \quad ,$$

$$k_1 = -6.4499 \times 10^{-2} \quad ,$$

and

$$k_2 = 1.1728 \times 10^{-5} \quad .$$

Specific heat capacity (j/kg K)

The specific heat capacity at constant pressure for liquid sodium is given by

$$C_p(T) = c_0 + c_1 T + c_2 T^2 \quad , \tag{5-30}$$

where

$$c_0 = 1630.22 \quad ,$$

$$c_1 = -0.83354 \quad ,$$

$$c_2 = 4.62838 \times 10^{-4} \quad .$$

Enthalpy (J/kg)

The enthalpy of saturated liquid sodium is given by

$$h_s(T) = h_0 + h_1 T + h_2 T^2 + h_3 T^3 \quad , \tag{5-31}$$

where

$$h_0 = -6.7511 \times 10^4 \quad ,$$

$$h_1 = 1630.22 \quad ,$$

$$h_2 = -0.41674 \quad ,$$

$$h_3 = 1.54279 \times 10^{-4} \quad .$$

For unsaturated liquid sodium, the enthalpy is written as

$$h = h_s - \frac{p_s}{\rho_s} + \frac{p}{\rho} \quad , \tag{5-32}$$

where the saturation vapor pressure and the liquid sodium density are given in the following. For incompressible sodium,

$$\rho(T,p) \equiv \rho(T) = \rho_s(T) \; ;$$

hence, Equation (5-32) becomes

$$h = h_s - \frac{p_s - p}{\rho} \quad . \tag{5-33}$$

For most purposes, the liquid sodium enthalpy may be approximated by the saturation value.

In the SSC code, we also need to compute liquid sodium temperature from its enthalpy value. Although it is computed iteratively in the code by inverting Equation (5-31), an approximate correlation was obtained:

$$T = c_0 + c_1 h_s + c_2 h_s^2 + c_3 h_s^3 + c_4 h_s^4 \quad , \tag{5-34}$$

where

$$c_0 = 55.5057 \quad ,$$

$$c_1 = 5.56961 \times 10^{-4} \quad ,$$

$$c_2 = 2.17341 \times 10^{-10} \quad ,$$

$$c_3 = -7.27069 \times 10^{-17} \quad ,$$

and

$$c_4 = 4.41118 \times 10^{-24} \quad .$$

Saturation vapor pressure (Pa, i.e., N/m^2)

The saturation vapor pressure of sodium is expressed by the following two equations:

$$\log_{10}P_s = p_1 + \frac{p_2}{T} + p_3\log_{10}T \qquad \text{for } T \leq T_1 \qquad (5\text{-}35)$$

and

$$\log_{10}P_s = p_4 + \frac{p_5}{T} + p_6\log_{10}T \qquad \text{for } T > T_1 \; , \qquad (5\text{-}36)$$

where

$$p_1 = 11.35977 \; ,$$

$$p_2 = -5567.0 \; ,$$

$$p_3 = -0.5 \; ,$$

$$p_4 = 11.68672 \; ,$$

$$p_5 = -5544.97 \; ,$$

$$p_6 = -0.61344 \; ,$$

and

$$T_1 = 1144.2 \; .$$

The saturation temperature of liquid sodium as a function of pressure is given by the following equation[5.11]:

$$T_s = \frac{c_0}{\ln(9.869 \times 10^{-6}p) - c_1} \; , \qquad (5\text{-}37)$$

where

$$c_0 = -12130.0 \; ,$$

$$c_1 = 10.51 \; ,$$

and p is the pressure in N/m^2.

Density (kg/m^3)

The density of saturated liquid sodium is given by the following relation:

$$\rho_S(T) = \rho_0 + \rho_1 T + \rho_2 T^2 + \rho_3 T^3 \qquad \text{for } T_1 \le T \le T_2 \,, \qquad (5\text{-}38)$$

where,

$$\rho_0 = 1011.597 \,,$$

$$\rho_1 = -0.22051 \,,$$

$$\rho_2 = -1.92243 \times 10^{-5} \,,$$

$$\rho_3 = 5.63769 \times 10^{-9} \,,$$

$$T_1 = 370.9 \,,$$

and,

$$T_2 = 1644.2 \,.$$

The density of unsaturated liquid sodium is related to that of saturated liquid through a compressibility factor, as follows:

$$\rho(T,p) = \rho_S(T) \exp \; \beta_T (p - p_S) \,, \qquad (5\text{-}39)$$

where $\rho_S(T)$ is given by Equation (5-38) and p_S is given by Equations (5-35) and (5-36). For incompressible assumption, $\beta_T \equiv 0$. Hence,

$$\rho(T,p) \equiv \rho(T) = \rho_S(T) \,. \qquad (5\text{-}40)$$

Dynamic viscosity $(P\ell, \text{ i.e., } N \, s/m^2)$

The dynamic viscosity of liquid sodium is represented as

$$\log_{10} n = c_1 + \frac{c_2}{T} + c_3 \; \ell pg_{10} T \,, \qquad (5\text{-}41)$$

where

$$c_1 = -2.4892 \quad ,$$

$$c_2 = 220.65 \quad ,$$

and

$$c_3 = -0.4925 \quad .$$

Heat of vaporization (J/kg)

The heat of vaporization, fitted over the range 1150 to 1500 K, is given by the following equation[5.11]:

$$\lambda(T) = \lambda_0 + \lambda_1 T + \lambda_2 T^2 \quad , \tag{5-42}$$

where

$$\lambda_0 = 4.40241 \times 10^6 \quad ,$$

$$\lambda_1 = -17.5055 \quad ,$$

$$\lambda_2 = -0.380184 \quad .$$

Specific heat capacity (J/kg K)

The specific heat capacity at constant pressure for sodium vapor was fitted over the range 1150 to 1500 K, and is given by the equation[5.11]:

$$c_{pv}(T) = c_0 + c_1 T + c_2 T^2 \quad , \tag{5-43}$$

where

$$c_0 = 4.4015 \times 10^3 \quad ,$$

$$c_1 = -2.2987 \quad ,$$

$$c_2 = 6.347 \times 10^{-4} \quad .$$

Density (kg/m³)

The density of sodium vapor is given by the following equation:

$$\rho_v = \frac{p \, A(T)}{T} \quad , \tag{5-44}$$

in which the factor $A(T)$ was fitted over the range 1150 to 1600 K and is given by the equation[5.11]:

$$A(T) = a_0 + a_1 T + a_2 T^2 , \qquad (5\text{-}45)$$

where

$$a_0 = 3.27317 \times 10^{-3} ,$$

$$a_1 = -8.72393 \times 10^{-7} ,$$

$$a_2 = 6.07353 \times 10^{-10} .$$

Enthalpy (J/kg)

At given pressure p, the sodium saturation temperature T_s is first calculated. The liquid saturation enthalpy $h_\ell(T_s)$ and heat of vaporization $\lambda(T_s)$ are then calculated. The vapor enthalpy is then given by the equation

$$h_v(T) = h_\ell(T_s) + \lambda(T_s) + h_{v_1}(T - T_s) + h_{v_2}(T^2 - T_s^2) + h_{v_3}(T^3 - T_s^3) ,$$

$$(5\text{-}46)$$

where

$$h_{v_1} = 4.4015 \times 10^3 ,$$

$$h_{v_2} = -1.14935 ,$$

$$h_{v_3} = 2.11567 \times 10^{-4} ,$$

$\lambda(T_s)$ is given by Equation (5-42), and $h_\ell(T_s)$ is given by Equation (5-31).

5.1.5 Water/Steam

The constitutive relations for water are given by correlations where the properties are evaluated as a function of enthalpy and pressure.[5.12]

Enthalpy of saturated liquid (J/kg)

The enthalpy of saturated water is given by

$$H_\ell(p) = a_0 + a_1 p + a_2 p^2 + a_3 p^3 + a_4 p^4 + a_5 p^5 , \qquad (5\text{-}47)$$

where

$$a_0 = 5.7474 \times 10^5 \quad,$$

$$a_1 = 2.09206 \times 10^{-1} \quad,$$

$$a_2 = -2.8051 \times 10^{-8} \quad,$$

$$a_3 = 2.38098 \times 10^{-15} \quad,$$

$$a_4 = -1.0042 \times 10^{-22} \quad,$$

$$a_5 = 1.6587 \times 10^{-30} \quad,$$

and p is pressure in N/m^2.

Enthalpy of saturated vapor (J/kg)

The enthalpy of saturated steam is given by

$$H_V(p) = b_0 + b_1 p + b_2 p^2 + b_3 p^3 + b_4 p^4 \quad, \tag{5-48}$$

where

$$b_0 = 2.7396 \times 10^6 \quad,$$

$$b_1 = 3.7588 \times 10^{-2} \quad,$$

$$b_2 = -7.1640 \times 10^{-9} \quad,$$

$$b_3 = 4.2002 \times 10^{-16} \quad,$$

$$b_4 = -9.8507 \times 10^{-24} \quad.$$

Temperature of compressed liquid (K)

The temperature of compressed liquid is given by

$$T(H,p) = c_0(p) + c_1(p)H + c_2(p)H^2 + c_3(p)H^3 \quad, \tag{5-49}$$

where

$$c_0(p) = c_{00} + c_{01}p \quad,$$

$$c_1(p) = c_{10} + c_{11}p \quad,$$

$$c_2(p) = c_{20} + c_{21}p \quad,$$

$$c_3(p) = c_{30} + c_{31}p \quad,$$

and the coefficients c_{ij} are given in Table 5-5.

Temperature of superheated vapor (K)

The temperature of superheated steam is given by

$$T(H,p) = d_0(p) + d_1(p)H + d_2(p)H^2 \quad, \tag{5-50}$$

where

$$d_0(p) = d_{00} + d_{01}p + d_{02}p^2 \quad,$$

$$d_1(p) = d_{10} + d_{11}p + d_{12}p^2 \quad,$$

$$d_2(p) = d_{20} + d_{21}p + d_{22}p^2 \quad,$$

and the coefficients d_{ij} are given in Table 5-6.

Density of compressed liquid (kg/m³)

The density of compressed water is given by

$$D(H,p) = \frac{e_8}{f_0 + f_1 Z + f_2 Z^2 + f_3 Z^3 + f_4 Z^4 + f_5 Z^5} \quad, \tag{5-51}$$

where

$$Z = e_7 \left[ER - PR \left(e_6 - \frac{e_5}{e_4 - ER} \right) \right] \quad,$$

$$ER = e_3 H \quad,$$

$$PR = e_1 p - e_2 \quad,$$

and the coefficients e_j and f_j are given in Table 5-7.

Density of superheated vapor (kg/m³)

The density of superheated steam is given by

$$D(H,p) = \frac{1}{g_0(p) + g_1(p)H} \quad, \tag{5-52}$$

Table 5-5

Values of Coefficients for
Temperature of Compressed Liquid Water

Coefficient	Value
c_{00}	2.7291×10^{2}
c_{01}	-1.5954×10^{-7}
c_{10}	2.3949×10^{-4}
c_{11}	-5.1963×10^{-13}
c_{20}	5.9660×10^{-12}
c_{21}	1.2064×10^{-18}
c_{30}	-1.3147×10^{-17}
c_{31}	-5.6026×10^{-25}

Table 5-6

Values of Coefficients for
Temperature of Superheated Water Vapor

Coefficient	Value
d_{00}	$6.5659 \times 10^{+2}$
d_{10}	-5.2569×10^{-4}
d_{20}	1.6221×10^{-10}
d_{01}	9.9066×10^{-5}
d_{11}	-3.4406×10^{-11}
d_{21}	1.8674×10^{-18}
d_{02}	-2.1879×10^{-12}
d_{12}	7.0081×10^{-19}
d_{22}	-1.4567×10^{-26}

Table 5-7

Values of Coefficients for
Density of Compressed Liquid Water

Coefficient	Value
e_1	1.4504×10^{-4}
e_2	2.0×10^{3}
e_3	4.2992×10^{-4}
e_4	8.0×10^{2}
e_5	1.1333
e_6	6.670×10^{-3}
e_7	1.0×10^{-3}
e_8	1.60185×10^{1}
f_0	-7.794×10^{-3}
f_1	2.7487×10^{-1}
f_2	-1.2212
f_3	2.7455
f_4	-3.0272
f_5	1.3459

where

$$g_0(p) = g_{00} + g_{01}p + g_{02}/p \quad ,$$

$$g_1(p) = g_{10} + g_{11}p + g_{12}/p \quad ;$$

and

$$g_{00} = -5.1026 \times 10^{-5} \quad ,$$

$$g_{01} = 1.1208 \times 10^{-10} \quad ,$$

$$g_{02} = -4.4506 \times 10^{+5} \quad ,$$

$$g_{10} = -1.6893 \times 10^{-10} \quad ,$$

$$g_{11} = -3.3980 \times 10^{-17} \quad ,$$

$$g_{12} = -2.3058 \times 10^{-1} \quad .$$

Specific heat of compressed liquid (J/m^{3}K)

The specific heat of compressed water is given by

$$Cp(H,p) = \frac{1}{a_0(p) + a_1(p)H + a_2(p)H^2} \quad , \qquad (5\text{-}53)$$

where

$$a_0(p) = a_{00} + a_{01}p \quad ,$$

$$a_1(p) = a_{10} + a_{11}p \quad ,$$

$$a_2(p) = a_{20} + a_{21}p \quad ;$$

and

$$a_{00} = 2.3949 \times 10^{-4} \quad ,$$

$$a_{01} = -5.1963 \times 10^{-13} \quad ,$$

$$a_{10} = 1.1932 \times 10^{-11} \quad ,$$

$$a_{11} = 2.4127 \times 10^{-18} \quad ,$$

$$a_{20} = -3.9441 \times 10^{-17} \quad ,$$

$$a_{21} = -1.6808 \times 10^{-24} \quad .$$

Specific heat of superheated vapor (J/m^3K)

The specific heat of superheated steam is given by

$$Cp(H,p) = \frac{1}{b_0(p) + b_1(p)H} \quad , \tag{5-54}$$

where

$$b_0(p) = b_{00} + b_{01}p + b_{02}p^2 \quad ,$$

$$b_1(p) = b_{10} + b_{11}p + b_{12}p^2 \quad ;$$

and

$$b_{00} = -5.2569 \times 10^{-4} \quad ,$$

$$b_{01} = -3.4406 \times 10^{-11} \quad ,$$

$$b_{02} = 7.0081 \times 10^{-19} \quad ,$$

$$b_{10} = 3.2441 \times 10^{-10} \quad ,$$

$$b_{11} = 3.7348 \times 10^{-18} \quad ,$$

$$b_{12} = -2.9134 \times 10^{-26} \quad .$$

Viscosity of compressed liquid (Ns/m^2)

The viscosity of compressed water is given by

$$
n(H,p) = c_0 + c_1X + c_2X^2 + c_3X^3 + c_4X^4
$$
$$
- (d_0 + d_1E + d_2E^2 + d_3E^3)(p - p_1) \quad H \leq H_1 \quad , \tag{5-55}
$$

$$n(H,p) = e_0(H) + e_1(H)(p - p_1) \qquad H_1 < H < H_2 \quad , \tag{5-56}$$

$$n(H,p) = f_0 + f_1Z + f_2Z^2 + f_3Z^3 + f_4Z^4 \qquad H \geq H_2 \quad , \tag{5-57}$$

where

$$X = g_0(H - g_1) \quad ,$$

$$E = g_2(H - g_3) \quad ,$$

$$Z = g_4(H - g_5) \quad ,$$

$$e_0(H) = e_{00} + e_{01}H + e_{02}H^2 + e_{03}H^3 \quad ,$$

$$e_1(H) = e_{10} + e_{11}H + e_{12}H^2 + e_{13}H^3 \quad ,$$

and the constants are given in Table 5-8.

Viscosity of superheated vapor (Ns/m^2)

The viscosity of superheated steam is given by

$$\eta(H,p) = (a_0 + a_1T) - D(b_0 + b_1T) \qquad \text{for } T \le 300, \qquad (5\text{-}58)$$

$$\eta(H,p) = (a_0 + a_1T) + (c_0 + c_1T + c_2T^2 + c_3T^3)D$$
$$+ D(d_0 + d_1T + d_2T^2 + d_3T^3)(e_0 + e_1D + e_2D^2) \qquad (5\text{-}59)$$
$$\text{for } 300 < T < 375,$$

$$\eta(H,p) = (a_0 + a_1T) - D(e_0 + e_1D + e_2D^2) \qquad \text{for } T \ge 375; \qquad (5\text{-}60)$$

where

$$T = T_v(H,p) - 273.15 \quad ,$$

$$D = D_v(H,p) \quad ,$$

and the constants are given in Table 5-9.

Conductivity of compressed liquid (W/m K)

The thermal conductivity of compressed water is given by

$$k(H,p) = a_0 + a_1X + a_2X^2 + a_3X^3 \quad , \qquad (5\text{-}61)$$

where

$$X = \frac{H}{5.815 \times 10^5}$$

Table 5-8

Values of Coefficients for
Viscosity of Compressed Liquid Water

Coefficient	Value
c_0	1.2995×10^{-3}
c_1	-9.2640×10^{-4}
c_2	3.8105×10^{-4}
c_3	-8.2194×10^{-5}
c_4	7.0224×10^{-6}
d_0	-6.5959×10^{-12}
d_1	6.763×10^{-12}
d_2	-2.8883×10^{-12}
d_3	4.4525×10^{-13}
e_{00}	1.4526×10^{-3}
e_{01}	-6.9881×10^{-9}
e_{02}	1.5210×10^{-14}
e_{03}	-1.2303×10^{-20}
e_{10}	-3.8064×10^{-11}
e_{11}	3.9285×10^{-16}
e_{12}	-1.2586×10^{-21}
e_{13}	1.2860×10^{-27}
f_0	3.0260×10^{-4}
f_1	-1.8366×10^{-4}
f_2	7.5671×10^{-5}
f_3	-1.6479×10^{-5}
f_4	1.4165×10^{-6}
H_1	2.76×10^5
H_2	3.94×10^5
p_1	6.8946×10^5
g_0	8.5813×10^{-6}
g_1	4.2659×10^4
g_2	6.4845×10^{-6}
g_3	5.5359×10^4
g_4	3.8921×10^{-6}
g_5	4.0147×10^5

Table 5-9

Values of Coefficients for
Viscosity of Superheated Water Vapor

Coefficient	Value
a_0	4.07×10^{-8}
a_1	8.04×10^{-6}
b_0	1.858×10^{-7}
b_1	5.9×10^{-10}
c_0	-2.885×10^{-6}
c_1	2.427×10^{-8}
c_2	-6.7893×10^{-11}
c_3	6.3170×10^{-14}
d_0	1.76×10^{2}
d_1	-1.6
d_2	4.8×10^{-3}
d_3	-4.7407×10^{-6}
e_0	3.53×10^{-8}
e_1	6.765×10^{-11}
e_2	1.021×10^{-14}

and

$$a_0 = 5.7374 \times 10^{-1} \quad,$$

$$a_1 = 2.5361 \times 10^{-1} \quad,$$

$$a_2 = -1.4547 \times 10^{-1} \quad,$$

$$a_3 = 1.3875 \times 10^{-2} \quad.$$

<u>Conductivity of superheated vapor (W/m K)</u>

The thermal conductivity of superheated steam is given by

$$k(H,p) = X + D\left(Z + \frac{cD}{T^{4\cdot2}}\right) \quad, \tag{5-62}$$

where

$$T = T(H,p) - 273.15 \quad,$$

$$D = D(H,p) \quad,$$

$$X = a_0 + a_1 T + a_2 T^2 + a_3 T^3 \quad,$$

$$Z = b_0 + b_1 T + b_2 T^2 \quad;$$

and

$$a_0 = 1.75 \times 10^{-2} \quad,$$

$$a_1 = 5.87 \times 10^{-5} \quad,$$

$$a_2 = 1.04 \times 10^{-7} \quad,$$

$$a_3 = -4.51 \times 10^{-11} \quad,$$

$$b_0 = 1.0351 \times 10^{-4} \quad,$$

$$b_1 = 4.198 \times 10^{-7} \quad,$$

$$b_2 = -2.771 \times 10^{-11} \quad.$$

In addition to the properties listed above, various partial derivatives of many of the functions were required. These were obtained by analytically differentiating the pertaining correlations.

5.2 CORRELATIONS

The required pressure drop and heat transfer correlations for the range of interest are included in this section. Representative values for various curve-fitted parameters are also noted in the SI units.

5.2.1 Friction Factor Correlations

Fluid flow and heat transfer correlations for the entire flow regime are required by the SSC code. The following is a compilation of the friction factor correlations that have been selected or developed so far.

The pressure change due to frictional effect is given by the following equation:

$$\frac{\Delta P}{\Delta L} = - \frac{f}{D_h} \left(\frac{1}{2} \rho U^2 \right) \quad , \tag{5-63}$$

where the hydraulic channel diameter, D_h, is defined as

$$D_h = \frac{4 \cdot (\text{flow area})}{\text{wetted perimeter}} \quad , \tag{5-64}$$

and U is the fluid velocity. The friction factor, f, depends on the Reynolds number Re and the surface roughness, ε. The friction factor for turbulent flow in a pipe is given in the Moody chart. The Moody chart is expressed as[5.13] the following transcendental equation:

$$\frac{1}{\sqrt{f}} = - 2.0 \; \log_{10} \left(\frac{\varepsilon / D_h}{3.7} + \frac{2.51}{Re\sqrt{f}} \right) \quad . \tag{5-65}$$

For smooth pipes, i.e., for $\varepsilon / D_h = 0$, the above equation simplifies to the following transcendental equation:

$$\frac{1}{\sqrt{f}} = 2.0 \; \log_{10} (Re \cdot \sqrt{f}) - 0.80 \quad , \tag{5-66}$$

which is the same as Prandtl's universal law of friction for smooth pipes.[5.14]

A simplified form of friction factor rather than the above-mentioned transcendental equation is desireable. The following explicit relation for f,[5.15] which is accurate within ±5%, has been coded in SSC.

$$f = 0.0055 \left\{ 1 + \left[20000 \cdot \frac{\varepsilon}{D_h} + \frac{10^6}{Re} \right]^{1/3} \right\} . \tag{5-67}$$

For smooth pipes, the above equation reduces to

$$f = 0.0055 + 0.55(Re)^{-1/3} , \tag{5-68}$$

which is very similar to the Koo correlation.[5.16]

A comparison for computing efficiency in calculating f from either Equation (5-65) or Equation (5-67) was made. The approximate representation, Equation (5-67), was found to be 25% more efficient. Since the friction factor needs to be evaluated for each pipe section or node section, only Equation (5-67) for f has been incorporated in SSC.

The friction factor for laminar flow is given by

$$f = \frac{64}{Re} . \tag{5-69}$$

The Reynolds number is evaluated at bulk temperature of the fluid.

In the case of two-phase flow of water, the effective friction factor is the product of f [Equation (5-67)] with a two-phase friction multiplier ϕ_{TP}. It is given by[5.17]:

$$\phi_{TP} = (1.0 + 8.0x) \left(\frac{p}{8.1685 \cdot 10^6} \right)^{0.04066 - 7.533X} \tag{5-70}$$

where p is the pressure in N/m^2 and x is the quality.

For wire-wrapped fuel rod bundles, the following correlation for friction factor is used[5.18]:

$$f_{bundle} = \left[\frac{1.034}{(P/D)^{0.124}} + \frac{29.7 \, (P/D)^{6.94} Re^{0.086}}{(P_w/D)^{2.239}} \right]^{0.885} 0.316 \, Re^{-0.25} . \tag{5-71}$$

This equation is found to compare favorably with FFTF tests (P/D $\geq$ 1.08).

For laminar flow in rod bundles, Axford gave the following expression[5.19]:

$$c_f \cdot Re_D = \frac{1}{M} \left[\frac{A_F}{(P/D)^2} \right]^2 \frac{16 \times 24}{\pi} \quad , \tag{5-72}$$

where

$$c_f = \frac{f}{4} \quad .$$

Re_D is the Reynolds number based on rod diameter, and M is a function of (P/D). This correlation can be rewritten in terms of Moody friction coefficient and Reynolds number based on hydraulic diameter as

$$f \cdot Re = \frac{2\pi}{3} \frac{1}{M} \frac{1}{(P/D)^4} \left[\frac{2\sqrt{3}}{\pi} \left(\frac{P}{D} \right)^2 - 1 \right]^3 \quad . \tag{5-73}$$

The parameter M is a complicated function of P/D. From the computed values[5.20] of M for P/D in the range 1.05 to 1.5 , a simple correlation for M was developed:

$$M = f_0 + f_1(P/D) + f_2(P/D)^2 + f_3(P/D)^3 \quad , \tag{5-74}$$

where

$$f_0 = 0.0618456 \quad ,$$

$$f_1 = -0.137837 \quad ,$$

$$f_2 = 0.0898949 \quad ,$$

and

$$f_3 = -0.013786 \quad .$$

The friction factor in the transition region can be determined by linear interpolation of values at the end of turbulent flow regime and that at the beginning of laminar flow regime.

5.2.2 Heat Transfer Correlations

The liquid metal heat transfer correlations for forced convection in a rod bundle have been developed by West, Schad, Graber and Rieger, and Borishanskii. These correlations have been compared with the experimental data by Kazimi.[5.21] In view of the comparison, the modified Schad correlation is selected. The following correlation is valid for Pe > 10, i.e., for turbulent flow regime:

$$Nu = \left[h_1 + h_2(P/D) + h_3(P/D)^2 \right] \cdot (a + b\, Pe^c) , \qquad (5-75)$$

where

$$h_1 = -16.15 ,$$

$$h_2 = 24.96 ,$$

$$h_3 = -8.55 ,$$

and

$$a = 0, \qquad b = 1, \quad c = 0.3 \qquad \text{for } Pe \geq 150 ,$$

or

$$a = 4.496, \quad b = 0, \quad c = 0.3 \qquad \text{for } Pe < 150 .$$

The above correlation also agrees well for laminar flow regime.

For liquid metal flow in a pipe, Aoki's[5.22] correlation for heat transfer is used:

$$Nu = 6.0 + 0.025(\overline{\psi}\, Pe)^{0.8} , \qquad (5-76)$$

where

$$\overline{\psi} = \frac{0.014(1 - e^{-71.8X})}{X} ,$$

$$X = \frac{1}{Re^{0.45}\, Pr^{0.2}} .$$

In the laminar region,

$$Nu = 4.36 \qquad \text{for } Re \leq 3000 . \qquad (5-77)$$

For the shell side in the intermediate heat exchanger, Nusselt number is obtained from the Graber-Rieger correlation[5.23]:

$$Nu = A + B Pe^C \qquad 110 \leq Pe \leq 4300 \qquad (5\text{-}78)$$
$$1.25 \leq P/D \leq 1.95 \ ,$$

where

$$A = 0.25 + 6.2(P/D) \ ,$$

$$B = -0.007 + 0.032 \ (P/D),$$

and

$$C = 0.8 - 0.024(P/D) \ .$$

The range of applicability is also indicated above. For Pe < 110, we use a constant value for Nu (= Nu at Pe = 110).

The heat transfer correlations for water/steam are given for four different modes of heat transfer. The first mode of heat transfer is forced convection. The Nusselt number for this mode is given as[5.24]

$$Nu = 0.023 \ Re^{0.8} \ Pr^{0.33} \ . \qquad (5\text{-}79)$$

The heat transfer for nucleate boiling is given as[5.25]

$$T_s - T_{sat} = 0.02253 \ \sqrt{q} \ \exp(-p/8.69 \cdot 10^6) \ , \qquad (5\text{-}80)$$

where T_s is the temperature at inner surface of tube, T_{sat} is the saturation temperature of water at pressure p, and q is the surface heat flux in W/m^2.

The heat transfer for film boiling regime is given as[5.26]

$$Nu = 0.0193 \ Re_\ell^{0.8} Pr_\ell^{1.23} \left(\frac{\rho_B}{\rho_g}\right)^{0.68} \left(\frac{\rho_\ell}{\rho_g}\right)^{0.068} \ , \qquad (5\text{-}81)$$

where subscripts ℓ and g denote, respectively, liquid and vapor phase at saturation and subscript B indicates bulk property of steam/water mixture.

For superheated steam, the following heat transfer correlation for forced convection is used[5.27]:

$$Nu = 0.0133 \ Re^{0.84} \ Pr^{0.333} \ .$$ (5-82)

The steam/water quality at the DNB point is given by[5.28]

$$X_{DNB} = \frac{4.38 \times 10^4 \ \rho_\ell}{H_{\ell g} \ \rho_g \ \sqrt{G/1350.0}} \qquad \text{for } q > 6.3 \times 10^5 \ ,$$ (5-83)

or

$$X_{DNB} = \frac{4.38 \times 10^4 \ \rho_\ell \ \cdot \ (5.3 \times 10^5/q)^{1.5}}{H_{\ell g} \ \rho_g \ \sqrt{G/1350.0}} \qquad \text{for } q < 6.3 \times 10^5 \ ,$$ (5-84)

where $H_{\ell g}$ is the latent heat of vaporization (J/kg), G is the mass flow rate per unit area (kg/s m^2), and q is in W/m^2.

REFERENCES

5.1   LIFE-II Committee, ANL, Priv. Comm., 1973.

5.2   R.G. Gibbym L. Leibowitz, J.F. Kerrisk and D.G. Clifton, "Analytical Expressions for Enthalpy and Heat Capacity for Uranium-Plutonium Oxide," HEDL-TME 73-60, June 1973.

5.3   B.F. Rubin, "Summary of (U, Pu) O_2 Properties and Fabrication Methods," GEAP-13582, November 1970.

5.4   M.F. Lyons et al., "UO_2 Properties Affecting Performance," Nucl Eng. & Design 21, 167 (1972).

5.5   Thermophysical Properties of Matter, "Thermal Radioactive Properties of Non-Metallic Solids," Vol. 8 edited by Y.S. Touloukian, 1972.

5.6   "Mechanical and Physical Properties of the Austenitic Chromium-Nickel Stainless Steels at Elevated Temperatures," The International Nickel Company, Inc., New York, 1963.

5.7   C.S. Kim, "Thermophysical Properties of Stainless Steel," ANL 75-55, 1975.

5.8   J. Humphries, "On the Thermal Emittance of Stainless Steels," J. of British Nucl. Energy Soc. 13, 271 (1974).

5.9   "A Compilation of Boron Carbide Design Support Data for LMFBR Control Elements," HEDL-TME 75-19, 1975.

5.10 G.H. Golden and J.V. Tokar, "Thermophysical Properties of Sodium," ANL-7323, August 1967.

5.11 F.E. Dunn, G.J. Fischer, T.J. Heames, P.A. Pizzica, N.A. McNeal, W.R. Bohl and S.M. Prastein, "The SAS2A LMFBR Accident Analysis Computer Code," ANL-8138, October 1974.

5.12 W. Wulff et al., "Development of a Computer Code for Thermal Hydraulics of Reactors (THOR)," Fifth Quarterly Progress Report, Sect. 3.2, BNL-NUREG-50534, July 1976.

5.13 C.F. Bonilla, "Fluid Flow in Reactor Systems," Nuclear Engineering Handbook, pp. 9-30, edited by H. Etherington, McGraw-Hill Book Company, Inc., New York, 1958.

5.14 H. Schlichting, Boundary Layer Theory, 4th Edition, p. 515, McGraw-Hill, Inc., New York, 1968.

REFERENCES (Cont)

5.15 S. Levy, "Fluid Flow," Ch. 15 in The Technology of Nuclear Reactor Safety, Vol. 2, edited by T.J. Thompson and J.G. Beckerly, The M.I.T. Press, Cambridge, Massachusetts, 1973.

5.16 W.H. McAdams, Heat Transmission, 2nd edition, McGraw-Hill, New York, 1942.

5.17 J.R.S. Thom, "Prediction of Pressure Drop During Forced Circulation Boiling of Water," Int. J. Heat Mass Transfer 7, 709 (1964).

5.18 E.H. Novendstern, "Turbulent Flow Pressure Drop Model for Fuel Rod Assemblies Utilizing a Helical Wire-Wrap Space System," Nucl. Eng. & Design 22, 19 (1972).

5.19 R.A. Axford, "Summary of Theoretical Aspects of Heat Transfer Performance in Clustered Rod Geometries," LA-AC-9786, 1968.

5.20 R.A. Axford, "Two-Dimensional Multiregion Analysis of Temperature Fields in Reactor Tube Bundles," Nucl. Eng. & Design 6, 25 (1967).

5.21 M.S. Kazimi, "Heat Transfer Correlation for Analysis of CRBRP Assemblies," WARD-D-0034, April 1974.

5.22 S. Aoki, "Current Liquid-Metal Heat Transfer Research in Japan," Progress in Heat & Mass Transfer, Vol. 7, pp. 569-573, edited by O.E. Dwyer, Pergamon Press, Inc., Elmsford, New York, 1973.

5.23 H. Graber and M. Rieger, "Experimental Study of Heat Transfer to Liquid Metals Flowing In-Line Through Tube Bundles," Progress in Heat & Mass Transfer, Vol. 7, pp. 151-166, edited by O.E. Dwyer, Pergamon Press, Inc., Elmsford, New York, 1973.

5.24 F.W. Dittus and L.K. Boelter, Univ. of Calif. Publs. Eng. 2, 433 (1930).

5.25 J.R.S. Thom, J.A. Clark, E.R. Lady and H. Merte, "Boiling Heat Transfer at Low Heat Flux," Trans. ASME, J. Heat Transfer 89, 235 (1967).

5.26 A.A. Bishop, R.O. Sandberg and L.S. Tong, "Forced Convection Heat Transfer at High Pressure after Critical Heat Flux," ASME Paper 65-HT-31, 1965.

5.27 J.B. Heineman, "An Experimental Investigation of Heat Transfer to Superheated Steam in Round and Rectangular Channels," ANL-6213, 1960.

5.28 R.B. Harty, "Modular Steam Generator Final Project Report," TR-097-330-010, September 1974.

6. CODE DESCRIPTION

6.1 CODING GUIDELINES

6.1.1 Applicable Coding Standards

A set of practices intended to insure uniform and concise notation as well as to simplify code conversions and modifications has been maintained throughout SSC-L. These guidelines were developed so as to adhere to the formal standards of the American National Standards Institute (ANSI) and the American Nuclear Society (ANS). The SSC standards adhere closely to the language specifications of[6.1] "USA Standard FORTRAN", ANSI X3.9-1966 and adhere closely to the recommendations set forth in the following documents:

- ANS STD.3-1971   "Recommended Programming Practices to Facilitate the Interchange of Digital Computer Programs"[6.2]

- ANSI Standard N413-1974   "Guidelines for the Documentation of Digital Computer Programs"[6.3]

- ANSI Standard X3.5-1968   "Flow Chart Symbols and Their Usage in Information Processing"[6.4]

Additionally, practices set forth in the preliminary draft of RDT F 1-4[6.5] were considered. Wherever possible, many of the recommendations contained in this pending standard were implemented into the SSC-L coding.

6.1.2 Code Structure and Data Management

SSC is a deliberately structured ensemble of modules each of which performs a well-defined set of tasks. A module is broken down into submodules such that each submodule performs a single task. Submodules are designed so

that they may be easily replaced or exported from the code. As much as possible, all data linkage is maintained via labeled common blocks. To assure agreement of data definitions, all nonexecutable statements defining variables in a given common are identical in every routine using that common (exception is made for a number of well-defined data management routines).

A variable dimensioning (dynamic allocation) scheme is used throughout the program. Data transfer of dimensional arrays is accomplished by passing a large container array via labeled common. The starting locations and lengths of each individual array within the container are also passed via labeled common. At the module and submodule level, equivalence statements are employed so that naming convention for variables (discussed later) can be maintained for better user understanding and readability. This particular scheme of variable dimensioning was selected because of its superior efficiency of data transfer and inherent characteristics for permitting a minimization of storage.

A symbolic naming scheme was adopted for SSC and used throughout. This was done to avoid the problems caused by naming ambiguities and degeneracies prevalent in other large system codes. Symbolic names are restricted to six or fewer characters and are used for several different types of entities, specifically:

Variables used by several modules via labeled common,

Common block names,

Routine names, and

Statement functions.

A summary of the SSC naming convention is given in the following section.

6.1.3 Symbolic Naming Convention

The naming convention attempts to convey as much information as possible about an entity while maintaining the final label as mnemonic as possible. To this end, SSC names reserve two (and occasionally three) characters to identify general entity type and purpose and leave four characters to be assigned mnemonically. Specifically, the symbolic naming convention for variables and names is as follows:

- LOCAL VARIABLES (including those shared via scratch COMMON):

    May not contain embedded digit; i.e., digits only at end.

    First character should conform to Table 6-1, if applicable.

- GLOBAL VARIABLES:

    First character is a letter specifying the type of quantity, e.g., P for pressure. See Table 6-1.

    Second character is a digit indicating module which alters the value (i.e., region of reactor system). See Table 6-2.

    Remaining characters (up to four; at least one) are assigned mnemonically, with no embedded digits. (Digits may occur at end, or starting with third character: P6ABC2, P67B5).

- ROUTINE NAMES:

    First two to four characters are mnemonically assigned, except that second may not be a digit.

    Next character is a digit indicating module (or region). See Table 6-2.

    Last character(s): one or two letters, indicating overlay name etc. See Table 6-3.

    Examples: READ1R, VRFY7R, MAIN9S, FUEL5S, PBAL9S.

Table 6-1

Initial Letters Used to
Indicate Type of Quantity and Units

A	Area	m^2
B	Mass	kg
C	Material properties; constants	(See Table 6-2.)
D	Density	kg/m^3
E	Energy; enthalpy	J; J/kg
F	Fractions, factors	-
G	Mass flow rate per unit area	$kg/s\ m^2$
H	Heat transfer coefficients	W/m^2K
P	Pressure; power	N/m^2; W
Q	Surface heat flux; catch-all	W/m^2; --
R	Reactivity; angular measure	$\Delta K/K$; radians
S	Time	s
T	Temperature	K (not C)
U	Velocity	m/s
V	Volume	m^3
W	Mass flow rate	kg/s
X	Distance (length or radius)	m
Y	Distance (width or diameter)	m
Z	Distance (height or axial)	m

I, J, K   Used for index values of dimensioned arrays (used in order).

L   Control flags, counters, etc.

M   Maximum compiled dimensions, other integer constraints.

N   Actual dimensions used (e.g., number of channels used).

Table 6-2

Digits Used to Indicate
Major Modules (or Regions)

1	Primary loop (NOT including IHX or vessel).
2	Secondary loop, including IHX (but not steam generator).
3	Tertiary loop and steam generator (but not turbine, condenser).
4	Turbine, condenser.
5	Fuel (and blanket) rods.
6	Reactor core coolant volumes.
7	Reactor vessel, structure, etc.
8	- (unassigned).
9	Global or general quantities, not pertaining to a specific module or modules (or regions).

NOTE: For entities pertaining to more than one region, the digit used is determined by whichever module creates or alters it.

For material properties constants (first character is "C"), the digits have a slightly different meaning:

1	Sodium.	2	Sodium vapor
3	Water or steam.	4	Reactor fuel blanket.
5	Reactor fuel.	6	Cladding of fuel rods.
7	Steel, other structural material.	8	Reactor cover gas.

Also, for material properties constants, the third character is meaningful; for example:

A	Coefficient of thermal expansion.		
C	Specific heat capacity.	K	Thermal conductivity.
D	Density.	N	Dynamic viscosity.
E	Emissivity.	P	Pressure.
H	Enthalpy	T	Temperature.

Table 6-3

Final Letters Used for Routine Names

R	Routines of the data reading and restart segment.
S	Routines of the steady-state calculation segment.
T	Routines of the transient time-stepping segment.
U	Utility routines used by more than one program segment.
F	Functions other than those calculating material properties.
*	The final letters of material properties functions generally correspond to those used for the third character for material properties constants (see Table 6-2).

6.2 FLOW CHART

The modularized structure of the SSC-L code lends itself to a natural subdivision. The code is divided into three sequentially disjointed processes as shown in Figure 6-1. These routines are the main driver programs of SSC and are called in succession by the controller routine, SSC-L. Each performs a unique set of tasks and is executed only once for any given case. It should be noted that this type of structure permits the use of system routines such as CDC's utility OVERLAY to make the most efficient use of field length. The flow chart of each of the drivers, along with its associated subroutines, is shown in Figures 6-2 through 6-10. The naming convention discussed earlier (Section 6.1.3) is used in selecting program and subprogram names. Only a short description of these subroutines is included in the following.

MAIN9R

This routine is the main driver for the input-initialization module. It calls the free-format card reader routines in a sequence specified by the user. The data verification, as well as a series of data management routines, are also called from this routine.

CALC1R

This routine initializes secondary and subsequent loop structures where the user has chosen to default these values to those entered for the primary loop.

CALC3R

This routine loads the input data into the data arrays, using the component order information generated by VRFY3R.

- 277 -
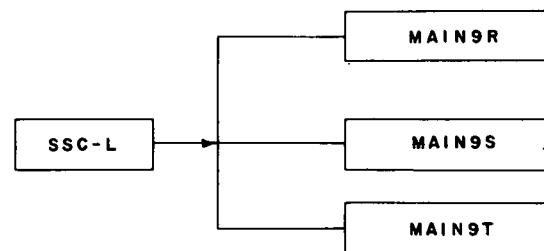
Figure 6-1. Three main driver programs of SSC-L.
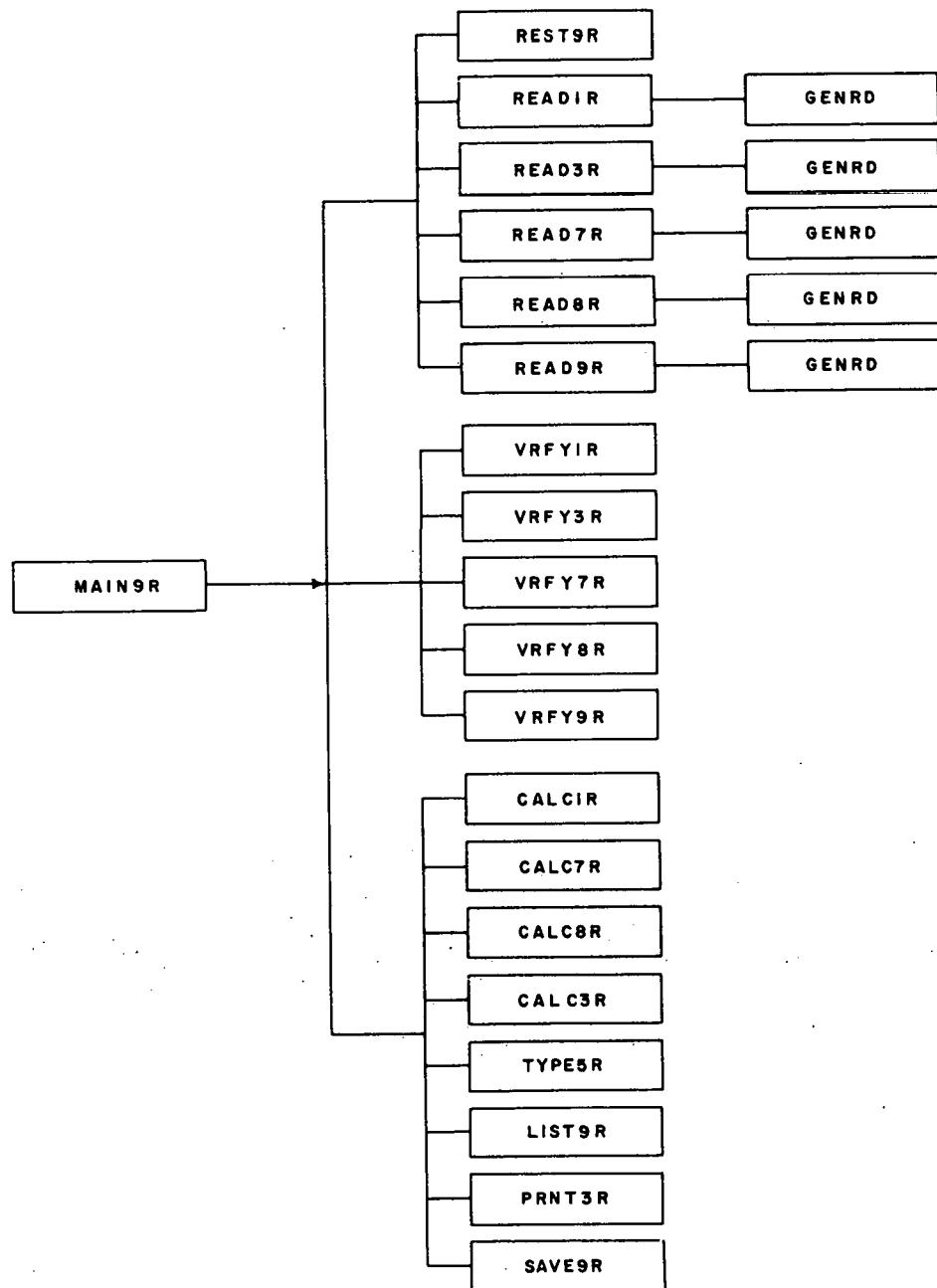
Figure 6-2. MAIN9R flow diagram.
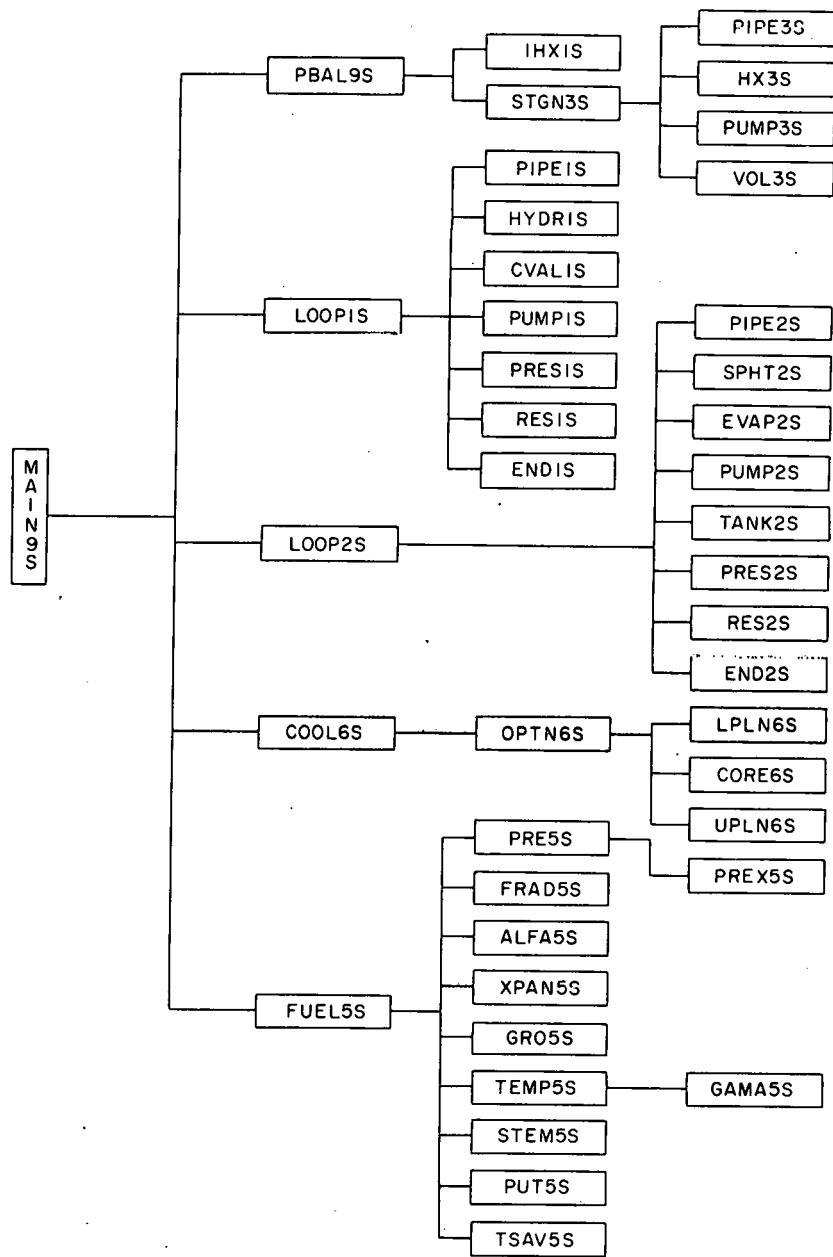
Figure 6-3. MAIN9S flow diagram.
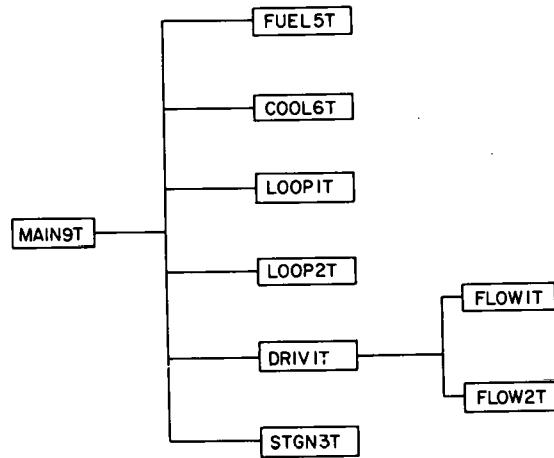
Figure 6-4. MAIN9T flow diagram.
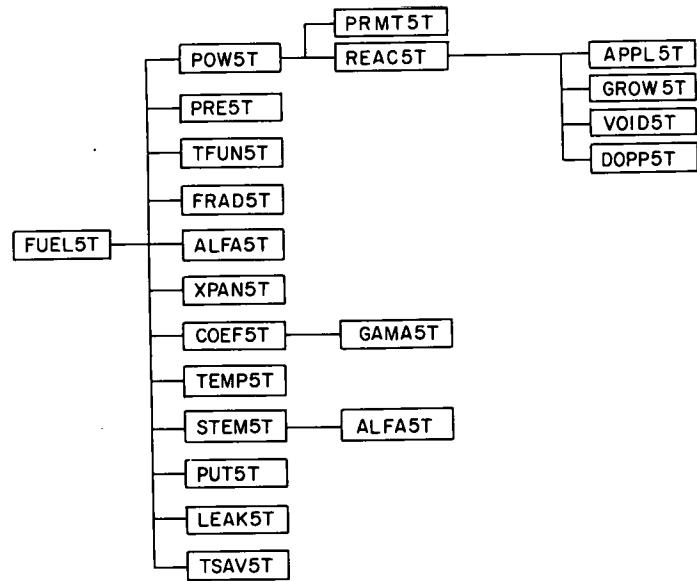
Figure 6-5. FUEL5T flow diagram.
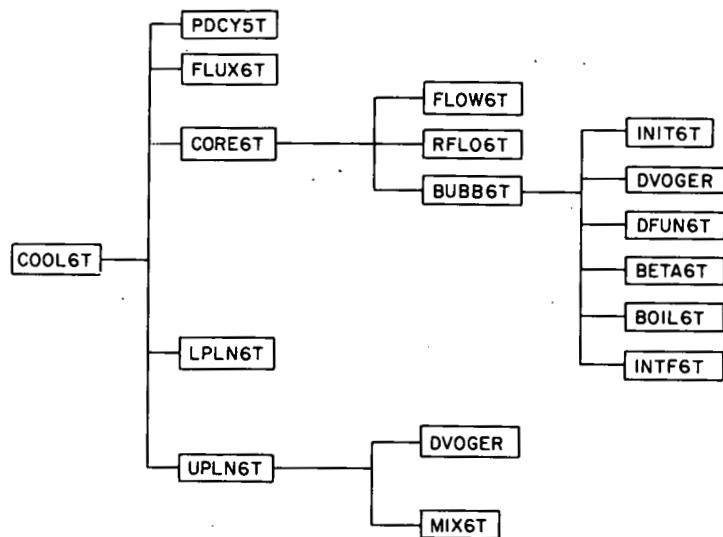
Figure 6-6. COOL6T flow diagram.
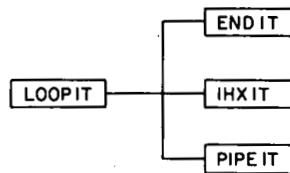

Figure 6-7. LOOP1T flow diagram.
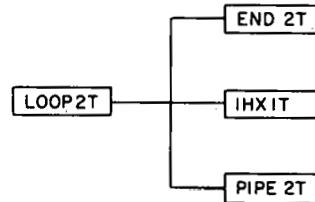
Figure 6-8. LOOP2T flow diagram.
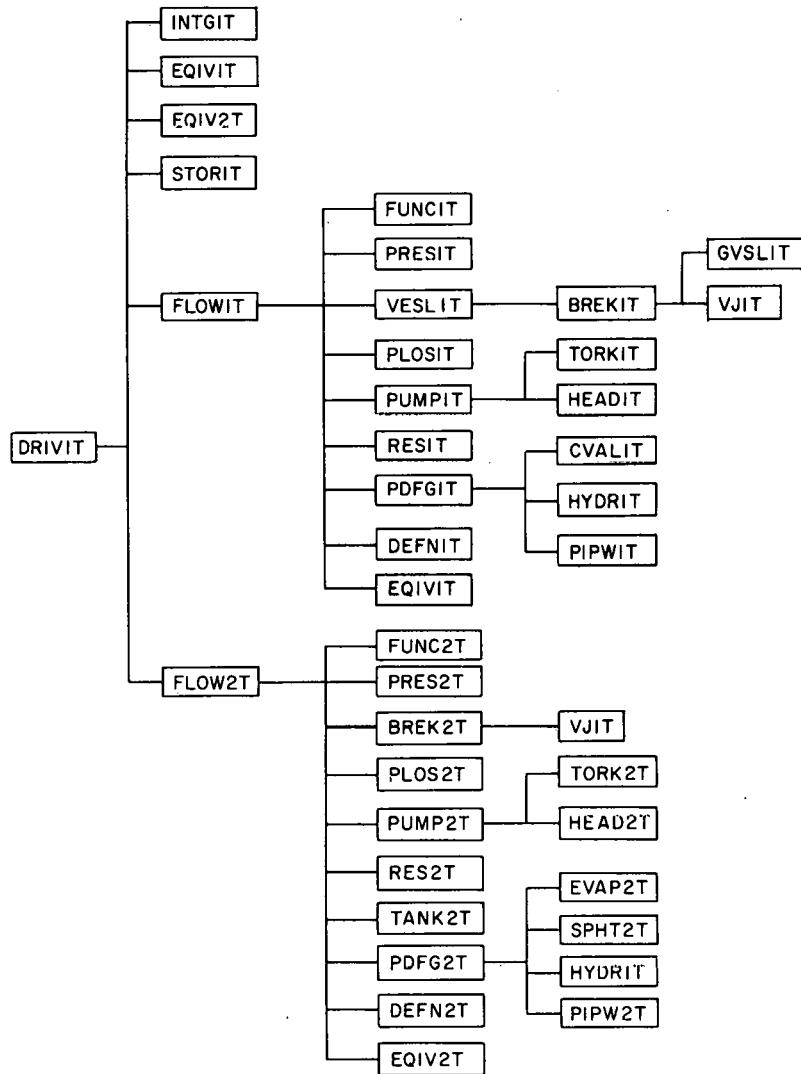
Figure 6-9. DRIV1T flow diagram.
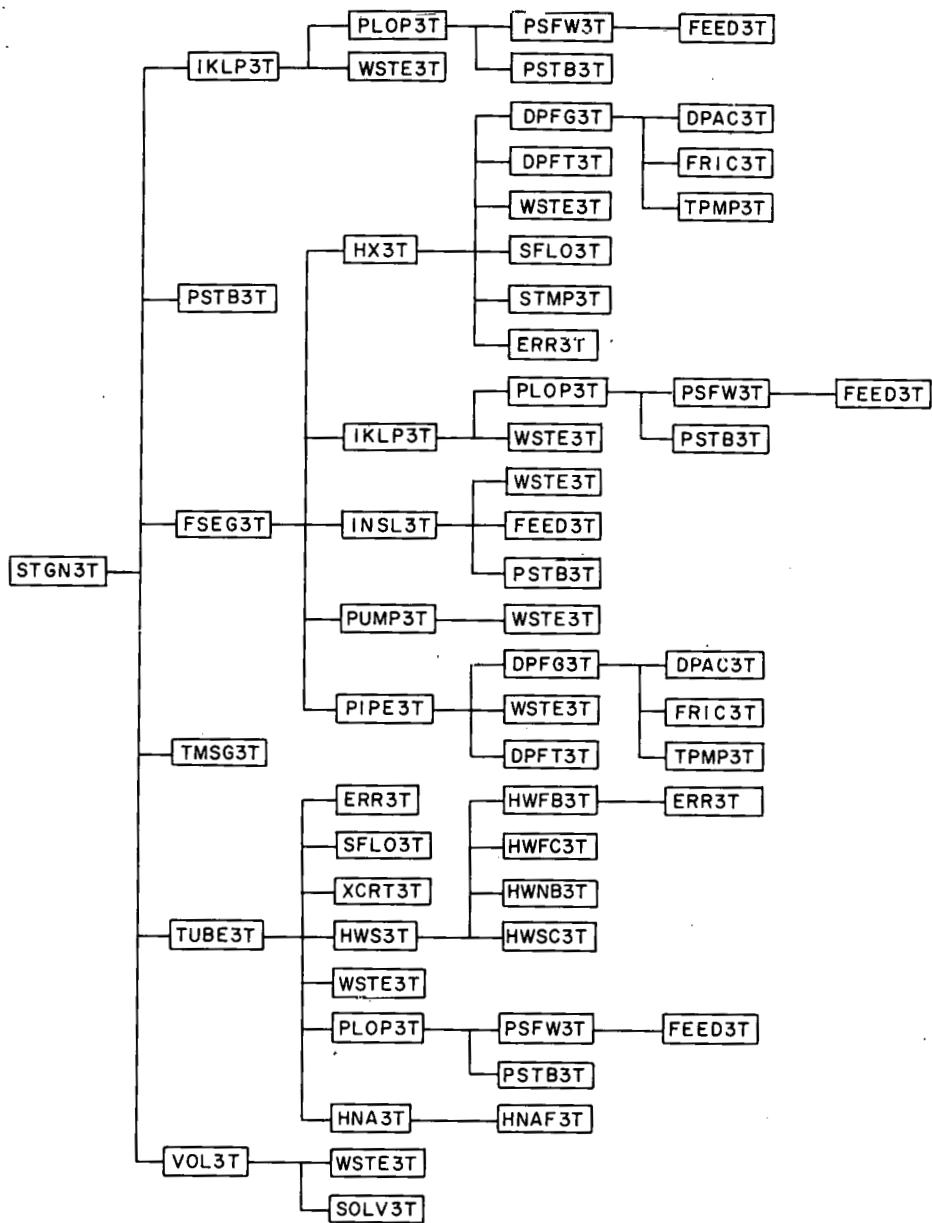
Figure 6-10.   STGN3T flow diagram.

CALC7R

This routine sets slice-type dependent arrays and determines normalized axial and radial power distribution.

CALC8R

This routine interprets the coded iterative scheme designated by the user for establishing the initial plant balance.

GENRD

This is a general purpose card reader routine as developed by the Los Alamos Scientific Laboratory[6.6] and modified for current usage.

LIST9R

This routine prints all data initialized in the input module.

PRNT3R

This routine prints all data initialized in the input module.

READ1R

This routine processes free-format card input for the initialization of the primary and secondary loop modules.

READ3R

This routine processes free-format card input for the initialization of the steam generator module.

READ7R

This routine processes free-format card input for the initialization of the in-vessel modules.

READ8R

This routine processes free-format card input for the initialization of the plant balance routine.

READ9R

This routine processes free-format card input for the initialization of the material property parameters.

REST9R

This routine reads a program generated file for the reinitialization of labeled commons in the event of a restart.

SAVE9R

This routine generated an ordered file for a reinitialization restart.

TYPE5R

This routine loads channel-dependent parameters for use in the slice-type-dependent in-vessel modules.

VRFY1R - VRFY9R

These routines validate the data processed by the corresponding READ routines against the criteria established in the data dictionary.

MAIN9S

This routine is the main driver for the steady-state calculations.

ALFA5S

This module calculated the coefficient of thermal expansion for each
node in the fuel slice.

COOL6S

This is the driver module for coolant calculations. It performs inter-
polation for fuel noding of temperature and heat transfer coefficients.

CORE6S

This is the coolant core module. It determines flow rate for L6ATYP(N6CHI)
channel. For all regions in the L6ATYP channel the module determines the node
size and number of nodes for each region, calculates axial temperature and
enthalpy gradients at each node for the region, determines friction factors at
each node for the region,and calculates pressure at each node for the region
and the orifice zone pressure difference at node one. It performs these cal-
culations for N6CHAN channels. It then calculates heat transfer coefficients
for all nodes in all N6CHAN channels and calculated the bypass flow.

CVAL1S

This routine computes the steady-state pressure drop over the check valve.

END1S

This routine calculates the temperature boundary conditions for the

subsequent pipe in the primary loop and, in doing so, accounts for the temperature rise across pump, as well as IHX plena temperatures at the proper locations.

END2S

This subroutine sets the inlet temperature and mass flow rate boundary conditions for pipe (J+1) in the intermediate coolant loop. It particularly accounts for temperature rise across pump and mass flow rate division due to branch lines for coolant flow at the steam generator.

EVAP2S

This subroutine calculates the pressure drop or loss coefficient on the shell side of the evaporator.

FRAD5S

This module calculates the average power generation for all nodes in the slice.

FUEL5S

This is the driver module for fuel heat conduction calculations. It treats a fuel slice as the basic computational element, calls all major fuel computational modules, and controls convergence.

GAMA5S

The module calculates the thermal conductivity for fuel and clad nodes for the slice and heat transfer coefficients for the interfaces.

GRO5S

This module sets pointers for restructuring in the slice.

HX3S

This routine performs the heat exchanger model calculations. It determines the pressure drop in the inlet plenum of the heat exchanger, calls the routines which determine the enthalpy and pressure distributions in the heat transfer tube, and calculates the pressure drop in the outlet plenum of the heat exchanger. In addition, it determines the location of the DNB point and adjusts the total heat transfer area to produce specified outlet conditions.

HYDR1S

This subroutine solves the steady-state momentum equations (hydraulics) for both primary and secondary sides of the IHX.

IHX1S

This routine solves the steady-state energy equations for the IHX. IHX1S and HYDR1S are the only interface between the primary and intermediate loop modules.

LOOP1S

This routine drives the primary loop steady-state calculation. In particular, it interprets the logical variables in order to select the proper calling sequence to the various subroutines. This routine also copies the results of the computations for loop 1 into the arrays for the rest of the loops.

LOOP2S

This routine drives the intermediate loop steady-state computation. The rest of the description is the same as for LOOP1S.

LPLN6S

Coolant lower plenum module. It initializes node-one values from input of temperature, enthalpy, and pressure. It calculates pressures at the bottom of the core.

OPTN6S

This routine computes the steady-state channel flow rate distribution or pressure loss coefficients, depending on user specified option.

PBAL9S

This routine performs the global thermal balance for the whole plant.

PIPE1S

This routine solves the steady-state energy and momentum equations for pipe J in the primary coolant loop. It is assumed that the pipe diameter is constant, and the pipe wall is in thermal equilibrium with the coolant.

PIPE2S

This routine solves the steady-state energy and momentum equations for pipe J in the intermediate coolant loop.

PIPE3S

This routine computes the pressure at the exit of a pipe from the

pressure losses for each node in the pipe and the fitting at the end of the pipe.

PRE5S

This module performs the initialization for FUEL5S by obtaining data computed by other modules. Amoung others, it sets the NR nodal temperature to T6COOL(J,K), places the heat transfer coefficient for that slice in a local variable HCOOL, initializes tags for restructuring, and calls PREX5S to initialize nodal distances XI at temperature T5REF.

PRES1S

This subroutine determines the pressures at pipe endpoints around the primary loop.

PRES2S

This subroutine determines the pressures at pipe endpoints around the intermediate loop.

PREX5S.

This module initializes nodal distances XI for either equiradial increments or equiarea increments of the fuel slice.

PUMP1S

This routine determines pump pressure rise by matching it with overall load in the primary circuit. It then sets up the polynomial equation for pump head and calls ROOT1U to calculate pump operating speed.

PUMP2S

This subroutine determines pump pressure rise by matching it with over-all load in the intermediate circuit. It then sets up the polynomial equation for pump head and calls ROOT1U to calculate pump operating speed.

PUMP3S

This routine computes either the pump outlet pressure at rated pump speed or the pump speed if the pump outlet pressure is specified.

PUT5S

This module moves the calculated steady-state values for the slice into storage locations.

RES1S

This routine computes the height of coolant in the primary pump tank, and the mass of cover gas above the coolant level.

RES2S

This routine computes the height of coolant in the intermediate pump tank, and the mass of cover gas above the coolant level.

SIMT6S

This routine contains seven equations for seven upper plenum temperatures, which are called by ZSYSTM, to obtain an iterative solution.

SPHT2S

This subroutine calculates the pressure drop or loss coefficient on the shell side of the superheater.

STEM5S

This module calculates the temperature of the fuel rod structure and fission gas plenum for steady-state.

STGN3S

This routine is the main driver for the steam generator calculations. In particular, it calls the various subroutines in the order in which the respective modules appear in the steam generator loops and copies the results of the computation for the intact loop into the arrays representing the damaged loop.

TANK2S

This subroutine computes the pressure in the loop at the location of the surge tank, and further, calculates the mass of gas in the surge tank.

TEMP5S

This module calculates the steady-state temperature distribution in the fuel rod and cladding.

TSAV5S

This routine determines the average temperature in each slice which contains fuel.

UPLN6S

This upper plenum coolant module calculates: the average values over N6CHAN channels of temperature and enthalpy; the total channel flow rate for N6CHAN channels; the upper plenum temperatures using ZSYSTM; the exit enthalpy, outlet, and top of core pressures and finds loss factors for each channel.

VOL3S

This routine calculates the mixed mean enthalpy in a volume based on the liquid level in the volume and the pressure specified in the volume.

XPAN5S

This module adjusts radii due to thermal expansion for each node in the fuel slice.

ZSYSTM

An IMSL routine[6.7] that determines a root of a system of N simultaneous nonlinear equations in N unknowns utilizing Brown's method.

MAIN9T

This is the driver routine for transient calculations. It also handles overall timestep control.

ALFA5T

This module calculates coefficient of thermal expansion for each node.

APPL5T

This module calculates the applied reactivity contributions (e.g., those due to scram and/or control rods) during the transient.

BETA6T

This calculates the critical pressure ratio for fission gas release.

BREK1T

This routine computes pressures at eventual break in primary loop.

BREK2T

This routine computes pressures at eventual break in intermediate loop.

BUBB6T

This is the main driver for the boiling and fission gas release calculation. It calculates initial and boundary conditions for the boiling and fission gas release.

COEF5T

This module calculates appropriate coefficients for the transient temperature calculations of fuel rod.

COOL6T

This module is the driver for the transient coolant dynamics calculations. It provides initial conditions; determines step size; and then employs several submodules to calculate temperature, pressure, enthalpy, and mass

flow rate of the coolant in all axial nodes of all channels. It then
stores values for subsequent timestep. Finally it provides boundary
conditions for fuel calculations.

CORE6T

This module calculates the enthalpy, temperature, and pressure of
liquid sodium for single-phase flow at all axial nodes of all channels. It
also acts as a subdriver for two-phase flow and reverse flow and directs
calculations to the bubble model or flow reversal model, respectively.

CVAL1T

This routine computes the pressure loss across the check valve.

DEFN1T

This routine defines pipe flow rates, and input and output pump flow
rates for primary loop.

DEFN2T

This routine defines pipe flow rates, and input and output pump flow
rates for intermediate loop.

DFUN6T

This routine calculates the derivatives for the functions calculated in
DVOGER.

DOPP5T

This module calculates the reactivity feedback due to the Doppler effect.

DPAC3T

This determines the coefficients of momentum flux pressure loss in control volume.

DPFG3T

This determines coefficients of total flow resistance in control volume.

DPFT3T

This routine determines coefficients of pressure drop in a fitting using form loss coefficient.

DRIV1T

This routine is the driver for heat transport system transient hydraulics.

DVOGER

This is an ISML routine[6.7] which integrates a system according to Gear's method.

END1T

This routine sets transient thermal boundary conditions from one pipe to the next in primary loop.

END2T

This routine sets transient thermal boundary conditions from one pipe to the next in intermediate loop.

EQIV1T

This routine equivalences the names of primary loop variables and functions of the model in terms of names in the integrating subroutine.

EQIV2T

This routine equivalences the names of intermediate loop variables and functions of the model in terms of names in the integrating subroutine.

ERR3T

This writes error message.

EVAP2T

This routine computes pressure loss across the shell side of evaporator.

FEED3T

This routine determines coefficients for feedwater flow rate.

FLOW1T

This routine sets proper calling sequence to primary loop hydraulic computation submodules.

FLOW2T

This routine sets proper calling sequence to intermediate loop hydraulic computation submodules.

FLOW6T

This module simulates the flow redistribution model. It calculates the mass flow rate in each channel and bypass channel.

FLUX6T

This routine calculates, at any timestep, heat flux from rod and structure into liquid sodium.

FRAD5T

This module calculates average power generation for all fuel nodes. It also calculates the power generation multiplier to be used later on in calculating the transient volumetric power generation.

FRIC3T

This determines friction factor as function of Reynolds number and surface roughness.

FSEG3T

This is a main driver for flow segment calculations.

FUEL5T

This module is the driver for the fuel rod and structure calculations. By calling series of modules in succession, it calculates, through these

submodules, quantities such as temperature and radii of the fuel, cladding, and structure nodes.

FUNC1T

This routine defines functions of differential equations (other than pump and reservoir) for primary loop hydraulics.

FUNC2T

This routine defines functions of differential equations (other than pump and reservoir) for intermediate loop hydraulics.

GAMA5T

This module calculates the thermal conductivity and emissivity for fuel and clad nodes and also computes the heat transfer coefficient for gaseous mistures, in the gap.

GROW5T

This module calculates the reactivity feedback due to axial expansion.

GVSL1T

This routine computes coolant level in guard vessel, pressure external to break, and d/dt for accumulated volume of coolant in the guard vessel.

HEAD1T

This routine computes head of primary pumps and defines its operational region.

HEAD2T

This routine computes head of intermediate pumps and defines its operational region.

HNA3T

This routine computes overall sodium side heat transfer coefficient.

HNAF3T

This routine computes sodium side surface heat transfer coefficient.

HWFB3T

This routine determines heat transfer coefficient in film boiling.

HWFC3T

This routine determines heat transfer coefficient in forced convection to liquid.

HWNB3T

This routine determines heat transfer coefficient in nucleate boiling of subcooled or saturated water.

HWS3T

This routine is the main driver for overall heat transfer coefficient calculation on water side of heat exchanger.

HWSC3T

This determines heat transfer coefficient in forced convection to superheated steam.

HX3T

This determines coefficients for energy and flow equation for water side of heat exchanger and advances sodium temperatures.

HYDR1T

This routine computes transient hydraulics in IHX.

IHX1T

This routine solves transient energy equations in the IHX.

IKLP3T

This determines pointers for all arrays needed in the flow segment calculations.

INIT6T

This calculates cladding temperature and cladding inside and outside radii for the new nodalization required by BUBB6T.

INSL3T

This determines coefficients of inlet enthalpy and flow rate of a flow segment in terms of accumulator conditions.

INTF6T

This calculates temperature at the interfaces for the lower and upper slug.

INTG1T

This routine advances the hydraulic equations using the predictor-corrector method of Adams type.

LEAK5T

This routine tests for cladding rupture due to fission gas pressure for each axial fuel slice in current channel. Cladding rupture conditions exists if difference between fission gas pressure and coolant pressure exceeds critical value defined by cladding dimensions and material yield point for the calculated cladding temperature.

LOOP1T

This routine is the main driver for transient thermal computations in primary loop.

LOOP2T

This routine is the main driver for transient thermal computations in intermediate loop.

LPLN6T

This module performs transient lower plenum calculations. It extrapolates boundary conditions. It terminates its procedure by calculating coolant and metal temperatures and pressure at the bottom of the core.

MIX6T

This module contains the solution vector at time t. This is required by DVOGER, the one-step integration package, as a formal parameter.

PDCY5T

This module handles the advancement in time of the decay heat power generation.

PDFG1T

This routine sets the logic to compute pressure losses across different elements of primary loops.

PDFG2T

This routine sets the logic to compute pressure losses across different elements of intermediate loops.

PIPE1T

This routine solves transient energy equations in the primary loop piping.

PIPE2T

This routine solves transient energy equations in the intermediate loop piping.

PIPE3T

This routine determines coefficients for energy and flow equations for a pipe.

PIPW1T

This routine computes pressure losses in pipe sections in primary loops.

PIPW2T

This routine computes pressure losses in pipe sections in intermediate loops.

PLOP3T

This routine determines reference pressure for a flow segment.

PLOS1T

This routine computes pressure losses in appropriate sections of primary loop from the losses in individual components.

PLOS2T

This routine computes pressure losses in appropriate sections of intermediate loop from the losses in individual components.

POW5T

This module serves as the driver for the rod transient fission power generation calculations.

PRE5T

This module gets the temperature from storage arrays into local scratch arrays for the particular slice in question, at the start of each timestep. It is mainly used as an initialization routine.

PRES1T

This routine sets inlet and outlet pressures of uniform mass flow rate sections in primary loops.

PRES2T

This routine sets inlet and outlet pressures of uniform mass flow rate sections in intermediate loops.

PRMT5T

This module handles the advancement in time of the fission power generation.

PSFW3T

This determines reference pressure for a flow segment.

PSTB3T

This determines turbine inlet pressure.

PUMP1T

This routine computes primary pump variables and d/dt for pump speed.

PUMP2T

This routine computes intermediate pump variables and d/dt for pump speed.

PUMP3T

This determines coefficients for energy and flow equation for a pump.

PUT5T

At the time this module is invoked, all formal calculations of the fuel and clad and structure have been completed for that timestep and for the given axial node. This module then moves all temperatures and radii so far calculated from local scratch variables into storage arrays for subsequent timesteps.

REAC5T

This module initiates calls to other modules to obtain the various applied and feedback reactivity contributions.

RES1T

This routine computes variables and d/dt for level in primary pump reservoir.

RES2T

This routine computes variables and d/dt for level in intermediate pump reservoir.

RFLO6T

This module calculates the temperature, pressure, and enthalpy of liquid sodium at all coolant nodes, when reverse flow occurs.

SFLO3T

This routine determines sodium mass flow rate from input boundary conditions.

SOLV3T

This routine solves accumulator equations by Gaussian elimination with pivoting.

SPHT2T

This routine computes pressure loss across the shell side of superheater.

STEM5T

This module calculates the temperature of the structure and the fission gas plenum.

STGN3T

This is the main driver for the steam generator calculation. It calls routines which computes accumulator conditions, backsubstitutes accumulator conditions to advance flow segment variables, and determines the maximum change in water side variables during this step.

STMP3T

This routine determines sodium temperature at heat exchanger inlet from boundary conditions.

STOR1T

This routine stores the intermediate updated values of flow rate.

TANK2T

This routine computes pressures and d/dt for level in surge tank.

TBOIL6T

This routine does the Lagrangian calculations for liquid temperature at fixed axial mesh points in upper and lower slugs. For the fixed mesh points in the bubble, it sets the temperature equal to the bubble temperature.

TEMP1T

This function program transforms enthalpy into temperature.

TEMP5T

This module calculates the temperatures at fuel and clad nodes for the new timestep.

TFUN5T

In this module, the previous temperature of the fuel and cladding are extrapolated to the present time to evaluate material properties.

TMSG3T

This calculates timestep in the steam generating system.

TORK1T

This routine computes hydraulic and friction torques for primary pumps.

TORK2T

This routine computes hydraulic and friction torques for intermediate pumps.

TPMP3T

This determines two-phase friction multiplier on the water/steam side of the steam generator.

TSAV5T

This module calculates certain fuel slice dependent quantities required in GROW5T, DUPP5T, and VOID5T.

TUBE3T

This calculates surface heat fluxes and tube wall temperatures in heat exchanger.

UPLN6T

This routine, by employing DVOGER, solves the systems of first order differential equations with the timestep provided by the main driver COOL6T. The final solution consists of sodium level; temperature of sodium in two mixing zones; temperature of cover gas; and temperatures of the inner structure, thermal liner, and the vessel closure head. It terminates by calculating the pressure at the vessel outlet.

VGSL1T

This routine retrieves information to interface with reactor vessel and sets calling sequence to compute pressures at eventual break in primary loops.

VJ1T

This routine determines velocity of jet out of a pipe break.

VOID5T

This module calculates the reactivity feedback due to sodium voiding.

VOL3T

This calculates coefficients for accumulators, eliminates flow segment terms from accumulator equations, and advances the accumulator variables.

WSTE3T

This determines water properties as function of enthalpy and pressure.

XCRT3T

This routine determines water quality at DNB point as function of pressure, enthalpy, and heat flux.

XPAN5T

This module recalculates the radii of the fuel and cladding, necessary because of the thermal expansion of the radial nodes. Two methods are employed in calculating radii. Equal area increment, and equal radii increment.

REFERENCES

6.1 "USA Standard FORTRAN," ANSI X3.9-1966, United States of America Standards Institute, New York.

6.2 "ANS Standard Recommended Programming Practices to Facilitate the Interchange of Digital Computer Programs," ANS STD.3-1971, American Nuclear Society.

6.3 "Guidelines for the Documentation of Digital Computer Programs," ANSI Standard N413-1974.

6.4 "Flow Chart Symbols and Their Usage in Information Processing," ANSI Standard X3.5-1968.

6.5 "Computer Coding, Documentation and Distribution," RDT Standard F 1-4, Unapproved Preliminary Draft, January 30, 1975.

6.6 C.W. Cox, "GENRD: A Free-Format Card Input Processor," Los Alamos Scientific Laboratory, LA-4793, January 1972.

6.7 International Mathematical and Statistical Library, IMSL Library 3, June 1974.